Non-invasive fetal electrocardiogram : analysis and interpretation

Citation for published version (APA):
Vullings, R. (2010). *Non-invasive fetal electrocardiogram : analysis and interpretation*. [Phd Thesis 1 (Research TU/e / Graduation TU/e), Electrical Engineering]. Technische Universiteit Eindhoven. https://doi.org/10.6100/IR692881

DOI:
10.6100/IR692881

Document status and date:
Published: 01/01/2010

Document Version:
Publisher's PDF, also known as Version of Record (includes final page, issue and volume numbers)

Non-invasive fetal electrocardiogram: analysis and interpretation

PROEFSCHRIFT

ter verkrijging van de graad van doctor aan de Technische Universiteit Eindhoven, op gezag van de Rector Magnificus, prof.dr.ir. C.J. van Duijn, voor een commissie aangewezen door het College voor Promoties in het openbaar te verdedigen op dinsdag 14 december 2010 om 16.00 uur

door

Rik Vullings

geboren te Venray

Dit proefschrift is goedgekeurd door de promotoren:

prof.dr.ir. J.W.M. Bergmans
en
prof.dr. S.G. Oei

Copromotor:
dr.ir. M. Mischi

This research was supported by the Dutch Technology Foundation STW (06480). Financial support for the printing of this thesis has been kindly provided by Maastricht Instruments, Nemo Healthcare, Technomed Europe, and Unitron Group.

CIP-DATA LIBRARY TECHNISCHE UNIVERSITEIT EINDHOVEN

Vullings, Rik

Non-invasive fetal electrocardiogram: analysis and interpretation / by Rik Vullings.
- Eindhoven : Technische Universteit Eindhoven, 2010.- Proefschrift.
A catalogue record is available from the Eindhoven University of Technology Library
ISBN 978-90-386-2395-5
NUR 954
Trefw.: biomedische signaalverwerking / foetale bewaking / electrocardiografie.
Subject headings: biomedical signal processing / fetal monitoring / electrocardiography.

Samenstelling van de promotiecommissie:

prof.dr.ir. J.W.M. Bergmans, promotor
Technische Universiteit Eindhoven, Nederland

prof.dr. S.G. Oei, promotor
Technische Universiteit Eindhoven, Nederland

dr.ir. M. Mischi, copromotor
Technische Universiteit Eindhoven, Nederland

prof.dr. K.G. Rosén, extern lid
University of Borås, Zweden

prof.dr. M.G. Signorini, extern lid
Politecnico di Milano, Italië

prof.dr. F.P.H.A. Vandenbussche, extern lid
Universitair Medisch Centrum St Radboud, Nijmegen, Nederland

prof.dr.ir. P.F.F. Wijn, lid TU/e
Technische Universiteit Eindhoven, Nederland

prof.dr.ir. A.C.P.M. Backx, voorzitter
Technische Universiteit Eindhoven, Nederland

Summary

Non-invasive fetal electrocardiogram: analysis and interpretation

High-risk pregnancies are becoming more and more prevalent because of the progressively higher age at which women get pregnant. Nowadays about twenty percent of all pregnancies are complicated to some degree, for instance because of preterm delivery, fetal oxygen deficiency, fetal growth restriction, or hypertension. Early detection of these complications is critical to permit timely medical intervention, but is hampered by strong limitations of existing monitoring technology. This technology is either only applicable in hospital settings, is obtrusive, or is incapable of providing, in a robust way, reliable information for diagnosis of the well-being of the fetus.

The most prominent method for monitoring of the fetal health condition is monitoring of heart rate variability in response to activity of the uterus (cardiotocography; CTG). Generally, in obstetrical practice, the heart rate is determined in either of two ways: unobtrusively with a (Doppler) ultrasound probe on the maternal abdomen, or obtrusively with an invasive electrode fixed onto the fetal scalp. The first method is relatively inaccurate but is non-invasive and applicable in all stages of pregnancy. The latter method is far more accurate but can only be applied following rupture of the membranes and sufficient dilatation, restricting its applicability to only the very last phase of pregnancy. Besides these accuracy and applicability issues, the use of CTG in obstetrical practice also has another limitation: despite its high sensitivity, the specificity of CTG is relatively low. This means that in most cases of fetal distress the CTG reveals specific patterns of heart rate variability, but that these specific patterns can also be encountered for healthy fetuses, complicating accurate diagnosis of the fetal condition. Hence, a prerequisite for preventing unnecessary interventions that are based on CTG alone, is the inclusion of additional information in diagnostics.

Monitoring of the fetal electrocardiogram (ECG), as a supplement of CTG, has been demonstrated to have added value for monitoring of the fetal health condition. Unfortunately the application of the fetal ECG in obstetrical diagnostics is limited because at present the fetal ECG can only be measured reliably by means of an invasive scalp electrode. To overcome this limited applicability, many attempts have been made to record the fetal ECG non-invasively from the maternal abdomen, but these attempts have not yet led to approaches that permit widespread clinical application.

One key difficulty is that the signal to noise ratio (SNR) of the transabdominal ECG recordings is relatively low. Perhaps even more importantly, the abdominal ECG recordings yield ECG signals for which the morphology depends strongly on the orientation of the fetus within the maternal uterus. Accordingly, for any fetal orientation, the ECG morphology is different. This renders correct clinical interpretation of the recorded ECG signals complicated, if not impossible.

This thesis aims to address these difficulties and to provide new contributions on the clinical interpretation of the fetal ECG. At first the SNR of the recorded signals is enhanced through a series of signal processing steps that exploit specific and a priori known properties of the fetal ECG. More particularly, the dominant interference (i.e. the maternal ECG) is suppressed by exploiting the absence of temporal correlation between the maternal and fetal ECG. In this suppression, the maternal ECG complex is dynamically segmented into individual ECG waves and each of these waves is estimated through averaging corresponding waves from preceding ECG complexes. The maternal ECG template generated by combining the estimated waves is subsequently subtracted from the original signal to yield a non-invasive recording in which the maternal ECG has been suppressed. This suppression method is demonstrated to be more accurate than existing methods.

Other interferences and noise are (partly) suppressed by exploiting the quasi-periodicity of the fetal ECG through averaging consecutive ECG complexes or by exploiting the spatial correlation of the ECG. The averaging of several consecutive ECG complexes, synchronized on their QRS complex, enhances the SNR of the ECG but also can suppress morphological variations in the ECG that are clinically relevant. The number of ECG complexes included in the average hence constitutes a trade-off between SNR enhancement on the one hand and loss of morphological variability on the other hand. To relax this trade-off, in this thesis a method is presented that can adaptively estimate the number of ECG complexes included in the average. In cases of morphological variations, this number is decreased ensuring that the variations are not suppressed. In cases of no morphological variability, this number is increased to ensure adequate SNR enhancement. The further suppression of noise by exploiting the spatial correlation of the ECG is based on the fact that all ECG signals recorded at several locations on the maternal abdomen originate from the same electrical source, namely the fetal heart.

The electrical activity of the fetal heart at any point in time can be modeled as a single electrical field vector with stationary origin. This vector varies in both amplitude and orientation in three-dimensional space during the cardiac cycle and the time-path described by this vector is referred to as the fetal vectorcardiogram (VCG). In this model, the abdominal ECG constitutes the projection of the VCG onto the vector that describes the position of the abdominal electrode with respect to a reference electrode. This means that when the VCG is known, any desired ECG signal

can be calculated. Equivalently, this also means that when enough ECG signals (i.e. at least three independent signals) are known, the VCG can be calculated. By using more than three ECG signals for the calculation of the VCG, redundancy in the ECG signals can be exploited for added noise suppression.

Unfortunately, when calculating the fetal VCG from the ECG signals recorded from the maternal abdomen, the distance between the fetal heart and the electrodes is not the same for each electrode. Because the amplitude of the ECG signals decreases with propagation to the abdominal surface, these different distances yield a specific, unknown attenuation for each ECG signal. Existing methods for estimating the VCG operate with a fixed linear combination of the ECG signals and, hence, cannot account for variations in signal attenuation. To overcome this problem and be able to account for fetal movement, in this thesis a method is presented that estimates both the VCG and, to some extent, also the signal attenuation. This is done by determining for which VCG and signal attenuation the joint probability over both these variables is maximal given the observed ECG signals. The underlying joint probability distribution is determined by assuming the ECG signals to originate from scaled VCG projections and additive noise. With this method, a VCG, tailored to each specific patient, is determined. With respect to the fixed linear combinations, the presented method performs significantly better in the accurate estimation of the VCG.

Besides describing the electrical activity of the fetal heart in three dimensions, the fetal VCG also provides a framework to account for the fetal orientation in the uterus. This framework enables the detection of the fetal orientation over time and allows for rotating the fetal VCG towards a prescribed orientation. From the normalized fetal VCG obtained in this manner, standardized ECG signals can be calculated, facilitating correct clinical interpretation of the non-invasive fetal ECG signals.

The potential of the presented approach (i.e. the combination of all methods described above) is illustrated for three different clinical cases. In the first case, the fetal ECG is analyzed to demonstrate that the electrical behavior of the fetal heart differs significantly from the adult heart. In fact, this difference is so substantial that diagnostics based on the fetal ECG should be based on different guidelines than those for adult ECG diagnostics. In the second case, the fetal ECG is used to visualize the origin of fetal supraventricular extrasystoles and the results suggest that the fetal ECG might in future serve as diagnostic tool for relating fetal arrhythmia to congenital heart diseases. In the last case, the non-invasive fetal ECG is compared to the invasively recorded fetal ECG to gauge the SNR of the transabdominal recordings and to demonstrate the suitability of the non-invasive fetal ECG in clinical applications that, as yet, are only possible for the invasive fetal ECG.

Samenvatting

Het uitwendige foetale electrocardiogram: analyse en interpretatie

Hoog-risico zwangerschappen komen steeds vaker voor doordat vrouwen op steeds latere leeftijd zwanger worden. Momenteel vinden bij ongeveer twintig procent van de zwangerschappen complicaties, zoals vroeggeboorten, zuurstoftekort voor de foetus, foetale groeivertraging of een hoge bloeddruk plaats. Een vroegtijdige detectie van deze complicaties is van kritiek belang om een tijdig medisch ingrijpen mogelijk te maken, maar deze detectie wordt bemoeilijkt door ernstige tekortkomingen aan de bestaande bewakingstechnologie. Deze technologie is ofwel alleen toepasbaar in het ziekenhuis, ofwel belastend voor de patiënt, ofwel niet goed in staat om op een robuuste wijze betrouwbare informatie te verschaffen die diagnose van de foetale conditie mogelijk maakt.

De meest gebruikte methode om de foetale conditie te bewaken is de interpretatie van veranderingen in het hartritme van de foetus die optreden als gevolg van activiteit van de baarmoeder (cardiotocografie; CTG). Het foetale hartritme kan op twee verschillende manieren bepaald worden in de verloskundige praktijk: op niet-belastende, uitwendige wijze met behulp van een (Doppler) ultrageluid probe op de buik van de moeder, of, op wèl belastende wijze, met een inwendige elektrode die op het hoofd van de foetus bevestigd wordt. De eerste methode is relatief onnauwkeurig maar kan in alle stadia van de zwangerschap toegepast worden. De tweede methode is veel nauwkeuriger dan de uitwendige methode maar kan alleen toegepast worden nadat de vliezen gebroken zijn en nadat er voldoende ontsluiting is. Dit beperkt de toepasbaarheid van de inwendige methode tot de allerlaatste fase van de zwangerschap. Behalve door de onnauwkeurigheid van de uitwendige methode en de beperkte toepasbaarheid van de inwendige methode is de waarde van CTG in de klinische praktijk ook om een andere reden beperkt. Namelijk, hoewel CTG een hoge mate van sensitiviteit heeft, is de specificiteit relatief laag. Dit betekent dat, hoewel CTG vrijwel altijd specifieke patronen in hartritme variabiliteit laat zien in gevallen van foetale nood, het deze patronen ook kan laten zien in gevallen dat er geen sprake is van foetale nood. Om onnodig ingrijpen in de zwangerschap, enkel gebaseerd op CTG, te voorkomen zal daarom aanvullende informatie gebruikt moeten worden in de diagnostiek.

Het is aangetoond dat de analyse van het foetale electrocardiogram (ECG) in combinatie met CTG analyse een toegevoegde waarde heeft in het bewaken van de foetale gezondheidstoestand. Het gebruik van het foetale ECG voor verloskundige diagnostiek is echter beperkt vanwege de invasiviteit van de scalp elektrode waarmee het ECG gemeten wordt. Om deze beperking te omzeilen en het ECG meer algemeen toepasbaar te maken zijn door de jaren heen verschillende pogingen ondernomen om het foetale ECG op een uitwendige wijze vanaf de buik van de moeder te meten. Helaas heeft door technologische moeilijkheden geen enkele van deze pogingen geleid tot een veelgebruikte klinische applicatie voor uitwendige bewaking van het foetale ECG. Eén van de voornaamste moeilijkheden bij het meten van het uitwendige ECG is het feit dat de signaal ruis verhouding (SNR; signal to noise ratio) van de ECG metingen relatief laag is. Echter, wat misschien nog wel belangrijker is, is dat de abdominale metingen ECG signalen opleveren waarvan de morfologie sterk afhangt van, onder andere, de oriëntatie van de foetus in de baarmoeder. Als een gevolg van deze afhankelijkheid is de morfologie van het foetale ECG anders voor elke foetale oriëntatie en is correcte klinische interpretatie van de gemeten ECG signalen erg lastig, zo niet onmogelijk.

In dit proefschrift richten we ons op problemen die gerelateerd zijn aan uitwendige metingen van het foetale ECG: de analyse van deze metingen en het verschaffen van nieuwe inzichten in de interpretatie van het foetale ECG. In de eerste plaats wordt de SNR van de gemeten signalen verbeterd door middel van een serie signaalverwerkingsstappen die gebruik maken van specifieke en *a priori* bekende eigenschappen van het foetale ECG. De dominante verstoring (i.e. het maternale ECG) kan bijvoorbeeld onderdrukt worden door de afwezigheid van een temporele correlatie tussen het maternale en foetale ECG te benutten. In deze onderdrukking wordt het maternale ECG op dynamische wijze gesegmenteerd in individuele ECG golven en wordt elk van deze golven afgeschat door overeenkomstige golven uit voorgaande ECG complexen te middelen. Het maternale ECG template dat ontstaat door de afgeschatte, individuele golven weer te combineren kan vervolgens afgetrokken worden van het oorspronkelijke ECG signaal om zodoende een uitwendige meting, waarin het maternale ECG onderdrukt is, over te houden. De prestatie van deze maternale ECG onderdrukkingsmethode is vergeleken met de prestatie van reeds bestaande onderdrukkingsmethoden. Deze vergelijking toont aan dat de ontwikkelde methode een hogere nauwkeurigheid heeft.

Andere verstoringen van het abdominaal gemeten foetale ECG en ruis worden (gedeeltelijk) onderdrukt door de quasi-periodiciteit van het foetale ECG te benutten (door middel van het middelen van opeenvolgende foetale ECG complexen) of door het benutten van de ruimtelijke correlatie van het ECG. Het middelen van verscheidene opeenvolgende ECG complexen, gesynchroniseerd op hun QRS complex, vergroot de SNR van het ECG maar kan ook leiden tot het onderdrukken van kli-

nisch relevante morfologische veranderingen in het ECG. De keuze voor het aantal ECG complexen dat gebruikt wordt in de middeling is daarom een afweging tussen de gewenste SNR toename aan de ene kant en het verlies aan morfologische variaties aan de andere kant. Om het belang van deze afweging te verzwakken wordt in dit proefschrift een methode gepresenteerd die een adaptieve schatting van het aantal ECG complexen in de middeling mogelijk maakt. In gevallen van morfologische variatie wordt dit aantal verminderd, er voor zorgend dat deze variaties niet onderdrukt worden. In gevallen van geen morfologische variatie wordt dit aantal vergroot, er voor zorgend dat de SNR toename afdoende is. De verdere onderdrukking van ruis door het benutten van de ruimtelijke correlatie van het ECG is gebaseerd op het feit dat alle ECG signalen, die op verschillende plaatsen op de maternale buik gemeten worden, hun oorsprong hebben in dezelfde elektrische bron, namelijk het foetale hart.

De elektrische activiteit van het foetale hart kan op elk tijdstip gemodelleerd worden als een enkele elektrische veld vector met een stationaire oorsprong. Zowel de amplitude als de oriëntatie van deze vector in de drie-dimensionale ruimte varieert gedurende de hartcyclus. Het pad dat de vector beschrijft gedurende een hartslag wordt het foetale vectorcardiogram (VCG) genoemd. In dit model van de foetale cardiale elektrische activiteit vormt het abdominale ECG een projectie van het VCG op de vector die de positie van de abdominale elektrode ten opzichte van een referentie-elektrode beschrijft. Dit betekent dat wanneer het VCG beschikbaar is, elk gewenst ECG signaal berekend kan worden. Dit betekent echter ook dat, wanneer genoeg ECG signalen (i.e. minimaal 3 onafhankelijke signalen) beschikbaar zijn, het VCG berekend kan worden. Door gebruik te maken van meer dan drie ECG signalen in de berekening van het VCG kan de redundantie in deze ECG signalen benut worden voor ruisonderdrukking.

Bij het berekenen van het foetale VCG uit de ECG signalen die gemeten zijn vanaf de buik van de moeder, is de afstand tussen het foetale hart en de elektroden op de buik helaas niet voor elke elektrode hetzelfde. Omdat de amplitude van de ECG signalen afneemt tijdens propagatie van de signalen naar het buikoppervlak, houden deze verschillen in afstand een specifieke, onbekende demping van elk individueel ECG signaal in. De bestaande methoden om het VCG uit te rekenen maken gebruik van een vaste, lineaire combinatie van de ECG signalen en kunnen, derhalve, geen rekening houden met deze verschillen in signaaldemping. Om dit probleem op te lossen en rekening te kunnen houden met foetale beweging (die de afstand tussen het foetale hart en de abdominale elektroden doet veranderen), wordt in dit proefschrift een methode gepresenteerd die niet alleen het VCG, maar ook, in enige mate, de signaaldemping afschat. Dit wordt gedaan door te bepalen voor welk VCG en voor welke signaaldemping de gezamenlijke probabiliteit over deze beide variabelen maximaal is, gegeven de gemeten ECG signalen. De onderliggende gezamenlijke probabiliteitsverdeling wordt bepaald door aan te nemen dat de gemeten ECG sig-

nalen combinaties zijn van geschaalde versies van VCG projecties en additieve ruis. Met deze methode kan een VCG, individueel afgestemd op elke patiënt, bepaald worden. In vergelijking tot de vaste, lineaire combinatie van ECG signalen presteert de gepresenteerde methode significant beter in het nauwkeurig afschatten van het VCG.

Naast het beschrijven van de elektrische activiteit van het foetale hart in drie dimensies, verschaft het foetale VCG ook een raamwerk waarbinnen rekening gehouden kan worden met de oriëntatie van de foetus in de baarmoeder. Dit raamwerk maakt de detectie van de foetale oriëntatie als een functie van de tijd mogelijk en verschaft bovendien de mogelijkheid om het foetale VCG te roteren naar een voorgeschreven oriëntatie. Van het gestandaardiseerde foetale VCG dat zo verkregen wordt kunnen vervolgens gestandaardiseerde ECG signalen berekend worden. Deze ECG signalen vergemakkelijken op hun beurt de correcte klinische interpretatie van het uitwendige foetale ECG.

De potentie van de gepresenteerde aanpak (i.e. de integratie van alle methoden die hierboven beschreven zijn) wordt geïllustreerd aan de hand van een drietal klinische voorbeelden. In het eerste voorbeeld wordt het foetale VCG gebruikt om aan te tonen dat het elektrische gedrag van het foetale hart significant afwijkt van dat van het volwassen hart. Sterker nog, dit gedrag wijkt zo sterk af dat diagnostiek op basis van het foetale ECG gebaseerd zou moeten zijn op andere klinische richtlijnen dan die gebruikt wordt in de diagnostiek voor volwassenen. In het tweede voorbeeld wordt het foetale ECG gebruikt om de oorsprong van ventriculaire extrasystoles te visualiseren. De resultaten van deze visualisatie suggereren dat het foetale ECG in de toekomst wellicht gebruikt kan worden als diagnostisch hulpmiddel om foetale arrhythmieën te relateren aan aangeboren hartziekten. In het laatste voorbeeld wordt het uitwendig gemeten foetale ECG vergeleken met het inwendig gemeten foetale ECG om zodoende de SNR van de metingen op de maternale buik te kunnen duiden. Bovendien wordt aldus getoond dat het uitwendig gemeten ECG bruikbaar kan zijn in klinische toepassingen die vooralsnog alleen mogelijk zijn met het inwendig gemeten foetale ECG.

Contents

Abbreviations, notation, and symbols

Abbreviations

aICA	Augmented independent component analysis
ANC	Adaptive noise canceller
aPCA	Augmented principal component analysis
BPM	Beats per minute
BSPM	Body surface potential map
BSS	Blind source separation
CTG	Cardiotocography
DC	Direct current
ECG	Electrocardiogram
EHG	Electrohysterogram
EMG	Electromyogram
ESAIC	Event synchronous adaptive interference canceller
ESC	Event synchronous interference canceller
FIR	Finite impulse response
HRV	Heart rate variability
ICA	Independent component analysis
IIR	Infinite impulse response
LMS	Least mean squared
LP	Linear prediction
MAP	Maximum *a posteriori*
MCG	Magnetocardiogram
ML	Maximum likelihood
M-PAQ	Maastricht programmable acquisition
MRI	Magnetic resonance imaging
MSE	Mean squared error
NEMO	Non-invasive electrophysiological monitor for obstetrics
NICU	Neonatal intensive care unit
PBSS	Physiology based source separation
PCA	Principal component analysis
PTV	Patient-tailored vectorcardiography

RMS	Root mean squared
ROI	Region of interest
SAD	Sum of absolute differences
SNR	Signal to noise ratio
SVD	Singular value decomposition
SVES	Supraventricular extrasystoles
TWA	T-wave alternans
VCG	Vectorcardiogram
WAMES	Weighted averaging of maternal ECG segments

Notation

x	Scalar
$\vec{x}$	Vector
$\mathbf{X}$	Matrix
$X_{i,j}$	Entry on i^{th} row and j^{th} column of $\mathbf{X}$
$\mathbf{X}^T$	Transpose of $\mathbf{X}$
$\mathbf{X}^{-1}$	Inverse of $\mathbf{X}$
$\mathbf{X}^{\dagger}$	Moore-Penrose inverse of $\mathbf{X}$
$\mathbf{X}_{-i}$	Matrix $\mathbf{X}$ for which the ith row is missing
$\lvert\vec{x}\rvert$	Modulus of $\vec{x}$
$\lvert\mathbf{X}\rvert$	Determinant of matrix $\mathbf{X}$
$\lVert\mathbf{x}\rVert_F^2$	Frobenius norm of $\mathbf{x}$
$\mathbf{tr}\left(\mathbf{X}\right)$	Trace of $\mathbf{X}$
$\hat{\mathbf{X}}$	Estimate of $\mathbf{X}$
$\mathbf{E}_y\left[x\right]$	Expected value of x with respect to the probability distribution y
$\mathbf{cov}\left(x\right)$	Covariance of x
$p\left(x\right)$	Distribution of x
$p\left(x\,\vert\,y\right)$	Conditional probability distribution of x given y
$p\left(x,y\right)$	Joint probability distribution of x and y
$\mathcal{N}\left(x,y\right)$	Gaussian distribution with mean x and variance y

Symbols

In case the symbol represents a physical quantity with non-dimensionless unit, this unit is indicated between square brackets.

a, b, c	Parameters for aligning ECG segments [V] (only for c; a and b are dimensionless)
$\mathbf{D}$	Dower matrix
$f(\vec{x},\vec{a})$	Function describing ellipse
F	Collection of maternal ECG samples that are not corrupted by artifacts
g	Scaling parameter for QRS detection threshold
G	Collection of maternal ECG segments/waves for which the associated averaging weights conform to a specific range
$\mathbf{I}$	Identity matrix
$\mathbf{J}_\tau$	Shift matrix
$\mathbf{K}$	Kalman gain
M	Length of ECG wave/segment [s] (or dimensionless in case the length is expressed in samples)
$\mathbf{M}$	Mixing matrix
$\mathcal{M}$	Measure for fetal movement
n	Number of ECG complexes included in average or in signal of specific length
N	Number of ECG signals
$\mathfrak{N}$	Number of model residuals averaged to improve statistical significance
$\mathbf{P}$	Orthonormal transformation matrix
$q(\cdot,\cdot)$	Variational distribution
$\vec{r}$	Spatial vector [m]
$\mathbf{R}$	Rotation matrix
$\mathbb{R}$	Collection of real numbers
$\mathbf{S}$	VCG [V]
$\mathcal{S}$	Source signals [V]
Δt_s	Time period between samples (inverse of sampling frequency) [s]
T	Length of ECG signals [s] (or dimensionless in case the length is expressed in samples)
ΔT	Delay between corresponding segments in different ECG complexes [s] (or dimensionless in case the length is expressed in samples)
$\mathbf{U}$	Matrix of scaled ECG signals [V]
$\vec{V}$, $\mathbf{V}$	ECG signal(s) [V]
$\vec{w}$	Weight for averaging maternal ECG segments
$\mathbf{Z}$	Wave/segment of ECG or VCG signals [V]
$\tilde{\mathbf{Z}}$	Interpolated or augmented wave/segment of ECG signals [V]
$\mathbf{Z}'$	Interpolated and aligned wave/segment of ECG signals [V]

$\mathbb{Z}$	Collection of integers
$\vec{\nabla}$	Gradient vector
α, $\vec{\alpha}$, α	Scaling of ECG or VCG signals
$\vec{\beta}$, $\mathbf{B}$	Lead-dependent scaling of VCG loop
Γ	Right eigenvectors
Δ	Number of additional samples
ε	Normalized mean squared error
$\vec{\zeta}$	Coefficients of parabolic fit
$\vec{\eta}$, $\mathbf{H}$	Noise signal(s) [V]
Θ	Left eigenvectors
$\vec{\lambda}$	Coefficients for ECG signal combination
$\vec{\Lambda}$	ECG process noise signal [V]
$\vec{\mu}_x$, μ_x	Mean (vector) of x
$\vec{\nu}$	Variation in the threshold for QRS detection [V]
$\vec{\xi}$	Threshold for QRS detection [V]
$\vec{\xi}_a$	Augmented threshold for QRS detection [V]
$\vec{\rho}$	Model residual vector [V]
σ, σ^2, Σ	Standard deviation, variance, and covariance, respectively
τ	Time interval [s] (or dimensionless in case the length of the time interval is expressed in samples)
$\vec{\phi}$	Rotation angles
$\psi_{\mathbf{SNR}}$	Measure for the SNR

Chapter 1

Introduction

Birth is among the biggest challenges a human being encounters in life. Not only does a newborn have to adjust to completely new surroundings, but, moreover, the transition from life inside the uterus to life outside it is often associated with temporal hypoxia, a decrease of the oxygen level in peripheral tissues. In order to withstand the difficulties of labor well, the fetus is equipped with several protective mechanisms that enable it to cope with substantial oxygen deficiency. A healthy fetus that encounters hypoxia during labor but is able to handle this adequately is likely to develop normally after birth [1].

The fetal protective mechanisms against oxygen deficiency consist of several reactions that enable the fetus to maintain sufficient oxygen supply to central organs such as the heart and brain. A first reaction to oxygen deficiency is a reduction of fetal activity, i.e. a reduction of fetal movement and respiration [1, 2]. When the lack of oxygen distributed to the fetus persists, the fetus reacts by redistributing its blood circulation to central organs at the expense of oxygen supply to peripheral organs [3, 4]. Furthermore, activity of the autonomic nervous system is increased, stimulating anaerobic metabolism in the peripheral organs [5, 6].

When the fetal protective mechanisms are fully intact, the fetus reacts optimally to hypoxemia (a decrease of the arterial blood oxygen level) and acute hypoxia during labor, minimizing the risk of fetal damage. However, when the fetal protective mechanisms fail, either because they have already been used or have not had the opportunity to develop, minimal reaction to hypoxia is observed. In this case, the risk of damage is significant and several non-characteristic signs of fetal distress can be expected [7].

In some situations, if detected and treated timely, fetal hypoxia is still reversible [8]. In other situations, earlier in pregnancy, physicians need to intervene, e.g. by inducing labor or by performing a Caesarean section. Monitoring of the fetal condition throughout all stages of pregnancy is therefore of the utmost importance, enabling physicians to intervene when an increased risk of long-term morbidity exists.

1.1 Present-day fetal monitoring

One of the main protective mechanisms of the fetus against hypoxia consists of blood flow regulation and distribution [3]. The driving force behind the control of variations in blood flow and blood pressure is the cardiovascular control system, which operates under the influence of the autonomic nervous system [9]. This system consists of two parts, the sympathetic nervous system and the parasympathetic nervous system, between which an essential difference exists. The sympathetic system uses a network of neurons and ganglia for the transfer of action potentials, whereas innervation by the parasympathetic system takes place directly [10]. As a result, the sympathetic system is significantly slower than the parasympathetic system.

The assessment of blood pressure by the autonomic nervous system occurs by means of so-called baroreceptors [9]. These baroreceptors are located in the wall of blood vessels and are sensitive to strain. A decrease in blood pressure results in a decrease in the stimulation of baroreceptors, which in turn leads to increased sympathetic activity and lowered parasympathetic activity [11]. This change in sympathetic and parasympathetic activity causes an increase in heart rate and cardiac contraction power [12] and the occurrence of vasoconstriction (the narrowing of blood vessels), which results in an increase in blood pressure [11]. Thus, regulation of blood flow by the cardiovascular control system is achieved in two different ways: the primary way is regulation of the arterial blood pressure by altering the degree of vasoconstriction in blood vessels and the secondary way is the regulation of the heart rate.

Unfortunately, it is impossible to determine the fetal blood pressure inside the uterus. The fetal heart rate, on the other hand, can be determined during pregnancy [13,14], and is currently the main source of information from which the physiological condition of the fetus is assessed.

The fetal heart rate can be determined in several ways, based on different physical principles. For instance, it can be determined with Doppler ultrasound measurements [15]. Ultrasonic waves experience a shift in frequency when they reflect at a moving interface. The magnitude and direction of this shift contains information about the motion of that interface. This effect is known as the Doppler effect [16]. Since both the valves and the blood move in the fetal heart during contraction, Doppler ultrasound can be used as a non-invasive technique to determine the fetal heart rate. A second way to determine the fetal heart rate is based on assessment of the electrical activity of the fetal heart. This electrical activity can be measured by positioning electrodes either directly on the fetus or on the maternal abdomen. Positioning the electrodes directly on the fetus is an invasive technique and can only be performed during labor when the fetal membranes have ruptured. Positioning the electrodes on the maternal abdomen is preferable since it is a non-invasive technique that, therefore, can be applied in all stages of pregnancy. However, due to the low signal to noise ratio (SNR) of the recorded signals, determination of the fetal heart rate from abdominal

electrophysiological recordings with existing techniques is still inaccurate and not reliable [17]. Currently, of the presented ways for monitoring the fetal heart rate, the Doppler ultrasound way is most widely used in clinical practice [17].

Besides the fetal heart rate, clinicians are generally also interested in monitoring of the maternal uterine activity. As uterine contractions can impose stress on the fetus, the relationship between uterine activity and fetal heart rate provides more information on the fetal condition than the fetal heart rate alone does. For example, uterine contractions can lead to (partial) occlusion of the umbilical cord, reducing the blood flow from the mother to the fetus. The capability of the fetus to respond to this temporary oxygen deficiency by, among other reactions, adapting its heart rate is indicative for the fetal condition [18]. The relationship between uterine activity and fetal heart rate has, therefore, been investigated extensively through the years. Many guidelines and scoring systems have been proposed for the interpretation of these simultaneous recordings, referred to as cardiotocography (CTG; the simultaneous recording of fetal heart rate (cardio-) and uterine activity (toco-)) recordings, and several of these guidelines are used in clinical practice [19]. However, the information provided by CTG has turned out to be only sufficient when the condition of the fetus is clearly good or clearly bad [20, 21]. Very often, it is not possible to draw conclusions from CTG recordings and additional tests, such as fetal blood sampling (i.e. examination of a small droplet of blood, obtained invasively, from the fetus), are required to evaluate the condition of the fetus [22]. Besides this lack of information for accurately evaluating the fetal condition, the use of CTG is also associated with the drawback that, since it is based on ultrasound, CTG is very sensitive to motion and noise [23]. Not only does the ultrasound probe require frequent repositioning due to fetal movement, but the dimensions of the ultrasound beam with respect to the dimensions of the fetal heart and vessels can cause other moving interfaces to contribute to the frequency shift of the reflected ultrasound beam. In addition, due to radiative loads, ultrasound cannot be applied 24/7.

From the above it is clear that any additional source of information from which the fetal condition can be assessed or any reliable and accurate alternative to determine the fetal heart rate is potentially valuable. Such an additional source of information might be provided by the fetal electrocardiogram (ECG) [24, 25]. The fetal ECG provides information on the depolarization and repolarization properties of the heart, which are expressed in the shape of the ECG waveform. Indications have been found that fetal hypoxia is reflected in the ECG as changes in the morphology of the waveform [2, 26, 27]. Since this finding, guidelines for clinical interpretation of the ECG morphology have been established and have in fact converged to the introduction of a commercially available fetal ECG analysis device, called STAN® (Neoventa Medical, Sweden). This STAN® monitor analyzes the ST segment, a specific part of the ECG associated to relaxation of the cardiac muscles, and the com-

bined monitoring of this ST segment with CTG has been demonstrated to improve perinatal outcome [28]. In addition to the analysis of the ST segment for detecting fetal hypoxia, more information might be available from the fetal ECG. For example, changes in the orientation of the fetus with respect to the uterus can in principle be determined from fetal ECG signals that are recorded from the maternal cutaneous surface. These changes in orientation can be related to fetal movement, providing yet another parameter that can have clinical relevance in assessing the fetal condition. It needs to be stressed here that, although the idea of monitoring fetal movement from the ECG has been published [29], no practical solution to realize this idea and apply the movement monitoring in clinical practice does as yet exist.

Similar as for the electrical determination of the fetal heart rate, the fetal ECG can be recorded by positioning electrodes either directly on the fetus or on the maternal abdomen (see Fig. 1.1). The ST analysis mentioned above is performed on the ECG signals obtained from a single invasive electrode. The detection of fetal movement from the ECG, on the other hand, requires several electrodes on the maternal abdomen. Unfortunately, as mentioned before for the fetal heart rate, with currently existing techniques, the fetal ECG cannot yet be determined accurately and reliably enough from these non-invasive recordings for the non-invasive fetal ECG analysis to be employed in clinical practice.

1.2 Future prospects of fetal monitoring: goals of this study

1.2.1 Goals of this study

From the previous section, it is evident that the fetal ECG provides additional information to assess the fetal condition, but that clinical application is hampered by either the limited applicability of the invasively recorded fetal ECG or by the low SNR of the non-invasively recorded fetal ECG. The focus of this study is directed towards the latter of these hamperings: to solve some of the problems associated with the recording of the non-invasive fetal ECG. These problems can essentially be divided into two main categories: those involved with analysis of the recorded signals and those involved with clinical interpretation of the results of this analysis.

The analysis of the recorded signals entails the enhancement of the SNR, or, in other words, the extraction of the relevant signals from the mixture of signals that is obtained from the maternal abdomen. These signals are not limited to the fetal ECG signals alone, but also include the three-dimensional representation of the electrical activity of the fetal heart: the fetal vectorcardiogram (VCG). The fetal VCG constitutes a simplified representation of the full three-dimensional electrical activity of the fetal heart [30, 31]. Contractions of the heart originate from the propagation of an action potential through the cardiac tissues [9]. This propagating action potential causes the simultaneous occurrence of numerous electrical dipoles in the heart. By

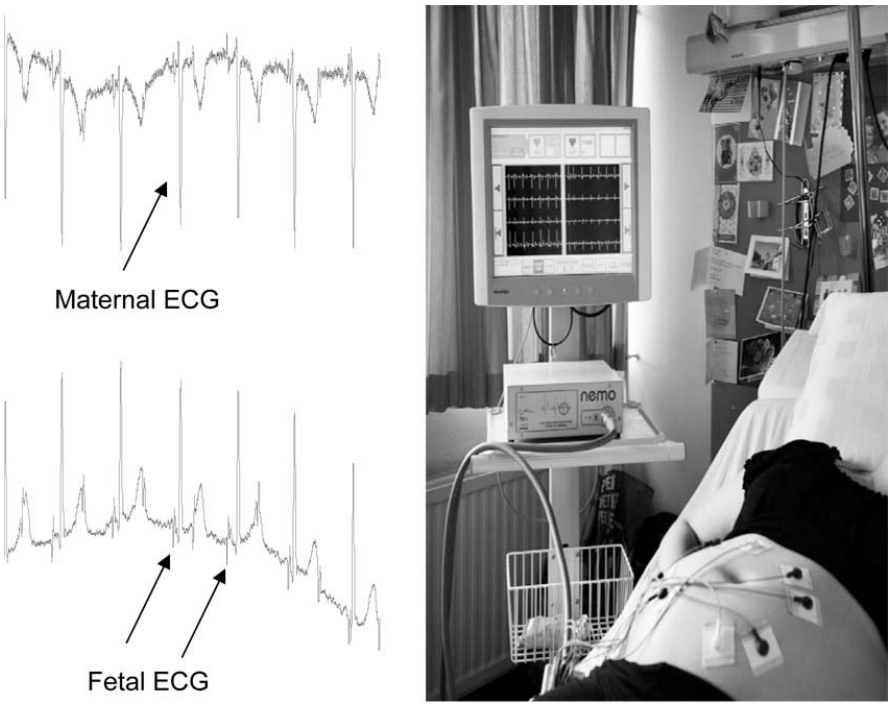

Figure 1.1: *Illustration of the abdominal fetal ECG recordings. On the right, electrodes are positioned on the maternal abdomen and the recorded electrophysiological signals are transmitted to the NEMO system where they are digitized and stored. On the left, two examples of recorded signals are depicted with arrows indicating the maternal and fetal ECG. Note that the fetal ECG amplitude for this particular recording is about a factor 10 smaller than the maternal ECG amplitude. (Photo by Bart van Overbeeke.)*

superimposing the dipoles at each point in time into a single dipole vector, the electrical activity of the heart can be described by an electrical field vector that varies in both amplitude and orientation over time [32, 33]. The time path of this electrical field vector during a single heartbeat, with the simplification that the origin of the vector is assumed to be stationary, is referred to as the VCG.

The interpretation of the results of the fetal ECG analysis basically entails the presentation of the SNR-enhanced fetal VCG in such a way that clinicians can readily assess the fetal condition. Continuing on the description of the electrical activity of the fetal heart in terms of the fetal VCG, the fetal ECG that is recorded at the maternal abdomen can be viewed as the potential caused by the electrical field vector [34]. Moreover, the difference between the potential at two locations on the maternal abdomen, i.e. a bipolar fetal ECG recording, can be viewed as the projection of the VCG onto the vector that describes the orientation of these recording locations with respect to one another [35]. The latter vector is referred to as the lead vector. The relation between the fetal VCG and ECG hence implies that the VCG can be projected onto any lead vector to yield the ECG lead desired by the clinician. The ECG lead is defined here as the ECG signal that corresponds to a particular lead vector. The determination of the desired lead vector is, however, complicated by the fact that for every change in the orientation of the fetus within the uterus, the lead vector needs to be modified. Specifically, when the fetus changes its orientation, the lead vectors need to be changed accordingly to ensure that the projected ECG signals do not exhibit orientation related changes. The assessment of the fetal orientation, therefore, forms a significant part of the fetal VCG interpretation problem.

The goal of this study can therefore be summarized as *the analysis of the composite abdominal signals to present the fetal ECG and VCG in such a way that it enables clinicians to readily assess the fetal condition*. The two key variables to achieve such a suitable presentation of the information are the fetal VCG and the orientation of the fetus with respect to the abdominal electrodes. With the fetal orientation known, the fetal VCG can be projected on those lead vectors that are clinically interpretable, e.g. the fetal ECG lead recorded by the invasive electrode and analyzed by the STAN® monitor or the ECG leads that are used in normal cardiology.

All these VCG projections implicitly assume uniform conduction from the fetal heart to the abdominal surface [36]. This assumption is only justified until the development of the vernix caseosa [37, 38], a waxy layer that electrically shields the fetus from its surroundings and that forms around 28 weeks of gestation and starts to shed around 32 weeks (see Fig. 1.2). The presence of this vernix limits the value of the VCG projections, yielding them less useful for gestational ages between 28 weeks and 32 weeks. In fact, not until about 37 weeks of gestation, when the vernix has completely dissolved in the amniotic fluid [39], can the conduction of the electrophysiological signals be reliably considered uniform and the proposed fetal ECG

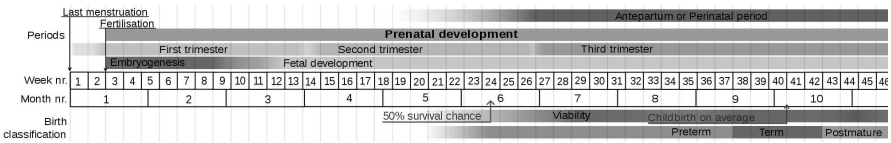

(a)

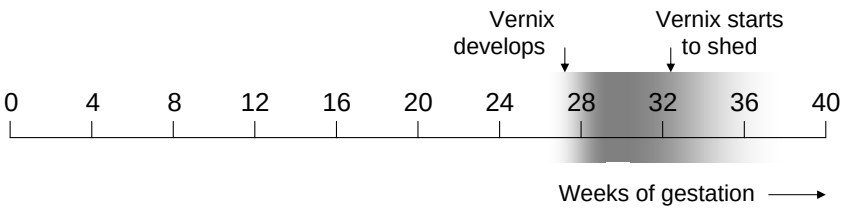

(b)

Figure 1.2: *Time line of pregnancy with in (a) the various periods during gestation and in (b)the periods in which the vernix caseosa is present (marked in gray).*

monitoring method applied to its full potential. At first glance, the vernix might seem to put a severe restriction on the applicability of the proposed monitoring method, but clinically the period between 20 and 28 weeks of gestation and the period near term are very relevant. From 20 weeks on, treatment of congenital cardiac diseases becomes feasible [40, 41]. In addition, from approximately 24 weeks on, the fetus can survive outside the uterus [42, 43]. The risk of preterm morbidity and mortality for these fetuses is however still substantial [44]. Therefore, in the period before 28 weeks of gestation, providing clinicians with more information than the fetal heart rate alone can result in improved judgement on whether or not to treat or intervene in the pregnancy. In the period near term, complications related to labor like hypoxemia or hypoxia, which might be detected from the non-invasive fetal ECG recordings, are most likely to occur [12, 45].

In conclusion, as stated above, this thesis aims to address some of the problems that need to be solved in order for non-invasive fetal ECG monitoring to be employed in clinical practice. In particular, this thesis focuses on the analysis of the non-invasive fetal ECG recordings to obtain the fetal VCG and on the interpretation of the fetal VCG and its projected ECG signals for fetuses with gestational ages before 28 weeks and after 32 weeks. To further mark this division between analysis and interpretation, the thesis is divided into two main parts, one concerning the fetal ECG analysis and the other concerning the fetal VCG and ECG interpretation. Note that interpretation of the fetal VCG in fact entails the projection of the fetal VCG onto lead vectors that yield clinically interpretable ECG signals. In future, extensive clinical studies need to be performed to assess which fetal ECG parameters are rele-

vant for fetal monitoring and how these parameters need to be presented to clinicians (e.g. onto which lead vectors the fetal VCG can best be projected). Nevertheless, to anticipate these studies, in this thesis some clinical parameters that are expected to be relevant are already exemplified.

1.2.2 Analysis and clinical presentation of fetal ECG

The first step towards the determination of the fetal VCG in the analysis of the abdominal fetal ECG recordings is the enhancement of the relatively low SNR of the abdominal recordings. The abdominally recorded signals constitute a mixture of several electrophysiological signals, including the fetal ECG, and noise. To enable the determination of the fetal VCG, first the fetal ECG has to be extracted from this mixture. Analogously, each of the interferences can be suppressed to render the fetal ECG the only signal left.

Suppression of the interferences is achieved in this thesis through a series of signal processing steps that exploit specific and *a priori* known properties of the abdominal fetal ECG signals. More particularly, the dominant interference (i.e. the maternal ECG [46]) is suppressed by exploiting the absence of temporal correlation between the maternal and fetal ECG [46]. Other interferences are (partly) suppressed by exploiting the quasi-periodicity of the fetal ECG through averaging consecutive ECG complexes and, subsequently, further suppressed by exploiting the spatial correlation of the ECG. The latter interference suppression approach is based on the fact that all fetal ECG signals recorded on the maternal abdomen constitute a projection of the fetal VCG onto the corresponding lead vectors and, therefore, have to be spatially correlated to one another [35]. In fact, by properly combining the abdominal fetal ECG signals, not only can (more of) the remaining noise be suppressed, but also can the fetal VCG be estimated [47, 48].

Besides representing the three-dimensional electrical activity of the fetal heart, the fetal VCG also provides a way for assessing the fetal orientation within the uterus, hence facilitating clinical interpretation of the fetal VCG. More particularly, fetal VCGs that correspond to different fetal orientations can be related to one another through a series of transformations, including a rotational transformation. By assessing this rotation and correcting for it, the VCGs can be aligned. In other words, the VCGs can be rotated in such a way that they correspond to a prescribed fetal orientation. From the universal fetal VCG thus obtained, standardized ECG signals can be calculated – by projecting the VCG onto the appropriate lead vectors –, facilitating correct clinical interpretation of the non-invasive fetal ECG recordings.

One of the VCG projections that could be of relevance in clinical practice is the standard 12-lead ECG that is used in cardiology [49]. Another presentation of the fetal ECG that can have direct value in clinical practice is the one that resembles the invasively recorded fetal ECG. As mentioned previously, for the latter ECG, guide-

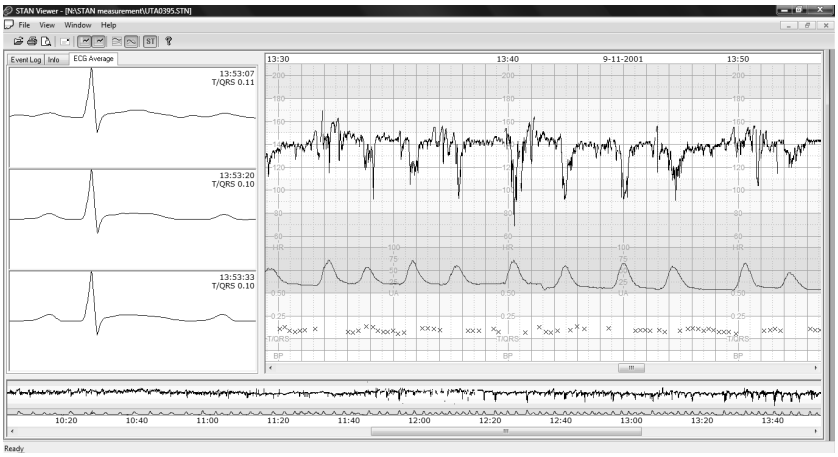

Figure 1.3: *Screenshot of the STAN® monitor. In the right panel the fetal heart rate (top graph) and maternal uterine activity (second graph from above) are depicted. For most uterine contractions, successive decelerations in the fetal heart rate are clearly visible. The crosses (x-marks) in the bottom graph of the right panel show the results of the ST analysis. In the left panel, three (processed) fetal ECG complexes are shown, each corresponding to a single cross.*

lines for clinical interpretation have been established [2, 26, 50] and incorporated in the STAN® monitor (Fig. 1.3). Notwithstanding the improvement in perinatal outcome achieved through the introduction of the STAN® monitor [28], the clinical value of the fetal ECG's ST analysis is limited in three ways. At first, as mentioned previously, ST analysis on the invasively recorded fetal ECG can only be performed during labor after rupture of the membranes and sufficient dilatation of the uterine cervix. Secondly, the combination of CTG and ST analysis still does not always provide sufficient information to conclusively assess the fetal condition [51,52]. Thirdly, the ST analysis is performed on the only fetal ECG signal available. This is not necessarily the optimal ECG lead signal for performing this particular analysis and could hence diminish the analysis' robustness and accuracy.

For the situations in which the combined use of CTG and ST analysis does not provide sufficient information, additional information provided by parameters that are extracted from the ECG can be of added value [53, 54]. One such parameter that is covered in this thesis is fetal movement. Other parameters that have relevance in clinical practice, but that will not be covered extensively in this thesis, are associated with growth restriction [55] and sleep and activity patterns of the fetus [56]. To improve the robustness and accuracy of the ST analysis and to extend its applicability to stages of pregnancy earlier than labor, the abdominally obtained fetal VCG could

be used to calculate a fetal ECG signal that has optimal properties for facilitating ST analysis.

1.3 Thesis outline

As the title of the thesis implies, the content of this thesis concerns the analysis and interpretation of the non-invasively obtained fetal ECG. Therefore, after having discussed some of the physiological and technical backgrounds in Chapter 2, this thesis is divided into two parts, one dealing with analysis of the non-invasive fetal ECG recordings (Part I) and the other with interpretation of the fetal VCG (and its projected ECG signals) that is obtained from the analysis (Part II).

The fetal ECG analysis in Part I consists of five chapters (see also Fig. 1.4). Chapter 3 deals with the suppression of the maternal ECG. As discussed, the maternal ECG constitutes the dominant interference in the abdominal fetal ECG recordings. Current methods for suppression of the maternal ECG include subtracting a template of the maternal ECG. This template exploits the lack of temporal correlation between the maternal ECG and the fetal ECG. Specifically, the heart rates of the mother and fetus are not correlated and hence, the averaging of several consecutive maternal ECG complexes results in an averaged maternal ECG that essentially shows no contribution of the fetal ECG anymore. The maternal ECG can now be suppressed by subtracting the maternal ECG template (i.e. the averaged maternal ECG) from the ECG complexes in the recorded signals.

Unfortunately, ECG complexes of consecutive heartbeats are never the same and thus also the maternal ECG template does not perfectly match the recorded maternal ECG complexes. In fact, the difference between the recorded maternal ECG complex and the template can be so large that the residual maternal ECG, remaining after subtraction of the template, has an amplitude that is still larger than that of the fetal ECG. To improve the accuracy of the maternal ECG template generation, in the method developed in this thesis each maternal ECG complex is subdivided into multiple physiological segments. Subsequently, for each of these segments a template is determined by averaging the corresponding segments of several preceding ECG complexes. In fact, prior to averaging these segments, they are first scaled, time-aligned, and offset compensated to further improve the accuracy of the generated template. By combining these separate segment templates, a maternal ECG template can be generated that can account, at least to some extent, for beat-to-beat variability in the morphology of the ECG complexes. The subtraction of this maternal ECG template is demonstrated in Chapter 3 to outperform existing methods – not only template subtraction methods, but also other methods like adaptive filtering and independent component analysis (ICA) – in the suppression of the maternal ECG.

To further enhance the SNR of the fetal ECG signals that remain after the sup-

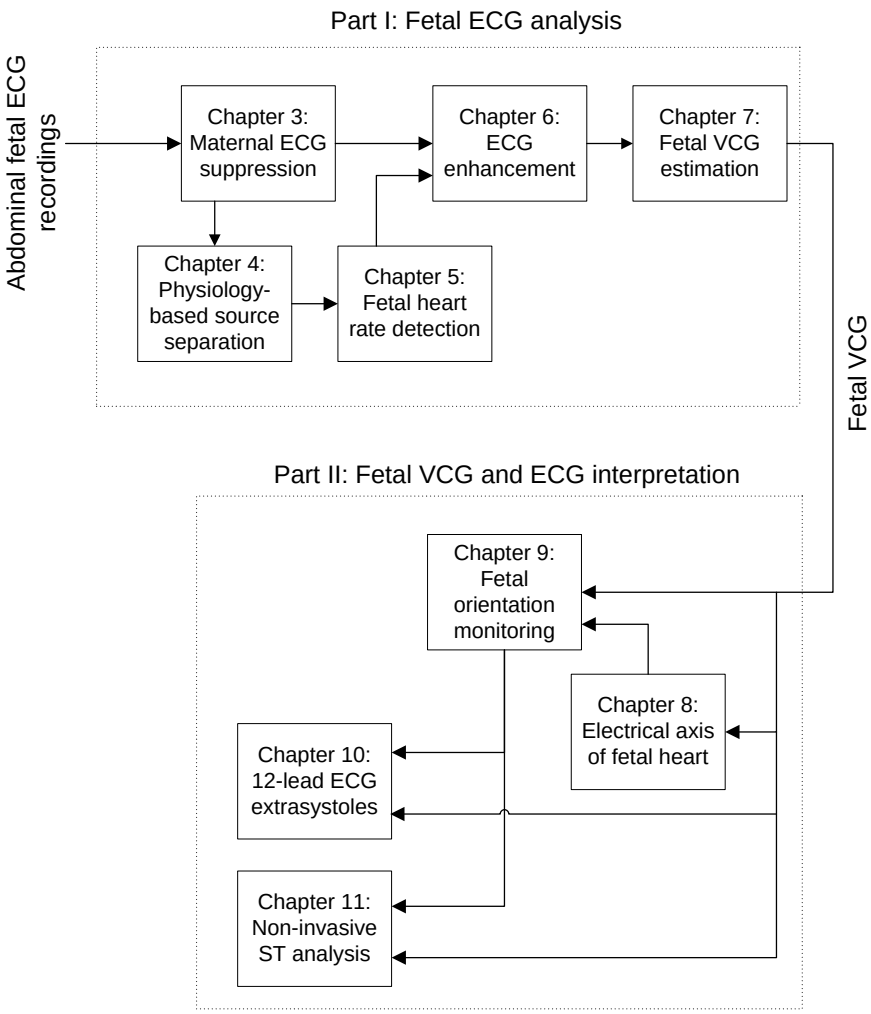

Figure 1.4: *Block diagram of the outline of the thesis. The arrows that connect the various chapters indicate that the results of the one chapter are used as input for the next chapter.*

pression of the maternal ECG, also consecutive fetal ECG complexes could be averaged. However, even after suppression of the maternal ECG, the SNR of the fetal ECG signals is often so low that the heart rate cannot be detected. Consequently, individual fetal ECG complexes cannot be defined and thus also not averaged. Since fetal ECG signals recorded at multiple locations on the maternal abdomen originate from the same source, they are spatially correlated to one another. This spatial correlation can be exploited by employing existing blind source separation techniques like ICA and principal component analysis (PCA). These techniques linearly combine the recorded signals to maximize the statistical independency (ICA) or variance (PCA) of the obtained linear combinations. Some of these linear combinations might represent the fetal ECG, others might represent noise contributions that are still present in the abdominal recordings. The linear combinations that represent the fetal ECG are referred to as the fetal ECG source signals. Both ICA and PCA, however, suffer from the drawback that they do not consider *a priori* knowledge on the abdominal electrode configuration and fetal heart activity. In cases of low-SNR abdominal fetal ECG signals, this renders ICA and PCA incapable of providing a fetal ECG source at all times. In Chapter 4 a physiology-based source separation technique is developed that operates more robustly than ICA and PCA. As its name suggests, the technique uses *a priori* knowledge on the origin of the fetal ECG to linearly combine the abdominal signals. Due to the robustness brought about by the usage of physiological knowledge, the developed technique is capable of providing fetal ECG source signals that have improved SNR over the abdominal fetal ECG signals, under almost all circumstances.

The detection of the fetal heart rate is discussed in Chapter 5 and is performed by means of finding local peaks in the fetal ECG source signal that exceed a variable threshold. To increase the accuracy of the detection and avoid artifacts from exceeding the threshold, the ECG source signal is transformed to exploit specific features of the QRS complex. The QRS complex is the part of the ECG that is associated with depolarization of the ventricles. The QRS complex generally exhibits a relatively large gradient with respect to other ECG segments and roughly lasts for a fixed amount of time. By summing the modulus of the gradient over a moving time window for which the length is chosen as the approximated length of the QRS complex, the QRS complexes are enhanced with respect to artifacts, noise, and other ECG segments, facilitating their accurate detection.

Together with the abdominal ECG signals that remain after Chapter 3, the detected heart rate is used as starting point for further enhancement of the fetal ECG signals in Chapter 6. The SNR of the fetal ECG signals can be improved by averaging several consecutive ECG complexes. However, in clinical practice, this averaging constitutes a trade-off between SNR enhancement and loss of clinically relevant information. Relatively fast fluctuations in the ECG morphology that have a physiolog-

ical origin might be lost due to extensive averaging, whereas including too few ECG complexes in the averaging restricts the SNR enhancement that can be achieved. In Chapter 6 a Kalman filter with adaptive noise estimation is developed that, in essence, can adaptively vary the number of ECG complexes included in the averaging, based on the signal properties. Hence, in case of morphological variations, the number of ECG complexes is reduced and in case of no such variations, the number of complexes is increased. Compared to a similar filter but without adaptive noise estimation, the developed filter is capable of more quickly adapting its output when the ECG exhibits relatively fast morphological variations (e.g. due to episodes of fetal movement) and is less sensitive to artifacts.

The enhanced fetal ECG signals are used in Chapter 7 to determine the fetal VCG. In the adult case, the VCG is generally determined by applying a fixed transformation (i.e. the Dower transformation [47]) to the ECG signals. However, such a fixed transformation requires *a priori* knowledge on the position of the heart with respect to the electrodes. As the fetus can take several orientations in the uterus, this position of the heart cannot be *a priori* known. Consequently, also the ECG signal attenuation or distortion that occurs during the propagation from the fetal heart to the abdominal electrodes cannot be known. Such a distortion can vary from additive noise to morphological changes in the ECG and is mostly due to non-uniform conductive properties of the tissues between the fetal heart and the abdominal electrodes [37]. In Chapter 7, a Bayesian method is developed that estimates the VCG and, to some extent, also the signal attenuation for each electrode. This is done by determining for which VCG and signal attenuation the joint probability over both these variables is maximal given the observed fetal ECG signals. The underlying joint probability distribution is determined by assuming the ECG signals to originate from scaled VCG projections and additive noise. With this method, a VCG, tailored to each specific fetal orientation, can be determined. Relative to the fixed Dower transformation, the developed method performs significantly better in determining the fetal VCG.

The fetal VCG that is determined in the first part of this thesis, is used as starting point for Part II. This part consists of four chapters. In Chapter 8 the electrical axis of the fetal VCG is discussed. As mentioned previously, the most straightforward method for clinically interpreting the fetal VCG is to project the VCG onto lead vectors that are known from adult electrocardiography. As straightforward as this projection might seem, the ECG that is obtained by projecting the fetal VCG onto the standardized lead vectors, is expected to look different for the fetus than for an adult. The reason for this difference is adaptation of the fetal heart to its alternative cardiovascular circulation. Rather than in the lungs, the fetal blood is oxygenated in the placenta, causing the right part of the heart to exert higher loads than the left part [57]. This is in contrast to the adult heart in which the left part exerts the highest loads. The adaptation to the alternative fetal circulation usually entails an increment

in the muscle mass of the right side of the fetal heart, which in turn is accompanied by a shift in the three-dimensional orientation of the VCG. To the best of our knowledge, in Chapter 8, this shift in direction is measured and visualized for the first time ever. In addition, the consequences of this shift for the as yet unexplored field of fetal electrocardiography are anticipated and briefly discussed.

The interpretation of the ECG signals that are generated by projecting the fetal VCG onto clinically relevant lead vectors is complicated when the orientation of the fetus in the uterus is unknown. Not only does this orientation vary between patients, but also does the orientation for a specific fetus fluctuate due to fetal movement. However, by aligning the vectorcardiographic loops (i.e. the parts of the fetal VCG associated with depolarization of the ventricles), most of this movement can be accounted for. This alignment has the additional benefit that, besides facilitating interpretation of the projected fetal ECG signals, the movement itself is also a parameter of particular relevance in clinical practice. The currently existing alignment method is based on a statistical model that accounts for scaling, rotation, and time-synchronization of the loops. The scaling in this model only comprises a scalar multiplication, accounting for loop contraction and dilatation but not for distortion effects (i.e. changes in the morphology of the loop) in the loops. For the fetal ECG, due to fetal movement, such distortions are, however, expected. Hence, the existing statistical model is extended in Chapter 9 with a lead-dependent scaling to account for distortion effects in the loops. The parameters for scaling, rotation, and time-synchronization are assessed by maximizing the likelihood function of the statistical model, using the expectation-maximization (EM) algorithm. The performance of the method is assessed by comparing it to that of the method with scalar scaling. This comparison shows a significant reduction in the morphological variability of the loops when using the developed EM method. The movement assessed from fetal ECG recordings is compared to simultaneously performed ultrasound recordings to demonstrate that the method can also be used to monitor fetal movement. Finally, the method is applied on an extreme case of morphological variability of the vectorcardiographic loops; it is used to align a fetal loop with a simultaneously recorded maternal loop. It is shown that the rotation assessed in this alignment provides information on the orientation of the fetus within the maternal uterus.

Hence, with the methods described in Chapters 3-9, the fetal VCG can be determined from non-invasive recordings on the maternal abdomen and this VCG can not only be corrected for fetal movement, but it can also be rotated towards a standardized presentation that is the same for all patients. Using this universal fetal VCG as basis, in Chapters 10 and 11 two clinical applications of the non-invasive fetal ECG are exemplified.

In Chapter 10, the 12-lead ECG presentation is used to visualize the difference between regular heartbeats and irregular heartbeats that originate from the heart's

ventricles. These irregular beats are referred to as ventricular extrasystoles. Using the 12-lead presentation, it might be possible to assess the origin of these extrasystoles and link them to either harmless events or (congenital) heart diseases.

In Chapter 11, the fetal VCG is projected onto the lead vector that produces an ECG signal that resembles the invasively recorded fetal ECG. It is shown that the SNRs of the non-invasive and invasive ECG signals are similar and it is studied whether the non-invasive fetal ECG might in future be used for performing ST analysis. Finally, in this chapter the optimal VCG projection for ST analysis is investigated (i.e. optimal in terms of providing an ECG signal from which the ST analysis can be performed most accurately) and it is shown that the invasive ECG signal, for fetuses in the normal so-called vertex position, is in fact not far from the optimal projection.

The chapters listed above are either published or submitted for publication. Hence, each chapter is written to be self-contained, causing some overlap in the introductory parts of the chapters.

1.4 Publications by author

Patents

PAT-1 R. Vullings and C.H.L. Peters, ”ECG signal processing”, EP2016894A1, 21 January 2009.

PAT-2 R. Vullings, C.H.L. Peters, S.G. Oei and P.F.F. Wijn, ”Fetal monitoring”, WO2009/013246A1, 29 January 2009.

Journal papers (only first author)

JP-1 R. Vullings, B. de Vries, and J.W.M. Bergmans, ”An adaptive Kalman filter for ECG signal enhancement”, *submitted*.

JP-2 R. Vullings, C.H.L. Peters, S.G. Oei and J.W.M. Bergmans, ”Vectorcardiographic loop alignment for non-invasive monitoring of fetal movement”, *submitted*.

JP-3 R. Vullings, M.J.M. Hermans, C.H.L. Peters, J.W.M. Bergmans, P.F.F. Wijn and S.G. Oei, ”Electrical axis of the human fetal heart during pregnancy – insights into fetal electrocardiography”, *submitted*.

JP-4 R. Vullings, C.H.L. Peters, M.J.M. Hermans, P.F.F. Wijn, S.G. Oei and J.W.M. Bergmans, ”A robust physiology-based source separation method for QRS detection in low amplitude fetal ECG recordings”, Physiol Meas. 2010; 31(7):935–51.

JP-5 R. Vullings, C.H.L. Peters, S.I. Mossavat, S.G. Oei and J.W.M. Bergmans, ”Bayesian approach to patient-tailored vectorcardiography”, IEEE Trans Biomed Eng. 2010 Mar; 57(3):586–95.

JP-6 R. Vullings, C.H.L. Peters, R.J. Sluijter, M. Mischi, S.G. Oei and J.W.M. Bergmans, ”Dynamic segmentation and linear prediction for maternal ECG removal in antenatal abdominal recordings”, Physiol Meas. 2009 Mar; 30(3):291–307.

Journal papers (not first author)

JP-7 J.O.E.H. van Laar, C.H.L. Peters, R. Vullings, S. Houterman, J.W.M. Bergmans and S.G. Oei, ”Fetal autonomic response to severe acidaemia during labour”, BJOG 2010 Mar; 117(4):429–37.

JP-8 J.O.E.H. van Laar, C.H.L. Peters, R. Vullings, S. Houterman and S.G. Oei, ”Power spectrum analysis of fetal heart rate variability at near term and post term gestation during active sleep and quiet sleep”, Early Hum Dev. 2009 Dec; 85(12):795–8.

International conference proceedings

IC-1 R. Vullings, C.H.L. Peters, J.O.E.H. van Laar, J.W.M. Bergmans and S.G. Oei, ”Objective and non-invasive detection of fetal movement”, 9th World Congress of Perinatal Medicine, Berlin, Germany, October 24–28, 2009, p. 260.

IC-2 C.H.L. Peters, R. Vullings, J.O.E.H. van Laar, S.G. Oei and P.F.F. Wijn, ”Fetal sympathetic nervous activity during the second trimester of pregnancy”, 9th World Congress of Perinatal Medicine, Berlin, Germany, October 24–28, 2009, p. 217.

IC-3 R. Vullings, C.H.L. Peters, M. Mischi, S.G. Oei and J.W.M. Bergmans, ”Fetal movement quantification by fetal vectorcardiography: a preliminary study”, IEEE-EMBS Proc. on the 30th Annual International Conference, Vancouver, Canada, August 20–24, 2008, pp. 1056–1059.

IC-4 C.H.L. Peters, R. Vullings, J.W.M. Bergmans, S.G. Oei and P.F.F. Wijn, ”The effect of artifact correction on spectral estimates of heart rate variability”, IEEE-EMBS Proc. on the 30th Annual International Conference, Vancouver, Canada, August 20–24, 2008, pp. 2669–2672.

IC-5 R. Vullings, C.H.L. Peters, J.O.E.H. van Laar, J.W.M. Bergmans and S.G. Oei, ”Fetal movement detection by non-invasive fetal vectorcardiography”, 35th Annual Meeting of the Fetal and Neonatal Physiological Society, Maastricht, the Netherlands, June 22–25 2008, p. 35.

IC-6 C.H.L. Peters, R. Vullings, J.O.E.H. van Laar, A.M. Bolderdijk, S.G. Oei and P.F.F. Wijn, ”Fetal Sympathetic Nervous Activity during the Second Trimester of Pregnancy: Preliminary Results”, 35th Annual Meeting of the Fetal and Neonatal Physiological Society, Maastricht, the Netherlands, June 22–25 2008, p. 70.

IC-7 R. Vullings, C.H.L. Peters, J.O.E.H. van Laar, M.J. Prudon, A.M. Bolderdijk, J.W.M. Bergmans and S.G. Oei, ”Non-invasive recording of multi-lead fetal ECG”, 8th World Congress of Perinatal Medicine, Florence, Italy, September 9–13, 2007, vol.35, supplement II, p. s97.

IC-8 R. Vullings, C.H.L. Peters, J.W.M. Bergmans and S.G. Oei, ”Maternal ECG removal from non-invasive fetal ECG recordings”, 8th World Congress of Perinatal Medicine, Florence, Italy, September 9–13, 2007, vol.35, supplement II, p. s295.

IC-9 C.H.L. Peters, R. Vullings, A.M. Bolderdijk, M. Mischi, L. Gourmelon, B. Feddes, S.G. Oei, ”Contactless measurement of the antepartum fetal ECG”, 8th World Congress of Perinatal Medicine, Florence, Italy, September 9–13, 2007, vol.35, supplement II, p. s84.

IC-10 J.O.E.H. van Laar, M.J. Prudon, R. Vullings, C.H.L. Peters, P.F.F. Wijn and S.G. Oei, ”Spectral analysis can discriminate between normal fetal condition and fetal acidosis”, 8th World Congress of Perinatal Medicine, Florence, Italy, September 9–13, 2007, vol.35, supplement II, p. s94.

IC-11 R. Vullings, C.H.L. Peters, M. Mischi, R.J. Sluijter, S.G. Oei and J.W.M. Bergmans, ”Artifact reduction in maternal abdominal ECG recordings for fetal ECG estimation”, IEEE-EMBS Proc. on the 29th Annual International Conference, Lyon, France, August 23–26, 2007, pp. 43–46.

IC-12 R. Vullings, C.H.L. Peters, M. Mischi, S.G. Oei and J.W.M. Bergmans, ”Maternal ECG removal from non-invasive fetal ECG recordings”, IEEE-EMBS Proc. on the 28th Annual International Conference, New York, USA, August 30 – September 3, 2006, pp. 1394–1397.

IC-13 C.H.L. Peters, R. Vullings, J.W.M. Bergmans, S.G. Oei and P.F.F. Wijn, ”Heart rate detection in low amplitude non-invasive fetal ECG recordings”, IEEE-EMBS Proc. on the 28th Annual International Conference, New York, USA, August 30 – September 3, 2006, pp. 6092–6094.

IC-14 R. Vullings, C.H.L. Peters, P. Andriessen, S.G. Oei and P.F.F. Wijn, ”Monitoring the fetal heart rate and fetal electrocardiogram: abdominal recordings are

as good as direct ECG measurements", 46th Annual Meeting of the European Society for paediatric research, Siena, Italy, August 31 – September 3, 2005.

IC-15 R. Vullings, C.H.L. Peters, J.O.E.H. van Laar, P.F.F. Wijn and S.G. Oei, "The fetal heart rate and sympathetic activity determined non-invasively from the maternal abdomen", 7th World Congress of Perinatal Medicine, Zagreb, Croatia, 2005.

Benelux conference proceedings

BC-1 R. Vullings, C.H.L. Peters, M. Mischi, S.G. Oei and J.W.M. Bergmans, "Prototyping of a fetal ECG monitoring system", 1st IEEE-EMBS Benelux Symposium, Brussels, December 7–8, 2006, pp. 191–194.

BC-2 C.H.L. Peters, R. Vullings, M.N. O'Riordan, P.R. Stone, P.F.F. Wijn, "Beat-to-beat heart rate detection in low amplitude non-invasive fetal ECG recordings: the effect on time and frequency domain parameters", 1st IEEE-EMBS Benelux Symposium, Brussels, December 7–8, 2006.

BC-3 R. Vullings, C.H.L. Peters, M. Mischi, S.G. Oei and J.W.M. Bergmans, "The fetal electrocardiogram", IEEE SPS DARTS Symposium, Antwerpen, March 28-29, 2006.

Chapter 2

Background

This chapter deals with the physiological and technical backgrounds of fetal ECG monitoring. To exemplify the potential value of the ECG, several parameters that can be derived from the ECG are discussed. It needs to be noted that some of these parameters do not necessarily need to be derived from the ECG, but can also be determined in alternative ways. Fetal movement, for instance, can be obtained from ECG recordings, as will be discussed in this section, but is nowadays monitored through either ultrasound analysis or movement counting by the mother. In addition, it has to be noted that although this chapter deals with some backgrounds on fetal ECG analysis, it does not present an extensive overview of the state-of-the-art in signal processing techniques for extracting and analysis of the fetal ECG from the acquired data. These techniques are discussed later on in this thesis in more detail.

The chapter is organized as follows. Firstly, the physiology of the fetal heart is discussed with special emphasis on the origin of the fetal ECG and its associated clinical parameters. Secondly, a brief overview of the clinical practice in fetal ECG monitoring is provided with special emphasis on some of the problems encountered in non-invasive fetal ECG analysis. Finally, the data acquisition approach adopted in this thesis is presented.

2.1 Physiology of the fetal heart and its role in fetal monitoring

2.1.1 Physiology of the heart

The adult heart

The adult heart is a muscular organ that consists of two separate pumps. The right part of the heart pumps blood through the lungs and the left part of the heart pumps the blood through the peripheral organs [9, 58]. Each of these parts is a pulsatile two-chamber pump composed of an atrium and a ventricle. The atrium functions in principle as a weak primer pump for the ventricle, helping the blood to move into

the ventricle. The ventricle, in turn, supplies the main force that thrusts the blood through either the pulmonary or peripheral circulation [9, 58].

The heart has a specialized system for generating rhythmical impulses – that cause rhythmical contractions of the heart muscle – and conducting these impulses rapidly throughout the heart [9]. When this system functions normally, the atria contract some time ahead of the ventricles, allowing additional filling of the ventricles before they thrust the blood through the lungs and peripheral circulation. Another special feature of this system is that it allows all parts of the ventricles to contract almost simultaneously, which is essential for effective pressure generation in the ventricular chambers.

The fibers of this specialized conducting system have the capability of self-excitation, a process that can cause automatic rhythmical discharge and subsequent contraction [58]. The fibers of the sinoatrial (SA) node exhibit this capability to the largest extent and, therefore, the SA node ordinarily controls the rate of contractions of the complete heart [9]. Specifically, the fibers of the SA node self-excite at the highest rate and the impulses generated by the SA node subsequently propagate throughout the entire heart. After depolarization of a cell, the cell exhibits a refractory period in which no excitation can occur. At the end of the refractory period, the SA node is generally again the first to self-excite and because of this, the SA node is responsible for the rate of contractions of the heart.

The nodal fibers of the SA node discharge spontaneously causing an action potential to propagate rapidly through both atria and from there through the atrioventricular (AV) bundle into the ventricles [58]. It is primarily this AV (or His) bundle that delays the transmission of action potentials from the atria into the ventricles, allowing time for the atria to empty their contents into the ventricles before ventricular contraction begins [58]. Fig. 2.1 shows an illustration of the conduction path of action potentials throughout the heart.

After penetration of the fibrous tissue between the atrial and the ventricular muscle, the distal part of the AV bundle passes downward in the ventricular septum and splits into left and right bundle branches [9, 58]. Each branch spreads downward to the apex of the ventricle, progressively splitting into smaller branches that spread around each ventricular chamber and back towards the base of the heart. The terminal Purkinje fibers penetrate about one third of the way into the muscular mass and then become continuous with the cardiac muscle fibers.

The Purkinje fibers lead from the AV node through the AV bundle branches into the ventricles and have characteristics quite opposite of those of the AV node. In order to allow all ventricular muscle fibers to contract almost simultaneously, the cardiac impulse has to appear at each muscle fiber at approximately the same time. For this reason, the Purkinje fibers are relatively large fibers that transmit the action potentials at velocities about six times larger than transmission velocities in cardiac

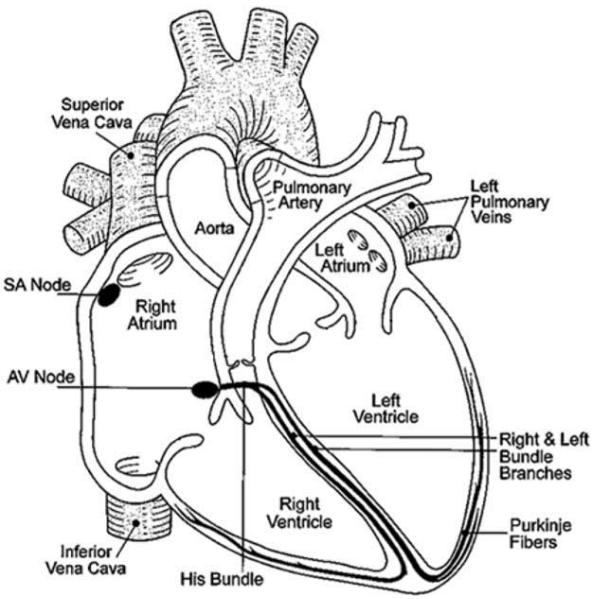

Figure 2.1: *Basic anatomy of the human adult heart with the main components of the action potential conduction system indicated.*

muscle fibers [9].

The fetal heart: differences with respect to the adult heart

Relative to the adult heart, the physiology and anatomy of the fetal heart exhibit some significant differences. These differences originate from the fact that the fetal cardiovascular circulation is different from the adult circulation [57, 59, 60].

In the adult, gas exchange (i.e. the secretion of carbon-dioxide from the blood and the intake of oxygen in the blood) takes place in the lungs [9]. From the lungs, the oxygenized blood flows through the left part of the heart into the peripheral circulation. Since this peripheral circulation is larger than the pulmonary circulation, the left ventricle has to generate a substantially higher pressure than the right ventricle to ensure sufficient perfusion to the organs. Consequently, the muscular mass of the left ventricle is larger than the mass of the right ventricle.

In the fetus, gas exchange takes place in the placenta [61]. As a result, the fetal blood circulation needs to operate differently from the adult. This different circulation manifests itself, among other differences, by interconnections between the left and right parts of the heart. These interconnections consist of the foramen ovale, a gap in the septum dividing both sides of the heart, and the ductus arteriosus, a shunt between the pulmonary artery and the aorta [61]. Both the foramen ovale and ductus arteriosus are schematically illustrated in Fig. 2.2.

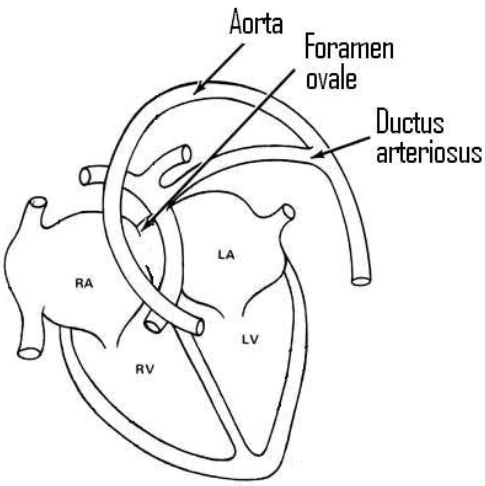

Figure 2.2: *Basic anatomy of the human fetal heart with the main differences with respect to the adult heart (see Fig. 2.1) indicated.*

Because of these interconnections, the left and right ventricle both generate the same pressure. However, in the fetal circulation, the right ventricle is responsible for about 60% of the total cardiac output whereas the left ventricle accounts for the remaining 40% [57]. As a result of this higher output, the right ventricle of the fetal heart has a muscular mass exceeding that of the left ventricle. The effect of these different mass distributions between the fetal and adult heart on the ECG is discussed in Section 2.1.3.

2.1.2 Origin of the ECG

Cardiac activity at cellular level

At rest, the potential of the intracellular fluid is negative with respect to the potential of the extracellular fluid [9, 58]. This is caused by the different concentrations of Na^+, K^+, and Ca^{2+} across the cell membrane. When an action potential propagates along the cell, this action potential causes an increase in the Na^+ permeability of the membrane [9, 58]. Consequently, large numbers of Na^+ ions flow into the interior of the cell, reversing the potential of the intracellular fluid with respect to the potential of the extracellular fluid: the cell is depolarized [58].

Besides the increase in Na^+ permeability, the propagating action potential also causes an increase in the K^+ and Ca^{2+} permeability of the cell membrane, forcing K^+ ions to flow from the interior of the cell to the extracellular fluid and forcing Ca^{2+} ions to flow from the exterior to the intracellular fluid [9, 58]. However, the increase in K^+ and Ca^{2+} permeability arises more gradually than the increase in

Na^+ permeability. In addition, the Ca^{2+} permeability decreases earlier than the K^+ permeability. As a result, the intracellular potential first rapidly increases to positive values due to the Na^+ inflow. Subsequently, the potential remains at a plateau for a short while due to the inflow of Ca^{2+} and outflow of K^+ ions. Finally, the potential returns to its rest value due to the persisting outflow of K^+ ions: the repolarization of the cell. In fact, towards the end of the plateau, the K^+ permeability even increases to ensure a rapid return to the rest potential [9]. It has to be noted that the description above only holds for cardiac cells and not for other excitable cells in the body, like nerve cells. Moreover, also the nodal cells in the heart that are responsible for the self-excitation of the heart behave differently [9].

Propagation of electrical impulses from cell to cell occurs in two manners, either passively or actively [58]. Passive propagation consists of the electrical conduction of stimuli that are too small to cause the depolarization of the cell. In this case, the cells act as a coaxial wire conducting the stimulus, but gradually reducing the stimulus amplitude due to leakage currents to the cell membrane. Active propagation occurs without degradation of the stimulus amplitude. The reason for this is that the depolarization of a particular cell causes a supraliminal stimulus in the adjacent cell, initiating the depolarization of this cell. Active propagation can therefore also be described as the propagation of action potentials.

Cardiac activity at tissue level

Next to effects at the cellular level, the propagation of action potentials also has effect at the tissue level. In fact, for the heart to contract, the propagating electrical stimulus needs to be converted to mechanical activity.

This conversion is accomplished in two steps: the electrical stimulus initiates a chemical process which in turn initiates the desired mechanical activity [58]. The propagating action potential causes the sarcoplasmic reticulum (Fig. 2.3) to release large quantities of Ca^{2+} ions into the myofibrils. These Ca^{2+} ions initiate attractive forces between the actin and myosin filaments in the fiber, causing them to slide together. This is the actual contraction of the muscle.

Besides this mechanical effect, the propagating action potentials also have an electrical effect on the tissue. As mentioned before, the depolarization of a particular cell causes a potential difference with respect to adjacent cells that are not yet depolarized. Consequently, the boundary between a depolarized cell and a cell at rest acts as a dipole. Moreover, as the action potentials propagate rather uniformly through the cardiac tissue, adjacent fibers depolarize virtually simultaneously: a dipole (or depolarization) wave travels through the heart [9].

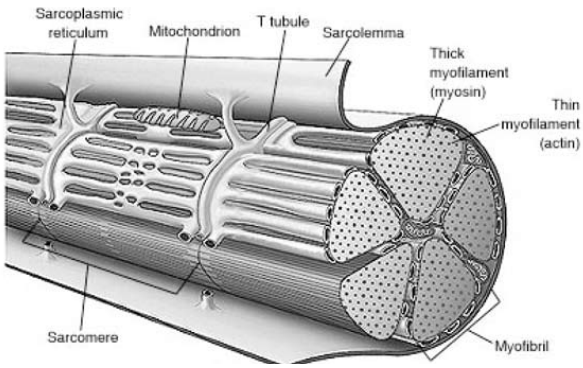

Figure 2.3: *Schematic view of a muscle fiber with the main components involved in the contraction of the fiber indicated.*

Cardiac activity at cutaneous level

The tissues surrounding the traveling dipole are, in general, conductive and hence the dipole wave acts as a source for a circular current that is substantially larger than the circular current caused by the cellular potential difference itself. These currents spread all the way to the body surface where the skin impedance causes potential differences [33].

As the dipole wave travels through the cardiac tissues, the potential at a specific position on the skin is not constant but varies with the traveling dipole. The representation of the skin potential as a function of time is called the electrocardiogram (ECG) and can be measured by positioning electrodes on the skin [9].

2.1.3 Characteristics of the ECG

One-dimensional ECG

The ECG is a representation of the skin potential as a function of time. In fact, the use of the word potential is not completely correct in this context: the ECG generally constitutes a representation of the potential-*difference* between two electrodes, referred to as a bipolar ECG recording [9]. The bipolar ECG (throughout this thesis simply referred to as the ECG) can be described by means of a few characteristic waves, which are associated with specific physiological events, and the segments and intervals between these waves. Fig. 2.4 shows an example of a typical ECG signal.

The *P-wave* is associated with the depolarization of the atria [9, 58]. When the atria are completely depolarized, the net electrical field generated by the traveling dipole is zero and the ECG consequently has zero amplitude. This isoelectrical period lasts until the action potential has propagated through the AV bundle to the Purkinje fibers and is represented in the ECG by the PR interval. The *QRS complex* is asso-

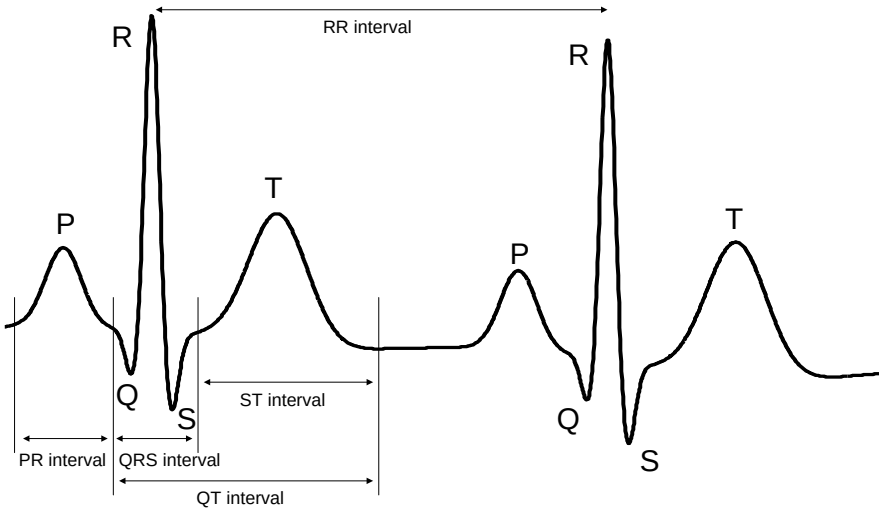

Figure 2.4: *Nomenclature of the ECG.*

ciated with ventricular depolarization [9, 58]. The amplitude of the QRS complex exceeds the amplitude of the P-wave dramatically as the amount of muscle fibers in the ventricular walls is much larger than the amount of muscle fibers in the atrial walls. The reason for this is that the ventricles need to propel the blood into the peripheral circulation whereas the atria only need to propel the blood into the ventricles. As a result of this and because the atrial repolarization coincides with the ventricular depolarization, the repolarization of the atria cannot be distinguished in the ECG. After the ventricles are depolarized completely, the net electrical field is again zero and the ECG has zero amplitude. The repolarization wave of the ventricles propagates in the opposite direction as the depolarization wave and is represented in the ECG by the *T-wave* [9,58]. Because of the reversed propagation direction and the inversion of the signs in the resulting dipole wave, the T-wave has the same polarity as the QRS complex.

Besides as the aforementioned potential-difference between two electrodes, the ECG can also be regarded as the projection of the electrical field generated by the traveling dipole onto the lead vector that describes the positions of the involved electrodes with respect to one another [35]. This view on the ECG will be described in more detail in the forthcoming section, but elucidates the title for this section: the ECG is a one-dimensional projection of the three-dimensional electrical field generated by the traveling dipole.

Three-dimensional VCG

The traveling dipole produces a varying electrical field in the heart, which to a first-order approximation can be described by a single vector: the heart (or cardiac) vector [32, 35]. When the orientation of the heart vector on the cutaneous level is perpendicular to the lead vector between two electrodes, both these electrodes measure the same electrical field amplitude and hence the bipolar ECG amplitude is zero. In other words, the projection of the heart vector onto the lead vector determines the instantaneous ECG amplitude. This is illustrated in Fig. 2.5, in which the three vectors composing the triangle are the lead vectors and the amplitude of the ECG is determined by the amplitude of the projection of the instantaneous heart vector onto these lead vectors [62]. In addition, this relation between the electrical field, the lead vector, and the ECG amplitude implies that the varying electrical field can be used to describe the ECG at the body surface. Consequently, one of the main interests in fetal ECG monitoring is the description of this electrical field vector over time: the fetal vectorcardiogram (VCG) [63].

Essentially, the VCG is the three-dimensional representation of the time-path of the heart vector during one cardiac cycle [31]. Fig. 2.5 shows a two-dimensional illustration of the VCG. In fact, this depicted VCG represents a simplification of the actual physiology. As the heart vector originates from the dipole wave, the origin of the vector travels with this wave through the heart. In the simplification used in the definition of the VCG, however, the origin of the heart vector remains stationary [64].

In general, the VCG consists of three closed loops associated with atrial depolarization, ventricular depolarization, and ventricular repolarization [63]. The largest of these loops, the ventricular depolarization loop, exhibits one particular direction for which the cardiac vector has maximum amplitude. This direction is referred to as the electrical axis of the heart or the main heart axis [9].

For adults, the main heart axis is on average tilted 57° with respect to the transverse plane, i.e. approximately corresponding to the direction from the right shoulder to the left ankle (Einthoven lead II [62]), but deviations from -30° to 90° are considered normal [9].

Differences between fetal and adult ECG

The direction of the electrical axis in the adult and fetal hearts are not the same. In the adult heart, the electrical axis points towards the left ventricle; the ventricle with the largest mass. For the fetal heart, however, the mass of the right ventricle is larger than that of the left one [60]. Hence, the electrical axis of the fetal heart is expected to point towards the right ventricle [59]. This shift in the electrical axis between the fetal and adult is firmly established in Chapter 8 of this thesis and implies that the fetal VCG is oriented differently as well with respect to the adult VCG. Hence, each

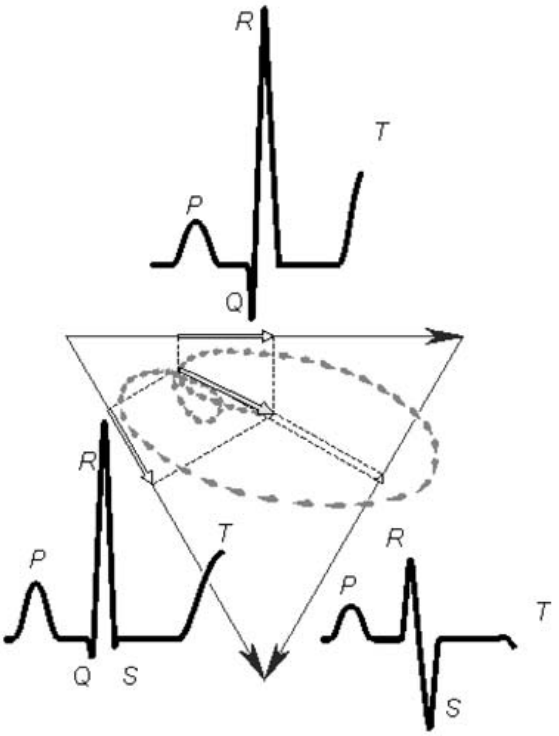

Figure 2.5: *Two-dimensional illustration of the vectorcardiogram (in gray) and the instantaneous projection of the cardiac vector on the three leads of the Einthoven triangle, resulting in three one-dimensional ECG leads [35].*

ECG representation for the fetus – being the projection of the fetal VCG onto the appropriate lead vector – differs from the same ECG representation for the adult.

For clinical interpretation of the fetal ECG, therefore, standard guidelines used in the field of cardiology may no longer be valid, requiring the formulation of new guidelines for the fetal cardiology field. In Chapter 8 of this thesis, the differences between the fetal and adult ECG are further elaborated on.

2.1.4 Clinical significance of the fetal ECG

Several parameters of the fetal ECG complex can be associated with the fetal condition. For instance, the dimensions of the fetal heart and hence the size of the fetus can be estimated from the lengths of the intervals in the ECG, while also indications for fetal oxygen deficiency can be discerned.

Fetal growth parameters

The time it takes for the traveling dipole wave to depolarize both atria is determined by the size of the atria and the conduction speed of the action potentials. As this conduction speed is rather constant, the interval between activation of the SA node and complete atrial depolarization is associated with the size of the atria [55]. This interval is reflected in the ECG by the length of the P-wave.

In addition, the QRS complex reflects the time interval between initial and complete depolarization of the ventricles [9]. The length of this interval is associated with the size of the ventricles. As the heart grows proportionally with the fetus, both the length of the P-wave and the length of the QRS complex are parameters that can be used to approximate the size of the fetal heart and consequently assess potential fetal growth restriction.

ST segment variability

The capability of the fetal heart to distribute the blood to the body depends on the critical balance between energy production and energy consumption. Under normal conditions, the available amount of oxygen exceeds the requested amount and the fetal heart utilizes aerobic (oxygen-dependent) metabolism for generating energy. In this situation, the energy balance is positive and the fetal ECG morphology is normal [1].

When the available amount of oxygen decreases while the requested amount persists, the energy balance becomes negative and myocardial hypoxia emerges. As a result of myocardial hypoxia the ECG morphology changes in such way that the ST segment obtains a downward slope: a biphasic ST segment [1]. The fetus responds to the negative energy balance by a sudden increase in adrenalin, activating

the myocardium even more and causing an rapid further decrease in the energy balance [12]. In addition however, this adrenalin initiates glycogenolysis, a process in which stored glucose is utilized for generating energy [65]. Consequently, the aerobic metabolism gets supported by anaerobic metabolism, restoring the energy balance to equilibrium [12].

However, in contrast to aerobic metabolism that, next to energy, produces carbon-dioxide and water, the anaerobic metabolism produces lactates which contribute to the development of metabolic acidemia [66]. Moreover, the process of glycogenolysis releases a surplus of K^+ ions increasing the amplitude of the T-wave. When the lack of oxygen supply continues and the rate of glycogenolysis rises, the T-wave amplitude increases ever more [2, 26].

The persisting lack of oxygen can result in a global oxygen deficiency that also includes the central organs. This is called asphyxia. In cases of severe and sustained asphyxia, the T-wave amplitude returns to its normal level due to the incapability of the fetus to respond to the situation [50, 67, 68]. At the same time, biphasic ST segments as are visible during the initial phase of hypoxia should no longer be expected in case of developing asphyxia due to the fact that the ability of the fetus to employ its protective mechanisms is declining [1]. Although this might, at first sight, impede the use of ST monitoring in clinical practice, in these asphyxia situations the CTG is usually conclusive, underscoring once more the necessity for combining the use of ST monitoring with CTG.

Fetal movement

As discussed before, each ECG complex can be considered the projection of the VCG on the appropriate electrode lead vector. For non-invasive fetal ECG recordings this implies that the fetal VCG is projected on electrode lead vectors on the maternal abdomen. Since these lead vectors are stationary, with the exception of abdominal movement, changes in the morphology of the ECG can be related to fetal movement. Naturally, changes in the morphology of the fetal ECG do not have to originate from fetal movement per se; changes in the physiological condition of the fetus can also affect the fetal ECG, as indicated above. Discrimination between either of these ECG changes is nevertheless made possible based on *a priori* physiological knowledge on the time scale on which each of these changes occurs. Particularly, ST waveform variations are expected to take place at a time scale in the order of 15 seconds or larger [69]. Fetal movement, on the other hand, is expected to take place at a much smaller time scale.

Besides discriminating ECG changes that originate from changes in the fetal physiological condition from ECG changes originating from movement, monitoring of fetal movement serves another purpose. In general, spontaneous fetal movement can be observed from 7 weeks of gestational age [56]. During the first part of preg-

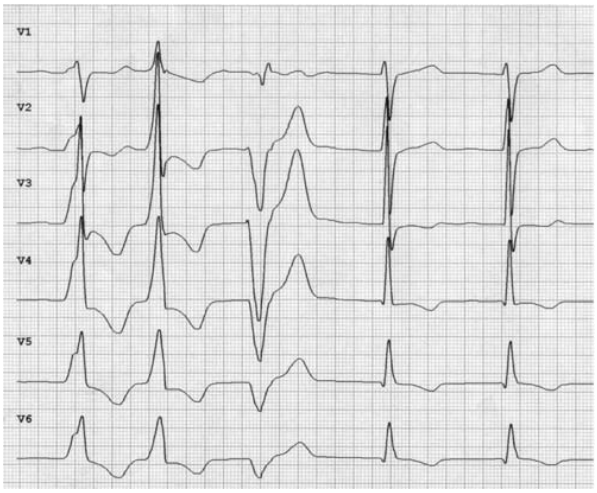

Figure 2.6: *Example of a SVES (third heartbeat) in the precordial leads of an adult patient.*

nancy, these movements take place randomly in time. As pregnancy progresses, they become more and more clustered into alternating episodes of rest and activity. These so-called rest-activity cycles are present from 20 weeks of gestation [70, 71]. In the second half of pregnancy, the rest-activity cycles become increasingly linked to fetal heart rate patterns and fetal eye movements and result in fetal behavioral states. The presence of these behavioral states is one of the indicators for maturity and integrity of the fetal nervous system [56]. In addition, severe and sustained reduction in fetal movement is an indication of fetal distress, often preceding fetal death [54, 72].

It has to be noted here that monitoring fetal movement through the fetal ECG only provides information about motion of the fetal heart or thorax; movement of the fetal limbs does not affect the transabdominal fetal ECG.

Extrasystoles

Extrasystoles, or more particularly supraventricular extrasystoles (SVES), are heartbeats that originate in the nodal cells of the ventricles and not in the SA node [9]. The conduction of the depolarization wave therefore occurs in opposite direction and does not exploit the high conduction velocities of the Purkinje fibers. In the ECG, this conduction translates to a widened QRS complex with opposite sign [9]. The P-wave, representing contraction of the atria, is absent for SVES (see Fig. 2.6).

In most cases, SVES are innocent and hence not very relevant for fetal monitoring. This innocence can be explained by the fact that the ventricles are filled with blood both actively (by contraction of the atria) and passively (because of the higher pressure in the vena cava) [60]. Sole contraction of the ventricles in periods of low

activity, is therefore sufficient to perfuse the fetal body with blood. In addition, the occurrence of SVES is in most cases associated with immaturity of the heart and not with congenital heart disease [73–76].

However, in the few cases that SVES do originate from congenital heart disease, the visualization of the fetal ECG can be of vital importance. This is so because timely detection of congenital heart disease can aid in either treatment of the disease during pregnancy, e.g. through administration of medication [77], or in the preparation for treatment directly after birth [78].

All the parameters discussed above illustrate that fetal ECG monitoring can have added value with respect to CTG monitoring. Not only can the fetal heart rate be assessed more accurately and more reliably, but also do the fetal growth, fetal oxygenation and fetal movement parameters provide information about fetal distress. This, however, raises the question why fetal ECG monitoring has not been used as a standard in clinical practice since many years. One of the answers to this question is the lack of signal acquisition and processing techniques that enable determination of the fetal ECG with sufficient accuracy and reliability in all stages of pregnancy. As mentioned in Chapter 1, this thesis aims to provide a contribution to the solution of the signal processing (and interpretation) issues. Hence, in the remainder of this chapter, firstly the problems that signal processing and analysis techniques have to overcome for non-invasive fetal ECG monitoring to be applied in clinical practice are discussed briefly. The existing solutions to these signal analysis problems themselves are detailed on in the remainder of this thesis. Secondly, the data acquisition and the patient population used throughout this thesis to evaluate the developed signal analysis techniques are described.

2.2 Problems encountered in non-invasive fetal ECG analysis

2.2.1 History of fetal ECG analysis

Ever since Cremer [79] in 1906 recorded the first fetal ECG, researchers have shown interest in reproducing this feat and studying the clinical relevance of the fetal ECG [12, 79–83]. In particular, interest has been focused towards the non-invasive recording of the fetal ECG, i.e. from the maternal abdomen. Notwithstanding the many attempts to improve the quality of the transabdominal fetal ECG [12], this quality remained too low to use the non-invasive fetal ECG as a diagnostic tool. Hence, the use of fetal ECG monitoring in clinical practice lost momentum and was disregarded until the introduction of the scalp electrode as a means of fetal heart rate monitoring by Hon in 1963 [13].

The introduction of this scalp electrode, i.e. an invasive electrode connected to the fetal scalp that provides an ECG signal with improved quality over the non-invasive fetal ECG, led to extensive new research regarding the diagnostic value of this improved quality fetal ECG [84–86]. Part of this research finally converged to the introduction of the STAN® monitor [2, 8, 25, 26, 50]; a monitor that analyzes the ST segment of the fetal ECG and, in combination with CTG, can be used to assess fetal hypoxia [28]. In recent years, this STAN® monitor has gained evermore momentum [52, 87, 88]. Unfortunately, STAN® can only be applied during parturition since it is based on the invasively recorded fetal ECG. Combined with the fact that the ST segment alone cannot discriminate between sustained asphyxia and normal oxygen levels [51], this stresses the need for a non-invasive method to record the fetal ECG. For example, in case of a fetus suffering from asphyxia before dilatation, the scalp electrode and thus STAN® analysis is commenced too late. Consequently, ST analysis does not assess the fetal condition correctly [51]. Naturally, the CTG registration of a fetus in this case should lead to a correct diagnosis and subsequent intervention by the physician, but when the ST analysis could have commenced earlier this would potentially have resulted in an earlier diagnosis.

Basically, this limited applicability of the STAN® monitor returns us to the problem that arose after Cremer recorded the first fetal ECG: how can we record the transabdominal fetal ECG with good enough quality to use it as a diagnostic tool in clinical practice? Over the years, many techniques have been proposed to extract the fetal ECG from the composite signals that are recorded from the maternal abdomen [89–96], but none prevailed.

The origin of the signals that mostly contribute to the composite abdominal signals and that corrupt the fetal ECG are discussed below. Techniques – both proposed in the literature and newly developed – to remove, suppress, or extract these contributing signals are discussed in Chapter 3, Chapter 6, and Chapter 7.

2.2.2 Signals recorded from the maternal abdomen

Physiological signals

As the maternal body acts as a conductor, several other electrophysiological signals that do not originate from the fetus are recorded by electrodes on the maternal abdomen [63]. These interferences include, but are not limited to, the maternal ECG, activity from the uterus (electrohysterogram, EHG) [97, 98], and abdominal muscle activity (electromyogram, EMG).

The maternal ECG has about the same spectral properties as the fetal ECG, that is, a frequency content ranging from about 2 Hz to 80 Hz as shown in Fig. 2.7 [99], but has amplitudes that can exceed those of the fetal ECG by a factor 10 (Fig. 2.8). The EHG, in contrast, has a frequency content ranging from 0 Hz to approximately

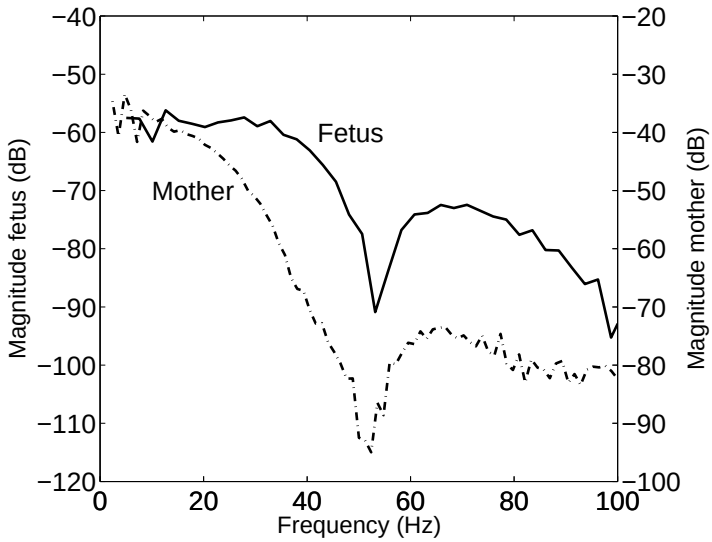

Figure 2.7: *Frequency content of both the fetal and maternal ECG. The dip around 50 Hz is due to a notch filter to suppress powerline interference.*

3 Hz [100], whereas the EMG exhibits frequencies ranging from 0 Hz to 200 Hz [101]. These three interferences alone already illustrate the difficulty of fetal ECG extraction and hence explain the wide range of techniques proposed to achieve this extraction. To further exemplify this, in Fig. 2.8 a composite abdominal fetal ECG recording is shown with some of the contributing signals indicated.

Non-physiological signals

Although many non-physiological interferences exist, e.g. imperfections in the analog-digital converter of the recording equipment, the non-physiological interferences are dominated by the powerline grid [102].

The interference from the powerline grid in the Netherlands is centered around 50 Hz with harmonics at multiples of 50 Hz and can be suppressed from the composite signal by either employing a series of notch filters with fixed cutoff frequencies or an adaptive interference canceler [102].

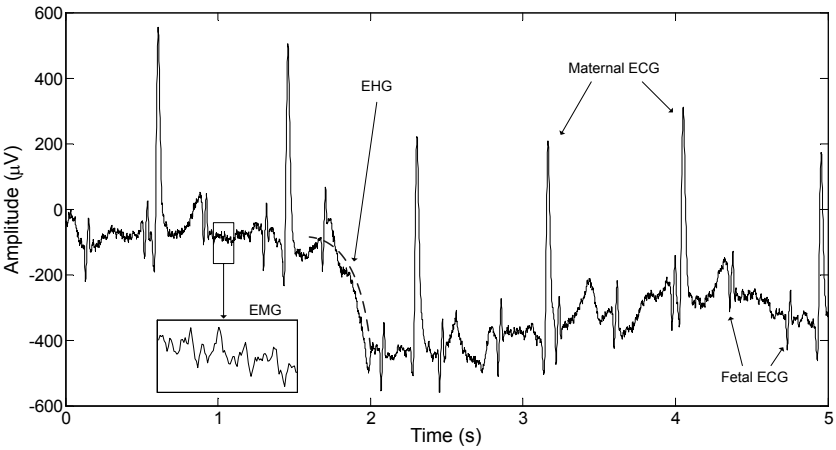

Figure 2.8: *Segment of composite abdominal fetal ECG recording. The contribution of the EHG is reflected by wandering of the baseline. This baseline wander is emphasized by the additionally drawn dashed arc.*

2.2.3 Complications in fetal ECG analysis due to changes in the volume conductor

In addition to the signals that corrupt the fetal ECG in the abdominal recordings, fetal ECG analysis is complicated for another reason as well. Changes in the volume conductor between the fetal heart on the one hand and the abdominal electrodes on the other hand can distort or attenuate/amplify the ECG [36, 37, 103, 104]. In general, these changes originate from movement of the fetus, development of the vernix caseosa [37, 39], and movement of the mother.

As stated previously, fetal movement is reflected in the transabdominal fetal ECG as spatially correlated changes in the morphology of the ECG waveform. In terms of the fetal VCG, movement of the fetus is reflected as a rotation of the VCG. However, fetal movement not only causes the fetal VCG to rotate with respect to the electrode configuration on the maternal abdomen, but it also causes the distance between the fetal heart and the various electrodes to change [29]. In case the conduction of the electrophysiological signals from the fetal heart to the maternal abdominal surface is not uniform, this change in distance causes both distortion and attenuation/amplification of the fetal ECG [37, 104]. In case of uniform conduction, only attenuation or amplification of the fetal ECG signals is expected. Specifically, in case fetal movement causes the distance between the heart and a particular electrode to decrease, amplification of the corresponding fetal ECG signal is expected. Conversely, an increase in the heart-electrode distance is expected to be accompanied by attenuation of the corresponding fetal ECG.

From about 28 weeks of gestation the fetus develops a protective layer called the vernix caseosa [37, 39, 105, 106]. The vernix caseosa isolates the fetus electrically from its surroundings, making it virtually impossible to record a fetal ECG on the maternal abdomen. However, from about 32 weeks of gestation this protective layer starts to break down, partly canceling the isolated environment of the fetus and thus restoring the possibility of transabdominal fetal ECG recording. As a consequence of the holes that are thus generated in the vernix caseosa, preferred conduction paths for the electrical signals arise [39]. These conduction paths constitute a transition from uniform conduction before 28 weeks of gestation to non-uniform conduction after 32 weeks of gestation, significantly affecting the transabdominal fetal ECG [63]. After about 37 weeks of gestation the vernix caseosa dissolves in the amniotic fluid restoring the uniform conduction characteristics of the volume conductor [37]. Since problems that arise from attenuation or amplification of the fetal ECG signals can be properly dealt with (as will be discussed in 7), limitations in fetal ECG analysis due to fetal movement and non-uniformity of the volume conductor are mainly expected between 28 weeks and 37 weeks of gestation.

Another change in the volume conductor that causes fetal ECG distortions on the abdominal surface is caused by fetal breathing. By filling its lungs with amniotic fluid [107], the fetus changes the impedance of the conduction path from its heart to the abdominal electrodes, affecting the recorded fetal ECG.

A final reason for changes in the volume conductor mentioned here is movement of the electrodes, resulting from movement of the mother. At first glance, electrode movement might seem more appropriately placed among non-physiological interferences of the fetal ECG, rather than among changes in the volume conduction. However, movement of the electrodes causes the conductive layer between the skin and the electrodes to change and hence causes a change in the properties of the volume conductor. This conductive layer is generated by the thermal excitation of metallic ions in the electrode [108]. These ions spread through the electrolyte, forming a layer balancing the electrode charge [108]. Although the ions can move freely through the electrolyte, the speed of movement is limited and hence electrode movement is likely to disturb the balancing layer and hence the electrode-skin bias [108], resulting in artifacts in the recorded fetal ECG.

2.3 Fetal data acquisition

The setup for the acquisition of the non-invasive fetal ECG throughout this thesis basically consists of three parts: the patient, the sensors, and the data acquisition system. This setup is depicted in Fig. 2.9 and each part is separately discussed below.

Besides the acquisition of the non-invasive fetal ECG, i.e. the fetal ECG recorded from the maternal abdomen, a few other signals from the fetus may be acquired as

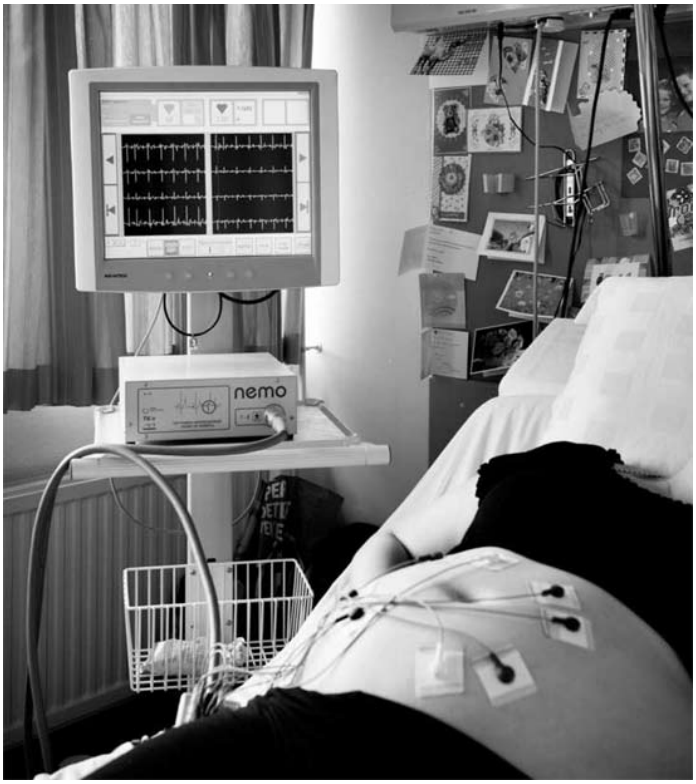

Figure 2.9: *Photograph of the data acquisition in operation. Self adhesive electrodes are positioned upon the maternal abdomen. The signals measured by these electrodes are stored on the panel PC via digitization by the NEMO amplifier. (Photo by Bart van Overbeeke.)*

well. These signals are mainly used for validation of the abdominally assessed fetal health parameters and consist of ultrasound recordings of the fetus and the invasively recorded fetal ECG. The latter signal is only recorded for a small number of patients. The acquisition of the ultrasound images is included in the measurement protocol and therefore performed for all patients.

2.3.1 Patient

In total about 50 patients were followed longitudinally throughout their pregnancy. Measurements started at 14 weeks of gestation and from then, were regularly repeated until term. To be precise, the measurements were, provided patient availability, conducted at 14, 18, 22, 24, 26, 30, 34, 36, 38, 40, 41, and 42 weeks of gestation. Up till 36 weeks, the measurements lasted 45 minutes and after 36 weeks they lasted 60

Table 2.1: *General information on patients that completed the longitudinal study. The asterisk * denotes that not for all patients the provided information is available.*

	Mean (Minimum – Maximum)
Number of patients	40
Age (years)	31.4 (21.1 – 41.0)
Gestational age at birth (weeks+days)	39+2 (31+3 – 42+0)
Birth weight (grams)	3380 (1020 – 5160)
1-minute Apgar scores	9.0* (8 – 10)
5-minute Apgar scores	9.9 (9 – 10)
Arterial blood pH	7.23* (7.07 – 7.42)
Venous blood pH	7.32* (7.21 – 7.48)
Number of recordings performed per patient	8.5 (3–10)

minutes. This elongation of the measurement length stems from the wish to eliminate the influence of fetal behavioral states on the results, which with progressing pregnancy will change less frequently. The study was approved of by the medical ethical committee of the Máxima Medical Center.

The choice for 50 patients was dictated by the aim to have 25 healthy women complete the study and provide a basis for defining preliminary, normal fetal parameter values. The other 25 women were anticipated to leave the study because of either complications arising after inclusion in the study or loss to follow up (”non-attenders”). In the end, over 40 women completed the study without complications.

Inclusion criteria for the patients were healthy women (low risk population) with an uncomplicated singleton pregnancy of at least 14 weeks of gestation. The participants were included in the study after informed consent. Exclusion criteria were women under the age of 18 years and multiple pregnancies. Pregnancies complicated by e.g. hypertension, preeclampsia, fetal growth restriction, diabetes mellitus, or fetal congenital malformations were also excluded from the longitudinal study, but in some cases analyzed separately. To ensure maximum signal quality, patients were prepared by gently scrubbing of their skin to remove dead cells. In Tables 2.1 some detail on patients that were included in the study is provided.

It has to noted that due to the alternative circulation of the fetus, as opposed to the circulation after birth, the arterial blood pH is lower than the venous blood pH (Table 2.1). After birth, this relation is inverted with the arterial blood carrying higher oxygen levels than the venous blood.

2.3.2 Non-invasive fetal ECG

Abdominal electrode configuration

The fetal ECG recordings comprise 8 bipolar signals, all with a common reference placed near the maternal umbilicus. A ground electrode, with right leg drive, is positioned near the side of the mother to minimize interference from the powerline grid. The electrode configuration is depicted in Fig. 2.10.

The choice for this particular electrode configuration constitutes a trade-off between patient comfort and signal processing capabilities on the one hand and the recorded amount of information on the other hand. Specifically, in order to assess the fetal health with as much accuracy as possible, as many as possible fetal ECG signals are preferred. This large number of fetal ECG signals, however, requires a multitude of electrodes on the maternal abdomen and many signals to be processed. To avoid significant patient discomfort resulting from all these electrodes and to facilitate real-time analysis of the recorded information, the number of abdominal electrodes should be kept rather small. Hence, the number of electrodes is chosen as 8. To ensure that, irrespective of the fetal position within the uterus, at least some of the electrodes are close to the fetal heart and thus record the fetal ECG with sufficient amplitude, the circular configuration of Fig. 2.10 is adopted.

Due to the rounding of the abdomen, this circular configuration exists in three-dimensional space. Specifically, the electrodes on the side of the abdomen (i.e. electrodes 1, 4, 5, and 8 in Fig. 2.10) are positioned closer to the back of the mother than the center electrodes (i.e. electrodes 2, 3, 6, and 7). The presence of this third dimension (i.e. the transversal direction; from front to back) enables the estimation of the fetal VCG in three dimensions (see Chapters 4 and 7). For pregnancies at low gestational ages, however, the rounding of the abdomen is smaller and hence, the accuracy of the three-dimensional electrode positions is relatively low. Based on photographs of the abdomen, taken from orthogonal directions, a fair indication on the electrode positions can nevertheless be obtained (see Fig. 2.10).

The electrodes used are Ag/AgCl electrodes. To minimize loss of signal quality during the conduction of the ECG signals from the electrode to the data acquisition system, the electrode cables are actively shielded.

Data acquisition

The ECG signals are digitized and stored by the NEMO system. This system comprises a programmable amplifier for acquiring electrophysiological signals and a panel PC for controlling the amplifier settings and storage of the recordings. This amplifier is based on the Maastricht Programmable AQuisition (M-PAQ) system (Maastricht Instruments BV, the Netherlands), but modified to maximize its performance in

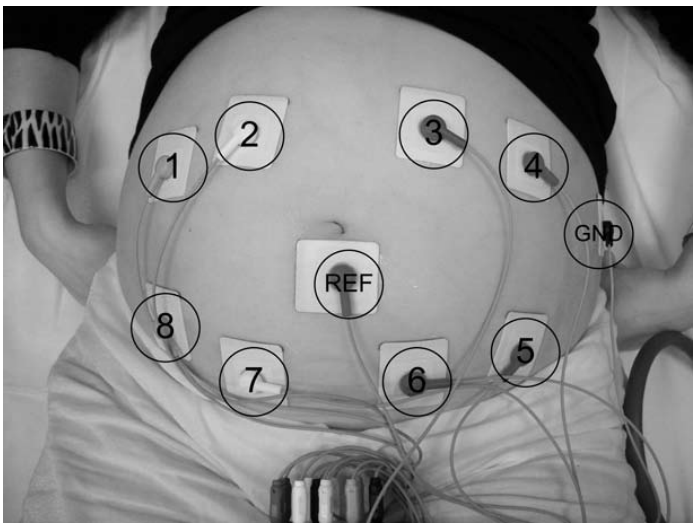

(a)

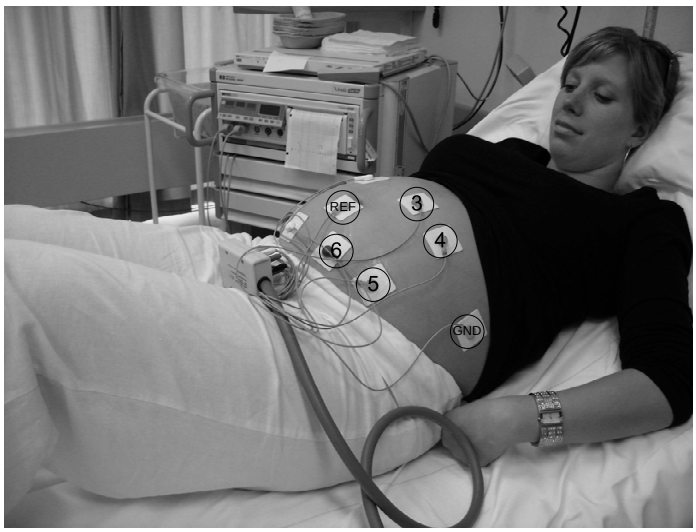

(b)

Figure 2.10: *Frontal view (a) and side view (b) of the electrode configuration used for recording the fetal ECG.*

Table 2.2: *Technical specifications and settings of the NEMO amplifier.*

Technical specifications	
ADC resolution	20 bit
Filters	2nd order IIR high-pass (0.01 Hz) and notch (50 Hz)
Maximum gain	200
Input impedance	100 MΩ
Input range	±10 V
Interface	USB 2.0
Number of channels	8 differential with common reference
Sampling rate	1 kHz per channel
Noise level	$< 5\ \mu V_{\mathrm{RMS}}$ (0.1–100 Hz)
Least significant bit	95 nV

recording the non-invasive fetal ECG. A few specifications of the NEMO amplifier are presented in Table 2.2.

With the general amplitude of the fetal ECG between 5 and 10 μV, the maximum allowed noise levels of the NEMO amplifier (Table 2.2) still require the most of the signal processing methods to extract the fetal ECG from the noise. At this moment, the largest part of this signal processing is done offline, but the panel PC of the NEMO system is capable of performing this processing in real-time, simultaneous with acquisition of the data.

2.3.3 Ultrasonic signals

Besides acquisition and storage of ECG data, the panel PC on the NEMO system is also capable of importing images acquired by a medical ultrasound device. The ultrasound device used is an Aloka SSD1100 (Aloka, Japan). This ultrasound device uses a standard obstetric probe to transmit 3.5 MHz ultrasound into the body and obtain images from the fetus. These images are transmitted via a coaxial cable to a frame-grabbing card in the panel PC, enabling synchronized acquisition of both the fetal ECG and ultrasound images.

2.3.4 Invasive fetal ECG

To evaluate newly developed signal processing techniques for non-invasive fetal ECG analysis, for some patients also the invasive fetal ECG is recorded simultaneously. As mentioned before, these measurements can only be performed during labor and impose some risk to the fetus. Hence, they are only performed based on medical need and as a result for only few of the women enrolled in the studies these signals have been acquired. The electrode used for these specific recordings entails a helix-shaped

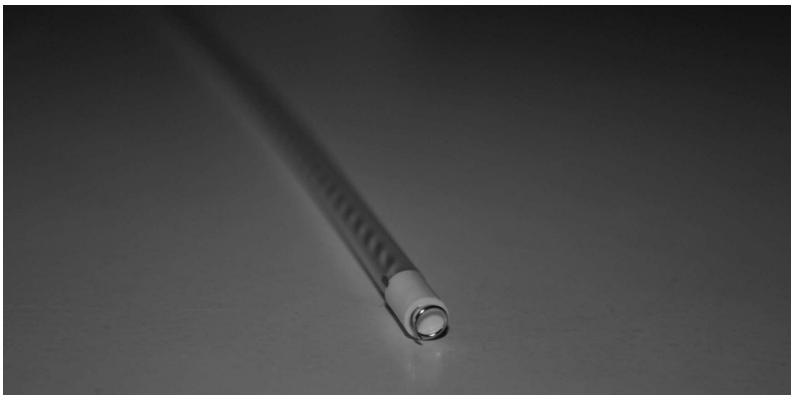

Figure 2.11: *Photograph of scalp electrode with a single helix needle.*

needle that is screwed into the fetal scalp. Hence, this electrode is generally referred to as a scalp electrode (Fig. 2.11).

For medical safety issues the invasive fetal ECG recordings are performed using a standard CTG monitor, albeit a rather old version (HP8040; Hewlett-Packard, USA). The advantage of this HP8040 is that it contains an analog output. This analog output is connected to the input of a 16-channel M-PAQ system, enabling simultaneous acquisition of the non-invasive and the invasive fetal ECG (Fig. 2.12). This 16-channel system has the same specifications as the NEMO system of Table 2.2, with the exception that the maximum selectable gain of the M-PAQ is increased to 2000.

2.4 Final remarks

In Section 2.1 of this chapter, the relevance of fetal ECG monitoring for supporting the diagnosis of the fetal condition was illustrated by exemplifying some clinically relevant parameters that can be extracted from the ECG. These examples only constitute a small fraction of the parameters that are used by clinicians to assess the fetal condition. Other parameters include results from fetal blood sampling [22], nuchal translucency [109] and fetal fibronectin [110]. The examples described in Section 2.1, nevertheless, are among the most relevant parameters and, moreover, are the ones extracted, assessed, or estimated throughout this thesis.

In Section 2.2 some of the problems that are encountered while trying to determine the non-invasive fetal ECG were discussed. Like with the fetal ECG parameters, also for Section 2.2 it holds that the listed problems only constitute a small part of the problems that are encountered in clinical practice. Similar as above, however, the problems discussed in this chapter are the ones most likely to occur and the ones for which this thesis aims to contribute in solving them. Other problems/challenges

Figure 2.12: *Photograph of the 16-channel M-PAQ system on the left and the HP8040 CTG device on the right.*

that can occur while recording the non-invasive fetal ECG in clinical practice include the separation of fetal ECG signals in twin or multiple pregnancies [111] and high electrode impedances that lead to low SNRs.

A high electrode impedance can originate from a bad galvanic contact between the skin and the silver plate in the electrode and can be avoided by careful preparation of the patient and positioning of the electrodes. In Section 2.3 this preparation was briefly addressed. Besides the patient preparation, Section 2.3 also addressed the data acquisition employed throughout the thesis and the included patient population. For the patient population, it needs to be mentioned that not all measurements were of similar quality, not only due to progressively alternating insights in the best measurement setup, but also due to differences in the position and size of the fetus, the skin impedance of the mother, and the presence of the vernix caseosa. As a consequence, in the various chapters of this thesis, different fetal ECG recordings are used to evaluate and illustrate the developed signal analysis technologies, each of these recordings selected based on favorable properties or features for its intended use.

Part I

Non-invasive fetal electrocardiogram analysis

In Part I of the thesis, the non-invasive fetal electrocardiogram (ECG) is analyzed. This analysis concerns the extraction of the fetal ECG from the mixture of signals that is recorded from the maternal abdomen and the further processing to yield the fetal vectorcardiogram (VCG). This VCG will be used as starting point in Part II of this thesis.

In Part I the ECG has to undergo a conversion in its dimensionality: the abdominally recorded fetal ECG consists of eight individual ECG signals while the intended result (i.e. the VCG) consists of three individual ECG signals. Moreover, in the process of getting from the eight-dimensional ECG to the three-dimensional VCG, the ECG is at first reduced to a one-dimensional signal. This signal is a linear combination of the eight fetal ECG signals and is merely used to detect the periodicity of the ECG (i.e. the heart rate). This periodicity is subsequently used as a basis for further processing of the eight-dimensional ECG towards the three-dimensional VCG.

The outline of this part of the thesis is as follows. In Chapter 3 a method is presented to suppress the maternal ECG from the abdominal recordings. This method operates by subsequent estimation and subtraction of individual ECG segments and performs more accurately in maternal ECG suppression than already existing methods. In Chapter 4 the signals remaining after suppression of the maternal ECG are linearly combined, based on a underlying physiological model, to yield a one-dimensional ECG signal with superior properties – as opposed to each of the eight signals remaining after maternal ECG suppression – to facilitate detection of the heart rate. The method used to detect this heart rate is discussed in Chapter 5. In Chapter 6 the heart rate is used as input for a filter that exploits the quasi-periodicity of the ECG, in the meantime ensuring that physiologically relevant variations in the, again eight-dimensional, ECG morphology are retained. Chapter 7 finally uses the eight filtered ECG signals to estimate the fetal VCG.

Chapter 3

Dynamic segmentation and linear prediction for maternal ECG suppression in antenatal abdominal recordings

In this chapter, a method is presented to suppress the maternal ECG from the non-invasive abdominal recordings and, hence, to enhance the signal to noise ratio of the remaining fetal ECG. The method operates by subdividing the maternal ECG complex into multiple physiological segments, by generating a dynamic template for each segment of the maternal ECG, and subsequently subtracting this template from the original signal.[1]

3.1 Introduction

Currently the most widespread method to monitor fetal health is cardiotocography (CTG) [112], which consists of the simultaneous monitoring of the fetal heart rate (fetal heart rate) and maternal uterine activity. However, in many cases the CTG does not provide conclusive information for accurate assessment of fetal health and, therefore, additional information is needed for clinical decision-making [28, 113].

The main additional sources of information to support the CTG are fetal blood sampling and fetal electrocardiogram (ECG) analysis using an invasive electrode. Both these methods require invasive measurements and consequently can only be applied during labor and entail an increased risk of infection. The spectral analysis of the fetal heart rate can also offer additional information [114, 115]. If this is performed on the non-invasively determined fetal heart rate, it can be applied in stages of pregnancy earlier than labor.

The non-invasive fetal heart rate is generally determined by means of Doppler ultrasound. This method, however, does not allow long-term monitoring since it is

[1]This chapter is based on the paper published as *R. Vullings, C.H.L. Peters, R.J. Sluijter, M. Mischi, S.G. Oei and J.W.M. Bergmans, "Dynamic segmentation and linear prediction for maternal ECG removal in antenatal abdominal recordings", Physiol Meas. 2009 Mar;30(3):291-307.*

sensitive to maternal and fetal motion, resulting in a relatively low signal to noise ratio (SNR), and since the ultrasound transducers transmit energy into the fetal body, potentially endangering fetal health.

To overcome low SNR problems, in modern CTG devices a buffer of consecutive heart beats is autocorrelated at constant frequency to provide a reliable, but slightly smoothed, fetal heart rate signal. Although this fetal heart rate measurement approaches the 'gold standard' of the fetal heart rate determined from a invasively recorded fetal ECG [15], particularly the high frequency parameters in the spectral analysis of the fetal heart rate are affected by the smoothing of the autocorrelation method.

From this it is clear that any non-invasive method to support the CTG, resolving the problems associated with Doppler ultrasound, can be highly valuable. One such method is fetal ECG monitoring with abdominal electrodes. Besides the fetal ECG, this method also enables accurate spectral analysis of the unsmoothed fetal heart rate, i.e., it can provide the fetal heart rate on a beat-to-beat basis, and due to its passive nature and relative insensitivity to fetal motion it can be used for long-term monitoring. In addition to improved spectral analysis of the fetal heart rate, the abdominally recorded fetal ECG also enables analysis of the fetal ECG. Relative changes in the segments and intervals of the fetal ECG are associated with fetal distress [2] and growth [55], implying that fetal ECG monitoring provides additional information on the fetal condition.

The fetal ECG recorded from the maternal abdomen is affected by noise consisting of a mixture of several interferences. As, in general, the maternal ECG is the predominant interference [116], several techniques for maternal ECG suppression from the abdominal signals are presented in literature [90–92, 94, 96, 117–120]. However, none of these techniques can suppress the maternal ECG completely or extract the fetal ECG [95] as the interferences in the abdominal recordings do not completely satisfy the assumptions implicitly made by the presented techniques.

Therefore, in this chapter a new technique is presented for the suppression of the maternal ECG. This technique is an extension of maternal ECG template subtraction techniques [92, 96, 118, 120] and is referred to as the weighted averaging of maternal ECG segments (WAMES). WAMES operates by dynamically dividing the maternal ECG complex in separate segments and generating an estimate for each individual segment. Each estimate is hereby obtained by the linear combination of time-shifted, offset compensated, and scaled corresponding segments in preceding maternal ECG complexes. This process can also be viewed as a dynamic segmentation and linear prediction of maternal ECG segments. By time-aligning, offset compensating and scaling the individual segments before linearly combining them, morphological variations in the maternal ECG complex can be dealt with accurately since the only assumption of WAMES is a quasi-periodicity of the maternal ECG segments. This is

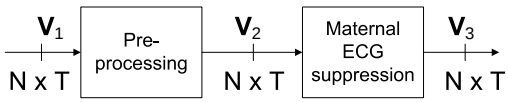

Figure 3.1: *Schematic view of fetal ECG extraction techniques.*

in contrast to other template subtraction techniques, which assume a larger degree of periodicity in the maternal ECG.

WAMES is evaluated in terms of maternal ECG estimation and fetal heart rate detection. Its performance is quantified on both modeled and real antenatal abdominal recordings, and compared to the performance of spatial filtering [91], adaptive filtering [117], template subtraction techniques [96, 118] and independent component analysis (ICA) [95, 111].

In Section 3.2 this new technique is described. Section 3.3 is devoted to the other techniques for comparison and validation. Section 3.4 discusses the abdominal recordings used for the comparison and details on the methodology of this comparison. Finally, Section 3.5 discusses the results and in Section 3.6 our conclusions are drawn.

3.2 Dynamic segmentation and linear prediction for maternal ECG suppression

Antenatal abdominal recordings generally constitute a mixture of fetal ECG, maternal ECG, and noise such as motion artifacts, muscular activity, and powerline interference. Consequently, most fetal ECG extraction techniques operate by means of consecutive suppression of each interference. Schematically, this can be seen as the two step procedure in Fig. 3.1, in which suppression of motion artifacts, muscular activity and powerline interference is referred to as preprocessing. This preprocessing block is detailed in Section 3.4. The abdominal recordings are represented in Fig. 3.1 by $\mathbf{V}_1$, which is a $[N \times T]$ matrix with N the number of electrodes on the maternal abdomen and T the length of the recording. The preprocessed signals $\mathbf{V}_2$ are subsequently fed into the maternal ECG suppression block; for WAMES this block is shown schematically in Fig. 3.2. Commonly, ECG complexes consist of a P-wave, a QRS complex (which can be subdivided into a separate Q-wave, R-wave, and S-wave), and a T-wave [9] (Fig. 3.3). Each maternal ECG complex in $\mathbf{V}_2$ is segmented by the maternal ECG segmentation block in Fig. 3.2 into individual waves, i.e., a separate P-, Q-, R-, S-, and T-wave. Each segment is subsequently estimated by linear prediction, using corresponding segments from preceding maternal ECG complexes. These estimated segments are finally combined to generate an estimate $\hat{\mathbf{V}}_2$ of the maternal ECG signal.

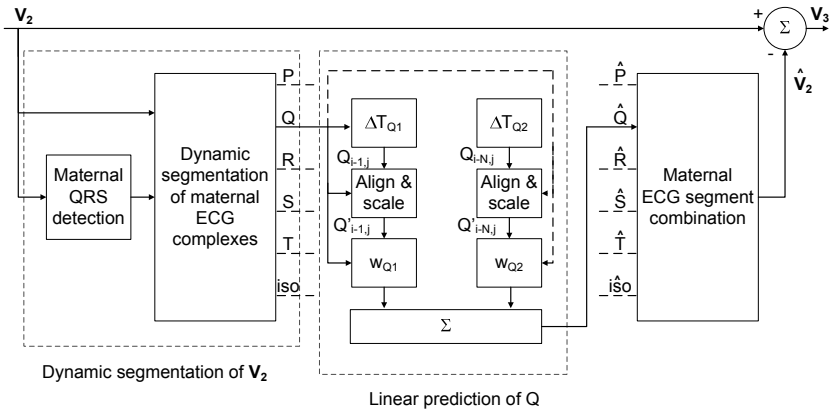

Figure 3.2: *Block scheme of the maternal ECG suppression by WAMES. The delays $\Delta T_{Q_1} \ldots \Delta T_{Q_N}$ correspond to the time intervals between the Q-wave that is estimated and n preceding Q-waves. These time intervals are approximated in the maternal QRS detection block, in which the time intervals between consecutive R-waves are determined. Part of this scheme has been adopted from [119]*

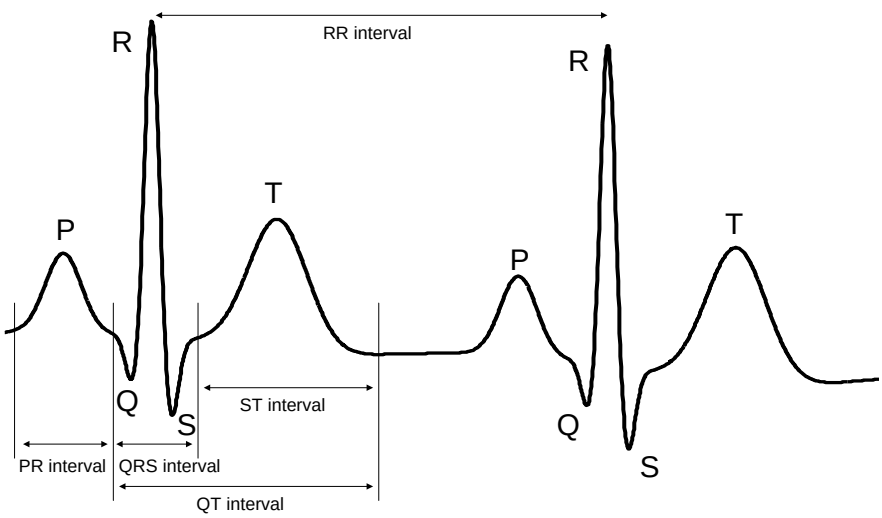

Figure 3.3: *ECG nomenclature.*

3.2.1 Dynamic maternal ECG segmentation

At a certain distance the heart can be modeled by a time-dependent dipole with variable amplitude and orientation [121]. In this framework, the ECG can be seen as the projection of the electrical field generated by this dipole on the measurement vector.

Respiration causes motion of the maternal abdomen and as a result the orientation of the measurement vector with respect to this electrical field varies over time. As each wave in the ECG exhibits its own orientation of the dipole, this variation is not proportional for each wave and therefore causes variability in the morphology of the ECG.

This morphological variability is the main reason for inaccuracies in existing template subtraction techniques. The template is not capable of accounting for all variations and consequently residuals of the maternal ECG remain after subtraction of the template. These residuals can have amplitudes that exceed the amplitude of the fetal ECG and therefore affect fetal heart rate detection. By generating a template for each individual wave the morphological variability can be accounted for more accurately, resulting in an improved maternal ECG subtraction.

The segmentation of the maternal ECG is performed in two steps. In the first step the signals are divided into individual maternal ECG complexes, based on the locations of the QRS complexes, and in the second step each maternal ECG complex is subdivided into the individual waves.

Maternal QRS detection

Depending on the position of the electrode on the maternal abdomen with respect to the position of the heart, some of the waves in Fig. 3.3 can be difficult to distinguish. Therefore, to facilitate the detection of maternal QRS complexes, the SNR of the maternal QRS complexes is enhanced by linearly combing the signals $\mathbf{V}_2$ in such way as to maximize the variance (principal component analysis, PCA) [122]. The linear combination with maximum variance is referred to as the principal component $\vec{V}_{\mathrm{PC}}$.

Maternal QRS complexes are detected in $\vec{V}_{\mathrm{PC}}$ by means of a peak detection method that is discussed in Chapter 5.

Dynamic segmentation of maternal ECG complexes

The segmentation of maternal ECG complexes is performed in two steps. In the first step for each wave a window is defined in which the wave is assumed to be present; in the second step the wave is detected in this particular window. Hereby each window is defined by its onset and its width which are both based on a physiological model and shown schematically in Fig. 3.4.

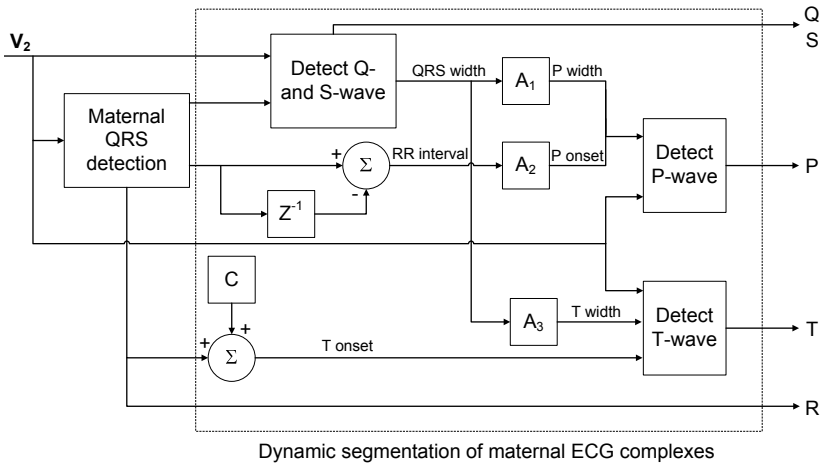

Figure 3.4: *Block scheme of the maternal ECG segmentation. The constants A_1, A_2, and A_3 are proportionality constants while the constant C represents a fixed delay between the QRS complex and the start of the T-wave.*

The P-wave is associated with the depolarization of the atria and therefore the width of this wave is related to the size of the atria and the conduction speed of the action potential through the atrial tissue. This conduction speed and size are assumed to be proportional to the conduction speed and size of the ventricles. Consequently, the width of the P-wave window is set proportional to the width of the QRS complex, which is associated with the conduction of the depolarization wave through the ventricles. The onset of the P-wave window is determined by the length of the PR interval (Fig. 3.3), which depends on the conduction speed through the AV node. As this conduction speed is regulated by the autonomous nervous system and this system is also responsible for heart rate variability, the onset of the P-wave window is set dependent on the instantaneous maternal heart rate.

Definition of the window for detecting the T-wave is analogous to the definition of the P-wave window. The main difference is that the length of the RT interval, and thus the onset of the T-wave window, is set at a fixed value C as the length of this interval is not regulated by neural stimulation. The width of the T-wave window is related to the repolarization of the ventricular tissues and is set proportional to the width of the QRS complex.

The windows for detecting the Q-, R-, and S-wave are set at fixed values assuming no cardiac pathology like bundle branch blocks. These fixed values are chosen small enough to enable WAMES to deal with high maternal heart rates adequately.

Ideally, the start and end of each wave are detected in the windows as the first local extrema on either side of the peak. However, generally the P-wave and T-wave

have a low SNR and, consequently, the detection of the start and end of the wave is less accurate. By defining an adaptive threshold that depends on the SNR within the window and performing the detection of the local extrema for the samples that do not exceed this threshold, the accuracy of this detection can be improved. The SNR within the window is approximated as the mean modulus of samples with moduli smaller than the mean modulus of all samples within the window.

Samples that are not detected in the individual ECG waves are included in the isoelectrical periods. These periods are associated with zero amplitude of the dipole or perpendicular orientation of the measurement vector with respect to the electrical field.

3.2.2 Linear prediction of maternal ECG segments

Alignment and scaling

Each wave in the maternal ECG is estimated by the weighted averaging of n corresponding waves in preceding maternal ECG complexes. Prior to averaging, the waves are aligned by synchronization on the start of the wave. As a result of the robustness in the maternal ECG segmentation, however, the accuracy of the segmentation is not optimal and hence this alignment can be inaccurate up to a few sampling period. To improve the alignment the waves are synchronized by minimizing the mean squared error (MSE):

$$b_{\min} = \arg\min_{b_{i-k}} \frac{1}{M} \sum_{j=1}^{M} \left(Z_{i,j} - Z_{i-k,j+b_{i-k}}\right)^2, b_{i-k} \in \mathbb{Z}, \tag{3.1}$$

with M the length of the wave, b_{i-k} the integer shift, $Z_{i,j}$ the wave that is estimated and $Z_{i-k,j}$ the corresponding wave of the kth preceding maternal ECG complex ($Z = \{P,Q,R,S,T,iso\}$, $iso =$ isoelectrical period). Hereby, for each i and k the value of M is set equal to the shortest length of the waves $Z_{i,j}$ and $Z_{i-k,j}$. Hence, for longer waves only part of the wave is estimated. However, as in practice the lengths of the waves vary only gradually, this omission has a negligible effect. Each of the preceding waves $Z_{i-k,j}$ is thus shifted over a length $b_{\min}$ corresponding to the minimum MSE for that particular wave.

Due to respiration the DC component and amplitude of $Z_{i-k,j}$ differ from the DC component and amplitude of $Z_{i,j}$. Moreover, because of the finite sampling frequency (1 kHz, see Section 3.4.1), misalignments smaller than one sampling period are expected, further decreasing the accuracy of the estimation. To improve accuracy, the DC component and amplitude of $Z_{i-k,j}$ have to be scaled properly and the time-shift (3.1) has to be extended with shifts smaller than one sampling period. To calculate the optimal parameters, in a least mean squared error sense, $Z_{i-k,j}$ require interpolation to obtain quasi-continuous signals. In this chapter a parabolic interpolation scheme

is used, i.e., for each sample a parabola is fitted through that particular sample and the adjacent samples on either side:

$$\tilde{Z}_{i-k,j} = \zeta_{1,j} j^2 + \zeta_{2,j} j + \zeta_{3,j}. \tag{3.2}$$

Here $\tilde{Z}_{i-k,j}$ is the interpolated wave and $\vec{\zeta}_j$ are the parabolic coefficients. The reason for using parabolic interpolation is that it is the lowest-order polynomial interpolation that can account for local extrema and has a continuous first derivative. Moreover, it computational simplicity is favored over more complex interpolation schemes. The time-shifted, DC offset compensated, and scaled wave $Z'_{i-k,j}$ can be calculated by:

$$\begin{aligned} Z'_{i-k,j} &= a\tilde{Z}_{i-k,j+b} + c, \\ a \in \mathbb{R}, b &\in \{\mathbb{R} \cap (-\Delta t_s, \Delta t_s)\}, c \in \mathbb{R}, \end{aligned} \tag{3.3}$$

with a the scaling parameter, b the required time-shift, c the DC component, and Δt_s the length of one sampling period. It has to be noted here that, as $\tilde{Z}_{i-k,j}$ is an interpolated wave, $Z'_{i-k,j}$ is an interpolated wave as well. The optimal parameters $\hat{a}$, $\hat{b}$, and $\hat{c}$ are calculated by minimizing the MSE between the estimated wave $Z_{i,j}$ and the time-shifted, offset compensated, scaled, and interpolated wave $Z'_{i-k,j}$:

$$\vec{\nabla}\left(\frac{1}{M'}\sum_{j\in F_{i-k}}\left(Z_{i,j} - Z'_{i-k,j}\right)^2\right) = \vec{0}, \tag{3.4}$$

where $\vec{\nabla}$ stands for the gradient $\left(\frac{\partial}{\partial a}, \frac{\partial}{\partial b}, \frac{\partial}{\partial c}\right)$. Here F_{i-k} is the set of samples that do not contain artifacts of fetal ECG complexes and M' is the number of samples included in F_{i-k}.

Artifacts and fetal ECG complexes affect the calculation of the parameters $\hat{a}$, $\hat{b}$, and $\hat{c}$ and therefore reduce the accuracy of the maternal ECG estimation. By excluding samples that possibly contain artifacts and fetal ECG complexes from the calculation of these parameters, the accuracy can be improved [123]. Artifacts and fetal ECG complexes generally distort the maternal ECG wave. Comparison of waves with normalized amplitudes provides information about the rate of distortion and consequently enables detection of samples containing artifacts or fetal ECG complexes [123].

Prediction

The waves $Z_{i,j}$ in the maternal ECG are estimated by the weighted averaging of the aligned and scaled waves of preceding maternal ECG complexes $Z'_{i-k,j}$ (3.3). The weights used in this averaging are determined as the reciprocals of the MSE:

$$w_{i-k} = \left(\frac{1}{M'}\sum_{j\in F_{i-k}}\left(Z_{i,j} - Z'_{i-k,j}\right)^2\right)^{-1}. \tag{3.5}$$

Since several preceding waves are included in the averaging, it can occur that both $Z_{i,j}$ and $Z_{i-k,j}$ for a particular k are similarly distorted by a fetal ECG complex. Consequently, exclusion of samples from F_{i-k} can be erroneous and as a result the weight w_{i-k} can be too large, i.e., a similar distortion of $Z_{i,j}$ and $Z_{i-k,j}$ causes the MSE to be relatively small and hence the weight to be relatively large. Furthermore, it can occur that preceding waves suffer from large distortions, resulting in relatively small weights w_{i-k}. These waves, however, still affect the averaged estimate of $Z_{i,j}$. To overcome these effects, only preceding waves are included in the weighted averaging for which the weights w_{i-k} are in the interval:

$$\mu_w - \sigma_w \leq w_{i-k} \leq \mu_w + \sigma_w, \tag{3.6}$$

with μ_w the mean weight and σ_w the square root of the weight variance.

The average maternal ECG wave $\hat{Z}_{i,j}$ can subsequently be calculated by:

$$\hat{Z}_{i,j} = \frac{\sum_{k \in G} w_{i-k} Z'_{i-k,j}}{\sum_{k \in G} w_{i-k}}. \tag{3.7}$$

Here, G is the set of preceding waves with weights satisfying (3.6). The maximum number of waves in G is restricted to the number of preceding waves N included in the estimation of the maternal ECG. Assuming that the fetal ECG and maternal ECG are not synchronized and disregarding the scaling of the waves, the amplitude of the fetal ECG in the average maternal ECG wave $\hat{Z}_{i,j}$ is reduced by a factor equal to the number of waves included in G. The desired reduction of the fetal ECG amplitude in the averaging is empirically set at 10. Since only preceding waves with weights satisfying (3.6) are included in the averaging, the number of preceding waves n included in the estimation has to exceed 10. Assuming a normal distribution of the weights, applying (3.6) results in $n = 15$.

3.2.3 Maternal ECG segment combination

As the waves $Z_{i,j}$ are estimated independently from each other, combination of the individual estimates $\hat{Z}_{i,j}$ into an estimate of the maternal ECG signal $\hat{\mathbf{V}}_2$ (Fig. 3.2) can result in discontinuities at the segment transitions due to different DC offsets. To avoid this, linear interpolation is applied on the segment transitions. This interpolation is performed in an interval of 10 ms centered around the actual segment transition.

3.3 Other methods for maternal ECG suppression

Several other techniques are implemented in the maternal ECG suppression block of Fig. 3.1 for comparison to WAMES. These techniques are discussed briefly in

this section. In addition, the performance of WAMES in fetal heart rate detection is compared to the performance of ICA and hence ICA is discussed in this section as well.

3.3.1 Spatial filtering

By regarding the abdominal maternal ECG as a superposition of three independent and orthogonal sources, three independent signals $\vec{V}_1$, $\vec{V}_2$, and $\vec{V}_3$ are sufficient to construct a fourth maternal ECG signal $\vec{V}_4$ [91]:

$$\vec{V}_4 = \lambda_1 \vec{V}_1 + \lambda_2 \vec{V}_2 + \lambda_3 \vec{V}_3. \tag{3.8}$$

The coefficients λ_1, λ_2, and λ_3 can be estimated by $\hat{\lambda}_1$, $\hat{\lambda}_2$, and $\hat{\lambda}_3$ by using the optimization procedure of Hildreth and d'Esopo [124].

According to [91] the estimated coefficients are stable for 4 seconds. Consequently, the optimization procedure is repeatedly applied on signal windows of 4 seconds. Moreover, the information contained in three signals appeared to be insufficient for all recordings [91], resulting in a suboptimal estimation of $\vec{V}_4$. For this reason, in this chapter (3.8) is extended to 8 signals $\vec{V}_i$ with $i = \{1, \ldots, 8\}$; each of the 8 recorded signals (Fig. 3.5) is estimated using the other 7 signals. The reason for extending (3.8) to 8 signals is the employed electrode configuration consisting of 8 abdominal electrodes; this configuration is discussed in Section 3.4.

3.3.2 Adaptive filtering

Noise canceling is a variation of adaptive filtering that can be highly advantageous for maternal ECG suppression in antenatal abdominal recordings [90]. Adaptive noise cancelers (ANC) build a reference maternal ECG and subtract this from the abdominal recordings that contain both maternal ECG and fetal ECG. As a result, the maternal ECG is attenuated whereas the fetal ECG remains unaffected. By using an artificial reference, generated by the event-triggered averaging of maternal ECG complexes, problems arising by the nonlinear propagation of the maternal ECG can be overcome [117]. In the case of antenatal abdominal recordings this means that a maternal ECG template is generated by averaging several consecutive maternal ECG complexes, synchronized on the QRS complex. This maternal ECG template is subsequently used as reference signal in the ANC; this technique is referred to as event synchronous adaptive interference canceling (ESAIC) and implemented as described in [117].

3.3.3 Template subtraction

Standard template subtraction techniques generate a maternal ECG template for the complete maternal ECG complex by event synchronous averaging, i.e. before aver-

aging the maternal ECG complexes are synchronized on the QRS complexes. This template is subsequently linearly scaled to minimize the MSE with respect to the maternal ECG complex that is estimated and subtracted [92].

Two different techniques to further improve this template and to generate this template are mentioned in literature: the event synchronous interference canceler (ESC) [96, 119] and linear prediction (LP) [118, 120], respectively.

Event synchronous interference cancelling

As respiration can cause variation in the amplitude of the maternal ECG complex, gain adaption is preferred within each maternal ECG complex [96, 119], i.e., the template is segmented and the required linear scaling is calculated for each segment separately. Implementation of ESC is performed according to [96]; segmentation of the template is performed similar to WAMES, as detailed in Section 3.2.1.

Linear prediction

After synchronization on the QRS complexes, for LP, the maternal ECG complexes are not averaged like for the ESC (with equal weights), but rather are the weights for the averaging calculated to minimize the MSE. Hence, the maternal ECG complex $\hat{\vec{V}}_i$ can be estimated by the linear combination of preceding maternal ECG complexes $\vec{V}_{i-j}$ with weights λ_{i-j}:

$$\hat{\vec{V}}_i = \sum_{j=1}^{n_{\mathrm{LP}}} \lambda_{i-j} \vec{V}_{i-j}, \tag{3.9}$$

with n_{LP} the order of the prediction model. By minimizing the MSE between the estimate $\hat{\vec{V}}_i$ and the actual maternal ECG complex $\vec{V}_i$ the weights $\vec{\lambda}_i = [\lambda_{i-1}, \ldots, \lambda_{i-n_{\mathrm{LP}}}]^T$ can be calculated:

$$\vec{\lambda}_i = \left(\mathbf{V}_i^T \mathbf{V}_i\right)^{-1} \mathbf{V}_i^T \vec{V}_i \tag{3.10}$$

with $\mathbf{V}_i = \left[\vec{V}_{i-1}, \ldots, \vec{V}_{i-n_{\mathrm{LP}}}\right]^T$. Implementation of LP is performed according to [118] and hence n_{LP} is set at 7.

Main differences with WAMES

As WAMES is based on template subtraction as well, both ESC and LP resemble WAMES to some extent. However, the main differences with ESC are that with WAMES the scaling of interpolated segments is performed before averaging, while ESC does not use interpolation and generates an average template before scaling its segments. Moreover, synchronizing of the segments in WAMES is not based on synchronization of the QRS complexes, but rather on minimizing the MSE between

the separate segments. Finally, in WAMES samples containing possible fetal ECG complexes or artifacts are excluded from scaling parameter calculations and not all preceding segments are included in the averaging (3.6). All these differences serve to increase the accuracy of maternal ECG estimation.

With respect to ESC, WAMES and LP are more different. LP does not use segmentation and artifact exclusion. Moreover, the weights for averaging in LP are determined on a minimum MSE basis while this approach is not beneficial for WAMES; due to segmentation, the contribution of noise in the weight calculation for the separate segments is too large, resulting in a reduced performance in the maternal ECG estimation.

3.3.4 Independent Component Analysis

ICA is a statistical signal processing technique for separating observed signal mixtures into latent source signals. Given a set of observed signals $\mathbf{V}$ and assuming that this set is generated by the statistically independent source signals $\mathcal{S}_{\text{ICA}}$, it can be stated that [125]:

$$\mathbf{V} = \mathbf{M}_{\text{ICA}}\mathcal{S}_{\text{ICA}} + H. \tag{3.11}$$

Here $\mathbf{M}_{\text{ICA}}$ is a constant full-rank matrix, referred to as the mixing matrix and H is additive noise.

The goal of ICA is to estimate the independent source signals matrix $\mathcal{S}_{\text{ICA}}$, or equivalently, to estimate the mixing matrix $\mathbf{M}_{\text{ICA}}$. When ICA is applied to antenatal abdominal recordings, the observed signals $\mathbf{V}$ are represented by the preprocessed signals $\mathbf{V}_2$ (Fig. 3.1) and the independent source signals $\mathcal{S}_{\text{ICA}}$ are represented by, among others, the fetal ECG and maternal ECG.

To account for non-stationarities in the mixing matrix $\mathbf{M}_{\text{ICA}}$ due to e.g. fetal movement, ICA is repeatedly applied on temporal windows of $\mathbf{V}_2$ with length of 4 seconds (Section 3.3.1), i.e. for each 4 seconds of data ICA is applied on the observed signals, resulting in a mixing matrix $\mathbf{M}_{\text{ICA}}$ that is updated every 4 seconds.

Restriction of ICA is that the order of the independent signals cannot be controlled and as a result, in consecutive calculations the source signals can be swapped. To overcome this signal swapping problem, half-overlapping windows are used in combination with a correlation scheme to re-order the independent signals [111].

The independent source signal representing the fetal ECG is selected automatically based on a physiological model of the fetal heart rate [126]. Independent source signals representing the maternal ECG but satisfying this model are excluded based on maternal heart rate information obtained through detection of the maternal QRS complexes in the recorded signals. When none of the independent signals satisfies the physiological fetal heart rate model, the window length used for the input signals of ICA is adapted; large non-stationarities can require shorter windows whereas estimation of a stationary mixing matrix is improved when the window length is enlarged.

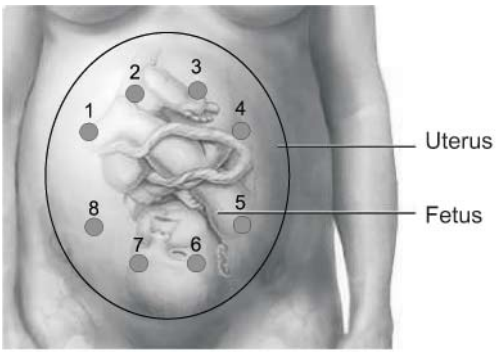

Figure 3.5: *Electrode configuration on the maternal abdomen.*

For implementation of ICA the Joint Approximate Diagonalization of Eigenmatrices (JADE) algorithm [127] is employed; a non-Gaussianity based solution to the ICA problem.

3.4 Data and methodology for evaluation

The performance of WAMES in estimating the maternal ECG is assessed by comparison with the performance of other techniques on modeled antenatal abdominal recordings. Reason for using modeled recordings is that in real abdominal recordings, the maternal ECG is affected by noise and fetal ECG and hence the absolute performance cannot be assessed quantitatively.

In addition, the performance of WAMES in fetal heart rate detection is assessed by comparing the performance to the performance of other techniques on real antenatal abdominal recordings. The detected fetal heart rate values are validated by comparison to the fetal heart rate detected from a simultaneously performed invasive fetal ECG recording from the fetal scalp.

3.4.1 Data acquisition and modeling

The abdominal recordings are conducted with an M-PAQ amplifier (Maastricht Instruments B.V., the Netherlands), a 16-channel system for physiological measurements with programmable gain and sampling frequency and high input impedance (10^8 Ω). For the abdominal recordings the gain is set at 500 and the sampling frequency at 1 kHz.

The adopted electrode configuration consists of eight contact electrodes on the maternal abdomen with a common reference as shown in Fig. 3.5. This configuration has been chosen since it covers most of the uterine surface, while patient discomfort, resulting from too many electrodes, is minimized.

Modeling antenatal abdominal recordings

Ten 8-channel abdominal recordings of 60 seconds each are performed on a non-pregnant subject with the electrode configuration of Fig. 3.5. To model antenatal abdominal recordings, a fetal ECG signal recorded directly from the fetal scalp during parturition and a Gaussian white noise source are superimposed on the maternal ECG recordings. Note that this model is not an accurate representation of actual antenatal abdominal recordings. However, it is suitable for the assessment of the maternal ECG suppression performance.

For each 8-channel recording, 49 modeled antenatal abdominal recordings are generated having different amplitude ratios between the maternal ECG, fetal ECG, and Gaussian noise. Moreover, the fact that the models are generated using ten different abdominal recordings ensures that the models comprise different degrees of variability in the maternal ECG morphology.

The amplitude ratios between maternal ECG, fetal ECG, and noise are defined as the ratio between the root mean squared (RMS) amplitudes. The employed maternal ECG to noise amplitude ratios range from 7 dB to 17 dB and the employed maternal ECG to fetal ECG amplitude ratios range from 3 dB to 13 dB. Finally, the morphological variability of the different abdominal recordings ranges from 0.15 to 0.32. This variability is defined as the RMS error between the normalized maternal ECG complexes and an maternal ECG template, generated by averaging the normalized maternal ECG complexes.

Real antenatal abdominal recordings

Seven 8-channel antenatal abdominal recordings of 10 minutes each are performed on pregnant subjects during parturition with the electrode configuration of Fig. 3.5. In addition, the direct fetal ECG is recorded simultaneously by an electrode positioned on the fetal scalp and passed on to the M-PAQ through the analog output of an HP8040 fetal monitor (Hewlett-Packard).

The patients have gestational ages ranging from 37 to 41 weeks and the medical indication for the group varies from healthy to preexistent hypertension and preeclampsia.

3.4.2 Preprocessing

As stated previously, antenatal abdominal recordings generally constitute a mixture of fetal ECG, maternal ECG and interferences such as motion artifacts, muscular activity, and powerline interference. In preprocessing the abdominal recordings each of these interferences is suppressed by means of applying a linear-phase filter.

Motion artifacts are suppressed by a 1000 tap FIR high-pass filter with fixed cutoff frequency of 1.5 Hz. This cutoff frequency maximizes the suppression of

the artifacts while minimizing distortion of the fetal ECG signals. The powerline interference is centered around 50 Hz and suppressed by a 1000 tap FIR notch filter with stop-band between 49 and 51 Hz. Harmonics of the powerline interference and part of the noise originating from muscular activity (electromyogram, EMG) are suppressed by a 1000 tap FIR low-pass filter with fixed cutoff at 70 Hz. As the EMG exhibits spectral properties ranging from 0 to 200 Hz this filter only suppresses part of the EMG. However, as the frequency range of the fetal ECG is limited by a upper bound of 70 Hz [99], a lower cutoff frequency would result in distortion of the fetal ECG.

3.4.3 Methodology of evaluation

The performance of WAMES in estimating the maternal ECG in the modeled antenatal abdominal recordings is compared to the performance of spatial filtering, ESAIC, ESC, and LP by assessing the normalized MSE ε between $\mathbf{V}_2$ and $\hat{\mathbf{V}}_2$ (Fig. 3.2):

$$\varepsilon = \frac{\sum\sum\left(\mathbf{V}_2 - \hat{\mathbf{V}}_2\right)^2}{\sum\sum\mathbf{V}_2^2}. \tag{3.12}$$

In addition, the performance of WAMES is compared to ICA by assessing the fetal heart rate detection in real antenatal abdominal recordings. The detection of the fetal heart rate is performed by calculating the interval lengths between consecutive fetal QRS complexes. In the independent source signal representing the fetal ECG the QRS complexes are detected as described in Chapter 5, i.e. as local extrema exceeding a variable threshold.

Detection of the fetal heart rate in the signals obtained by maternal ECG suppression through WAMES is not as straightforward as detection of the fetal heart rate in the independent source signals; in contrast to ICA, WAMES provides an fetal ECG signal for each recorded signal. Through PCA the inter-channel correlation of these fetal ECG signals can be exploited, performing the previously described fetal heart rate detection method on the principal component and hence solving this problem.

Performance of the fetal heart rate detection by both WAMES and ICA is assessed by the sensitivity Se and the positive predictive value PPV:

$$\text{Se } (\%) = \frac{\text{TP}}{\text{TP}+\text{FN}} \cdot 100, \tag{3.13}$$

$$\text{PPV } (\%) = \frac{\text{TP}}{\text{TP}+\text{FP}} \cdot 100. \tag{3.14}$$

Here TP is the number of correctly detected fetal QRS complexes, FN the number of undetected QRS complexes, and FP the number of falsely detected QRS complexes. The golden standard to establish whether fetal QRS complexes are correctly detected or missed are the QRS complexes detected from the simultaneously recorded fetal ECG signal from the fetal scalp.

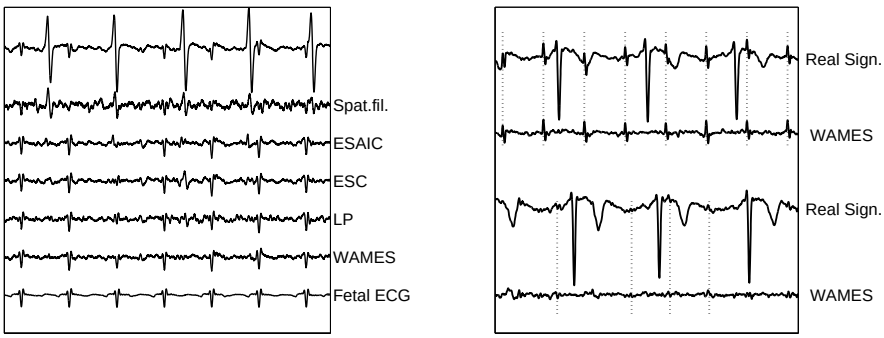

(a) (b)

Figure 3.6: *Results of maternal ECG subtraction on (a) modeled antenatal abdominal recordings and 3.6(b) preprocessed real antenatal abdominal recordings. The maternal ECG subtraction in (a) is performed by spatial filtering, ESAIC, ESC, LP, and WAMES. The upper graph shows the modeled antenatal abdominal recording with maternal ECG to noise ratio 17 dB and maternal ECG to fetal ECG ratio 6 dB. The 5 centered graphs show the resulting signals after subtraction of the maternal ECG estimates. The bottom graph shows the fetal ECG signal (for clarity shortened to fECG) used in the modeled abdominal recording. The maternal ECG subtraction in 3.6(b) is performed by WAMES alone and comprises a best-case scenario in the upper two graphs and a worst-case scenario in the bottom two graphs. The dotted lines indicate the positions of detected fetal QRS complexes. Note that for the worst-case scenario the peaks are detected in the principal component which, in contrast to the real signal shown, does exhibit some fetal ECG signal.*

3.5 Results and discussion

3.5.1 Comparison on maternal ECG estimation

Fig. 3.6(a) shows a modeled antenatal abdominal recording and the signals resulting after subtraction of the maternal ECG estimates by the different techniques. The depicted signals comprise 3 seconds of a 60 second recording. To evaluate the modeled antenatal abdominal recordings with respect to real recordings, in Fig. 3.6(b) the subtraction of maternal ECG estimates by WAMES on real antenatal abdominal recordings is depicted. Fig. 3.7 shows ε for different amplitude ratios between the maternal ECG, the fetal ECG, and the noise and for different degrees of variability in the maternal ECG morphology.

The results depicted in Fig. 3.7 show that WAMES performs better in subtracting

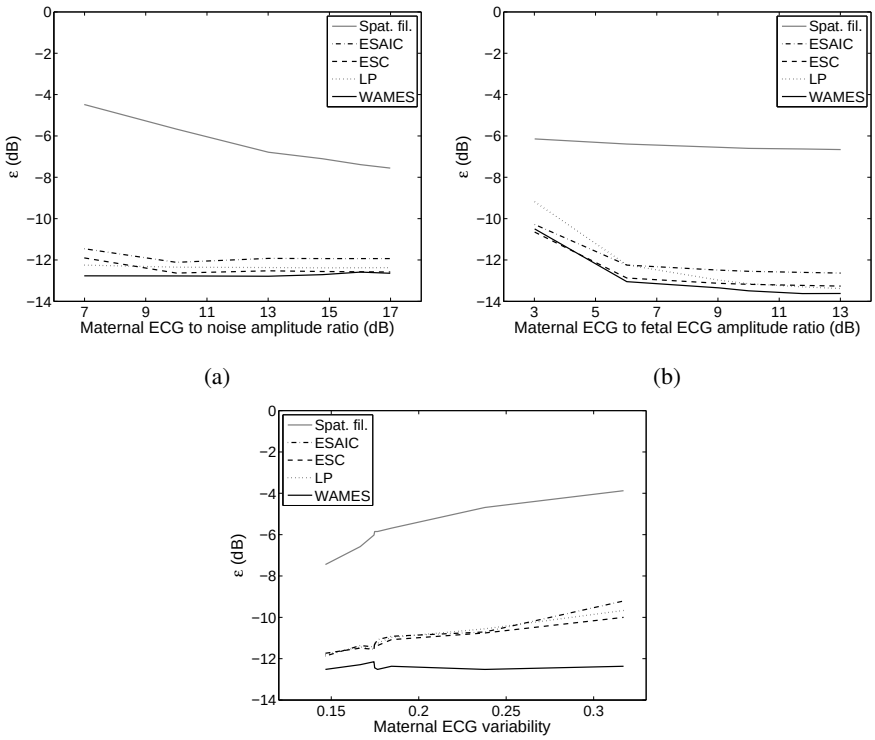

Figure 3.7: *Normalized mean squared error* ε *between the maternal ECG (here, for clarity shortened to mECG) used in the modeled antenatal abdominal recordings and the estimate of this maternal ECG for (a) different maternal ECG to noise amplitude ratios, (b) different maternal ECG to fetal ECG (also shortened to fECG) amplitude ratios, and (c) different degrees of maternal ECG morphological variability. For each plot the values of* ε *are obtained by averaging over the other dimensions, e.g. for (a) the values of* ε *are obtained by averaging over all maternal ECG to fetal ECG amplitude ratios and maternal ECG variability values.*

Table 3.1: *Performance assessment of the detection of fetal QRS complexes. The values in this table represent percentages (%).*

	Se	σ_{Se}	range	PPV	σ_{PPV}	range
Spat. fil.	82.7	3.4	80.0-90.4	91.6	2.8	85.7-94.1
ESAIC	89.8	3.6	87.2-97.2	94.2	2.8	88.4-96.7
ESC	90.1	3.5	87.6-97.5	94.4	2.7	88.9-96.8
LP	90.1	4.0	86.3-97.6	94.2	2.8	88.7-98.9
ICA	91.8	4.0	88.2-99.4	94.8	2.6	89.6-97.3
WAMES	94.8	3.7	89.6-99.3	95.1	1.8	92.5-97.7

the maternal ECG than spatial filtering, ESAIC, ESC, and LP for almost all modeled antenatal abdominal recordings. Moreover, although the differences in performance by WAMES on the one hand and ESAIC, ESC, and LP on the other hand appear to be small, in particular for Fig. 3.7(a) and Fig. 3.7(b), even these small differences in performance can be of major significance. The error in the maternal ECG subtraction is generally of the same order of magnitude as the fetal ECG, especially in early stages of pregnancy, and hence it can significantly corrupt the remaining fetal ECG signal.

For recordings with a small maternal ECG to fetal ECG amplitude ratio, i.e. a large fetal ECG signal, WAMES underperforms ESC. The large amplitude of the fetal ECG complexes causes significant inaccuracies in the maternal ECG segmentation, resulting in a decreased accuracy of maternal ECG estimation. Since ESC performs segmentation after averaging of consecutive maternal ECG complexes, the fetal ECG amplitude is reduced in this average maternal ECG complex and hence the segmentation is affected to a smaller extent. It has to be remarked, though, that this maternal ECG to fetal ECG amplitude ratio is not commonly encountered in medical practice.

Increased variability in the maternal ECG morphology causes no significant difference in estimation error ε for WAMES. In contrast, the other techniques suffer from an increased ε with increasing variability.

3.5.2 Comparison on fetal heart rate detection

In total 70 minutes of data is analyzed, containing 10^4 fetal QRS complexes. The performance of the detection of these complexes by the aforementioned techniques including ICA is presented in Table 3.1, in which Se and PPV are the values averaged over the 7 recordings, σ_{Se} and σ_{PPV} are the standard deviations, and range indicates the minimum and maximum values.

The results presented in Table 3.1 show that the performance of WAMES in detecting the fetal heart rate is slightly better than the performance of the other techniques; the Se of WAMES is 3% larger than the Se of the second best technique

(ICA). The PPV of WAMES is nearly equal to the PPV of the other techniques.

3.5.3 Discussion

In general, WAMES performs better in maternal ECG subtraction and fetal heart rate detection than the other techniques. At first, the 3% difference with ICA might seem rather small. However, since WAMES provides spatial information on the fetal ECG, whereas ICA cannot provide this information unless three independent fetal ECG sources are determined, this 3% difference should be considered as an additional advantage.

Notwithstanding this advantage of WAMES, in cases of maternal ectopic beats, WAMES is expected to underperform in suppressing the maternal ECG and detecting the fetal heart rate with respect to ICA. WAMES is incapable of handling the additional maternal ECG complexes sufficiently accurately as WAMES assumes only small variations in the maternal ECG morphology.

Moreover, subtraction of the estimated maternal ECG signal by WAMES is analogous to the superposition of an error signal to the fetal ECG signal. This error signal constitutes the difference between the maternal ECG and the maternal ECG estimate, and generally has a peaky nature. For recordings with a smaller fetal ECG amplitude, i.e., recordings in stages of pregnancy much earlier than labor, these peaks can be expected to have the same order of magnitude as the fetal ECG and hence might affect the performance of WAMES. For these recordings the fetal heart rate detection by ICA is therefore expected to outperform the fetal heart rate detection by WAMES. In future implementations of fetal heart rate detection methods it can, however, be advantageous to use WAMES as preprocessing step for ICA, exploiting the strong features of both techniques.

A final remark about the presented fetal heart rate detection performances can be made by stating that these results can be improved by applying a dedicated fetal QRS detection method instead of the method discussed in Section 3.2.1.

3.6 Conclusions

In this chapter, a new technique (WAMES) is presented to suppress the maternal ECG from antenatal abdominal recordings in order to extract the fetal ECG and fetal heart rate. WAMES is compared to several other maternal ECG suppression techniques, viz. spatial filtering, ESAIC, ESC, and LP. Moreover, the suitability of WAMES for fetal heart rate monitoring is assessed by comparing the performance in detecting the fetal QRS complexes to the performance of the aforementioned techniques plus ICA. WAMES proves to be more accurate in maternal ECG suppression than the other techniques and performs also better in fetal heart rate detection. In addition, imple-

mentations of WAMES in Matlab® (The Mathworks, Inc.) on a laptop computer with a 1.7 GHz Pentium® processor show that the maternal ECG can be suppressed in real-time. This implementation is executed on a clinical prototype, NEMO, that is currently evaluated in the Máxima Medical Center, the Netherlands. Provisional experience of clinicians is very positive; the added value of the fetal ECG and spectral analysis of the fetal heart rate, however, still needs to be further investigated.

Although WAMES outperforms the other techniques in maternal ECG subtraction, the differences in performance by WAMES and the other techniques appear to be rather small. However, in clinical practice the variability in the maternal ECG morphology is significantly larger than the variability in the recordings used in this study. The reason for this is that the subjects participating in this study were, due to ethical considerations, in general healthy women lying in a comfortable position during the recordings. However, in practice, the most relevant cases are those pregnancies where either mother or fetus is suffering from illness or distress and consequently the mother is not lying comfortable and still anymore. In these situations the maternal ECG morphological variability is expected to be 0.25 or larger (Fig. 3.7(c)) and, as a result, the performance of WAMES is expected to improve with respect to the other techniques.

In conclusion, it can be stated that WAMES provides a tool for maternal ECG suppression in antenatal abdominal recordings for which the performance is relatively insensitive to noise and variability in the maternal ECG morphology. When the main interest for maternal ECG suppression is monitoring of the fetal heart rate, no conclusive statement can be made whether WAMES should be preferred over the other techniques as the available amount of abdominal recordings is not sufficient to render statistical significance. However, for the recordings that are available, WAMES slightly outperforms the other techniques. When the aim is to monitor and analyze of the fetal ECG, WAMES is preferred over the other techniques as it provides relatively accurate spatial information on the fetal ECG, possibly enabling future implementations of fetal vectorcardiography.

Future research, besides the combined employment of WAMES and ICA, fetal vectorcardiography, and development of a dedicated fetal QRS detection method, includes extraction and enhancement of fetal ECG complexes and assessment of the performance of WAMES in cases of maternal or fetal pathology.

Chapter 4

A robust physiology-based source separation method for QRS detection in low amplitude fetal ECG recordings

The signals remaining after subtraction of the maternal ECG in general do not have a signal to noise ratio that renders them suitable for estimation of the fetal VCG right away. In order to enhance the signals, the periodicity of the ECG can be exploited. However, in order to exploit the periodicity, the instantaneous fetal heart rate needs to be accurately known. To facilitate detection of the heart rate, in this chapter a method is presented that utilizes physiological information of the fetal ECG to produce a linear combination of the signals remaining after maternal ECG suppression. This linear combination entails an ECG signal with improved signal to noise ratio and hence facilitates detection of the fetal heart rate.[1]

4.1 Introduction

High-risk pregnancies are becoming more prevalent because of the progressively higher age at which women get pregnant. Ten to twenty percent of all pregnancies are complicated by preterm delivery, fetal hypoxia, fetal growth restriction, or hypertension, yielding a large need for pregnancy monitoring technologies. For monitoring of the well-being of the fetus, the cardiotocogram (CTG; a recording of fetal heart rate in combination with uterine contractions) is commonly used. Subtle changes in fetal heart rate variability may occur as the first signs of fetal distress [8], which could still be reversible at this point if appropriately treated. Extensive studies have, however, shown that the diagnostic predictive value of the CTG is low [20]. To improve this predictive value, additional information is needed, either from more sophisticated analysis of the CTG, such as spectral analysis of the fetal heart rate variability [115],

[1]This chapter is based on the paper published as *R. Vullings, C.H.L. Peters, M.J.M. Hermans, P.F.F. Wijn, S.G. Oei, and J.W.M. Bergmans, "A robust physiology-based source separation method for QRS detection in low amplitude fetal ECG recordings", Physiol Meas. 2010;31(7):935–51.*

or from other sources such as the fetal electrocardiogram (ECG).

With respect to fetal ECG monitoring as an additional source of information, the currently available technique has one important limitation. This limitation is that recording of the fetal ECG is currently only possible during labor, by applying an electrode to the fetal scalp. Applying this electrode is cumbersome for both patient and clinician. As an alternative, the fetal ECG can also be recorded non-invasively from the maternal abdomen. In contrast to the invasive ECG, this abdominal ECG recording can be performed in all stages of pregnancy, but due to the typically low signal to noise ratio (SNR) of the abdominal fetal ECG, this non-invasive technique has not found its way to clinical practice yet.

The maternal ECG is generally the dominant interference in the abdominal fetal ECG recordings. Numerous methods to suppress this maternal ECG have been proposed in literature [92, 94, 95, 118] and in Chapter 3, of which many perform reasonably well. Even so, because the fetal ECG recordings are also corrupted by other interferences and noise, even after suppression of the maternal ECG, the SNR of the fetal ECG is generally still relatively low. The most straightforward approach to overcome this problem is to enhance the SNR of the fetal ECG by averaging several consecutive ECG complexes, all synchronized on their QRS complex. Unfortunately, this approach requires knowledge on the locations of QRS complexes, which are difficult to determine from the low SNR fetal ECG recordings [128, 129].

Consequently, in order to fully exploit the time correlation of the fetal ECG, the abdominal fetal ECG recordings need additional processing – next to maternal ECG suppression – to facilitate detection of the QRS complexes. In a simplified model, the electrical activity of the heart can be assumed to be represented by a single electrical field vector that varies in amplitude and orientation over time [32, 64]. The time-path of this field vector is referred to as the vectorcardiogram (VCG). In this model, each ECG signal corresponds to the projection of the VCG onto the lead vector indicating the electrode position with which the ECG signal is obtained. This projection constitutes a linear combination of the three orthogonal components into which the VCG can be decomposed. As a consequence all abdominal fetal ECG signals have to be spatially related to one another.

To exploit this spatial relation, several powerful mathematical techniques are available, of which *principal component analysis* (PCA) and *independent component analysis* (ICA) are the most prominent [130, 131]. These techniques operate by linearly combining the fetal ECG signals in such way that the resulting combinations exhibit either maximum variances (PCA) or maximum statistical independency (ICA) [132]. A disadvantage of these techniques is that the resulting linear combinations are randomly ordered, requiring additional processing to determine which combination should be attributed to the fetal ECG.

Another disadvantage is that PCA and ICA, although they are categorized as

source separation techniques, in general do not provide all three independent, orthogonal components (i.e. separate sources) of the VCG, but usually only one or two [133]. In addition, they do not include physiological considerations and, hence, are generally referred to as blind source separation (BSS) techniques. This lack of physiological basis can render the BSS techniques less effective in separating the fetal ECG signals from a mixture of these ECG signals and noise. In fact, typically in cases of low SNR, it occurs frequently that the BSS techniques are not capable of extracting the fetal ECG signals. To overcome this problem of robustness against noise – and as a side effect, also the problem of unknown order of the generated linear combinations – in this chapter a physiology-based source separation (PBSS) technique is developed.

The PBSS technique operates by spatially combining the abdominal signals, based on knowledge about the positions of the recording electrodes, to obtain a three-dimensional representation of the signals. This three-dimensional representation is related to the fetal VCG and, although it is still corrupted by noise, typically exhibits a higher SNR than the signals that were available before the spatial combining. The main advantage of this SNR enhancement is that it is relatively robust to noise. After spatial combination of the fetal ECG signals, the three-dimensional representation is approximated by fitting an ellipse to the combined data points. The paradigm of fitting a two-dimensional ellipse to three-dimensional data is explained in Section 4.2. The sources that are associated to the fetal ECG can, subsequently, be obtained by projecting the three-dimensional representation of the abdominal signals onto the long axis, the short axis and the normal vector of this ellipse.

To recapitulate, in this chapter a PBSS technique is developed that overcomes robustness issues that are associated with blind techniques such as PCA and ICA. The PBSS technique is used to generate a linear combination of fetal ECG signals in such way that it exhibits increased SNR with respect to the original fetal ECG signals, thus facilitating detection of the QRS complexes. By averaging consecutive ECG complexes, synchronized on the QRS complexes, in turn, the non-invasive fetal ECG signals can be enhanced, potentially providing them with sufficient quality to support clinical decision-making.

The PBSS technique is evaluated by assessing its performance in spatially combining fetal ECG signals obtained from real abdominal recordings on women with various gestational ages and detecting the QRS complexes from the spatially combined signal. The performance is gauged by comparing it to the performance of both PCA and ICA on the same abdominal signals. More specifically, the performance of the PBSS technique is compared to that of PCA and ICA on unprocessed abdominal recordings (i.e. without suppression of the maternal ECG) and to that of PCA and ICA on preprocessed abdominal recordings (i.e. after suppression of the maternal ECG). The latter two approaches are expected to improve the performance of the re-

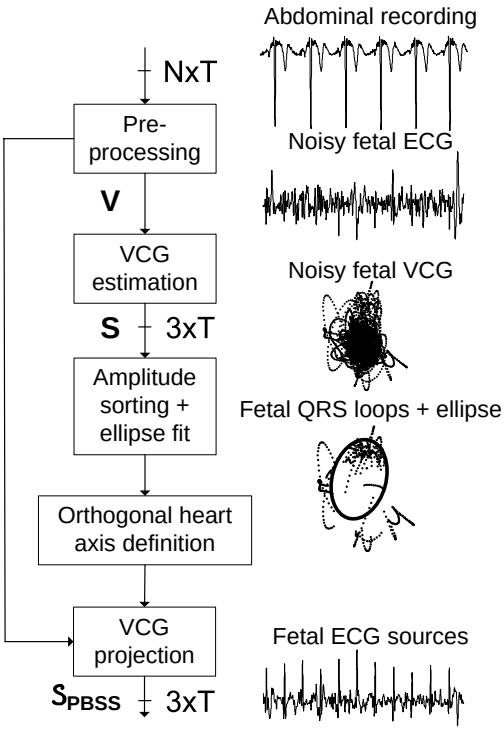

Figure 4.1: *Block scheme of the physiology-based source separation technique. Each of the blocks is discussed in detail in Section 4.2 with the exception of the Preprocessing block, which is discussed in Section 4.4. On the right, typical examples of the signals that are used as inputs for the various blocks are depicted.*

spective BSS techniques PCA and ICA in the sense that the maternal ECG does not longer play a role in the source separation. The PCA and ICA technique are briefly discussed in Section 4.3, while the methodology for the comparison is discussed in Section 4.4. The results are presented in Section 4.5 and finally discussed in Section 4.6.

4.2 Physiology-based source separation

The PBSS technique is discussed in separate parts, each in a different subsection. The mutual connection between these parts of the PBSS technique is schematically depicted in Fig. 4.1.

4.2.1 VCG estimation

The abdominal fetal ECG signals can be assumed linear combinations of three orthogonal signals that together constitute the VCG. This implies that three independent ECG signals are enough to fully describe the VCG, meaning that all additional ECG signals are redundant, yet can be used to enhance the robustness of the VCG determination against noise. Taking the VCG to be represented by the $[3 \times T]$ matrix $\mathbf{S}$, where each row represents one of the orthogonal signals of length T, and taking the N abdominal fetal ECG signals to be represented by the $[N \times T]$ matrix $\mathbf{V}$, the relation between the VCG and ECG can be described by

$$\mathbf{V} = \mathbf{DS}, \tag{4.1}$$

with $\mathbf{D}$ the $[N \times 3]$ matrix containing electrode positions. This matrix is determined from analysis of photographs of the abdomen, taken from several, orthogonal directions. The linear combination of the three orthogonal signals is, thus, described by the projection of the VCG $\mathbf{S}$ onto the electrode position vector (i.e. lead vector), as mentioned in Section 4.1. Inverting Eq. (4.1) gives

$$\mathbf{S} = \left(\mathbf{D}^T\mathbf{D}\right)^{-1}\mathbf{D}^T\mathbf{V} = \mathbf{D}^\dagger\mathbf{V} \tag{4.2}$$

where $\mathbf{D}^\dagger$ is the Moore-Penrose inverse of the matrix $\mathbf{D}$, also referred to as the inverse Dower matrix [47]. The calculation of the VCG is illustrated in Fig. 4.1 as *VCG estimation*. It has to be noted, here, that the ECG signals $\mathbf{V}$ comprise several heartbeats and that the VCG $\mathbf{S}$ therefore shows the time path of the electrical field vector for several heartbeats overlayed on one another.

In addition, it has to be noted that the VCG estimation limits the SNR gain that can be potentially reached by the PBSS technique. That is, by the weighted combination of individual ECG signals – as done, albeit in different forms, by PCA and ICA – the possible increase in SNR is larger than can be reached from the projection of $\mathbf{S}$ onto any vector. However, since the goal of the PBSS technique is not to obtain a maximum SNR but to provide a means for robustly detecting QRS complexes, this limitation of the PBSS technique is of minor concern. In fact, the reason for adopting the VCG estimation approach in the PBSS technique is to ensure that spatial correlation is exploited in all cases – even when this correlation cannot be directly assessed from the ECG signals themselves – to, at least, some extent.

4.2.2 Amplitude sorting

The QRS complexes of the ECG generally entail the parts with the largest amplitude. However, because these QRS complexes also comprise only a small fraction of the ECG signals, the fetal VCG $\mathbf{S}$ usually represents itself as a scatter plot in which most

points in the plot will be focused near the origin of the axes system. Since these points (i.e. the points near the origin) are not associated to the QRS complexes, omitting these points from the scatter plot results in a scatter plot in which most points are associated with the QRS complexes. This omission is justified since the purpose of the PBSS technique is to spatially combine the fetal ECG signals in such way that the SNR of the QRS complexes is enhanced, rather than that the SNR of the complete ECG signals is enhanced. As the QRS complex of a fetus lasts about 40 ms [55] and the time between two heartbeats lasts about 400 ms (i.e. a heartrate of 150 beats per minute), only the top 10% of the points needs to be retained (i.e. the points with the largest distance from the origin of the scatter plot). To prevent potentially present artifacts from affecting the further processing of the data points, any point that is further away from the origin than twice the mean distance, determined over the points remaining after omission of the bottom 90%, is omitted as well. The omission of the low amplitudes and potential artifacts in the VCG scatter plot is indicated in Fig. 4.1 as *amplitude sorting*.

Besides the fact that the QRS complexes exhibit a superior SNR with respect to the rest of the ECG, they have another property that renders them advantageous to the purpose of the PBSS technique: they have an almost planar shape [134]. As a consequence of this planar shape, the scatter plot of the overlayed QRS complexes can be approximated by a two-dimensional mathematical function. Since random noise would cause the scatter plot to have a circular shape (i.e. a spherical shape in three dimensions), any spatial correlation would interfere with the symmetrical shape of this circle, causing it to obtain a preferential direction. This preferentially directed scatter plot of overlayed QRS complexes is approximated here by an ellipse.

4.2.3 Ellipse fitting

To facilitate the fitting of the two-dimensional ellipse to the three-dimensional scatter plot, each point in the scatter plot can be projected onto the three orthogonal planes of a Cartesian coordinate system. In each of these planes, the scatter plot can again be approximated by an ellipse, but now in a two-dimensional plane. At first sight this might pose a problem to the ellipse approximation in the three-dimensional scatter plot, as the three orthogonal ellipses fitted in the two-dimensional planes cannot readily be combined to yield a single ellipse in three-dimensional space. However, the main interest in the PBSS technique is to find the preferential direction of the scatter plot (i.e. the direction of the long axis of the ellipse) and this direction can be readily obtained from combination of the preferential directions in the three two-dimensional ellipse fits. In addition, as in each of the orthogonal planes two components of the three-dimensional preferential direction are determined, each component is determined twice. That is, in the xy-plane, the x and y component of the preferential direction are determined and in the xz-plane the x component is determined a

second time. The match between these two independent determinations yields a direct way to assess the reliability of the ellipse fits; good correspondence between the various components signifies an accurate ellipse fit in each of the orthogonal planes, whereas poor correspondence signifies an inaccurate ellipse fit and thus an inaccurate estimation of the preferential direction in the scatter plot.

The ellipses are fitted in the two-dimensional planes using a least squares approach. In this approach the ellipse is described by the conic equation:

$$f(\vec{x},\vec{a}) = a_1x^2 + a_2xy + a_3y^2 + a_4x + a_5y + a_6 = 0. \tag{4.3}$$

For given $\vec{a}$, the ellipse is fully described and only for points $\vec{x}_i$ that lie exactly on the ellipse the conic equation of Eq. (4.3) will equal zero. Any deviation in the conic equation for $\vec{x}_i$ will therefore yield a measure for the error of the ellipse fit. By minimizing the mean square of this error, ε:

$$\varepsilon = \frac{1}{T}\sum_{i=1}^{T}\left(a_1x_i^2 + a_2x_iy_i + a_3y_i^2 + a_4x_i + a_5y_i + a_6\right)^2 \tag{4.4}$$

the optimal estimate $\hat{\vec{a}}$ for the ellipse parameters can be assessed.

Prior to estimation of the ellipse parameters, the potential bias of the ellipse is removed by subtracting the mean value of the scatter points across each dimension. The fitting of an ellipse to the scatter plot is indicated in Fig. 4.1 as *ellipse fit*.

4.2.4 Orthogonal heart axis definition

As mentioned previously, the preferential direction of the scatter plot is approximated by the direction of the long axis of the ellipse. In the two-dimensional planes onto which the scatter plot is projected, the direction and the amplitude of this long axis can be readily assessed by determining the distance $|\vec{r}_{\text{long}}|$ and the orientation ϕ_{long} between the origin of the fitted ellipse and the point on the ellipse for which the distance to the origin is largest.

With the amplitude and orientation of the long axis determined for each orthogonal plane, the long axis can be decomposed into two components; e.g. for the xy-plane it can be decomposed into

$$r^x_{\text{long}} = \left|\vec{r}_{\text{long}}\right|\cos\phi_{\text{long}} \qquad \text{and} \qquad r^y_{\text{long}} = \left|\vec{r}_{\text{long}}\right|\sin\phi_{\text{long}}. \tag{4.5}$$

The direction of the long axis in three-dimensional space follows from fitting the ellipse in all three orthogonal planes and subsequent averaging of each of the twice determined (as discussed in Section 4.2.3) long axis components, i.e. r^x_{long}, r^y_{long}, and r^z_{long}.

By projecting the scatter plot onto this three-dimensional long axis, one of the three fetal ECG sources $\mathcal{S}_{\text{PBSS}}$ can be obtained. The other two sources can be determined straightforwardly, i.e. by projecting the scatter plot onto the short axis of the fitted ellipse and onto the normal vector of the ellipse plane. The direction of the short axis of the ellipse is determined similarly as the direction of the long axis, except that the length $|\vec{r}_{\text{short}}|$ and orientation ϕ_{short} of the short axis are determined from the point on the ellipse at orientation $\phi_{\text{short}} = \phi_{\text{long}} + \frac{\pi}{2}$. The direction of the normal vector, in turn, is determined by

$$\vec{r}_{\text{normal}} = \vec{r}_{\text{long}} \times \vec{r}_{\text{short}}, \tag{4.6}$$

where $\bullet \times \bullet$ denotes the vector-product. The determination of the directions of these three axes (i.e. the long axis, short axis, and normal vector) are indicated in Fig. 4.1 as *orthogonal heart axis definition*.

4.2.5 VCG projection

Although the projection of the scatter plot onto the three axes of the fitted ellipse provides three linearly independent sources of the fetal ECG, the method as described in this section may not seem a source separation technique. However, when recalling that the scatter plot of the fetal VCG is obtained by multiplying the ECG signals matrix $\mathbf{V}$ with $\mathbf{D}^{\dagger}$, the mixing matrix $\mathbf{M}_{\text{PBSS}}$ that maps the ECG signals onto the independent sources can be expressed as

$$\mathbf{M}_{\text{PBSS}} = \begin{pmatrix} \vec{r}_{\text{long}} \\ \vec{r}_{\text{short}} \\ \vec{r}_{\text{normal}} \\ \vdots \end{pmatrix} \mathbf{D}^{\dagger}. \tag{4.7}$$

Here, the dots on the bottom rows indicate potential projections onto other directions. These latter projections, however, do not represent any of the fetal ECG sources. The independent sources $\mathcal{S}_{\text{PBSS}}$ are subsequently determined as

$$\mathcal{S}_{\text{PBSS}} = \mathbf{M}_{\text{PBSS}}\mathbf{V}. \tag{4.8}$$

The projection of the VCG onto the axes of the fitted ellipse is indicated in Fig. 4.1 as *VCG projection*.

In Fig. 4.2, the PBSS method is illustrated by means of three examples. These examples comprise some of the original fetal ECG signals, the amplitude sorted VCG's and their corresponding ellipse fits, and the fetal ECG signals originating from the VCG projection. The three depicted examples each have different SNR; the first has relatively high SNR, the second has average SNR, and the last has an SNR of zero (i.e. the fetal ECG signals are replaced by Gaussian noise signals).

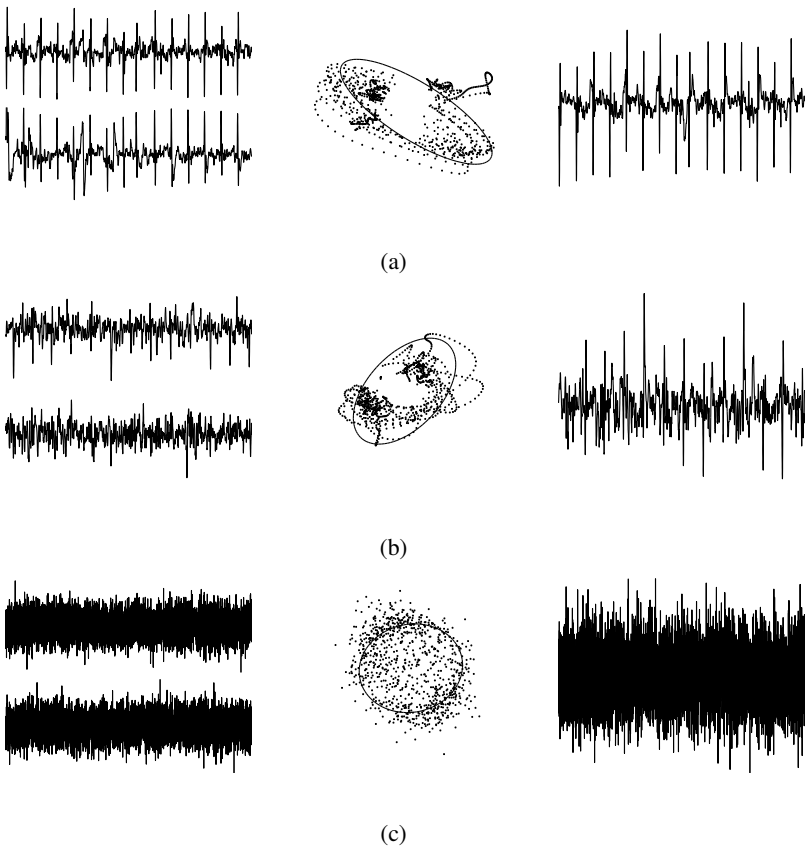

Figure 4.2: *Illustration of the PBSS method. In (a) the method is applied on fetal ECG signals with a relatively high SNR, in (b) the method is applied on signals with an average SNR, and in (c) the method is applied on Gaussian noise signals. For each of the examples, the graphs on the left show two of the N recorded fetal ECG signals. The center plot shows the scatter plot of the amplitude sorted VCG and its associated ellipse fit. The right plot shows the source signal resulting from projection of the VCG onto the long axis of the ellipse.*

From the examples in Fig. 4.2 it can be seen that, as expected, the fitted ellipse becomes more and more spherical with lower SNR. That is, the VCG scatter plot loses its preferential direction when the noise becomes more dominant.

4.3 Blind source separation

4.3.1 Principal component analysis

In PCA the correlated fetal ECG signals $\mathbf{V}$ are transformed into a number of uncorrelated signals called principal components. The first principal component accounts for as much of the variability in $\mathbf{V}$ as possible. In turn, each succeeding components accounts for as much of the remaining variability as possible.

The principal components can be calculated using the covariance method [135]. In this method, the fetal ECG signals $\mathbf{V}$ are multiplied with an orthonormal transformation matrix $\mathbf{P}$ such that the resulting sources $\mathcal{S}_{\text{PCA}}$ are uncorrelated:

$$\mathcal{S}_{\text{PCA}} = \mathbf{P}^T\mathbf{V} \tag{4.9}$$

with the constraints that $\text{cov}(\mathcal{S}_{\text{PCA}})$ is a diagonal matrix and that $\mathbf{P}^T = \mathbf{P}^{-1}$. Consequently, with substitution of Eq. (4.9)

$$\begin{aligned} \text{cov}\left(\mathcal{S}_{\text{PCA}}\right) &= \mathbf{E}\left[\mathcal{S}_{\text{PCA}}\mathcal{S}_{\text{PCA}}^T\right] \\ &= \mathbf{P}^T\mathbf{E}\left[\mathbf{V}\mathbf{V}^T\right]\mathbf{P} \\ &= \mathbf{P}^T\text{cov}\left(\mathbf{V}\right)\mathbf{P}. \end{aligned} \tag{4.10}$$

Since $\text{cov}(\mathcal{S}_{\text{PCA}})$ is a diagonal matrix, Eq. (4.10) is nothing more than an Eigenvector problem:

$$\mathbf{P}\text{cov}\left(\mathcal{S}_{\text{PCA}}\right) = \text{cov}\left(\mathbf{V}\right)\mathbf{P}. \tag{4.11}$$

Thus, by solving the Eigenvector problem of Eq. (4.11), the orthonormal transformation matrix $\mathbf{P}$ can be assessed and, using Eq. (4.9), the sources $\mathcal{S}_{\text{PCA}}$ determined.

The source that represents the fetal ECG is selected from the N sources by visual inspection.

4.3.2 Independent component analysis

The assumption of uncorrelated source signals in PCA is extended by the assumption of statistical independency for ICA. ICA operates by estimating both the independent sources of the fetal ECG $\mathcal{S}_{\text{ICA}}$, defined as

$$\mathcal{S}_{\text{ICA}} = \mathbf{M}_{\text{ICA}}\mathbf{V}, \tag{4.12}$$

and the mixing matrix $\mathbf{M}_{\mathrm{ICA}}$ by linearly combining the fetal ECG signals $\mathbf{V}$ in such way that the resulting combinations exhibit a distribution that is as little Gaussian as possible. The Central Limit Theorem states that the distribution of a sum of random variables tends towards a Gaussian distribution [136]. Thus, a combination of two random variables exhibits a distribution that is closer to a Gaussian distribution than the distribution of any of the two original variables. Hence, minimizing the Gaussianity of the source signals, maximizes their statistical independency.

In fact, the ICA approach is to some extent similar to the developed PBSS technique. Since signals containing only Gaussian noise would yield a spherical scatter plot in the PBSS technique, the search for a preferential direction in the scatter plot can be regarded as the maximization of the non-Gaussianity of the source signals. The main difference between the two techniques, however, is that the PBSS technique, before maximizing the non-Gaussianity, uses physiological knowledge on the spatial correlation of the signals by calculating the VCG, reducing the dimension of the problem from N to 3.

For implementation of ICA implementation, the FastICA algorithm [137] is used. As with PCA, the source representing the fetal ECG is selected from the calculated independent sources by visual inspection.

4.3.3 Application of BSS techniques

The PCA and ICA techniques are both applied on the fetal ECG signals in two different ways. In the first way, they are applied similar to the PBSS technique: both PCA and ICA are applied on fetal ECG signals that have been preprocessed to suppress the maternal ECG. The results of these approaches are labeled as augmented PCA (aPCA) and augmented ICA (aICA). In the second way, both BSS techniques are applied on fetal ECG signals in which the maternal ECG has not yet been suppressed. The reason for using this second approach as well is that both PCA and ICA are capable of extracting a fetal ECG source signal from unprocessed abdominal fetal ECG recordings [130, 131]. The source signals resulting from this approach might differ significantly from the ones determined from the preprocessed ECG recordings as potential negative aspects of the maternal ECG suppression do no longer play a role. The source signals resulting from the second approach are labeled PCA and ICA.

It has to be noted the comparison between the PBSS technique, aPCA, and aICA on the one hand and PCA and ICA on the other hand at first sight seems to be unfair as PCA and ICA have to deal with more interferences (i.e. the maternal ECG) than PBSS, aPCA, and aICA. However, as most applications of PCA and ICA in the field of fetal monitoring are used in the way that PCA and ICA are used here, the application of PCA and ICA is included in this chapter for reasons of completeness.

As with the aPCA and aICA approach, also for PCA and ICA the source sig-

Figure 4.3: *Photograph of the electrode configuration and the NEMO data acquisition system. The common reference electrode near the umbilicus is not attached in this photograph. (Photo by Bart van Overbeeke.)*

nal that represents the fetal ECG is selected from the calculated sources by visual inspection.

4.4 Evaluation

4.4.1 Fetal ECG signals

Data acquisition and preprocessing

The fetal ECG signals are recorded from the maternal abdomen using 8 contact electrodes on the maternal abdomen with a common reference near the umbilicus (see Fig. 4.3). The signals recorded with these electrodes are digitized using the NEMO system (Maastricht Instruments BV, the Netherlands), an 8-channel dedicated amplifier with programmable gain and sampling frequency, set at 500 and 1 kHz, respectively, and high input impedance.

The signals acquired from the maternal abdomen contain a mixture of fetal ECG, maternal ECG, muscular activity, and other interferences. The maternal ECG, being the predominant interference, is suppressed by the dynamic template subtraction technique presented in Chapter 3. The other interferences are partly suppressed using frequency-selective filtering, but due to the overlap with the frequency content of the

fetal ECG [99] a significant fraction of these interferences remains. The filtering and the suppression of the maternal ECG are referred to in Fig. 4.1 as *preprocessing*.

Patient demographics

In total, 17 recordings of 5 minutes each are performed on 17 different patients, ranging between 21 weeks of gestational age and term. For one of the recordings at term, also the invasive fetal scalp ECG was simultaneously recorded. All women were healthy and had uncomplicated singleton pregnancies.

4.4.2 Evaluation criteria

The performance of the developed PBSS technique is evaluated by comparing it to the performance of the BSS techniques aPCA and aICA (and PCA and ICA). To quantify the performance, the quality of the determined linear combination (i.e. source signal) of the fetal ECG signals, two approaches are used.

In the first approach, the percentage of fetal QRS complexes that are detected correctly in the linear combination serves as measure of the performance. The percentage of correctly detected QRS complexes is expressed here by the sensitivity Se and positive predictive value PPV:

$$\text{Se } (\%) = \frac{\text{TP}}{\text{TP}+\text{FN}} \cdot 100 \tag{4.13}$$

$$\text{PPV } (\%) = \frac{\text{TP}}{\text{TP}+\text{FP}} \cdot 100, \tag{4.14}$$

with TP the number of correctly detected fetal QRS complexes (true positives), FN the number of undetected QRS complexes (false negatives), and FP the number of falsely detected QRS complexes (false positives). For the first sixteen recordings mentioned above, these numbers are assessed by visual analysis, while for the last recordings they are assessed from the comparison to the simultaneously performed invasive scalp ECG recording. The QRS complexes are detected in the linearly combined signal as peaks exceeding an adaptive threshold [46, 138]. This detection method is further detailed in Chapter 5.

For the second approach of quantifying the performance, the SNR of the determined linear combination is estimated. This is achieved by using the detected QRS complexes to calculate an average ECG complex for the linear combination. By comparing this average ECG complex $\hat{\vec{V}}$ to the various ECG complexes $\vec{V}_i$ in the linear combination, a measure ψ_{SNR} for the SNR can be obtained:

$$\psi_{\text{SNR}} \text{ (dB)} = 10\log \frac{1}{n}\sum_{i=1}^{n} \frac{\hat{\vec{V}}\hat{\vec{V}}^T}{\left(\vec{V}_i - \hat{\vec{V}}\right)\left(\vec{V}_i - \hat{\vec{V}}\right)^T}, \tag{4.15}$$

with n the number of ECG complexes in the 5 minute long signals. Note that both the averaged ECG and the individual ECG complexes are represented by a $[1 \times T]$ row vector here instead of by a $[N \times T]$ matrix as in Eq. (4.1) because the linear combination yields only one signal.

4.5 Results

In Fig. 4.4(a) an example of an 8 lead fetal ECG recording is shown for the patient at term, for which also the invasive fetal ECG was recorded simultaneously. In Fig 4.4(b) the calculated sources for each source separation technique (i.e. PBSS, aPCA, aICA, PCA, and ICA) are shown, together with the simultaneously recorded fetal scalp ECG signal. The circles in the plot indicate the detected QRS complexes and for the PBSS technique only the source along the long axis of the fitted ellipse is depicted. Note that for the aPCA method, at about 8.7 s, one of the fetal QRS complexes is missed by the peak detection algorithm. The graphs in Fig. 4.4 only show the signals for a period of 10 s and for one patient.

The results of the evaluation of either method in terms of the sensitivity, the positive predictive value, and the SNR for all recordings is shown in Figs. 4.5, 4.6, and 4.7.

The results in Figs 4.5–4.7 indicate that PCA and ICA perform worse than the other techniques for almost all recordings. Intuitively, this difference in performance can be explained by the fact that both PCA and ICA can maximally calculate 8 source signals from the 8-channel abdominal fetal ECG recordings [135,136]. Without prior suppression of the maternal ECG and other interferences, most of the 8 calculated source signals still are a linear combination of the actual source signals. That is, if each of the abdominal signals constitutes a linear combinations of e.g. 10 independent source signals, the $[8 \times T]$ matrix $\mathbf{V}$ cannot be fully decomposed into a $[10 \times T]$ matrix $\mathbf{S}$ but only into a $[8 \times T]$ matrix. Hence, the 8 source signals calculated by PCA and ICA cannot fully correspond to the 10 original independent sources signals. This implies that the source signal representing the fetal ECG will be a linear combination of the actual fetal ECG and noise. For PBSS, aPCA, and aICA, on the other hand, some of the independent source signals (i.e. maternal ECG and part of other interferences) are *a priori* suppressed from $\mathbf{V}$, facilitating improved decomposition of $\mathbf{V}$ into the original source signals.

From Figs. 4.5–4.7 it can also be seen that where aPCA and aICA show occasional reductions in Se, PPV, or ψ_{SNR}, the performance of PBSS is rather constant. Moreover, the performance of the PBSS technique is in most cases larger, albeit marginally, than the performance of aPCA and aICA. From this finding it can, therefore, be concluded that the PBSS technique performs similarly well as, or even better than, the aPCA and aICA techniques and has the additional advantage that its perfor-

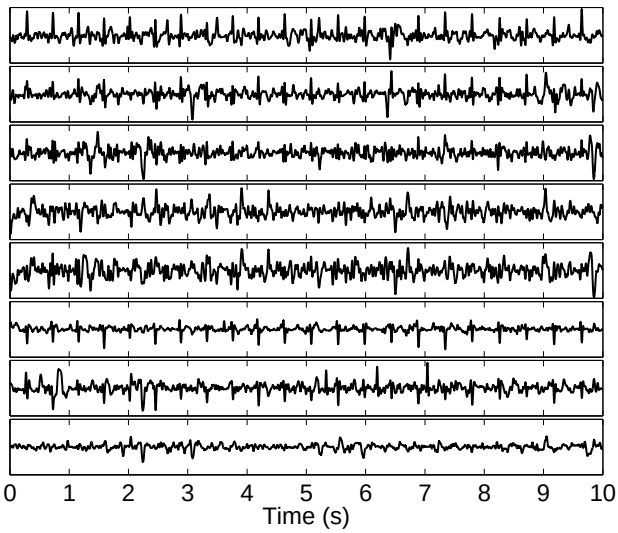

(a)

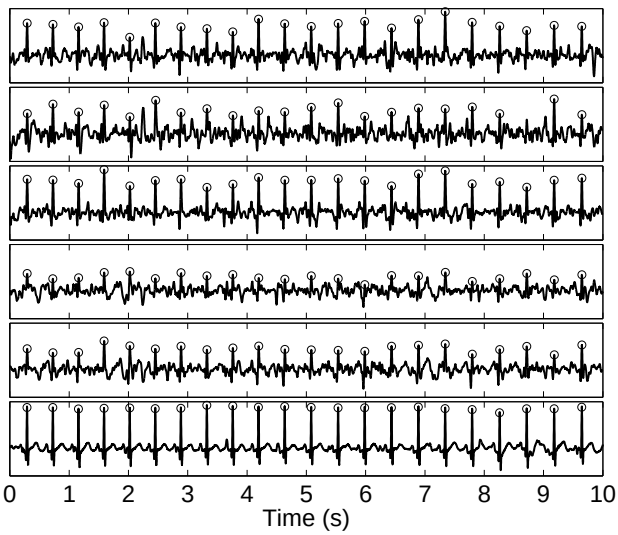

(b)

Figure 4.4: *Example of (a) 8 lead fetal ECG signals obtained with the electrode configuration of Fig. 4.3 and (b) the calculated sources signals from PBSS (top graph), aPCA (second graph), aICA (third graph), PCA (fourth graph), and ICA (fifth graph) plus the simultaneously recorded invasive fetal scalp ECG (bottom graph). The detected fetal QRS complexes are indicated with the circles.*

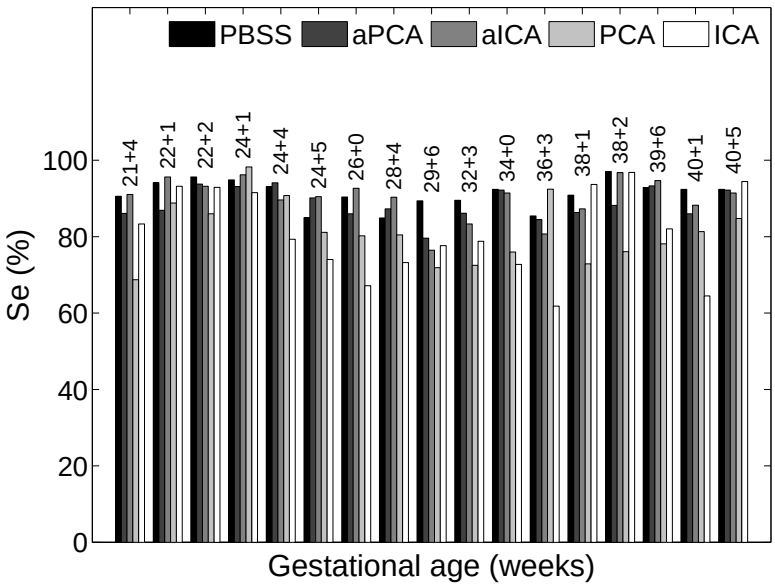

Figure 4.5: *Sensitivity of the QRS detection for all 17 recordings and for each of the source separation techniques.*

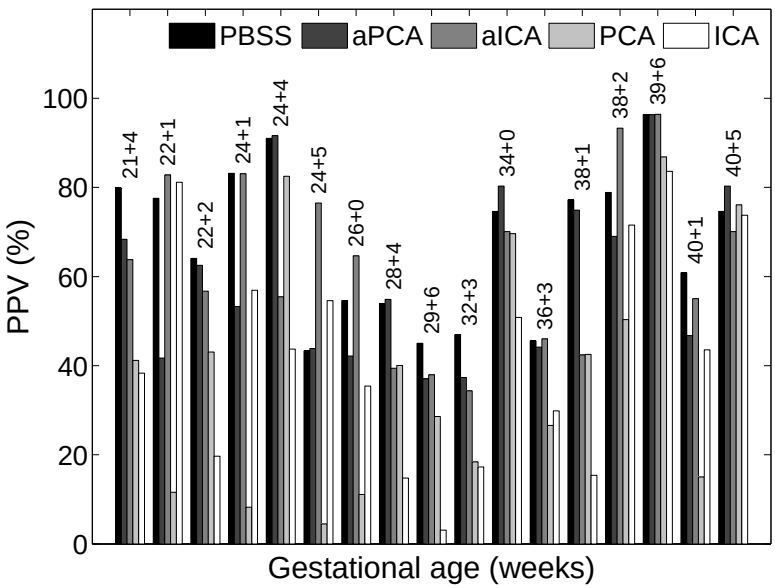

Figure 4.6: *Positive predictive value of the QRS detection for all 17 recordings and for each of the source separation techniques.*

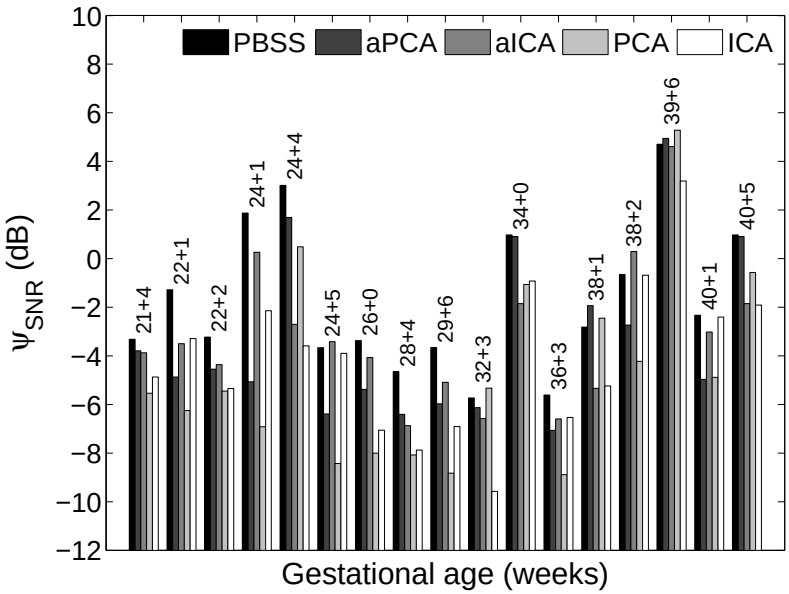

Figure 4.7: *SNR ψ_{SNR} of the source signals for all 17 recordings and for each of the source separation techniques.*

mance is more robust.

Finally, Figs. 4.5–4.7 show that the performance of all methods exhibits a reduction between 26 and 32 weeks of gestation. This reduction in performance can be explained by the development of the vernix caseosa, a waxy layer that electrically isolates the fetus from its surroundings, develops around 28 weeks of gestation, and start to shed around 32 weeks of gestation. In addition, it can be seen that, whereas the performance in terms of the Se is rather constant, the performance in terms of ψ_{SNR} and PPV value fluctuates more and shows a relation between ψ_{SNR} and PPV. That is, for high σ also the PPV is relatively high; for low ψ_{SNR}, also the PPV is low. This relation can be explained by the fact that a small ψ_{SNR} signifies more noise in the ECG signal. This higher noise level, in turn, increases the possibility of the noise to be (incorrectly) detected as a QRS complex. The fact that Se is less affected by noise can be explained by the fact that the Se is governed by the ratio between the correctly detected QRS complexes (TP) and the missed QRS complexes (FN). These missed complexes not only occur as a result of increased noise levels, but also occur due to the fact that during the suppression of the maternal ECG some of the fetal QRS complexes are suppressed or affected as well. The latter effect is independent of noise levels and hence explains the relation between Se and ψ_{SNR}.

As mentioned in Section 4.1, a side effect of the developed PBSS technique is that it also overcomes the problem of unknown order of the source signals determined by aPCA and aICA (and PCA and ICA). Due to this problem, these techniques required

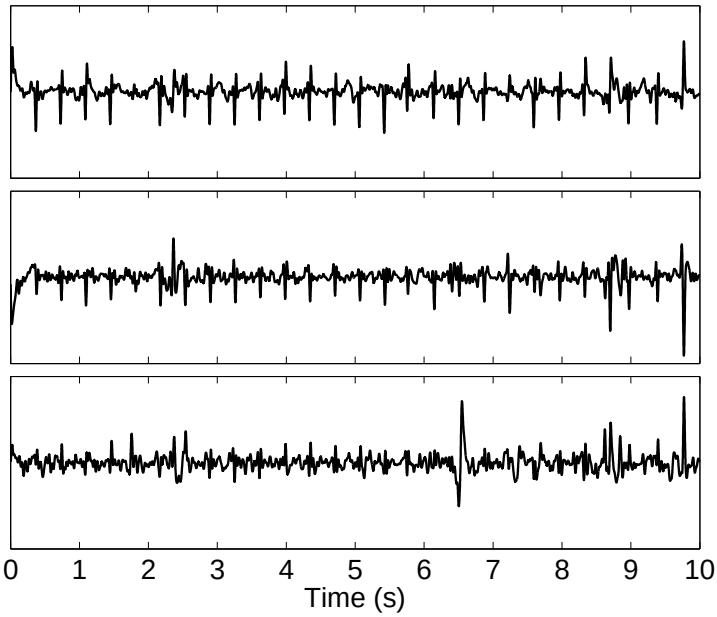

Figure 4.8: *Three source signals determined for the fetal ECG recording at 28 weeks of gestation. The top graph shows the projection of the VCG onto the long axis of the fitted ellipse. The middle graph shows the projection on the short axis of the ellipse and the bottom graph show the projection onto the normal vector of the ellipse plane.*

additional signal processing to identify which of the calculated source signals represents the fetal ECG. Although this is a triviality in source signals with a relatively high SNR, for signals with a low SNR this can impose a significant problem to automated applications of the techniques. In addition, neither of these BSS techniques provides all three orthogonal sources of the ECG in all situations. The PBSS technique, on the other hand, is capable of calculating all three sources, as shown in Fig. 4.8 for the patient at 28 weeks of gestation.

In each of the three sources in Fig 4.8 the fetal ECG can be distinguished, although the projection normal to the ellipse plane shows significant artifacts. These artifacts are caused by residues of the maternal ECG, originating from imperfections in the dynamic template subtraction technique [46].

4.6 Discussion & Conclusions

The developed PBSS technique provides a method for linearly combining low SNR fetal ECG signals in such way that the linear combination has an improved SNR, thus facilitating detection of the fetal QRS complexes. The method performs more robustly than the BSS techniques aPCA and aICA and has the additional advantages that no additional signal processing for identifying the source signal that represents the fetal ECG is required and that it always provides three linearly independent sources of the fetal ECG. In addition, the PBSS technique (and also aPCA and aICA) significantly outperforms PCA and ICA for all abdominal fetal ECG recordings.

In terms of the SNR of the determined source signals, the PBSS technique does not perform optimally. The reason for this suboptimal performance is the fact that the technique is aimed to enhance the SNR of the QRS complexes alone and does not consider the other features of the ECG. Consequently, in some situations aPCA and aICA outperform the PBSS technique as these techniques do consider the whole ECG complex, rather than the QRS complex alone. So when the interest of the source separation is not on QRS complex detection alone, but on ECG segment or interval analysis, it can be advantageous to use the source signals determined by aPCA and aICA. To overcome the problem of unknown order of the source signals in these situations, the source signals from the PBSS technique can be used as reference. That is, the aPCA and aICA source signal that shows maximum correlation with the PBSS source signals is most likely the source signal that represents the fetal ECG.

Since the amplitude of the fetal ECG is expected to rise with progressing pregnancy due to the growth of the fetus and its heart, the SNR of the abdominally recorded fetal ECG signals is also expected to rise. Naturally, with the exception of the period between 28 and 32 weeks, in which the fetus is covered by the vernix caseosa. Taking this expectation into account, then from Fig. 4.7 it can be concluded that the difference between the SNR of the source signals determined by the PBSS technique on the one hand, and the SNR of the source signals determined by aPCA and aICA on the other hand decreases with increasing SNR of the abdominal recordings. This effect can be explained by the fact that aPCA and aICA operate by maximizing the variance and statistical independency of the source signals, respectively. Although these approaches suffer from significant inaccuracies for low SNR recordings, they are relatively accurate for high SNR recordings. The ellipse fit employed by PBSS, on the other hand, suffers less from inaccuracies in low SNR recordings as it uses prior, physiology based information to spatially combine the abdominal ECG signals and enhance the SNR. However, in all cases, also for high SNR recordings, the ellipse fit in PBSS is not completely accurate, reducing the performance of PBSS. This reduction in performance becomes more evident for the high SNR recordings.

The inaccuracies in the ellipse fit originate from the fact that the least squares fitting employed does not guarantee an optimal fit as fitting errors can be unwillingly

weighted and are generally biased [139]. These problems can be resolved using a geometric fitting approach in which the mean orthogonal distance between the ellipse and each data point is minimized. This method, however, requires an iterative approach and significantly larger computation times. The latter is the main reason why in our technique the less accurate, yet faster, least squares fit is preferred; With this least squares fit approach, the PBSS technique requires, on average and on a standard-issue desktop computer, 1.2 seconds to calculate the source signals for fetal ECG recordings with lengths of 1 minute.

Besides the fact that the performance of the PBSS technique depends on the SNR of the recorded fetal ECG signals, the performance is also expected to depend, albeit less strongly, on the orientation of the fetus within the uterus. Variations in the orientation of the fetus mostly result in rotations of the VCG and, thus, also in rotations of the fitted ellipse and its associated orthogonal axes. The projection of the rotated VCG onto these rotated axes will nevertheless be the same as before the fetal rotation. However, for each orientation of the fetus, the distances between the fetal heart and the abdominal electrodes will be different. These differences, in turn, result in different signal attenuations for each ECG signal and, as a result, in distortion of the VCG [140]. This distortion can affect the performance of the PBSS technique to some extent. However, as the shape of the QRS loop is expected to remain planar and will therefore still allow for elliptic fits, this effect is expected to be small. Naturally, larger signal attenuations will reduce the SNR of the fetal ECG signals and, as such, still affect the performance of the PBSS technique.

In future, for developing real-time fetal monitoring applications, the PBSS technique can be used for estimating which of the abdominal fetal ECG signals has the largest SNR. That is, by determining which signals contribute most to the linear combination, it can be assessed which abdominal signal contains the most fetal ECG. This abdominal signal ”ordering” can be used to reduce computation times (i.e by omitting signals that do not contain a fetal ECG with sufficient SNR) or improve patient comfort by reducing the number of electrodes on the abdomen, and is therefore subject of ongoing research. Next to this ongoing research, another subject for research is to explore whether the improved accuracy of a geometric ellipse fitting approach outweighs the associated increase in computational complexity.

Chapter 5

Fetal heart rate detection

In the two previous chapters the detection of the maternal and fetal QRS complexes was already briefly addressed. However, both in Chapter 3 and Chapter 4 the fetal heart rate detection was only used to quantitatively evaluate the performance of the maternal ECG suppression method (Chapter 3) or the performance of the source separation technique (Chapter 4). In neither of these chapters, the fetal heart rate detection constituted an essential part of the presented methodology. The maternal heart rate detection, or equivalently the detection of the maternal QRS complexes, in Chapter 3, on the other hand, constitutes an essential part of the maternal ECG suppression method. As this QRS complex detection might have been done using a more simple peak detection method [122], elaboration of the QRS detection was postponed until the current chapter. The reason for this was that, when considering the chain of signal processing and analysis steps shown in Fig. 1.4, the correct position of the discussion on fetal heart rate detection is here: after Chapters 3 and 4.

The goal of this chapter is to elaborate on this detection method, provide a general discussion on its shortcomings, and present a solution to overcome some of these shortcomings.

5.1 Introduction

The fetal heart rate variability (HRV) has direct clinical significance and is, in fact, the most widely used fetal health parameter currently used in clinical practice. Moreover, when using Doppler ultrasound to determine the fetal heart rate non-invasively, the fetal HRV is basically the only source of information available.

Since HRV is regulated by the autonomous nervous system, analysis of the HRV can provide information on the functioning and stage of development of this nervous system. More particularly, since the sympathetic and parasympathetic parts of the nervous system operate in different bandwidths of the HRV spectrum, spectral analysis of HRV can provide information on both parts of the nervous system. This, in turn, can provide clinicians with information to assess fetal distress.

To ensure accurate and reliable spectral analysis, however, the HRV information

needs to be determined on a beat-to-beat basis and should essentially be artifact free [141, 142]. Doppler ultrasound devices generally provide a heart rate that is averaged over several beats and hence obscures HRV [143]. To overcome this problem of not having a beat-to-beat heart rate from the Doppler ultrasound, in Peters et al. [23] a method is presented that is capable of providing a fetal heart rate on a beat-to-beat basis. This method operates by processing the signal obtained from the analog output of a second-generation fetal CTG-monitor with a 1.024 MHz probe. Apart from demodulation, bandpass filtering between 100 and 475 Hz, and taking the envelope of the ultrasonic signal, this analog output is the same as the input to the ultrasound device and as such still contains beat-to-beat information on the fetal heart rate [23].

Notwithstanding this solution to the beat-to-beat problem, HRV determined with Doppler ultrasound typically also suffers from substantial artifacts (e.g. movement of the fetus often leads to the need of repositioning the ultrasound probe; in the time between repositioning no heart rate data can be recorded) and thence provides inaccurate and unreliable spectral analysis results.

Both the aforementioned problems (i.e. HRV not available on beat-to-beat basis and artifacts in the data) can be solved when determining the HRV from the fetal electrocardiogram (ECG). During labor, this ECG can be recorded with an invasive electrode connected to the fetal scalp. Using electrodes positioned on the maternal abdomen, however, the fetal ECG can also be obtained in earlier stages of pregnancy.

Several approaches to detect the heart rate from an ECG signal are mentioned in literature, of which matched filtering [144–146], autocorrelation [128], wavelet analysis [147, 148], and thresholding [128, 145] are mentioned the most. It has to be noted here, that thresholding approaches in general use a preprocessing step (e.g. wavelet analysis or matched filtering) prior to detecting the QRS complexes as (preprocessed) signal components that exceed a specific threshold. The approach adopted in this chapter operates as a thresholding approach and, although it might perform less accurately or reliably as some of the other approaches, it was chosen for its mathematical simplicity and low computational complexity.

Finally, it has to be noted that, despite the direct value of HRV in clinical practice, the main goal for detecting the fetal heart rate in this thesis is to enable exploitation of the (quasi-)periodicity of the fetal ECG. Specifically, by aligning consecutive ECG complexes on their QRS complex and subsequently averaging the complexes, the signal to noise ratio (SNR) can be improved significantly.

This chapter is organized as follows. In Section 5.2 the detection of the QRS complexes is discussed and in Section 5.3 the performance of this detection method is briefly evaluated. Finally, Section 5.4 provides a discussion on the QRS detection method.

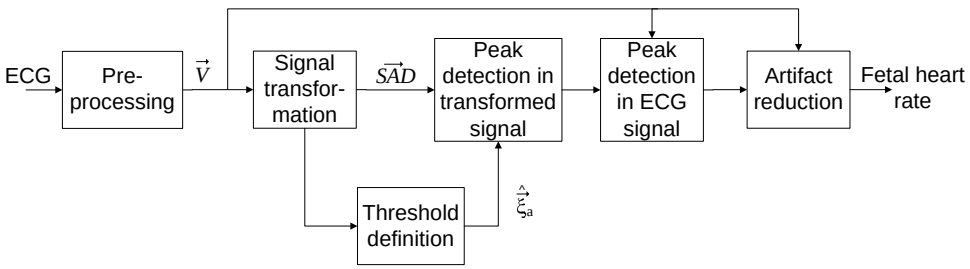

Figure 5.1: *Block diagram of fetal heart rate detection method.*

5.2 QRS detection

The detection of QRS complexes is performed through a series of signal processing steps, illustrated in Fig. 5.1. With exception of both peak detection blocks, each of the blocks in Fig. 5.1 is discussed in more detail below. Elaboration on the two peak detection blocks (i.e. *Peak detection in transformed signal* and *Peak detection in ECG signal*) is integrated in the discussions on the other blocks.

5.2.1 Preprocessing the ECG signal

Prior to detecting the QRS complexes, the ECG signals can be enhanced by exploiting knowledge on the spectral properties of the QRS complexes. Specifically, for the fetal ECG, the frequency content of the QRS complex is dominated by the 10 to 30 Hz range [99] (see also Fig. 2.7). Hence, by applying a bandpass filter set for this specific range, the SNR of the QRS complexes can be *a priori* enhanced.

It has to be noted that the application of the bandpass filter causes distortion of the QRS complexes. However, this effect is too small to have negative effects on the detection of the QRS complexes. After the QRS complexes have been detected in the bandpass-filtered ECG signals, the temporal information on these QRS complexes can be used on the unfiltered ECG signals to exploit their (quasi-)periodicity, as discussed in Section 5.1.

5.2.2 Signal transformation to enhance QRS complexes

One of the main shortcomings in QRS detection methods that operate by means of thresholding is that (physiological) artifacts or other parts of the ECG can cause the recorded signals to exceed the threshold. These events result in erroneously detected QRS complexes and therefore need to be minimized as much as possible. One way to do this is by exploiting *a priori* knowledge on the physiological origin of the ECG, and more particularly, of the QRS complex. The QRS complex is associated with depolarization of the heart's ventricles. This depolarization originates from the prop-

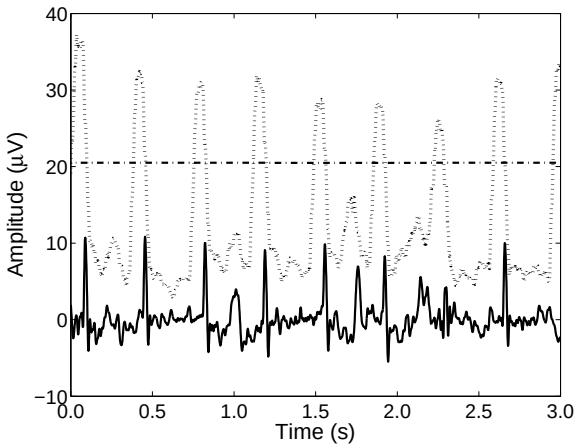

Figure 5.2: *Example of an ECG signal (solid line) with the corresponding SAD signal (dotted line) and the threshold (dash-dot line) required for detecting the peaks in the SAD signal. The advantages of using the SAD signal are most evident for the artifacts around 1.0 and 1.8 seconds: these are significantly smaller in the SAD signal.*

agation of an activation wave through the ventricular tissues and is characterized by the simultaneous electrical activation of numerous cells. In addition, the propagation of the activation wave is basically the same in both direction and speed for each heartbeat and is relatively fast with respect to the repolarization of the ventricles. Hence, the gradient of the QRS complex is expected to be large with respect to the gradient of other parts of the ECG. In addition, while the QRS complex lasts for about 90 ms in adults and 45 ms in neonates and fetuses [55], artifacts generally last much shorter.

Therefore, by summing the absolute values of the gradient of the ECG signal $\vec{V}$ (or $\vec{V}_{\mathrm{PC}}$, as discussed in chapter 3) over a time window M_{QRS} that corresponds to the length of the QRS complex, the amplitude of the resulting signal is expected to be substantially higher for the QRS complex than for other parts of the recorded signals. Moreover, as the gradient of the QRS complex generally changes sign more than once during contraction of the ventricles, the absolute value of the gradient should be summed. This process is commonly known as the sum of absolute differences (SAD) [149] and used mostly in the field of video compression:

$$\mathrm{SAD}_t = \sum_{j=1}^{M_{\mathrm{QRS}}} \left| V_{t+j+1} - V_{t+j} \right| . \tag{5.1}$$

An example of an ECG signal and its associated SAD signal are shown in Fig. 5.2.

From Eq. (5.1) it can be derived – or analogously from Fig. 5.2 it can be seen – that the peaks in the SAD signal precede the QRS complexes in the ECG signal.

Hence, after the peaks in the SAD signal are detected as local extrema that exceed the threshold, the QRS complexes can be detected in the ECG signal as local extrema within a *a priori* specified time interval (depending on M_{QRS}) after the peaks in the SAD signal.

5.2.3 Threshold definition

As mentioned, the method operates by detecting local peaks that exceed a certain threshold. The definition of this threshold is therefore critical in ensuring that all QRS complexes – or, in fact, the SAD transformations of the QRS complexes – exceed the threshold and that all other events in the signal do not exceed the threshold. Since, in particular for the fetal ECG, the signal properties (e.g. the noise level) can vary substantially and abruptly, the use of a variable threshold is favored over the use of a fixed threshold.

The instantaneous threshold is taken to be ξ_t:

$$\xi_t = g \max\left\{\left|\mathrm{SAD}_{t-\tau_{\mathrm{RR}}}\right|, \ldots, \left|\mathrm{SAD}_t\right|\right\} \tag{5.2}$$

with g a parameter that is empirically determined at 0.6 and τ_{RR} the time interval corresponding to the interval between the last two detected QRS complexes. The threshold at sample t is, thus, determined at 60% of the maximum amplitude within the window of length τ_{RR} that precedes sample t. We denote the estimated variance of this instantaneous threshold as $\sigma^2_{\xi,t}$, i.e. the variance of the SAD signal within the same time window.

To avoid artifacts in the SAD signal causing abrupt variations in the threshold, a new augmented version of the threshold is defined: $\xi_{a,t}$. This augmented threshold essentially constitutes a filtered counterpart of the instantaneous threshold ξ_t and the output of the filter is sequentially updated as a non-stationary mean of the instantaneous threshold ξ_t. In a state-space representation, the evolution of the augmented threshold and its relation to the instantaneous threshold can be described as (see also Fig. 5.3):

$$\begin{cases} \xi_{a,t+1} &= \xi_{a,t} + \nu_t \\ \xi_{t+1} &= \xi_{a,t+1} + \eta_{t+1} \end{cases} . \tag{5.3}$$

Here, ν_t represents the variation between the states $\xi_{a,t+1}$ and $\xi_{a,t}$ and is assumed to be Gaussian distributed with zero mean and variance $\sigma^2_{\nu,t}$. Analogously, η_{t+1} describes the contribution of artifacts in the instantaneous threshold ξ_{t+1} and is also taken to be Gaussian distributed with zero mean and variance $\sigma^2_{\eta,t+1}$. The assumption for Gaussian distributions is dictated by the wish to have an analytical solution and small computational complexity for the estimation of the augmented threshold.

The uncertainties in the state-space model of Eq. (5.3) suggest the use of a probabilistic approach for finding the solution to the augmented threshold estimation problem. Using Bayes' rule [150], the *posterior* probability distribution $p(\xi_{a,t}|\xi_t, \sigma^2_{\nu,t}, \sigma^2_{\eta,t})$

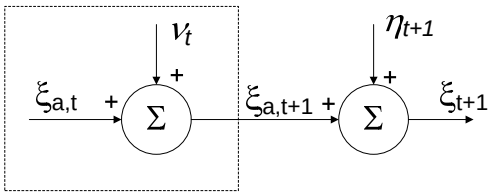

Figure 5.3: *Illustration of the state-space model that describes the evolution of the augmented threshold for QRS detection. In the square box, the evolution of the augmented threshold is depicted.*

for the augmented threshold $\xi_{a,t}$, given the instantaneous threshold ξ_t and the variances $\sigma^2_{\nu,t}$ and $\sigma^2_{\eta,t}$, can be written as:

$$\begin{aligned} &p\left(\xi_{a,t+1}\left|\xi_{t+1},\sigma^2_{\nu,t},\sigma^2_{\eta,t+1}\right.\right) \\ &\quad \frac{p\left(\xi_{a,t+1}\left|\sigma^2_{\nu,t},\sigma^2_{\eta,t+1}\right.\right)p\left(\xi_{t+1}\left|\xi_{a,t+1},\sigma^2_{\nu,t},\sigma^2_{\eta,t+1}\right.\right)}{p\left(\xi_{t+1}\left|\sigma^2_{\nu,t},\sigma^2_{\eta,t+1}\right.\right)} \\ &\quad \propto p\left(\xi_{a,t+1}\left|\sigma^2_{\nu,t},\sigma^2_{\eta,t+1}\right.\right)p\left(\xi_{t+1}\left|\xi_{a,t+1},\sigma^2_{\nu,t},\sigma^2_{\eta,t+1}\right.\right). \end{aligned} \tag{5.4}$$

The last two terms in Eq. (5.4) are referred to as the *prior* and *likelihood*, respectively.

Given the Gaussian behavior of ν_t, the prior can be written as $\mathcal{N}(\hat{\xi}_{a,t},\sigma^2_{\xi_a,t}+\sigma^2_{\nu,t})$ where $\hat{\xi}_{a,t}$ represents the estimate for $\xi_{a,t}$, $\sigma^2_{\xi_a,t}$ is the variance of $\xi_{a,t}$ and $\mathcal{N}(x,y)$ is a Gaussian distribution with mean x and variance y. Analogously, the likelihood can be written as $\mathcal{N}(\xi_{a,t+1},\sigma^2_{\eta,t+1})$. Substituting these expressions in Eq. (5.4) gives:

$$p\left(\xi_{a,t+1}\left|\xi_{t+1},\sigma^2_{\nu,t},\sigma^2_{\eta,t+1}\right.\right)=\mathcal{N}\left(\hat{\xi}_{a,t+1},\sigma^2_{\xi_a,t+1}\right), \tag{5.5}$$

with

$$\hat{\xi}_{a,t+1}=\hat{\xi}_{a,t}+K_t\left(\xi_{t+1}-\hat{\xi}_{a,t}\right) \tag{5.6}$$

and

$$\sigma^2_{\xi_a,t+1}=\sigma^2_{\xi_a,t}+\sigma^2_{\nu,t}-K_t\left(\sigma^2_{\xi_a,t}+\sigma^2_{\nu,t}\right). \tag{5.7}$$

The Kalman gain K_t in Eq. (5.6) and (5.7) is determined as:

$$K_t=\left(\sigma^2_{\xi_a,t}+\sigma^2_{\nu,t}\right)\left[\sigma^2_{\eta,t+1}+\sigma^2_{\xi_a,t}+\sigma^2_{\nu,t}\right]^{-1}. \tag{5.8}$$

The initial settings $\hat{\xi}_{a,0}$ and $\sigma^2_{\xi_a,0}$ are set equal to the instantaneous threshold determined over the time window comprising the first two seconds of the SAD signal and the variance of the SAD signal in this time window, respectively. The choice for

two seconds is made to ensure that at least one QRS complex is present in the time window. Note that in case of normal fetal heart rate (i.e. a heart rate between 110 and 150 beats per minute (BPM) [1]), it is more likely that 4 or 5 fetal QRS complexes are present within the two-second time window.

To demonstrate the estimation of the augmented threshold, the threshold is depicted in Fig. 5.2 alongside its parental SAD signal.

5.2.4 Artifact reduction

Despite the preprocessing and signal transformation to minimize the occurrence of artifacts or noise exceeding the threshold and leading to incorrectly detected QRS complexes, it cannot be excluded that some of the detected QRS complexes are still incorrect. In addition, besides erroneously detected QRS complexes (e.g. artifacts that exceed the threshold), it can also occur that the transformed QRS complex does not exceed the threshold and thus that the QRS complex is not detected.

To overcome both problems to some extent, the physiological properties of the heart can be exploited. Specifically, due to the relatively slow operation and relatively small influence of the autonomous nervous system in regulating the heart rate, variations in the instantaneous RR intervals (i.e. the interval between consecutive heartbeats) are gradual rather than abrupt. In addition, the heartbeat is generally also restricted by a physiological upper and lower bound. More specifically, RR intervals smaller than 0.2 s or larger than 1 s are labeled as incorrect. In addition, fluctuations in the RR interval that are larger than 25% of the mean RR interval of the 5 directly preceding heartbeats are also labeled as incorrectly detected.

The most common events that are labeled as incorrect are due to QRS complexes that do not exceed the threshold, yielding an RR interval that is about twice as large as the preceding RR intervals or two consecutive RR intervals of which the first is small and the second large (or vice versa) and the mean is in line with the preceding RR intervals. The latter event occurs as a result of a incorrectly detected QRS complex between two correctly detected QRS complexes. Both examples (i.e. missing QRS complex and incorrectly detected QRS complex) are illustrated in Fig. 5.4.

It has to be noted that the margins listed above are rather wide. In practice, the upper and lower limits of the fetal RR interval will be about 0.6 s and 0.3 s and variations will constitute much less than 25% of the mean RR interval. However, to ensure that bradycardias (heart rates below a certain, age-dependent range), tachycardias (heart rates that exceed the healthy range), and extrasystoles, generally originating from immaturities of the heart and not from regulation of the nervous system, are not erroneously labeled as incorrect, these margins are chosen as wide as this.

Once incorrect RR intervals have been labeled, in some situations they can be adapted by improving the detection of the involved QRS complexes. This is achieved by performing a local search near the expected location of the QRS complex. This

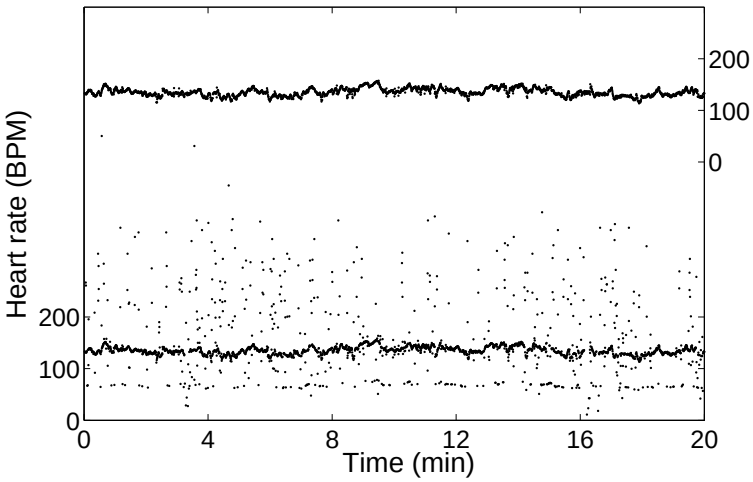

Figure 5.4: *Example of detected fetal heart rates with (top graph) and without (bottom graph) correction for artifacts. The heart rate on the vertical axis is expressed in BPM.*

expected location is defined based on the location of the previously detected QRS complex and the mean RR interval of the last five heartbeats. Only when a local extremum is found near the expected location and when this local extremum shows sufficient correlation with other detected QRS complexes, the originally detected QRS complex is replaced or the ”gap” between two detected complexes is filled.

5.3 Evaluation of QRS detection

The QRS detection algorithm is evaluated here by comparing the fetal heart rate information assessed from a non-invasive fetal ECG recording to the heart rate assessed from a simultaneously performed invasive fetal ECG recording (see Section 2.3 for details on the acquisition of the invasive ECG). The patient on which this recording was performed had a gestational age of 40+1 weeks and the length of the recording was slightly over 20 minutes. For analgetic reasons, the patient was given an epidural injection.

In Fig. 5.5 the heart rate traces for both the non-invasive and invasive fetal ECG signals are depicted.

From Fig. 5.5 it can be seen that both heart-rate traces resemble one another to a large extent. To quantify this resemblance, in Fig. 5.6 both heart-rate traces are related to one another as a scatter plot. This scatter plot contains over 2500 heart beats and shows a correlation coefficient between both heart rate traces of over 97%.

The correlation coefficient of 97% is relatively high and signifies that the fetal heart rate determined from the non-invasive fetal ECG is almost identical to the

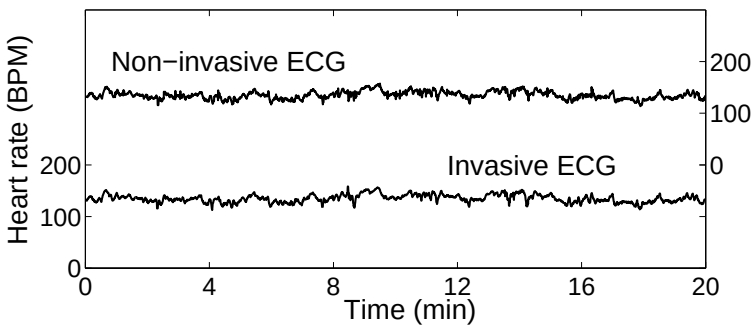

Figure 5.5: *Fetal heart rate traces assessed from both the non-invasive fetal ECG (top graph) and the invasive fetal ECG (bottom graph).*

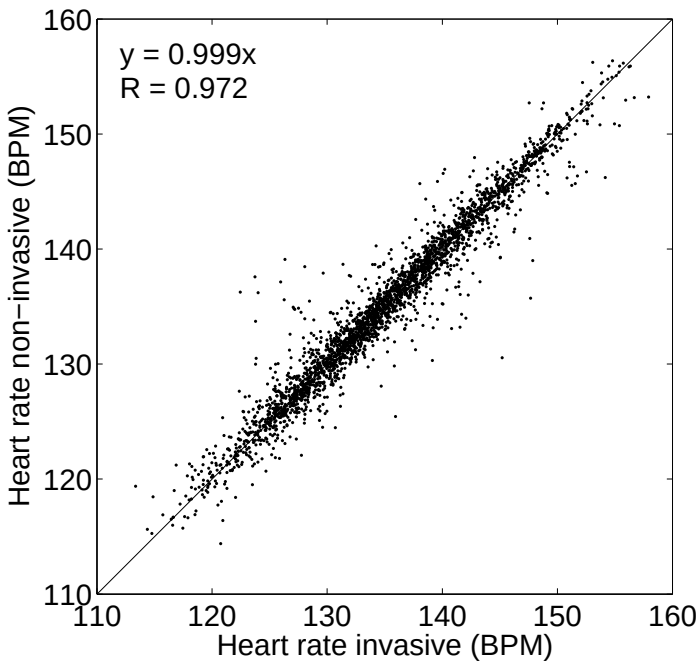

Figure 5.6: *Scatter plot of the fetal heart rate determined from the invasive fetal ECG and the heart rate determined from the non-invasive fetal ECG.*

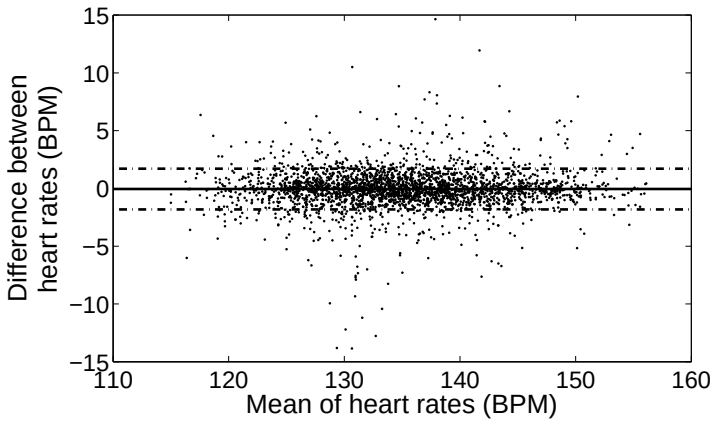

Figure 5.7: *Bland-Altman plot of the fetal heart rates determined from the invasive and non-invasive fetal ECG. On the horizontal axis for each heartbeat the mean value between both methods is shown. On the vertical axis the difference between both methods is shown. The solid horizontal line in the graph represents the mean of the depicted points. The dash-dot lines indicate the standard deviations with respect to this mean.*

fetal heart rate detected from the invasive fetal ECG. This is confirmed in the Bland-Altman plot [151] of Fig. 5.7. In this plot, the mean value on the vertical axis is 0.0 BPM with a standard deviation of 1.6 BPM. The Bland-Altman plot hence is consistent with the regression plot of Fig. 5.6, indicating good resemblance between the invasively and non-invasively determined fetal heart rates.

However, most of the recordings from the patient study mentioned in Section 2.3 do not show the same signal quality as the recording used here. As a result, the accuracy of heart-rate traces determined from non-invasive fetal ECG recordings is expected to be worse. The potential implications of this expectation are detailed in the next section.

5.4 Discussion

In this chapter a method for detecting QRS complexes in an ECG signal was presented. This method operates by transforming the ECG signal by calculating the SAD function and detecting peaks in this SAD function by using an adaptive threshold. The peaks in the SAD function serve as reference points for a restricted search for local extrema in the ECG signal.

As mentioned in Section 5.1, the presented method is not expected to perform

better than some of the methods mentioned in literature, but because of its computational efficiency and sufficiently good performance, it is anyhow used throughout this thesis. The statement of sufficiently good performance however raises the question of which degree of accuracy is considered to be still good. In addition, it also raises the question of how this performance can be assessed in cases where no objective evaluation as in Section 5.3 can be made. It needs to be stressed here that the evaluation in Section 5.3 is not completely objective. The QRS complexes detected in the non-invasive fetal ECG recording are compared to the QRS complexes detected in the invasive recording. This comparison implicitly assumes that the developed detection method operates flawlessly on the invasive fetal ECG signal. Otherwise, evaluation of the developed method would be performed by comparing the detected QRS complexes to an erroneously determined golden standard. Moreover, this golden standard will probably be biased towards a good correlation since possible shortcomings in the detection method will have a similar effect on the QRS detection in both the invasively and non-invasively recorded ECG signals. Hence, to prevent such a bias, the QRS complexes detected in the invasively recorded fetal ECG are validated by visual inspection.

The answer to the first question above depends on the intended goal. If the goal of the fetal heart rate is visual analysis of the CTG, then relatively low correlation coefficients are good enough. Even when the heart rate data is significantly corrupted by artifacts, visual analysis as a rule is not affected much. This is illustrated in Fig. 5.4 in which visual analysis of the bottom graph indicates a similar pattern as can be seen in the top graph; Artifacts are usually ignored by the analyst. Determination of the correlation coefficient between the bottom graph of Fig. 5.4 and the heart rate data obtained from the invasive fetal ECG (Fig. 5.5), however, yields a correlation of 67%, demonstrating that for visual analysis relatively low correlation coefficients are indeed still good enough.

If the goal is accurate and reliable spectral analysis of HRV, then larger correlation coefficients are required. In fact, to ensure accurate spectral analysis, the artifact reduction algorithm cannot be permitted to correct more than 25% of the determined fetal QRS locations [142].

Finally, if the goal of the heart rate data is to aid in the enhancement of fetal ECG signals (as is the mainly intended goal in this thesis), required correlation coefficients for reliable enhancement are expected to lie somewhere in between the required correlations for visual CTG analysis and spectral analysis. Because several consecutive ECG complexes will be aligned on their QRS complexes and subsequently averaged, the erroneous contribution of a complex that is misaligned due to inaccurate QRS detection is reduced by the averaging process. In fact, since consecutive ECG complexes have to resemble one another to a significant extent, a sanity check, e.g. by means of the correlation coefficient between ECG complexes, can be used to *a priori*

detect misaligned ECG complexes and exclude these from the averaging.

The fact that consecutive ECG complexes resemble one another can also be exploited to improve the QRS detection. Specifically, by generating a template of the ECG complex through averaging of several consecutive, aligned ECG complexes, this template can serve as a matched filter, enhancing the ECG signal prior to QRS detection.

The second question raised was how to assess the performance of the QRS detection in cases where no objective means of validation are present. One possible approach for this assessment was presented in Chapter 4. In fact, using the PBSS technique of Chapter 4 to preprocess the ECG signals, the performance of the QRS detection method was demonstrated to be, on average, around 90% in terms of the sensitivity (see Eq. (4.13)) and, on average, around 70% in terms of the positive predictive value (Eq. (4.14)). Although these are different performance measures than the correlation coefficient, these measures indicate that the general performance of the QRS detection can be anticipated to be adequate for the enhancement of fetal ECG signals. This enhancement is discussed in Chapter 6.

It can be noted here that, when not using an averaging process to enhance the ECG, the requirements for the performance of the QRS detection in this thesis can be lower. Apart from the ECG enhancement in Chapter 6, the fetal ECG signals that remain after suppression of the maternal ECG in Chapter 3 (see Fig. 1.4) are essentially only further analyzed during the estimation of the fetal VCG in Chapter 7 and during the subsequent estimation of the fetal orientation in Chapter 9. The estimation of the fetal VCG only assumes spatial correlation between the fetal ECG complexes recorded at different locations on the maternal abdomen and no temporal correlations or (quasi-)periodicity. Since the fetal ECG complexes in all abdominal signals are defined similarly, based on the QRS complexes that are detected in a single signal (see Chapter 4), the spatial correlation between the fetal ECG complexes is not affected by misdetection of a QRS complex. The estimation of the fetal orientation in Chapter 9 aligns the VCGs of consecutive heartbeats by, among other transformations, time-synchronization of the VCGs. Any delay in either one of the involved VCGs can therefore be accounted for during the time-synchronization, irrespective whether this delay originates from an erroneously detected QRS complex or from an physiological event.

Hence, the propagation of errors in the QRS detection further down the chain of signal processing and analysis steps occurs mainly during the averaging of fetal ECG complexes. The complications caused by the inclusion of misaligned ECG complexes in the averaging process are, nevertheless, not expected to be substantial. During the averaging, the misaligned ECG complex is essentially smeared out over more complexes. Particularly, for each average in which n ECG complexes are included, a misaligned complex contributes to about $(1/n)^{\text{th}}$ of the average ECG complex. On

the one hand, this smearing out of the effect of an erroneously detected QRS complex is convenient, as it can prevent artifacts from disturbing signal processing or VCG and ECG interpretation steps further down the chain. The fact is, in most cases, the erroneous detection of an QRS complexes is caused by the presence of an artifact with an amplitude that is so large that the amplitude of the SAD transformed artifact still exceeds the threshold. On the other hand, the averaging of n complexes of which one is misaligned also means that n averaged ECG complexes are to some extent (i.e. $(1/n)^{\text{th}}$) distorted in case the averaging is performed using a moving window of length n. The effect of these often relatively small but yet persistent distortions on other links in the signal processing chain has to be studied in the future.

Other subjects for future study are the overall improvement of the QRS detection. Besides using a matched filter as indicated above, also wavelet-based QRS detection methods, whether or not in combination with statistical models such as hidden Markov models [152] , need to be considered.

Chapter 6

An adaptive Kalman filter for ECG signal enhancement

As mentioned in the beginning of Chapter 4, knowledge on the fetal heart rate, or more particularly on the QRS locations, can be used for the enhancement of the ECG signals. This enhancement typically occurs by aligning individual ECG complexes on their QRS complex and subsequently averaging the complexes. However, as a result of averaging, physiologically relevant variations in the ECG can be lost. To avoid this loss, the number of ECG complexes used in the averaging process needs to depend on the dynamics of the signal. In this chapter, a method is presented that does exactly this; it varies the number of preceding ECG complexes included in the enhancement of a particular ECG complex.[1]

6.1 Introduction

Monitoring and analysis of the electrocardiogram (ECG) has long been used in clinical practice. In recent years, the application field of ECG monitoring is expanding to areas outside the clinic. An example of such an area is at-home monitoring of patients with sleep apnea [153]. Also within the clinic a transition in ECG monitoring applications is taking place. With developments in sensor technology (e.g. textile electrodes and capacitive electrodes), sensors that are incorporated in garments or the matrass of an incubator [154] have become available.

As a result of these new sensor technologies, the comfort of the patient is improving progressively. Where some years ago the patient had to reconcile him- or herself with the discomforts of the only available technology, nowadays patients prefer the more comfortable ways of recording the ECG. However, in most cases, this increased comfort comes at the expense of signal quality. Electrodes that are incorporated in garments generally provide signals with a lower signal to noise ratio (SNR) and more artifacts than contact electrodes that are glued to the body [155].

[1]This chapter has been submitted as *R. Vullings, B. de Vries, J.W.M. Bergmans, "An adaptive Kalman filter for ECG signal enhancement"* to be considered for publication.

Another example of ECG signals with a typically low SNR are fetal ECG signals, either recorded invasively after membrane rupture [13] or non-invasively from the maternal abdomen [116].

Some of the SNR and artifact problems that arise during these recordings can be suppressed by simple, frequency-selective filtering [116, 156, 157]. However, due to the partial overlap of signal and noise bandwidths [99, 158], this frequency selective filtering can only help to some extent. Further improvement of the ECG can be achieved by exploiting its (quasi-)periodicity. Consecutive ECG complexes resemble one another and are, moreover, in general uncorrelated with noise and artifacts. Hence, by averaging several consecutive ECG complexes, the SNR can be improved. For additive Gaussian noise, this improvement is directly related to the number of ECG complexes included in the average [159]. The drawback of averaging multiple consecutive ECG complexes is that, besides noise, also the physiological dynamics of the ECG are suppressed. That is, changes in the ECG that originate from physiological events – for instance, changes in the ST segment that might be associated to metabolic acidosis [2] – are suppressed in the averaging, complicating clinical diagnosis.

From this it is clear that the averaging of ECG complexes entails a trade-off between the pursued increase in SNR and the time scale at which physiologically relevant changes in ECG morphology are expected to occur. Hence, for each specific application, the number of complexes n included in the averaging needs to be reconsidered. If it were possible, however, to dynamically adapt the number of complexes in the average, based on newly arriving data, the problem of selecting a proper value for n could potentially be overcome. In this paper, we develop a filter that can do exactly this.

The filter is derived using a Bayesian framework and constitutes a Kalman filter in which the dynamic variations in the ECG are modeled by a covariance matrix that is adaptively estimated every time new data arrives. In contrast to filters that filter the ECG by modeling it by parametric functions [160], the presented filter uses the actual recorded ECG as basis and infers whether this ECG is corrupted by noise or dynamic variations. As a result, unanticipated physiological anomalies in the ECG, that cannot be easily captured by simple parametric functions, can be accurately modeled. For parametric functions, to capture such physiological anomalies, large families of analytical functions or many function parameters need to be considered, both inherently slowing down the filter process.

The derivation of this filter is provided in Section 6.2. The ECG data set, on which the filter is evaluated, is discussed in Section 6.3 and the results of this evaluation are provided in Section 6.4. Finally, discussion and conclusions are provided in Section 6.5.

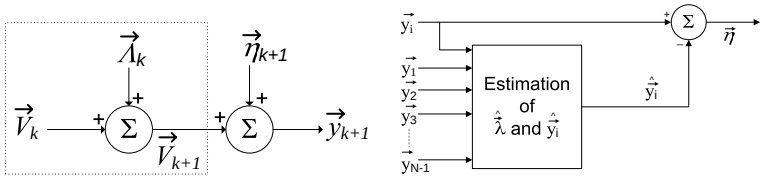

Figure 6.1: *(a): Illustration of the state-space model that describes the evolution of the ECG over time. The evolution of the state vectors is indicated by the dotted box. (b): Illustration of the measurement noise estimation.*

6.2 Derivation of adaptive Kalman filter

6.2.1 Bayesian model

Typically, ECG complexes that originate from consecutive heartbeats are very similar but not identical. Moreover, when recording the ECG, the signals are corrupted to some extent by noise and artifacts. In a simplified form, both the relation between consecutive ECG complexes and the corruption of the recorded ECG can be described by means of a state-space model (see also Fig. 6.1(a)):

$$\begin{cases} \vec{V}_{k+1} &= \vec{V}_k + \vec{\Lambda}_k, \\ \vec{y}_{k+1} &= \vec{V}_{k+1} + \vec{\eta}_{k+1}. \end{cases} \tag{6.1}$$

Here, $\vec{V}_k$ denotes the $[1 \times T]$ ECG complex for heartbeat k and $\vec{y}_k$ denotes the $[1 \times T]$ recorded signal where T is the length of the ECG complex. The isolation of individual ECG complexes from the recorded signals is discussed in Section 6.3.3. Also in this section, the choice for T and the implicit assumption of equal lengths for all ECG complexes is discussed. The evolution of the ECG complexes between heartbeats is modeled by the $[1 \times T]$ stochastic component $\vec{\Lambda}_k$ (also referred to as the process noise). The measurement noise, i.e. corrupting signals such as electromyographic signals, movement artifacts, and interferences from the powerline grid, is represented by the $[1 \times T]$ vector $\vec{\eta}_k$.

When critically assessing Eq. (6.1) and Fig. 6.1, it is clear that based on the state-space model alone, no clear distinction between the process noise $\vec{\Lambda}_k$ and the measurement noise $\vec{\eta}_k$ can be made. Therefore, a separate model (illustrated in Fig. 6.1(b)) is used for estimating the measurement noise. In this model, the spatial correlation between ECG signals recorded simultaneously at different locations is exploited. This spatial correlation renders it possible to approximate a particular ECG signal by the combination of the other, simultaneously recorded ECG signals. The part of the ECG signal that cannot be approximated by the combination of the

other signals, is subsequently assumed to be measurement noise. The estimation of the measurement noise will be discussed in more detail below in Section 6.2.2. With regard to the process noise, $\vec{\Lambda}_k$ is assumed to be zero mean with adaptive covariance Σ_{Λ_k}. Similarly, the measurement noise $\vec{\eta}_k$ is assumed to be zero mean with covariance Σ_{η_k}. The assumption of zero mean for both $\vec{\Lambda}_k$ and $\vec{\eta}_k$ can be justified by highpass filtering the ECG signals, as will be described in Section 6.3.2.

In the state-space description of Eq. (6.1), the problem of enhancing the SNR of the ECG is reduced to the problem of sequentially estimating the model parameter vector $\vec{V}_{k+1}$ and the noise covariances Σ_{η_k} and Σ_{Λ_k}. Here, sequential estimation refers to the estimation of the relevant parameters based on the previous estimate and all newly arriving data.

6.2.2 Estimation of measurement noise

When recording several ECG signals simultaneously, these signals are spatially correlated to some extent. Specifically, the electrical activity of the heart can be modeled as a time-dependent dipole that is variable in both amplitude and (three-dimensional) orientation. In this model, each ECG signal constitutes the projection of the electrical field generated by this dipole onto the vector that describes the position of the recording electrode. Hence, each ECG signal can be constructed from the linear combination of three independent ECG signals [64]. For N recorded ECG signals this means that the ECG signal $\vec{V}_i$ can be modeled (see also Fig. 6.1(b)) as

$$\vec{V}_i = \vec{\lambda}\mathbf{V}_{-i}. \tag{6.2}$$

Here, $\mathbf{V}_{-i}$ is a $[(N-1)\times T]$ matrix of which the N ECG signals $\vec{V}_j$ constitute the row vectors and for which the ith row is missing. The $[1\times(N-1)]$ vector $\vec{\lambda}$ comprises the coefficients of the linear combination. The index k that denotes the heartbeat in Eq. (6.1) is omitted from this description for clarity.

With the adopted dipole model of the heart's electrical activity, it can be argued that dynamical variations in the ECG morphology are reflected in all recorded ECG signals $\mathbf{Y}$. Analogously, measurement noise $\vec{\eta}$ that does not exhibit the same spatial correlation as the ECG is suppressed in the linear combination of ECG signals. As a result, the measurement noise vector $\vec{\eta}_i$ for ECG signal i can be approximated by $\hat{\vec{\eta}}_i$ using the estimate $\hat{\vec{y}}_i = \vec{\lambda}\mathbf{Y}_{-i}$:

$$\hat{\vec{\eta}}_i = \vec{y}_i - \hat{\vec{y}}_i, \tag{6.3}$$

also yielding an estimate for the measurement noise covariance Σ_η.

The estimates $\hat{\vec{\lambda}}$ that minimize the mean squared error (MSE) between $\mathbf{y}_i$ and its estimate $\hat{\vec{y}}_i = \hat{\vec{\lambda}}\mathbf{Y}_{-i}$ can be determined by:

$$\hat{\vec{\lambda}} = \vec{y}_i\mathbf{Y}_{-i}^T\left(\mathbf{Y}_{-i}\mathbf{Y}_{-i}^T\right)^{-1}. \tag{6.4}$$

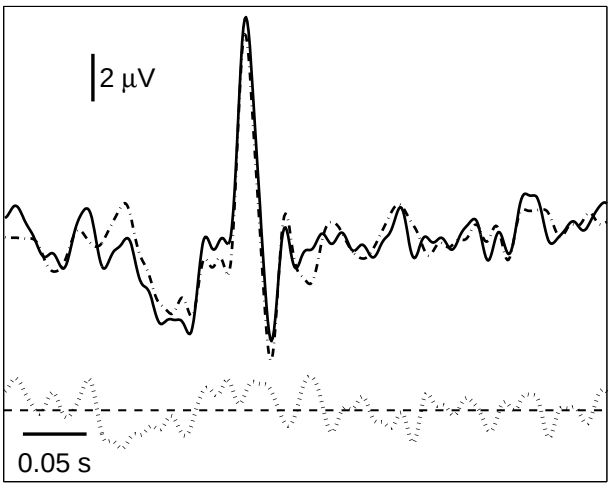

Figure 6.2: *Example of the estimation of the measurement noise in an ECG complex obtained from an eight-channel, non-invasive fetal ECG recording (see Section 6.3). The solid line represents the recorded ECG complex and the dash-dot line represents the estimate of this ECG complex obtained by the linear combination of the 7 simultaneously recorded signals. The differential signal, represented by the dotted line, constitutes an approximation of the measurement noise. Note that for clarity the measurement noise signal is depicted with a vertical offset; The scalings of all signals are the same.*

The matrix inversion in this equation exists in case the row vectors in $\mathbf{Y}_{-i}$ are linearly independent [161]. This condition of linear independence is satisfied in the case of ECG signals, for one due to the fact that each row vector is corrupted by independent, additive noise. The estimation of the measurement noise is illustrated in Fig. 6.2.

The main limitation of this method for estimating the measurement noise is that, at any time, at least four ECG signals have to be recorded: three independent ones to estimate the fourth. For most cases exemplified in Section 6.1, however, the recording of multiple ECG signals is standard procedure and hence, the requirement for more than three signals does not impose a serious restriction to the applicability of the proposed SNR enhancement method.

6.2.3 Kalman filter for parameter estimation

The uncertainty in the state-space model of Eq. (6.1) and in the associated noise parameters suggests the use of a probabilistic approach for solving the parameter es-

timation problem [162]. In addition, the sequential nature of the estimation problem motivates the use of a Bayesian framework in which the prior probability distribution assigned to the unknown parameters is updated every time new data arrives. Here, again, sequential refers to the estimation of model parameters based on previous parameter estimates and on newly arriving data.

Using Bayes' rule, the solution to the parameter estimation problem can be described as

$$p\left(\vec{V}_{k+1}\,|\vec{y}_{k+1},\Sigma_{\Lambda_k},\Sigma_{\eta_k}\right) = \frac{p\left(\vec{y}_{k+1}\,\middle|\vec{V}_{k+1},\Sigma_{\Lambda_k},\Sigma_{\eta_k}\right)p\left(\vec{V}_{k+1}\,|\vec{y}_k,\Sigma_{\Lambda_k},\Sigma_{\eta_k}\right)}{p\left(\vec{y}_{k+1}\,|\vec{y}_k,\Sigma_{\Lambda_k},\Sigma_{\eta_k}\right)}. \tag{6.5}$$

The conditional probability density function $p(\vec{V}_{k+1}|\vec{y}_{k+1},\Sigma_{\Lambda_k},\Sigma_{\eta_k})$ is referred to as the *posterior*. Since it contains all statistical information about $\vec{V}_{k+1}$ given the measurement $\vec{y}_{k+1}$ and the initial ECG complex $\vec{V}_0$, this posterior constitutes the complete solution to the parameter estimation problem [163]. The probability density functions on the right-hand side of Eq. (6.5) are referred to as the *likelihood* and the *prior*, respectively, for the numerator and as the *evidence* for the denominator.

By assuming the prior and likelihood to be Gaussian, the posterior and evidence are necessarily Gaussian as well. The use of Gaussian approximations is dictated by the fact that they render the posterior describable by a limited number of parameters and, as such, enable the estimation of the ECG in a maximum *a posteriori* (MAP) fashion [162]. For applications in which the posterior is expected to be multi-modal (i.e. a function with several peaks), a combination of Gaussians can be used, each describing a different mode of the posterior. The fact that, here, the posterior is assumed as a single Gaussian, implies that the parameter vector estimate $\hat{\vec{V}}_{k+1}$ and its associated covariance $\Sigma_{V_{k+1}}$ together completely describe the posterior probability density function and can be inferred analytically. Hence, using Eq. (6.5) and the assumptions in the state-space model, the posterior is given by [162]:

$$\mathcal{N}\left(\hat{\vec{V}}_{k+1},\Sigma_{V_{k+1}}\right) = \frac{\mathcal{N}\left(\vec{V}_{k+1},\Sigma_{\eta_{k+1}}\right)\mathcal{N}\left(\hat{\vec{V}}_k,\Sigma_{V_k}+\Sigma_{\Lambda_k}\right)}{\mathcal{N}\left(\hat{\vec{V}}_k,\Sigma_{V_k}+\Sigma_{\Lambda_k}+\Sigma_{\eta_{k+1}}\right)}, \tag{6.6}$$

where $\mathcal{N}(x,y)$ denotes a Gaussian probability distribution with mean x and covariance y.

By rewriting Eq. (6.6), the optimal Bayes estimate $\hat{\vec{V}}_{k+1}$ and its variance $\Sigma_{V_{k+1}}$, (i.e. optimal in the sense of the MAP estimate), can be sequentially updated according to:

$$\hat{\vec{V}}_{k+1}^T = \hat{\vec{V}}_k^T + \mathbf{K}_{k+1}\left(\vec{y}_{k+1}^T - \hat{\vec{V}}_k^T\right) \tag{6.7}$$

$$\Sigma_{V_{k+1}} = \Sigma_{V_k} + \Sigma_{\Lambda_k} - \mathbf{K}_{k+1}\left(\Sigma_{V_k}+\Sigma_{\Lambda_k}\right), \tag{6.8}$$

where $\mathbf{K}_{k+1}$ is known as the Kalman gain [164]:

$$\mathbf{K}_{k+1} = \frac{\Sigma_{V_k} + \Sigma_{\Lambda_k}}{\Sigma_{\eta_{k+1}} + \Sigma_{V_k} + \Sigma_{\Lambda_k}}. \tag{6.9}$$

Together, Eqs. (6.7), (6.8), and (6.9) constitute the Kalman filter equations.

6.2.4 Adaptive process noise covariance estimation

A limitation of the derived Kalman filter is its implicit assumption of known *a priori* statistics for the measurement noise $\vec{\eta}_k$ and process noise $\vec{\Lambda}_k$. Moreover, in the ECG monitoring applications for which the filter is intended, the noise statistics are expected to be non-stationary and hence, any choice for particular noise covariances potentially leads to large estimation errors [165]. These estimation errors can nonetheless be restricted by including a sequential estimation of the noise statistics in the Kalman filter equations.

The estimation of the measurement noise statistics has been discussed in Section 6.2.2. The discussion in this section is hence limited to the estimation of the process noise covariance Σ_{Λ_k}.

Again using Bayes' rule, the conditional probability density function for Σ_{Λ_k}, given the recorded signal $\vec{y}_{k+1}$ is given by:

$$p\left(\Sigma_{\Lambda_k} \left| \vec{y}_{k+1}, \Sigma_{\eta_k}\right.\right) = \frac{p\left(\vec{y}_{k+1} \left| \vec{y}_k, \Sigma_{\Lambda_k}, \Sigma_{\eta_k}\right.\right)}{p\left(\vec{y}_{k+1} \left| \vec{y}_k\right.\right)} p\left(\Sigma_{\Lambda_k} \left| \vec{y}_k, \Sigma_{\eta_k}\right.\right). \tag{6.10}$$

It can be noted here that the likelihood of the noise covariance $p\left(\vec{y}_{k+1} \left| \vec{y}_k, \Sigma_{\Lambda_k}, \Sigma_{\eta_k}\right.\right)$ is identical to the evidence function in the parameter estimation level of Eq. (6.5). Hence, maximizing the evidence function in this parameter estimation level is analogous to maximizing the likelihood of Σ_{Λ_k} for newly arriving data. Maximization of the evidence function, however, yields that the estimated noise covariance constitutes the maximum likelihood (ML) estimate instead of the MAP estimate, implying the assumption of no knowledge of the prior at the noise estimation level [162].

When defining the model residual to be

$$\begin{aligned} \vec{\rho}_{k+1} &\triangleq \vec{y}_{k+1} - \mathbf{E}\left[\vec{y}_{k+1} \left| \vec{y}_k, \Sigma_{\Lambda_k}, \Sigma_{\eta_k}\right.\right] \\ &= \vec{y}_{k+1} - \hat{\vec{V}}_k, \end{aligned} \tag{6.11}$$

it can easily be calculated that $\mathbf{E}[\vec{\rho}_{k+1}|\vec{y}_k] = \vec{0}$ and $\mathbf{E}[\vec{\rho}_{k+1}^T \vec{\rho}_{k+1}|\vec{y}_k] = \Sigma_{V_k} + \Sigma_{\Lambda_k} + \Sigma_{\eta_{k+1}}$. Since in addition $\mathbf{E}[\vec{\rho}_k^T \vec{\rho}_l|\vec{y}_k] = 0$, it follows that

$$p\left(\vec{\rho}_{k+1}\right) = \frac{\exp\left[-\frac{1}{2}\vec{\rho}_{k+1}\left(\Sigma_{V_k} + \Sigma_{\Lambda_k} + \Sigma_{\eta_{k+1}}\right)^{-1}\vec{\rho}_{k+1}^T\right]}{(2\pi)^{T/2}\left|\Sigma_{V_k} + \Sigma_{\Lambda_k} + \Sigma_{\eta_{k+1}}\right|^{1/2}}$$

is equivalent to the evidence function at the parameter estimation level, given in Eq. (6.6). Hence by maximizing $p(\vec{\rho}_{k+1})$ with respect to the process noise covariance Σ_{Λ_k}, the ML estimates for this covariance can be obtained.

The maximization of $p(\vec{\rho}_{k+1})$ can be simplified if we return to the intended purpose of the Kalman filter; to adaptively vary the number of averages n used in the enhancement of the ECG complexes, depending on the dynamic variations in signal morphology. From Eq. (6.7) it can be inferred that this purpose means that the Kalman gain $\mathbf{K}_k$ can be simplified to a scalar matrix (i.e. a diagonal matrix with all entries equal), or even a scalar. Specifically, by varying the scalar value of $\mathbf{K}_k$ in Eq. (6.7), either more or less weight can be ascribed to the newly arriving ECG complex $\vec{y}_{k+1}$. In other words, the relative contribution of preceding ECG complexes to the estimate $\hat{\vec{V}}_{k+1}$ varies with the value of $\mathbf{K}_k$, essentially similar to adaptation of the number of averages used. The scalar value for $\mathbf{K}_k$ here ensures that all T samples in $\vec{y}_{k+1}$ and all T samples in $\hat{\vec{V}}_k$ are assigned the same weight ($\mathbf{K}_k$ for $\vec{y}_{k+1}$ and $(1-\mathbf{K}_k)$ for $\hat{\vec{V}}_k$), preventing distortion of the ECG complexes. With the assumption of the Kalman gain being a scalar matrix, from Eq. (6.9) it then follows that also Σ_{V_k}, Σ_{Λ_k}, and Σ_{η_k} can be assumed scalar matrices (i.e. $\sigma^2_{V_k}\mathbf{I}$, $\sigma^2_{\Lambda_k}\mathbf{I}$, and $\sigma^2_{\eta_k}\mathbf{I}$, respectively, with $\mathbf{I}$ the $[T\times T]$ identity matrix $\mathbf{I}$ and where σ^2_x is the variance of vector $\vec{x}$), implicitly also assuming that both the measurement and process noise are spatially uncorrelated. The effect of the latter assumptions will be discussed in Section 6.5. With this simplification, not only can each of the scalar covariance matrices be regarded as the matrix representation of the variances of the vectors $\vec{V}_k$, $\vec{\Lambda}_k$, and $\vec{\eta}_k$, but also does the maximization of (the logarithm of) $p(\vec{\rho}_{k+1})$ reduce to the derivative of $\ln p(\vec{\rho}_{k+1})$ with respect to $\sigma^2_{\Lambda_k}$ equated to zero:

$$\begin{aligned}\frac{\partial}{\partial\sigma^2_{\Lambda_k}}\ln p\left(\vec{\rho}_{k+1}\right) = \\ \frac{1}{2}\mathrm{tr}\left[\vec{\rho}_{k+1}\left(\sigma^2_{V_k}\mathbf{I}+\sigma^2_{\Lambda_k}\mathbf{I}+\sigma^2_{\eta_{k+1}}\mathbf{I}\right)^{-2}\vec{\rho}^T_{k+1}\right] \\ -\frac{1}{2}\mathrm{tr}\left[\left(\sigma^2_{V_k}\mathbf{I}+\sigma^2_{\Lambda_k}\mathbf{I}+\sigma^2_{\eta_{k+1}}\mathbf{I}\right)^{-1}\right]=0.\end{aligned} \tag{6.12}$$

Here, $\mathrm{tr}[\cdot]$ denotes the matrix' trace. The use of $\ln p(\vec{\rho}_{k+1})$ instead of the use of $p(\vec{\rho}_{k+1})$ is justified by the monotonic behavior of the logarithm function.

Solving Eq. (6.12) for $\sigma^2_{\Lambda_k}$ yields an estimate for the process noise covariance:

$$\hat{\sigma}^2_{\Lambda_k} = \frac{1}{T}\vec{\rho}_{k+1}\vec{\rho}^T_{k+1} - \sigma^2_{V_k} - \sigma^2_{\eta_{k+1}}. \tag{6.13}$$

By computing the second derivative of $p(\vec{\rho}_{k+1})$ it is straightforward to prove that this result indeed corresponds to a global maximum in $p(\vec{\rho}_{k+1})$. In case the model errors

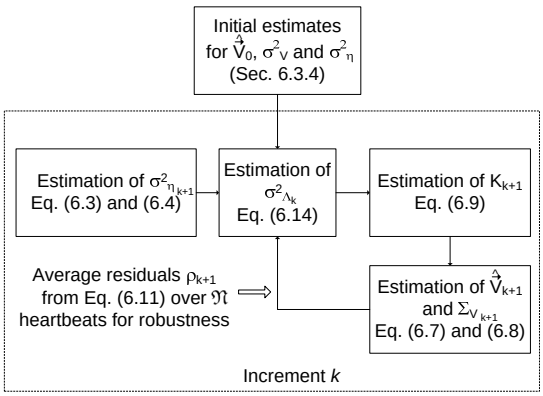

Figure 6.3: *Illustration of the algorithmic implementation of the developed adaptive Kalman filter.*

$\frac{1}{T}\vec{\rho}_{k+1}\vec{\rho}^T_{k+1}$ are smaller than what the theoretical value of the measurement noise $\sigma^2_{\eta_{k+1}}$ predicts, no additional process noise input is required. This leads to the estimator:

$$\sigma^2_{\Lambda_k} = \begin{cases} \frac{1}{T}\vec{\rho}_{k+1}\vec{\rho}^T_{k+1} - \sigma^2_{\hat{V}_k} - \sigma^2_{\eta_{k+1}} & \text{if positive,} \\ 0 & \text{otherwise.} \end{cases} \tag{6.14}$$

The operation of the filter can be explained as follows. In case the model error $\frac{1}{T}\vec{\rho}_{k+1}\vec{\rho}^T_{k+1}$ is larger than what its theoretical value $\sigma^2_{\eta_{k+1}}$ predicts, $\sigma^2_{\Lambda_k}$ increases and this in turn leads to an increase in the Kalman gain. Hence, more emphasis is put on newly arriving data [162]. To improve the robustness and statistical significance of the estimator of Eq. (6.14), instead of a single residual $\vec{\rho}_{k+1}$, the sample mean of $\mathfrak{N}$ residuals will be used [165]. The effect of the chosen value for $\mathfrak{N}$ will be evaluated in Section 6.4.

Implementation of the methods described above in an algorithm constitutes the sequential execution of Eqs. (6.4) and (6.3) to estimate the measurement noise covariance and, subsequently, Eqs. (6.9), (6.7), (6.8), (6.11), and (6.14) for estimation of the ECG signals and process noise covariances. The algorithm is illustrated schematically in Fig. 6.3.

6.3 Data preparation and initial filter settings

6.3.1 Data acquisition

To evaluate the developed Kalman filter a diversity of ECG signals is used. These signals comprise ECG signals of adult patients that suffer from T-wave alternans

(TWA; a condition that renders the amplitude or shape of the ECG's T-wave to often vary significantly between heartbeats), fetal ECG signals recorded from the maternal abdomen, and neonatal ECG signals recorded with textile electrodes.

The three categories of ECG signals are mainly used to illustrate the performance of the filter. The first category (i.e. adult ECG signals with TWA), however, is also used for quantitative evaluation of the filter. In total, 12-lead ECG signals from 23 patients suffering from TWA and of 2 minutes length each are used in this evaluation. The signals are obtained from the MIT-BIH TWA challenge database [166]. To map the filter's performance as a function of the SNR of the recorded signals as well, next to the performance's dependence on $\mathfrak{N}$, the ECG signals are corrupted with additive Gaussian noise of various amplitudes, yielding ECG signals with SNR's ranging from -3 dB to 18 dB.

The TWA signals comprise a rather ideal data set for evaluating the performance of the developed filter. They exhibit relatively high SNR values that can be made smaller by additive Gaussian noise and that moreover facilitate quantitative assessment of the filtered ECG signals (i.e. by comparing the filtered, with additive noise corrupted, ECG signals to the original ECG signals). In addition, the TWA signals exhibit morphological variability in the ECG that originates from underlying physiology.

6.3.2 Preprocessing

The acquired ECG data is preprocessed to remove noise, artifacts, and baseline wander that do not exhibit spectral overlap with the ECG. To this end, two fourth-order Butterworth filters [167] are used; one high-pass filter with cutoff frequency at 0.5 Hz and one low-pass filter with cutoff frequency at 90 Hz.

To suppress the interferences from the powerline grid, a notch filter centered around 50 Hz (or 60 Hz for USA recordings) is used. Again this filter is implemented as a fourth order Butterworth filter. In contrast to the high-pass and low-pass filters mentioned above, this filter, however, also affects the ECG due to the fact that the frequency content of the ECG extends from frequencies of about 1 Hz to frequencies beyond 50 Hz. By choosing the width of the notch filter relatively small – but wide enough to account for fluctuations in the power-line frequency – the distortion of the ECG signals can be kept small.

For the transabdominally recorded fetal ECG recordings, it has to be noted that these are processed as described above, but with an additional processing step in which the interfering maternal ECG is eliminated. The details of this maternal ECG removal are provided in [46] and Chapter 3.

6.3.3 Demarcation of individual ECG complexes

The consecutive individual ECG complexes that are used as input for the filter are defined based on their QRS complexes. Specifically, the QRS complexes are detected in the signals by the method presented in Chapter 5 and the ECG complexes are subsequently defined as the signal within a predefined time-window around the QRS complex. After these ECG complexes have been filtered by the developed Kalman filter, the filtered counterparts of the original ECG signals are generated by placing the filtered ECG complexes back on their original positions. Because the Kalman filter is limited by the fact that the length of the input ECG complexes needs to be fixed (i.e. the length should be T seconds) and because the interval between consecutive ECG complexes varies over time, this ECG signal generation approach suffers from the drawback that in some cases there will be overlap between consecutive filtered ECG complexes and in some cases there will be a gap. By choosing the time-window for the ECG complexes such as to minimize the number of gaps, as much of the original ECG signals as possible is filtered. The gaps that inevitably remain are smoothed by interpolation of the data between successive complexes. The overlapping signal parts, in turn, are smoothed by gradually averaging the contributions of both overlapping complexes. Specifically, the contribution of the first ECG complex is gradually reduced and the contribution of the trailing complex is gradually increased. The value of T chosen here is 120% of the mean interval between consecutive heartbeats.

As mentioned above, before defining the individual ECG complexes, the QRS complexes need to be detected. To facilitate this detection, the SNR of the ECG signals is *a priori* enhanced by linearly combing the signals in such way as to maximize the variance (principal component analysis, PCA) [122]. The linear combination with maximum variance is referred to as the principal component. The QRS complexes are subsequently detected in the principal component as local extrema that exceed an adaptive threshold (Chapter 5). This adaptive threshold is updated continuously by means of a simple Kalman filter and depends on the SNR of the ECG signals complexes in the principal component [46]; when the SNR changes, the threshold is adapted to prevent noise from exceeding it, in the mean time ensuring that the QRS complexes still exceed the threshold. For a more detailed description of the QRS complex detection, the reader is referred to [46] and [138].

6.3.4 Initializing the filter

Before commencing the filtering of the ECG signals, all variables and parameters need to be initialized. For the initial estimate of the ECG complex $\hat{\vec{V}}_0$ the mean ECG complex over $\mathfrak{N}$ heartbeats is used. Here, $\mathfrak{N}$ is the same value as used for estimation of σ^2_Λ. The initial estimate for the measurement noise vector $\hat{\vec{\eta}}_1$ is determined according to its description in Section 6.2.2. The initial estimates for the noise variances $\sigma^2_{V_0}$

and $\sigma^2_{\eta_1}$ are determined as the variances of the respective vectors $\hat{\vec{V}}_0$ and $\vec{\eta}_1$.

For $\mathfrak{N}$, various values ranging between 1 and 25 are used and the performance of the filter for each particular value is evaluated in Section 6.4.

6.4 Evaluation of filter

6.4.1 TWA signals

As mentioned above, the performance of the filter is assessed as a function of both $\mathfrak{N}$ (i.e. the number of residuals $\vec{\rho}$ averaged for robust estimation of the process noise covariance) and the SNR, using the TWA signals of 23 different patients. The performance is quantified by calculating ε, the normalized mean squared error (MSE) between the filtered ECG signals $\hat{\vec{V}}$ and the original ECG signals $\vec{V}$ used (i.e. the signals without additive noise):

$$\varepsilon = \frac{\sum_k \left(\vec{V}_k - \hat{\vec{V}}_k\right)\left(\vec{V}_k - \hat{\vec{V}}_k\right)^T}{\sum_k \vec{V}_k \vec{V}_k^T}, \tag{6.15}$$

where the summation indicates that ε is averaged over all heartbeats in the TWA signals. In addition, as the TWA signals comprise 12 individual ECG signals, ε is averaged over these signals as well (not indicated in Eq. (6.15) for clarity). Note that the original ECG signals $\vec{V}$ are not completely free of noise. However, as the amplitude of this noise is small compared to the amplitude of the ECG signals, the effect of this noise on the calculated ε values is small and disregarded in further discussions on the performance of the filter.

In Fig. 6.4 the normalized MSE ε is plotted as a function of both $\mathfrak{N}$ and the SNR. The results in Fig. 6.4 are averaged over all 23 TWA patients.

From Fig. 6.4(a) it can be seen that for the ECG signals with SNR of -3 dB and 0 dB, ε decreases with increasing $\mathfrak{N}$. That is, for the 0 dB signal, ε increases until $\mathfrak{N} = 5$ and decreases slightly for larger $\mathfrak{N}$. For the ECG signals with SNR larger than 0 dB, ε increases with $\mathfrak{N}$. These findings can be explained as follows. The fact that for high-SNR ECG signals ε is minimal for small $\mathfrak{N}$ stems from the fact that, with almost no noise present, most variations in the ECG signals are of physiological origin. Since a large value for $\mathfrak{N}$ causes slow adaptation of the process noise covariance, a large $\mathfrak{N}$ would yield underestimation of the process noise covariance σ^2_Λ and consequently a too small weight ascribed to newly arriving data. Low-SNR signals, on the other hand, are mostly affected by measurement noise rather than by morphological variability. In this case, large values for $\mathfrak{N}$ ensure that the process noise covariance is not overestimated, hence rendering the weight ascribed to newly arriving data relatively small.

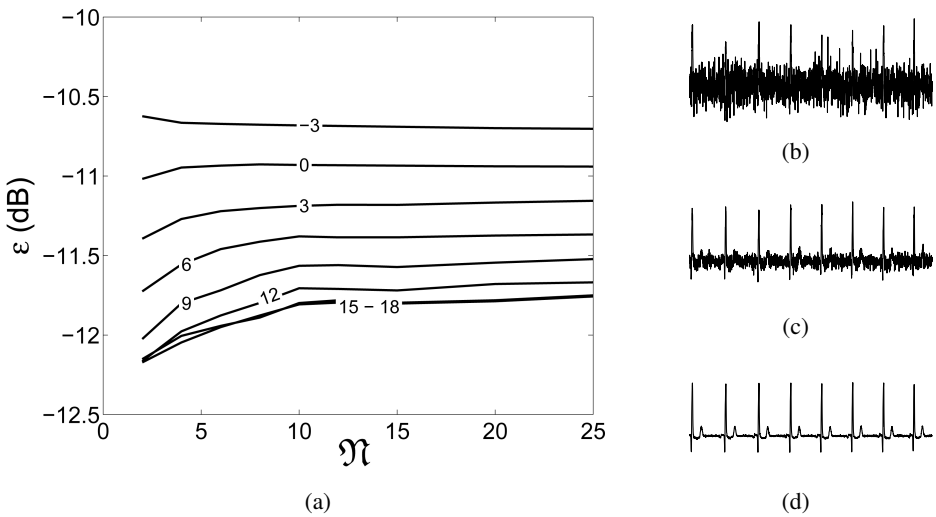

Figure 6.4: *In (a) the performance of the developed Kalman filter, expressed in terms of the normalized MSE* ε*, is plotted as a function of the SNR and the number of ECG complexes* $\mathfrak{N}$ *used in the estimation of the noise covariances. The SNR values corresponding to each of the lines are provided in the graphs and expressed in dB. In (b), (c), and (d) examples of the TWA signals are plotted (each 4 seconds long). The SNRs of these signals are -3 dB, 6 dB, and 24 dB, respectively.*

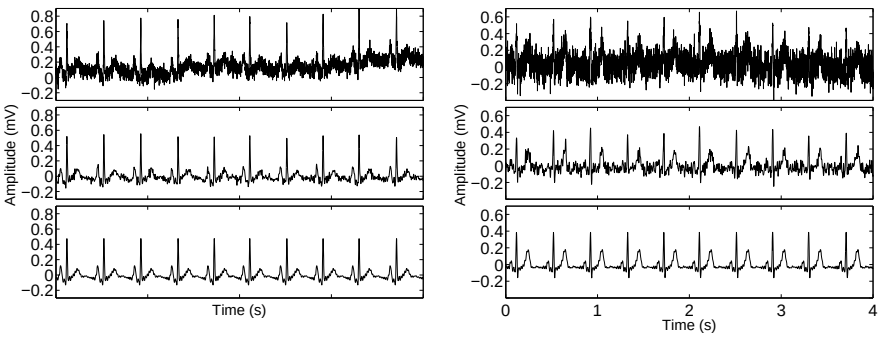

(a) (b)

Figure 6.5: *Examples of TWA signals before filtering (top graph), after preprocessing (center graph), and after filtering with the developed adaptive Kalman filter (bottom graph) filtering, with $N = 5$. In (a) the SNR of the TWA signal is 8 dB and in (b) this SNR=0 dB.*

From the discussion above, it is straightforward to state that the choice for $\mathfrak{N}$ involves a trade-off between robustness against measurement noise and flexibility of the process noise estimation. In Fig. 6.5 the performance of the developed filter (with $\mathfrak{N}$ chosen as 5) is exemplified on two TWA signals.

To illustrate this trade-off, in Fig. 6.4(a) it can be seen that for all recordings, specifically the high-SNR recordings, the normalized MSE ε saturates at about -12 dB. This saturation is due to the persistent underestimation of the process noise covariance for large $\mathfrak{N}$. As a result, the output of the filter cannot fully keep track of morphological variations in the TWA signal, leading, in this particular case, to an estimation error of -12 dB. To ensure optimal performance of the developed filter, the choice for $\mathfrak{N}$ should be based on expected signal behavior. For the TWA signals, $\mathfrak{N}$ is chosen as 5. Due to the larger measurement noise amplitudes anticipated in the fetal and neonatal ECG signals that will be discussed shortly, for these signals $\mathfrak{N}$ will be chosen as 10. From the relatively small gradients in Fig. 6.4(a) it can, nevertheless, be concluded that the specific choice for $\mathfrak{N}$ does not strongly affect the performance of the filter. In other words, irrespective which value for $\mathfrak{N}$ is used, the performance of the developed filter will be about the same. Based on this conclusion, it can be argued that with the adaptive noise covariance estimation, the problem of *a priori* selecting the noise covariances, mentioned in the beginning of Section 6.2.4, is overcome and replaced by the much less critical problem of selecting $\mathfrak{N}$. To substantiate this remark, in Fig. 6.6 the performance of the developed filter is compared to the performance of the same Kalman filter, but now with the adaptive noise covariance estimation replaced by a fixed *a priori* estimation. The estimation of the measurement noise covariance is kept the same for both filters. The values for σ_Λ^2 in this comparison range between -40 dB and 40 dB and are defined relative to the

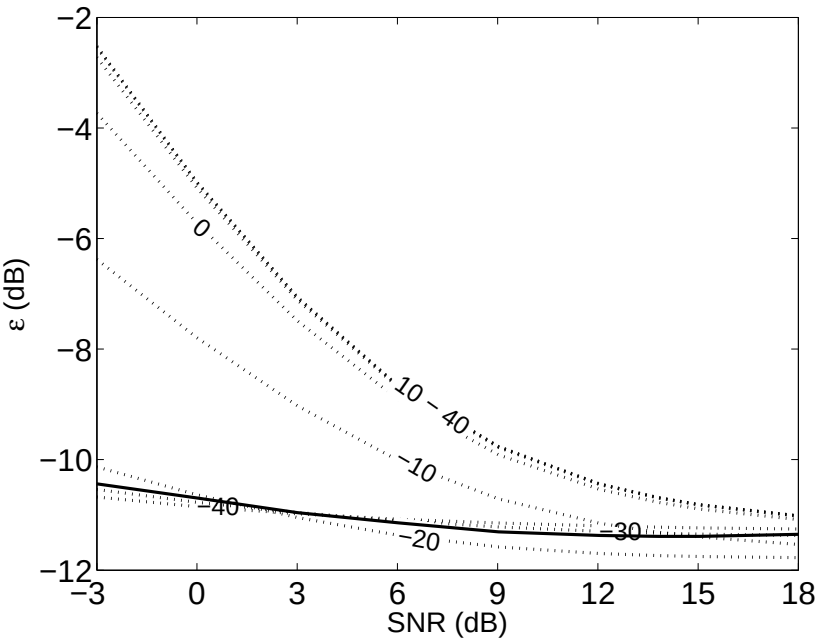

Figure 6.6: *Plot of the performance of the developed Kalman filter, expressed in terms of* ε*, as a function of the SNR of the ECG signals. The performance of the filter with adaptive noise covariance estimation is indicated with the solid line (*$\mathfrak{N}$ *is chosen as 5). The performances of the filters with fixed noise covariance are represented by the dotted lines. The selected noise covariances* σ_Λ^2 *are indicated in the graphs. Due to overlapping, the graphs for 10 dB, 20 dB, 30 dB, and 40 dB are jointly labeled as 10 – 40.*

amplitude of the ECG signals.

From Fig. 6.6 it can be seen that for the Kalman filter with fixed process noise covariance, for simplicity from here on referred to as the fixed Kalman filter, the performance improves with decreasing σ_Λ^2, until σ_Λ^2=-20 dB; from here on, the performance slightly deteriorates. This behavior is consistent with the discussion above that the choice for σ_Λ^2 affects the performance of the filter more strongly than the choice for $\mathfrak{N}$. Underestimation of σ_Λ^2 will result in a relatively small Kalman gain and hence little flexibility of the filter output to account for morphological variations in the ECG. Overestimation of σ_Λ^2 on the other hand, yields a relatively large Kalman gain leading to an output of the filter that not only accounts for morphological variations but also for measurement noise. Straightforwardly, an optimal value exists for

which the performance of the filter is rather good. In the case of the TWA signals used in Fig. 6.6, this optimal value is around -20 dB, but for other ECG signals, this value needs to be re-evaluated.

6.4.2 Fetal ECG signals

When comparing the performance of the fixed filter with σ_Λ^2=-20 dB in Fig. 6.6 to the performance of the adaptive Kalman filter, it can be concluded that this performance is about the same, with the fixed Kalman filter performing slightly better for high-SNR signals. It however needs to be emphasized once more that the fixed Kalman filter operates with a process noise covariance that is fixed at a rather optimal value. When employing both filters for long-term monitoring tasks, a proper *a priori* selection of σ_Λ^2 becomes virtually impossible. Moreover, even when it is possible to *a priori* assess for which value of σ_Λ^2 the filter will perform optimally, the long-term nature of the recording renders the ECG signals likely to exhibit dynamical variations. With these variations, the *a priori* assessed value for σ_Λ^2 needs to be re-evaluated and adapted. Since the adaptive Kalman filter is capable of making this adaptation, it is expected to outperform the fixed Kalman filter for long-term monitoring tasks. To study the behavior of both filters for a dynamical variation in the ECG signal, in Fig. 6.7 a transabdominally recorded fetal ECG signal is presented, exhibiting significant morphological variation as a result of movement.

From Fig. 6.7 it can be seen that, as expected, the estimated adaptive process noise covariance σ_Λ^2 increases when variations in the ECG signal occur (e.g. around 5 seconds and 45 seconds). Especially the variation in the ECG around 45 seconds is of relevance because the fetus shows significant movement here, as was demonstrated by a echocardiographic analysis performed simultaneously with the ECG recording. After the movement epoch, the fetus has taken a slightly different orientation with respect to the electrodes on the maternal abdomen, affecting the morphology of the ECG signal. When the movement sets in, the increased process noise covariance causes an increase in the Kalman gain, hence ascribing more weight to the newly arriving data, as intended.

When comparing the Kalman gains of both the adaptive and fixed Kalman filter – for the latter, σ_Λ^2 is empirically set at $2 \cdot 10^{-13}\,\mathrm{V}^2$ – it strikes that the gain of the fixed filter shows significantly fewer fluctuations than the gain of the adaptive Kalman filter. Consistent with the discussion above on long term monitoring, this rigidity of the fixed Kalman filter renders the fixed Kalman filter less capable of accounting for fast morphological changes in the ECG. This statement is substantiated by the filtered ECG signals in the top panel of Fig. 6.7. After the movement of the fetus, the fixed Kalman filter needs about 10 seconds to completely adapt its output to the new ECG morphology, whereas adaptation by the Kalman filter with adaptive noise covariance is almost instantaneous.

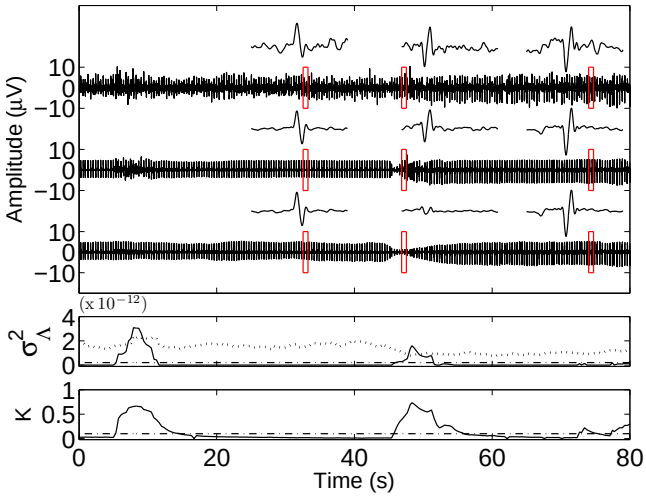

(a)

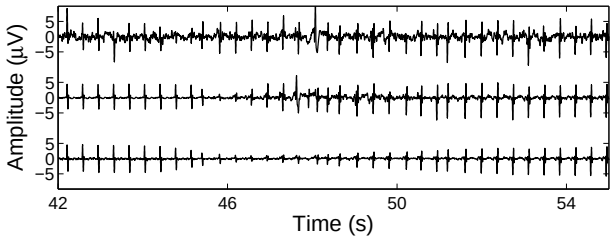

(b)

Figure 6.7: *(a): The top panel shows a fetal ECG signal recorded from the maternal abdomen, before filtering (top graph), after filtering with the adaptive Kalman filter (center graph) and after filtering with the fixed Kalman filter (bottom graph). The ECG complexes indicated in the rectangles are shown zoomed in on in the accompanying graphs. The second panel shows the estimated process noise covariance* σ_Λ^2 *for the adaptive Kalman filter (solid line), the process noise covariance for the fixed Kalman filter (dash-dot line) and the estimated measurement noise covariance* σ_η^2 *(dotted line). The bottom panel shows the Kalman gain* $\mathbf{K}$ *for both the adaptive (solid line) and fixed (dash-dot line) filters. For the estimation of* σ_Λ^2 *and* $\mathbf{K}$ *in the adaptive Kalman filter,* $\mathfrak{N}$ *is chosen equal to 10. Since the process noise covariance is often estimated as 0 (see Eq. (6.14)),* σ_Λ^2 *cannot be expressed in dB as in Fig. 6.6. Hence,* σ_Λ^2 *is expressed here in an absolute sense (i.e. in* V^2*). In (b) a zoom of the top panel between 42 and 55 seconds is depicted.*

Regarding the measurement noise covariance σ_η^2, it can be seen in Fig. 6.7 that it decreases as a result of the fetal movement. This decrease can be explained by the fact that, whereas the noise amplitude remains about the same, the signal amplitude increases as a result of the movement. This rise in the ECG amplitude can be explained by e.g. a movement-inflicted reduction in the heart-electrode distance.

6.4.3 Neonatal ECG

For the (maternal) movement artifact occurring around 5 seconds in Fig. 6.7, it can be argued that the fixed Kalman has an advantage over the adaptive Kalman filter in that it is less affected by the movement artifact. However, when examining the original, unfiltered ECG signal, this signal appears so corrupted that it hardly contains any ECG information. The output generated by the fixed Kalman filter therefore mostly comprises information from previous heartbeats. Naturally, in case of a local artifact that only affects a single ECG signal also the adaptive Kalman filter does not update the estimated ECG. That is, when the artifact occurs locally, the estimated measurement noise covariance will be relatively large, significantly decreasing the Kalman gain. Conversely, in cases where the artifact occurs simultaneously at more than one location, the estimated measurement noise will decrease and both the estimated process noise covariance and Kalman gain will increase. This process is illustrated in Fig. 6.8 in which a neonatal ECG, recorded in an incubator with textile electrodes, is depicted.

The neonatal ECG signals shown in Fig. 6.8 illustrate that in case of an artifact that occurs in more than one ECG signal at the same time, the newly arriving data is ascribed more weight (i.e. the Kalman gain is increased) to ensure rapid updating of the ECG estimate. For local artifacts, such as in the upper neonatal ECG signal occurs around 55 seconds, the Kalman gain changes only little, ensuring that the artifact is no longer present in the filtered ECG signal.

6.5 Discussion & Conclusions

In this paper a Kalman filter with adaptive noise covariance estimation has been developed and evaluated on a variety of ECG signals to assess whether the filter is capable of enhancing the SNR of these signals, while at the same time preserving clinically relevant morphological variations in the ECG. The filter operates by sequentially estimating the measurement and process noise covariances and uses these covariances to estimate the Kalman gain and update the estimated ECG complexes. In cases where the variations between consecutive ECG complexes can no longer be explained as measurement noise, the variations are taken to be morphological variations and the process noise covariance is increased. This, in turn, leads to an increase

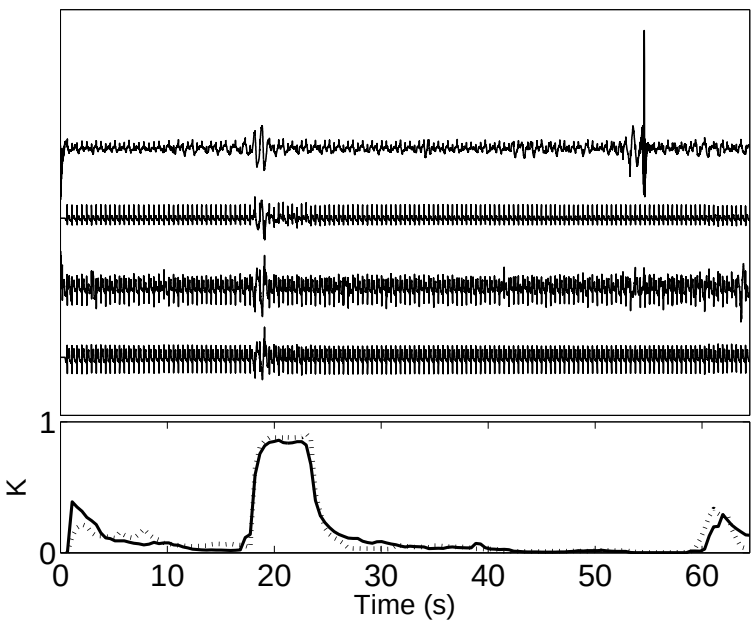

Figure 6.8: *In the top panel, two neonatal ECG signals recorded in the incubator using textile electrodes are depicted. The first and third signal from above are the preprocessed ECG signals and the second and fourth signals are the corresponding signals after filtering with the adaptive Kalman filter. In the bottom panel, the Kalman gains for both filtered signals are plotted. The solid line corresponds to the upper ECG signal and the dotted line corresponds to the lower ECG signal.*

of the Kalman gain and consequently, more weight is ascribed to the newly arriving ECG complex.

The performance of the filter is compared to the performance of a similar Kalman filter with fixed process noise covariance. For this fixed Kalman filter the process noise covariance needs to be *a priori* estimated and hence, to ensure adequate performance of the filter, requires rather detailed information on the ECG signal dynamics. The comparison between the fixed and adaptive Kalman filters demonstrates that the adaptive filter performs almost as well as a fixed Kalman filter with optimally chosen process noise covariance. In addition, for long-term monitoring tasks in which the ECG signal characteristics change, the adaptive Kalman filter is capable of quickly adapting its noise estimation to match the filter's output to the new input. The fixed Kalman filter, on the other hand, needs about 10 seconds to adjust its output due to its less flexible estimation of the Kalman gain.

In the derivation of the adaptive Kalman filter several assumptions are made for mathematical simplicity, but that might limit the applicability of the filter. For one, the ECG is assumed to have a Gaussian probability distribution, or equivalently, both the process and measurement noise are assumed to be Gaussian. In addition, the measurement and process noise are assumed to be uncorrelated. The latter assumption might limit the performance of the filter to some extent as, in particular, the process noise generally exhibits spatial correlation across the individual ECG signals. This limitation seems however small, as evidenced by the results. The same thing holds for the assumption of Gaussian noise. Although this assumption might impose a rather severe limitation to the filter's applicability, the evaluation of the filter on the fetal and neonatal ECG signals – that are corrupted by physiological noise, rather then by Gaussian noise – demonstrates that the filter also performs relatively well for non-Gaussian ECG signals. Besides providing a rather elegant solution to the filter problem, the mathematical simplification also relaxes the computational complexity of the filter, rendering an implementation of the filter in Matlab® (The Mathworks, Inc.) capable of filtering at least 12 ECG signals simultaneously in real-time.

Another decision that might limit the applicability of the developed filter is the fixed choice for the length of the ECG complexes (i.e. 120% of the mean interval between consecutive heartbeats). In cases of significant heart rate variability, it can occur that a single ECG complex contains information that originates from two consecutive heartbeats. Problems associated with this fixed ECG complex length can, however, be circumvented by only including those parts of the ECG complex that correspond to the same heartbeat in the calculation of the measurement noise, process noise, and Kalman gain. Upon reassembling the filtered ECG complexes into a filtered ECG signal that is composed of a multitude of heartbeats, the redundant parts of the filtered ECG complexes can be omitted.

As mentioned previously, the TWA signals comprise a rather ideal set for quanti-

tative evaluation of the developed filter. Here, however, distinction needs to be made between TWA signals that exhibit morphological variability at the microvolt level and macroscopic TWA signals that exhibit substantially more morphological variability. In our evaluation, only the latter TWA signals were used. With regard to the preprocessing of the TWA (and fetal and neonatal ECG) signals, the high-pass filter is expected to slightly distort the susceptible ST segment. Preprocessing is nevertheless performed to ensure that the measurement noise has indeed zero mean, as assumed in Section 6.2. The effect of omitting the preprocessing, in order to yield as little distortion of the filtered ECG signals as possible, on the performance of the filter is subject of future research. Also subject of future research is the evaluation of the filter's performance on ECG signals that are even more ideal than the TWA signals, such as ECG signals with isolated or slow pattern changes.

The accurate estimation of the measurement noise covariance is rather critical for the performance of the adaptive Kalman filter. When this covariance is overestimated, all ECG signal variations will be be ascribed to measurement noise and hence the process noise covariance will be underestimated, rendering the filter less capable of quickly adapting to dynamical signal variations. Conversely, underestimation of the measurement noise covariance leads to overestimation of the process noise covariance, causing the filter to also ascribe more weight to ECG complexes that are corrupted by measurement noise. The estimation of the measurement noise covariance is performed by exploiting the spatial correlation of simultaneously recorded multi-channel ECG signals. In a simplified model, all ECG signals can be assumed to originate from the same three-dimensional source and hence, three independent ECG signals should be enough to predict the morphology of a fourth ECG signal. Those parts of the fourth ECG signal that cannot be accounted for by the three other ECG signals, can therefore be marked as noise contributions. One of the main drawback of this approach is that for enhancing the ECG of one signal, at least three other ECG signals need to be recorded. However, for most clinical applications several ECG signals are recorded and even if there is no clinical relevance of recording several channels, it hardly constitutes a technological challenge to record more than three ECG signals simultaneously. Another drawback lies in the adopted model for the spatial correlation between the ECG signals. In this model, all ECG signal components that cannot be accounted for by the three-dimensional source are taken to be measurement noise, leading to underestimation of the process noise. By using more than four ECG signals, e.g. a standard configuration of 12 electrodes, this problem can be largely overcome.

For non-invasive fetal ECG recordings performed on the maternal abdomen, the requirement of at least four ECG signals of which three are linearly independent could be troublesome. Approximately between the 28th and 34th week of gestation, the fetus is covered by a waxy layer (i.e. vernix caseosa) that electrically isolates the

fetus, apart from a few places that are hypothesized to be over the oro-nasal area and the umbilical cord [39]. As a result of this layer, preferred conduction paths for the ECG signals arise, potentially making the number of independent ECG signals drop below three. Additional research to determine whether the presented method indeed fails in presence of the vernix caseosa is however required.

Additional research is also required to assess whether the application field of the filter can be extended. For ECG enhancement, the filter basically operates by averaging consecutive ECG complexes and varying the number of complexes included in the average, based on the amount of variation in the data. This approach can, however, also be applied in enhancement of other quasi-periodical signals that may vary due to either changes in the process or changes in the measurement noise. An example of such an application is the SNR enhancement of event-related potentials in electroencephalography studies [168].

6.6 Comments

In Chapter 5, it was mentioned that the effect of incorrectly detected QRS complexes is relatively small because upon averaging the contribution of the corresponding ECG complexes is reduced. The averaging filter developed in this chapter can nevertheless assign a relatively large weight to the incorrect ECG complex under the assumption of a physiological event occurring. However, because the noise covariances are estimated based on several consecutive ECG complexes (for the fetal EGC, $\mathfrak{N}$ is chosen 10), the influence of an incorrectly detected QRS complex is relatively small.

Chapter 7

Bayesian approach to patient-tailored vectorcardiography

The enhanced fetal ECG signals can be combined with knowledge on the employed electrode configuration to yield the fetal VCG. In general, the VCG is calculated by linearly combining the recorded ECG signals based on the locations of the electrodes that recorded them. In case of the fetal VCG, the amount of maternal tissue in between the fetal heart and the abdominal electrodes is different for each electrode. As a result, signal attenuation effects are different for each abdominal fetal ECG signal and hence, calculation of the VCG using only the electrode locations and not compensating for attenuation effects will yield a VCG that can be significantly distorted. In this chapter, the relation between VCG, ECG, and signal attenuation is described in a simplified model. Based on this model and the recorded ECG signals, the (undistorted) VCG and signal attenuation are subsequently estimated by means of an iterative procedure.[1]

7.1 Introduction

Cardiac contractions originate from the propagation of an action potential through the cardiac tissues. The front of the propagating action potential causes the occurrence of numerous electrical dipoles. By superimposing these electrical dipoles at each point in time, the electrical activity of the heart can be modeled as a single electrical field vector, originating in the heart, that varies in both amplitude and orientation over time [32, 33]. The time path of this electrical field vector during a single cardiac contraction is referred to as the vectorcardiogram (VCG). The electrocardiogram (ECG) recorded at the cutaneous surface can be viewed as the potential caused by this electrical field vector and therefore depends on both the distance between the recording electrode and the heart and on the conductive properties of the intermediate tissues.

[1]This chapter is based on the paper published as *R. Vullings, C.H.L. Peters, S.I. Mossavat, S.G. Oei and J.W.M. Bergmans, "Bayesian approach to patient-tailored vectorcardiography", IEEE Trans Biomed Eng. 2010 Mar;57(3):586-95.*

It has to be noted here that in this dipole model, the electrical field vector (and with that the VCG) is reported to only describe between 70 and 95% of the power of the ECG [33, 169, 170]. The remaining 5 to 30% of the ECG originates from insufficiencies in the dipole model such as the inclusion of non-dipolar components [31] and movement of the dipole origin [30].

The problem of improving the dipole model, with the goal of completely imaging and visualizing the electrical activity of the heart, has been addressed by researchers in the field of cardiac electrical imaging [171–173]. However, as nearly all the proposed methods for imaging the electrical activity are based on body surface potential maps (BSPM), i.e. lead systems consisting of a relatively large number of electrodes [174], for reasons of workability none of these methods has made its way into clinical practice. Clinicians generally prefer to use the standard 12-lead ECG for assessing the condition of the heart, in spite of the diagnostic inferiority of the 12-lead ECG with respect to BSPM.

With recent improvements in (wireless) data acquisition technology, the interest in ambulatory ECG monitoring is rapidly increasing. In order to increase patient comfort and reduce bandwidth requirements, the use of as few ECG leads as possible is preferred. However, as mentioned above, clinicians are accustomed to using the 12-lead ECG, theoretically implying that all 12 ECG leads need to be recorded and subsequently transmitted. By determining the VCG from fewer than 12 leads and using this VCG to predict the remaining leads, nevertheless, the problem of patient discomfort can be overcome. In addition, for assessing specific cardiac pathologies like right ventricular hypertrophy and myocardial infarcts, direct analysis of the VCG is considered to be superior with respect to 12-lead electrocardiography [48].

As mentioned previously, the relation between the ECG at the cutaneous surface and the VCG depends on the distance between the heart and the electrodes and the conductive properties of the intermediate tissues. The currently most widely used method to determine the VCG from a ECG recording, referred to as the inverse Dower method [47], accounts for both this distance and conductive properties. It entails a fixed, numerical description of a matrix that maps the VCG onto the 12-lead ECG. Due to this fixed numerical description, however, it assumes the same geometry and conductive properties for all patients. Consequently, it cannot provide accurate VCGs for patients that do not conform to the assumed conduction characteristics, such as patients that suffer from severe obesity. This category of patients has an increased risk of cardiac failure [175] and is therefore in more need of VCG examination than ”standard” patients.

When determining the VCG of the fetus through ECG recordings on the maternal abdomen, the problem of patients not conforming to the model is even more evident [39]. Not only does the position of the fetal heart with respect to the abdominal electrodes vary between patients, but also do, among other variations, the

amount of amniotic fluid, placental position, and abdominal fat differ from one pregnant woman to the other. Hence, for determining the fetal VCG, the inverse Dower matrix can only contain information on the electrode positions and not on the unknown heart-electrode distance and conduction properties. These conduction properties are unknown as, in contrast to the regular VCG, few models on the fetal signal propagation exist and the models that do exist cannot account for all possible positions of the fetal heart [63]. Even so, determining the fetal VCG can have significant value in fetal health monitoring. Changes in orientation of the QRS loop, for instance, can be an indication of fetal movement [176], while fetal ECG analysis – which can provide information on fetal oxygenation [2] – is facilitated by projecting the VCG onto leads that are familiar to physicians [177]. In addition, early-stage diagnosis of fetal congenital heart disease might in future become treatable and is facilitated by vectorcardiography, i.e, by projecting the VCG onto the leads used in standard 12-lead ECG analysis.

The common problem in these VCG applications is the lack of a way to account for variations in the composition and geometry of the tissues between the heart and cutaneous surface, leading to inaccurate VCG estimates for patients that do not conform to the standard. Naturally, by performing MRI or ultrasound imaging prior to the ECG recording, the geometry of the intermediate tissues can be estimated and accounted for [104]. However, particularly in case of the fetal VCG, the geometry is not expected to remain the same throughout the recording. Moreover, for ambulatory applications the use of MRI or ultrasound imaging is not practical. To nevertheless account for variations in the composition and geometry of intermediate tissues, in this chapter a method is developed for patient-tailored vectorcardiography (PTV), i.e. for determination of the VCG from multi-lead ECG recordings considering the geometrical and compositional variations. For quantitative evaluation, the method is applied to both non-standard adult ECG and fetal ECG recordings.

The method uses Bayesian probability theory to determine the joint probability distribution for both the VCG and a scaling matrix that models the attenuation at each recording site, given the recorded ECG. This probability distribution is based on a simplified model of the relation between the VCG and ECG. This model stipulates that the ECG at each recording site is generated by the projection of the VCG onto the corresponding ECG lead vector. To account for attenuation effects, each projected VCG is scaled by an *a priori* unknown scaling parameter. Inaccuracies in the model and noise in the ECG are assumed to originate from a Gaussian distribution. The optimal VCG estimate, in the sense of the maximum a posteriori (MAP) solution, is obtained from the joint probability distribution by means of an approximate inference technique referred to as variational inference [132].

Besides analysis of the contour and orientation of the QRS loop, the VCG is mainly used for predicting the shape of ECG signals that are not physically recorded.

This provides a way for evaluating the developed method, namely, the method can be evaluated by recording separate reference ECG signals and comparing these to the prediction of these signals from the VCG. To quantitatively evaluate the performance of the developed method on nonstandard adult patients, this evaluation approach is applied on randomly scaled adult ECG signals.

To recapitulate, the developed method for vectorcardiography models the conductive properties of the tissues between cutaneous electrodes and the heart and estimates the parameters of this model to obtain a patient-tailored estimate of the VCG. Applications of this method include improved assessment of the adult VCG, in particular for non-average patients, and assessment of the fetal VCG from non-invasive recordings. As a basis of reference for the developed method in Section 7.2 the inverse Dower matrix method is discussed briefly. In Section 7.3 the developed method is presented. Section 7.4 discusses the acquisition of the data and the evaluation of the method, while in Section 7.5 the results are presented. Finally, in Section 7.6 these results are discussed and conclusions are drawn.

7.2 Inverse Dower matrix for vectorcardiography

The Dower matrix was introduced by Dower *et al.* in [47] and describes the matrix that maps the VCG onto the 12-lead ECG signals, taking into account standardized electrode positions and non-linear signal attenuation effects. Even though the Dower matrix does not account for inter-patient variability, in practice the resulting VCG estimate is clinically useful [47].

By defining $\mathbf{V}$ as the $[N \times T]$ ECG matrix and $\mathbf{D}$ as the $[N \times 3]$ Dower matrix, the relation between these matrices can be described by

$$\mathbf{V} = \mathbf{DS} + \mathbf{H}, \tag{7.1}$$

with $\mathbf{S}$ the $[3 \times T]$ VCG matrix and $\mathbf{H}$ a $[N \times T]$ noise matrix with zero-mean Gaussian distribution for each row.

The model of Eq. (7.1) is significantly simplified. In reality, not only is the noise expected to be non-Gaussian, including non-dipolar components of the electrical activity of the heart, but also do boundary effects and inhomogeneities of the conductive medium play a significant role. To account for these effects, the fixed numerical Dower matrix $\mathbf{D}$ is defined in such a way that is does not only consider the electrode positions with respect to one another, but also considers the boundary and conductivity effects to some extent. More in particular, for an infinite uniform medium the mapping matrix between the VCG and ECG would only contain electrode positions. Any difference between the Dower matrix and electrode positions has, thus, been intended to account for boundary effects and tissue inhomogeneities.

In this simplified model of Eq. (7.1), the optimal VCG estimate $\hat{\mathbf{S}}_{\text{Dower}}$ can be assessed as the maximum likelihood (ML) solution:

$$\hat{\mathbf{S}}_{\text{Dower}} = \left(\mathbf{D}^T\mathbf{D}\right)^{-1}\mathbf{D}^T\mathbf{V} = \mathbf{D}^{\dagger}\mathbf{V}, \tag{7.2}$$

with $\mathbf{D}^{\dagger}$ the Moore-Penrose pseudoinverse [178, 179] of the Dower matrix.

7.3 Bayesian vectorcardiography

7.3.1 Inter-patient ECG variability

For each patient the position of the heart with respect to the cutaneous electrodes and the conductive properties of the intermediate tissues is different. Because of its fixed numerical nature, the Dower matrix cannot account for any of these differences. However, although the matrix that maps the VCG onto the ECG is expected to vary in a non-linear way as a function of inter-patient differences in geometry and conductivity, by assuming an individual scaling for each ECG signal, these non-linear variations can be approximated to a first order as (see also Fig. 7.1):

$$\mathbf{V} = \alpha\mathbf{DS} + \mathbf{H}. \tag{7.3}$$

Here, α is an $[N \times N]$ diagonal scaling matrix of which the diagonal elements α_i represent the linear scaling of the ECG signals $\vec{V}_i$ and $\mathbf{H}$ is a $[N \times T]$ matrix representing noise in the ECG signals. The reason that α is taken a diagonal scaling matrix follows directly from the assumption of individual scaling for each ECG signal. Namely, the ith row of the matrix $\mathbf{V}$ represents the projection of the VCG $\mathbf{S}$ onto the ith row of $\mathbf{D}$, scaled with a constant α_i. The matrix representation of this scaling yields a matrix with α_i on the diagonal and zeros elsewhere. The reason for keeping the matrix multiplications $\mathbf{D}$ and α separated in this model is the fact that the matrix $\mathbf{D}$ is assumed known, i.e. the Dower matrix, while the elements of α are as yet unknown model parameters.

Since both $\mathbf{S}$, α, and $\mathbf{H}$ are unknown, the VCG $\mathbf{S}$ cannot be readily assessed from $\mathbf{V}$. However, by employing a statistical analysis, the VCG can be estimated, given only the ECG $\mathbf{V}$, Dower matrix $\mathbf{D}$, and noise variance Σ plus some assumptions on statistical independencies and noise characteristics, which are made explicit in Section 7.3.2.

7.3.2 Statistical analysis

Assuming the noise $\mathbf{H}$ to have a Gaussian probability distribution with zero mean and variance Σ and using Bayes' theorem [150], the joint probability distribution of $\mathbf{S}$ and

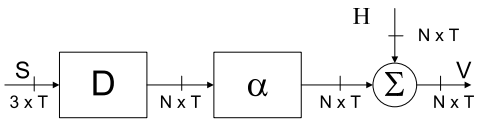

Figure 7.1: *Schematic overview of the model describing the relation between the VCG and the ECG. The VCG is projected onto the matrix* **D** *containing electrode positions and subsequently scaled by the diagonal matrix* α *to model attenuation effects. Imperfections in this model and additional noise are described by the noise matrix* **H**.

α, given **V**, **D**, and Σ obeys

$$p(\mathbf{S},\alpha|\mathbf{V},\mathbf{D},\Sigma) = p(\mathbf{S},\alpha|\mathbf{D},\Sigma)\,\frac{p(\mathbf{V}|\mathbf{D},\mathbf{S},\alpha,\Sigma)}{p(\mathbf{V}|\mathbf{D},\Sigma)}. \tag{7.4}$$

The reason for assuming the noise to have a zero-mean Gaussian distribution is similar as for Eq. (7.1); boundary effects and tissue inhomogeneities are taken to be accounted for by the definition of the Dower matrix **D**. In addition, inter-patient variability in these boundary effects and inhomogeneities are approximated by the linear scaling α. The reason for using this simplified model of the inter-patient variability and noise is to yield an analytical tractable solution for the VCG estimation problem.

Considering the evidence $p(\mathbf{V}|\mathbf{D},\Sigma)$ in Eq. (7.4) a normalization term, assuming α and **S** *a priori* statistically independent, and assuming no prior knowledge on **S**, hence taking $p(\mathbf{S}|\mathbf{D},\Sigma)$ to be a uniform distribution, Eq. (7.4) can be rewritten as

$$p(\mathbf{S},\alpha|\mathbf{V},\mathbf{D},\Sigma) \propto p(\alpha|\mathbf{D},\Sigma)\,p(\mathbf{V}|\mathbf{D},\mathbf{S},\alpha,\Sigma). \tag{7.5}$$

The terms on the right-hand side of Eq. (7.5) are referred to as the prior probability distribution and likelihood, respectively. The assumption of α and **S** to be *a priori* statistically independent can, intuitively, be explained by the fact that **S** is affected by changes in the electrical activity of the heart while α is only affected by changes in the propagation path between the heart and the cutaneous surface.

As mentioned previously, α represents a first-order approximation of the variations in the ECG caused by inter-patient differences in boundary effects and tissue inhomogeneities. As a result, the elements of α are, among other factors, related to the distance between heart and electrodes. With information on the distance between the heart and electrode i also providing information on the distance between the heart and electrode k, the elements α_i are mutually dependent. For reasons of mathematical simplicity, however, the elements of α are assumed to be statistically independent [180] and thus the prior probability distribution can be expressed as

$$p(\alpha|\mathbf{D},\Sigma) = \prod_i p(\alpha_i|\mathbf{D},\Sigma). \tag{7.6}$$

The probability distribution for each of the individual scaling elements, $p(\alpha_i|\mathbf{D},\Sigma)$, can be defined based on available models of torso geometry and conductivity [181, 182]. This would, however, lead to a mathematically complex prior distribution. To simplify the final algorithm, the prior distribution is chosen uniform yielding no prior information on α:

$$p(\alpha|\mathbf{D},\Sigma) = \text{constant}. \tag{7.7}$$

The impact of these physically unjustified – but mathematically simplifying – assumptions, i.e. mutual independency of the elements of α and an uniform prior probability distribution for $p(\alpha|\mathbf{D},\Sigma)$, on the performance of the developed PTV method is discussed later on in Section 7.6.

As mentioned previously, the noise $\mathbf{H}$ is assumed to have a zero-mean Gaussian distribution with variance Σ. Combining this with the model of Eq. (7.3) and the assumption that the rows of both $\mathbf{V}$ and $\mathbf{H}$ are statistically independent, the likelihood is given by:

$$p(\mathbf{V}|\mathbf{D},\mathbf{S},\alpha,\Sigma) = \prod_i \exp\left[-\frac{1}{2\sigma_i^2}\left(\vec{V}_i - \alpha_i\vec{D}_i\mathbf{S}\right)\left(\vec{V}_i - \alpha_i\vec{D}_i\mathbf{S}\right)^T\right], \tag{7.8}$$

where σ_i^2 is the variance of the ith row of $\mathbf{H}$. Moreover, $\vec{V}_i$ is a time vector describing the ECG signal recorded at position $\vec{D}_i$, so that $\vec{V}_i$ is a $[1 \times T]$ vector and $\vec{D}_i$ is a $[1 \times 3]$ vector.

The statistical independence between the rows of $\mathbf{V}$ is justified by applying d-separation [132] on the likelihood. Intuitively, this independence can be explained by the fact that for given $\mathbf{D}$, $\mathbf{S}$, α, and Σ, variations in one ECG signal do not affect any of the other ECG signals. More precisely, although the ECG signal changes, none of the variables $\mathbf{D}$, $\mathbf{S}$, α, and Σ change (as they are given), hence not affecting the other ECG signals. The assumption on statistical independence between the rows of $\mathbf{H}$ is justified analogously.

Substituting Eq. (7.7) and (7.8) in Eq. (7.5) yields the joint posterior probability distribution for $\mathbf{S}$ and α:

$$\begin{aligned} p(\mathbf{S},\alpha|\mathbf{V},\mathbf{D},\Sigma) &\propto \prod_i \exp\left[-\frac{1}{2\sigma_i^2}\left(\vec{V}_i - \alpha_i\vec{D}_i\mathbf{S}\right)\left(\vec{V}_i - \alpha_i\vec{D}_i\mathbf{S}\right)^T\right] \\ &= \exp\left[-\sum_i \frac{1}{2\sigma_i^2}\left(\vec{V}_i - \alpha_i\vec{D}_i\mathbf{S}\right)\left(\vec{V}_i - \alpha_i\vec{D}_i\mathbf{S}\right)^T\right]. \end{aligned} \tag{7.9}$$

7.3.3 Variational inference on the vectorcardiogram

Although the MAP solution for the VCG, which in this case is equivalent to the maximum likelihood solution, can be assessed by integrating Eq. (7.9) over α and determining for which $\mathbf{S}$ the resulting probability distribution is maximal, the required

integral is impossible to evaluate analytically. However, by employing variational inference [132], in factorized form also known as mean field theory [183], the MAP solution for the VCG can be approximated.

In variational inference, the posterior probability distribution $p(\mathbf{S},\alpha|\mathbf{V},\mathbf{D},\sigma^2)$ is approximated by the variational distribution $q(\mathbf{S},\alpha)$:

$$p\left(\mathbf{S},\alpha\middle|\mathbf{V},\mathbf{D},\sigma^2\right) \approx q\left(\mathbf{S},\alpha\right). \tag{7.10}$$

The goal of variational inference is now to restrict the family of possible distributions $q(\mathbf{S},\alpha)$ sufficiently that it comprises only tractable solutions, while at the same time allowing it to be sufficiently rich and flexible to obtain a good approximation to the true posterior probability distribution.

A way of restricting the family of distributions is by assuming it to factorize into

$$q\left(\mathbf{S},\alpha\right) = q_{\mathbf{S}}\left(\mathbf{S}\right)\prod_j q_{\alpha_j}\left(\alpha_j\right). \tag{7.11}$$

Substituting the factorized probability distributions from Eq. (7.11) into a lower bound for the true posterior, provided and discussed extensively in [132], results in an expression for the optimal solutions $\hat{q}_{\mathbf{S}}(\mathbf{S})$ and $\hat{q}_{\alpha}(\alpha)$ [132]:

$$\ln\hat{q}_{\mathbf{S}}\left(\mathbf{S}\right) = \mathbf{E}_{\alpha}\left[\ln p\left(\mathbf{V},\mathbf{S},\alpha\,|\mathbf{D},\Sigma\right)\right] + \text{const.} \tag{7.12}$$

$$\ln\hat{q}_{\alpha}\left(\alpha\right) = \mathbf{E}_{\mathbf{S}}\left[\ln p\left(\mathbf{V},\mathbf{S},\alpha\,|\mathbf{D},\Sigma\right)\right] + \text{const.} \tag{7.13}$$

Here, $\mathbf{E}_y[x]$ denotes the expected value of x with respect to the probability distribution $q(y)$.

Assuming a Gaussian distribution for $q_{\alpha_j} = \mathcal{N}(\alpha_j|\mu_{\alpha_j},\sigma^2_{\alpha_j})$ with mean μ_{α_j} and variance $\sigma^2_{\alpha_j}$, the optimal solution for the VCG $\mathbf{S}$ can be evaluated as

$$\begin{aligned}\ln\hat{q}_{\mathbf{S}}\left(\mathbf{S}\right) &= \int\prod_j \mathcal{N}\left(\alpha_j\middle|\mu_{\alpha_j},\sigma^2_{\alpha_j}\right)\ln p\left(\mathbf{S},\alpha\,|\mathbf{V},\mathbf{D},\Sigma\right)\mathrm{d}\alpha_j + \text{const.} \qquad (7.14)\\ &= -\sum_i\left\{\frac{1}{2\sigma_i^2}\left(\vec{D}_i\mathbf{S}\right)\left(\vec{D}_i\mathbf{S}\right)^T\left(\sigma^2_{\alpha_i}+\mu^2_{\alpha_i}\right) - \vec{D}_i\mathbf{S}\sigma_i^{-2}\vec{V}_i^T\mu_{\alpha_i}\right\} + \text{const.}\end{aligned}$$

Since the term on the right-hand side of Eq. (7.14) is quadratic with respect to $\mathbf{S}$, $\hat{q}_{\mathbf{S}}(\mathbf{S})$ is a Gaussian distribution. For reasons of convenience this distribution is expressed with respect to $\vec{D}_i\mathbf{S}$. From Eq. (7.14) it follows that this distribution has mean $\vec{\mu}_{\vec{D}_i\mathbf{S}_i}$ and variance $\Sigma_{\vec{D}_i\mathbf{S}_i}$ given by:

$$\vec{\mu}_{\vec{D}_i\mathbf{S}_i} = \frac{\mu_{\alpha_i}}{\sigma^2_{\alpha_i}+\mu^2_{\alpha_i}}\vec{V}_i \qquad \text{and} \qquad \Sigma_{\vec{D}_i\mathbf{S}_i} = \frac{\sigma_i^2}{\sigma^2_{\alpha_i}+\mu^2_{\alpha_i}}. \tag{7.15}$$

Substituting this result in Eq. (7.13) gives, analogous to Eq. (7.14)

$$\ln \hat{q}_\alpha(\alpha) = -\sum_i \left\{ \frac{\alpha_i^2}{2\sigma_i^2} \left(\Sigma_{\vec{D}_i \mathbf{S}_i} + \vec{\mu}_{\vec{D}_i \mathbf{S}_i} \vec{\mu}^T_{\vec{D}_i \mathbf{S}_i} \right) - \frac{\alpha_i}{\sigma_i^2} \vec{\mu}_{\vec{D}_i \mathbf{S}_i} \vec{V}_i^T \right\} + \text{const.}, \tag{7.16}$$

which reflects a Gaussian distribution for $\hat{q}_\alpha(\alpha)$ as well, with mean μ_{α_i} and variance $\sigma^2_{\alpha_i}$ given by:

$$\mu_{\alpha_i} = \frac{\vec{\mu}_{\vec{D}_i \mathbf{S}_i} \vec{V}_i^T}{\Sigma_{\vec{D}_i \mathbf{S}_i} + \vec{\mu}_{\vec{D}_i \mathbf{S}_i} \vec{\mu}^T_{\vec{D}_i \mathbf{S}_i}} \qquad \text{and} \qquad \sigma^2_{\alpha_i} = \frac{\sigma_i^2}{\Sigma_{\vec{D}_i \mathbf{S}_i} + \vec{\mu}_{\vec{D}_i \mathbf{S}_i} \vec{\mu}^T_{\vec{D}_i \mathbf{S}_i}}. \tag{7.17}$$

Implementing Eq. (7.15) and (7.17) into an iterative procedure, an estimate for $\vec{D}_i \mathbf{S}$ can be determined. Convergence of this iteration scheme is ensured by the convexity of Eq. (7.12) and (7.13) with respect to $q(\mathbf{S})$ and $q(\alpha)$, respectively. The VCG estimate $\hat{\mathbf{S}}$ can subsequently be determined from

$$\hat{\mathbf{S}}_{PTV} = \mathbf{D}^\dagger \mathbf{U}, \tag{7.18}$$

with $\mathbf{D}^\dagger$ the Moore-Penrose pseudoinverse of $\mathbf{D}$ and $\mathbf{U}$ an $[N \times T]$ matrix with rows $\vec{\mu}_{\vec{D}_i \mathbf{S}_i}$.

7.4 Data acquisition and evaluation

To evaluate both VCG methods, the 12-lead ECG from adult patients and the fetal ECG are used. The approach used to evaluate both methods is discussed in more detail below (Section 7.4.2).

To model the VCG of non-standard adult patients, the 12 ECG signals from the 12-lead ECG are randomly scaled. When dealing with real recordings of such patients this scaling is expected not to be random. In fact, electrodes close to one another are expected to exhibit similar scaling parameters. However, with a random scaling being an even more challenging test, this approach suffices for evaluation of the PTV and Dower method. To minimize the effect of the randomized scaling factor generation, the final results are averaged over all heartbeats. The scaled 12-lead ECG, the original 12-lead ECG itself, and the fetal ECG acquisition are discussed in more detail below.

7.4.1 Data acquisition

12-lead adult ECG

The most widely used clinical ECG system is the 12-lead ECG system, consisting of the leads: I, II, III, aV_R, aV_L, aV_F, V_1, V_2, V_3, V_4, V_5, and V_6 [9].

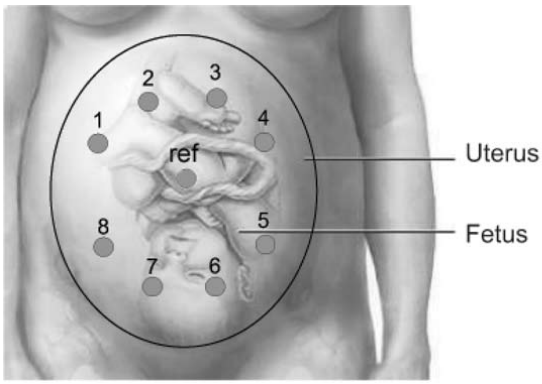

Figure 7.2: *Electrode positions for recording the fetal ECG and VCG from the maternal abdomen. This figure has been adopted from [100].*

The 12-lead ECG recordings used in this chapter are taken from the MIT/BIH PTB diagnostic ECG database [184]. Next to the 12-lead ECG signals, this database also contains the corresponding Frank XYZ signals. The Frank XYZ lead system is a system comprising three orthogonal leads that, due to this orthogonality, fully describe the three dimensions of the VCG [64]. The Frank XYZ signals can, therefore, be used to evaluate the predicting performance of both the PTV and Dower methods.

A total of 10 recordings is used from the database (Patients 104, 105, 116, 117, 121, 122, 235, 242, 263, and 264) with a total number of 693 heartbeats. All recordings are 60 seconds long and all patients are healthy.

Fetal ECG

As mentioned previously, the fetal ECG can be recorded from the maternal abdomen. In this chapter, the fetal ECG is recorded from a single patient of 24 weeks of gestation, using the electrode configuration of Fig. 7.2. The total length of the signal is over 300 seconds and it contains more than 800 fetal heartbeats. For this gestational age of 24 weeks, the fetus is not yet covered by the isolating vernix caseosa and hence, the conduction of fetal ECG signals towards the maternal abdominal surface can be assumed uniform [39, 63].

The signals acquired from the maternal abdomen, at a sampling rate of 1 kHz, contain a mixture of fetal ECG, maternal ECG, muscular activity and other interferences. The fetal ECG is extracted from this mixture using filtering and a dynamic template subtraction method [46] (Chapter 3). The electrode positions on the maternal abdomen with respect to one another are estimated by positioning the electrodes as accurately as possible in the configuration of Fig. 7.2 and estimating the shape/rounding of the abdomen.

The electrode configuration of Fig. 7.2 is designed in such way that all electrodes

are relatively close to the fetal heart. As this configuration is different from the electrode configuration used for the 12-lead ECG [31], the numerical description of the Dower matrix **D** cannot be used to determine the fetal VCG. Therefore, for estimation of the fetal VCG, the matrix **D** only contains the electrode positions and does not account for boundary effects and tissue inhomogeneities.

7.4.2 Evaluation of methods

As mentioned previously, both the PTV and Dower methods are evaluated by assessing the performance of both methods in predicting ECG signals. This entails the projection of the VCG onto ECG lead vectors $\vec{D}_j$ of which the corresponding signals $\vec{V}_j$ are not included in the estimation of the VCG. These excluded ECG signals are the signals from the previously mentioned Frank XYZ system, but also signals from the 12-lead ECG that are just not used in the calculation of the VCG and that are randomly selected. The reason for not using all of the 12-lead ECG signals is to also assess the sensitivity of both VCG methods to the number of electrodes. It has to be noted here, that for the estimation of the VCG a minimum number of 3 ECG signals is required at all times. Again, the performance of both methods is described by means of the resemblance between the ECG signals resulting from projection of the VCG and the actually recorded ECG signal.

The resemblance between projected and recorded ECG signals is expressed quantitatively by means of ε, the normalized mean squared error (MSE) between the recorded ECG signal and the VCG projection:

$$\varepsilon_{\mathrm{PTV}} = \frac{1}{N}\sum_{i=1}^{N} \frac{\left(\vec{V}_i - \hat{\alpha}_i \vec{D}_i \hat{\mathbf{S}}_{\mathrm{PTV}}\right)\left(\vec{V}_i - \hat{\alpha}_i \vec{D}_i \hat{\mathbf{S}}_{\mathrm{PTV}}\right)^T}{\vec{V}_i \vec{V}_i^T} \tag{7.19}$$

$$\varepsilon_{\mathrm{Dower}} = \frac{1}{N}\sum_{i=1}^{N} \frac{\left(\vec{V}_i - \vec{D}_i \hat{\mathbf{S}}_{\mathrm{Dower}}\right)\left(\vec{V}_i - \vec{D}_i \hat{\mathbf{S}}_{\mathrm{Dower}}\right)^T}{\vec{V}_i \vec{V}_i^T}. \tag{7.20}$$

As mentioned previously in Section 7.1, on average about 83% (i.e. approximately the mean between 70 and 95%) of the power of the ECG signals can be predicted by projection of the VCG. Consequently, MSE values of about -7.5 dB, i.e. 17%, signify a relatively accurate VCG. That is, MSE values larger than about -7.5 dB indicate that, besides imperfections in the dipole model, additional inaccuracies in the VCG methods have to be present as well.

The fetal VCG determined from real fetal ECG signals cannot be validated with respect to Frank XYZ signals. Therefore, the performance of both VCG methods is only evaluated by calculating the fetal VCG with fewer than the 8 electrodes depicted in Fig. 7.2 and subsequently comparing VCG projections to the omitted ECG signals. The performance is again expressed quantitatively by means of ε.

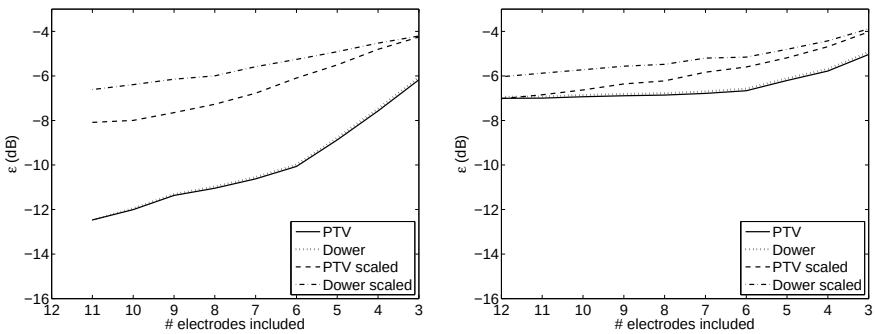

Figure 7.3: *Normalized MSE ε between the ECG signals determined from projection of the VCG and the recorded ECG signals. The MSE ε is determined for both the PTV method and the Dower method for both scaled and unscaled ECG signals. In (a), the VCG projections are compared to the omitted ECG signals and in (b) the VCG projections are compared to the Frank XYZ leads. Note that in both graphs, for the unscaled ECG signals, the values for ε for both methods are practically overlapping.*

Finally, for both the adult 12-lead ECG and the fetal ECG recordings, the variance Σ is determined by assessing, for each individual ECG complex, the variance of the signal that is obtained by subtracting a template ECG complex from the recorded ECG complexes. This template ECG complex is generated by averaging all ECG complexes within each signal.

7.5 Results

7.5.1 12-lead ECG

In Fig. 7.3, the MSE ε is depicted for both the PTV method and the Dower method. Fig. 7.3(a) and 7.3(b) show ε for the predictive performance of the VCG with respect to omitted electrodes and Frank XYZ leads, respectively. The values of ε are determined as a function of the number of ECG signals included. As mentioned previously, the signals that are omitted (i.e. horizontal axis values larger than zero) are randomly selected and the depicted values represent the mean values across all the heartbeats for all of the patients.

From Fig. 7.3 it can be seen that the performance of both methods is approximately the same for unscaled ECG signals, with the developed method performing marginally better. Since the Dower method has been developed for these recordings,

not much improvement would have been expected here though. It is, however, striking that even for small numbers of electrodes included, the VCG determined with the Dower method still is as accurate as a method that can, to some extent, account for inter-patient differences in signal propagation. The most probable reason for this is that the inaccuracy in the Dower method, also for few electrodes included, is smaller than the error originating from non-dipolar effects (Section 7.4.1). This argumentation is confirmed by the fact that all values for ε, except the ones for only 3 or 4 electrodes included, are smaller than -7.5 dB, indicating a relatively accurate VCG estimation. For the scaled ECG signals, the developed PTV method significantly outperforms the Dower method with MSE values below -7.5 dB in most situations.

From these figures it can also be seen that the variational inference only approximates the MAP solution for $\mathbf{S}$ in Eq. (7.9). Namely, in case the variational inference method would generate the true MAP solution, the PTV values for ε between scaled and unscaled ECG signals would nearly be the same.

In addition, from Fig. 7.3(a) and 7.3(b) it can be seen that, for the modeled non-standard patients (and thus scaled signals), for the PTV method the number of included electrodes larger than the minimally required number of three electrodes can be halved with respect to the Dower method in order to still obtain similar ε values. This can result in more patient-friendly, comfortable ECG measurements as fewer electrodes need to be positioned on the patient's skin.

Although the difference in performance between the PTV method and the Dower method for scaled ECG signals appears to be small in Fig. 7.3(b), it yields a significant difference in the VCG estimates of Fig. 7.4. More precisely, because the Frank XYZ leads together comprise the VCG, comparing the VCGs of both methods to one another gives some insight into how this small difference in MSE ε translates to actual VCG estimates. Fig. 7.4 indicates that the non-standard patients' VCG estimated by the PTV method resembles the VCG determined from unscaled ECG signals significantly better than the VCG estimated by the Dower method. Here, the unscaled VCG serves as reference for the VCGs determined from the scaled signals. The significance in this difference lies in the fact that some ECG applications call for comparison of two or more vectorcardiographic loops, serial ECG analysis probably being the most notable [185]. Such comparisons can be considerably affected by slight inter-recording changes in the VCG. For instance, a small Q-wave in a projected ECG complex may completely vanish in the consecutive complex. This is illustrated in Fig. 7.5, in which the VCGs of Fig. 7.4 are projected onto a specific lead vector. Notwithstanding this improved performance of the PTV method with respect to the Dower method, the PTV method also suffers from inaccuracies, as can be seen from the difference between the unscaled VCG and the VCG estimated by the PTV method in Fig. 7.4. These inaccuracies are mostly due to approximations made by the variational inference and the fact that attenuation effects are assumed

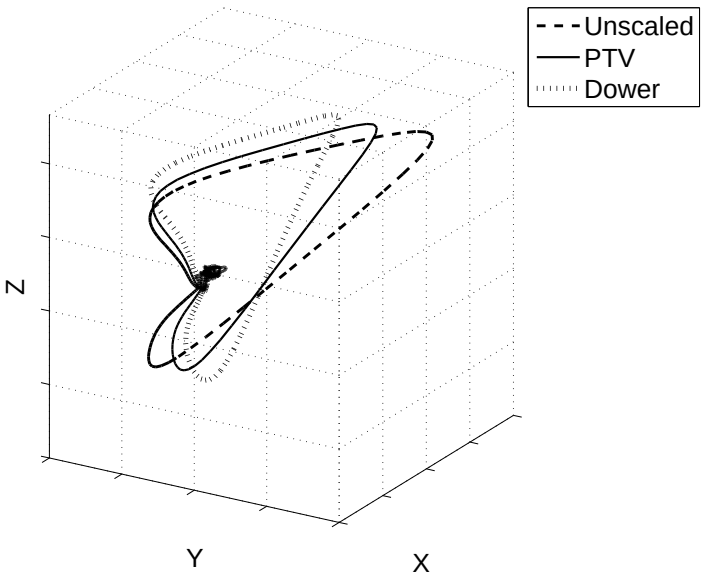

Figure 7.4: *VCG determined from scaled ECG recordings with the developed PTV method and with the conventional Dower method. For reference, also the corresponding VCG from the unscaled ECG recordings is depicted.*

isotropic, i.e. that the ratios between elements within each row of **D** are kept fixed.

7.5.2 Fetal ECG

In Fig. 7.6, the MSE ε is depicted for the VCG determined from actually recorded fetal ECG signals.

From Fig. 7.6 it can be seen that also for ECG signals with a lower signal to noise ratio, the developed PTV method outperforms the Dower method. The difference between both methods is illustrated once more in Fig. 7.7 in which the fetal VCG determined with both methods is depicted.

The difference between both VCGs can, according to the model of Eq. (7.3), be explained by the different attenuation effects on the ECG signals recorded with different electrodes.

7.6 Discussion & Conclusions

The presented method outperforms the currently existing method for VCG determination in all situations, although the difference between both methods for patients

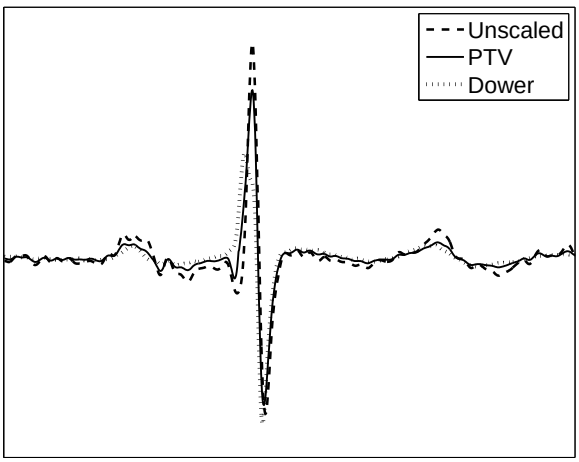

Figure 7.5: *Projections of the VCGs of Fig. 7.4 onto the normalized lead vector (0, 0.96, -0.27). In contrast to the ECG determined by the PTV method and the unscaled reference ECG, in the ECG determined by the Dower method the Q-wave is absent.*

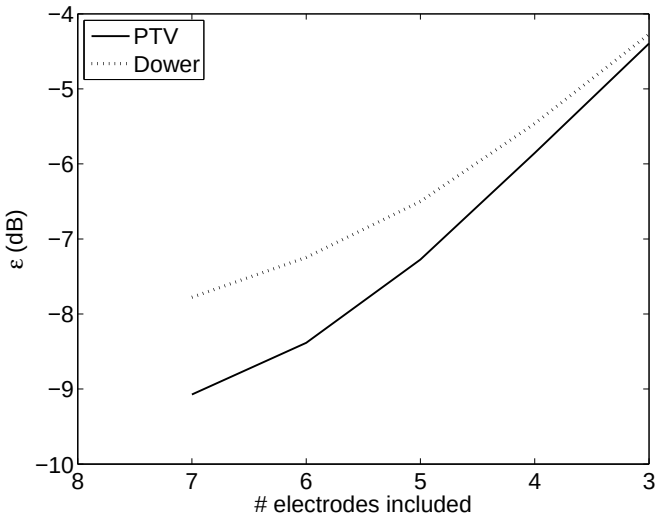

Figure 7.6: *Normalized MSE* ε *between the fetal ECG signals determined from projection of the fetal VCG and the fetal ECG signals that are omitted from the calculation of the VCG. The MSE* ε *is determined for both the PTV method and the Dower method.*

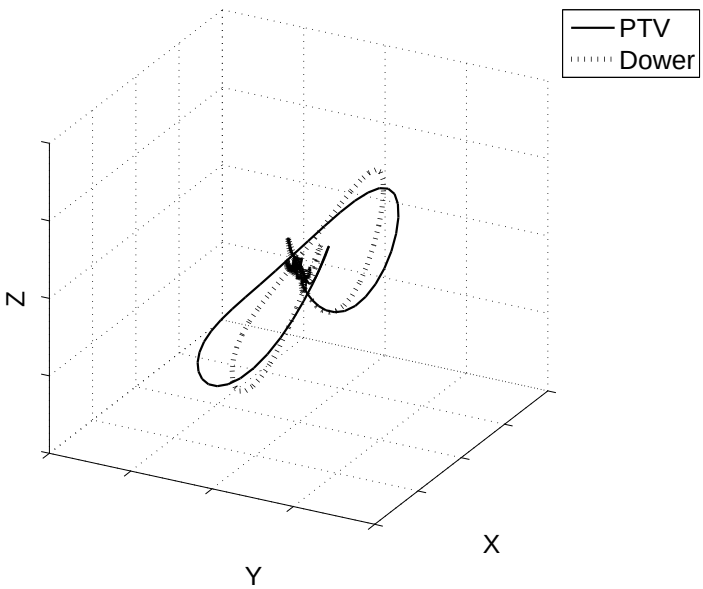

Figure 7.7: *Fetal VCG determined with both the PTV method and the conventional method.*

with standard body composition and geometry is negligible. For patients that do not conform to the standard, such as fetuses, however, the performance of the developed method appears to be significantly better than the performance of the conventional method.

Notwithstanding this improvement in VCG determination, the developed method is liable to inaccuracies since the applied variational inference method only approximates the MAP solution. By extending this method with other probability distributions, instead of just the Gaussian, performance of this method can be improved, however potentially leading to a computational higher complexity, e.g. due to required numerical evaluation instead of analytical evaluation as is the case with the Gaussian distribution. At this moment, for both scaled and unscaled ECG recordings, the PTV method requires, on average, less than 5 iterations to converge to a stationary solution, yielding a relatively small computational load.

Other ways of improving the developed method are the inclusion of prior information on the scaling parameters α, more precisely determined electrode positions, and the extension of the dipole model to enable it to also deal with non-dipolar components. For the latter, an overview of ways to extend the dipole model is provided in [34], including the addition of another dipole and the use of multi-poles. More recent extensions of the dipole model include the use of distributed source models, as discussed in [186]. Including prior information on α implies the inclusion of prior

information on spatial information, i.e. the heart-electrode distances, as well [187]. Following the principle of maximum entropy [180] to determine the appropriate corresponding prior probability distribution and including this distribution in Eq. (7.9) would result in an analytically unsolvable expression for the posterior probability distribution. In turn, this would require the use of computationally more complex numerical approaches to infer the MAP solution. The extension of the dipole model would also lead to computational more complex numerical approaches. Although all these improvements are expected to lead to a more accurate VCG estimation, this increased accuracy is expected to be overshadowed by the inaccuracies caused by non-dipolar contributions in the ECG, as described in the first paragraph of Section 7.1, with the exception of improvements in the variational inference and the extension of the model. Hence, the proposed improvements to the developed method are expected to cause higher computational complexity (improved variational inference, prior information on α, and extension of the model) and yield more laborious measurements (more precise electrode positions), while the benefits of most improvements are negligible. In addition, a higher computational complexity prevents the use of the PTV method in real-time applications.

For development of the PTV method, several assumptions have been made, including the Gaussian distribution of the noise and mutual independence of the scaling parameters α. The assumption of the noise having a zero-mean Gaussian distribution is adopted from the inverse Dower matrix method. In this method, inaccuracies in the dipole model regarding boundary effects, tissue inhomogeneities, and non-dipolar components are assumed to be accounted for by the numerical description of the Dower matrix. Although this assumption is not completely valid, resulting in reduced accuracy in VCG estimation, the method is reported to perform sufficiently well to support clinical decision-making [47]. With the PTV method outperforming the inverse Dower matrix method, the PTV method is expected to also perform sufficiently well for clinical decision-making. This, however, remains to be demonstrated in clinical practice. The mathematical benefits of the Gaussian noise assumption, yielding the final algorithm analytically solvable, can, therefore, be considered of larger interest than the modelling error it provokes. The assumption of the scaling parameters α being mutually independent is, in contrast to other statistical independencies, not justified by applying d-separation. In fact, both this assumption of independence and the assumption of a uniform prior for α are inaccurate and result in decreased performance of the PTV method. These assumptions are nevertheless needed for the sake of tractability. However, even with these inaccurate assumptions, the results in Fig. 7.3 and Fig. 7.6 show that the PTV method outperforms the Dower method. Including prior information on α is nevertheless expected to lead to substantially improved performance of the PTV method.

The normalized MSE ε in predicting ECG signals from the VCG is, for the un-

scaled ECG recordings, smaller than -10 dB for VCGs determined from 6 included electrodes or more. Although this error can be fully attributed to non-dipolar components in the precordial ECG leads, part of this error should be attributed to inaccuracies in the linearization of boundary effects and tissue inhomogeneities as well. Here, the main inaccuracy is caused by the assumption of the scaling α being isotropic – and hence the assumption of the ratio between the elements within each row of $\mathbf{D}$ being fixed. For scaled ECG signals and the fetal ECG, besides model inaccuracies also the approximation in the variational inference and decreased signal to noise ratios (for the fetal ECG) give rise to increased MSE. Based on the differences between scaled and unscaled PTV results in Fig. 7.3 (as discussed in Section 7.5.1), this increase in ε due to variational inference can be up to 5 dB.

From Fig. 7.3 and 7.6 it can be seen that the PTV method requires less ECG signals than the Dower method to obtain similar MSE values in the prediction of reference ECG signals. Consequently, the use of the PTV method in ambulatory ECG monitoring is expected to decrease patient discomfort and reduce bandwidth requirements for wireless data transmission.

Notwithstanding the inaccuracies mentioned above, the developed method provides a way for estimating a VCG, tailored to each specific patient. For patients conforming to the standard, the improvement with respect to the conventional method is negligible, but for non-standard patients the improvement is significant. On the one hand, the VCG can be determined with increased accuracy, which for the fetus may result in improved early stage diagnosis and perhaps even treatment of congenital heart diseases, whereas, on the other hand, for adult patients it can result in a smaller number of required electrodes, improving patient comfort and facilitating ambulatory monitoring applications.

Additionally, since the method also estimates α in Eq. (7.9), for the fetal VCG, the method can in future be used to estimate the position of the fetal heart with respect to the electrodes – requiring assumptions on tissue homogeneity – and hence the position of the fetus inside the uterus. In addition, the estimation of α might in future be used to estimate distributed electrical activity of the heart. Furthermore, because of the similar nature of the problem in fetal magnetocardiography [188], the method may also be applied on fetal magnetocardiogram (MCG) signals. With regard to fetal ECG/MCG monitoring, the capability of the method to predict the morphology of fetal ECG/MCG signals that cannot be recorded directly can have significant value in clinical practice, e.g. through determination of the 12-lead ECG/MCG. This prediction of the 12-lead ECG and its use in clinical practice is, therefore, a possible subject of further studies as well.

Part II

Fetal vectorcardiogram and electrocardiogram interpretation

In this part of the thesis, the vectorcardiogram (VCG) that has been estimated in Part I is used to assess clinically relevant information. The most straightforward method of extracting information from the VCG is by deriving electrocardiogram (ECG) signals from the VCG that are similar to the ECG signals recorded from adults and children. These signals are familiar to clinicians and as such facilitate clinical interpretation. However, two problems arise when trying to derive these ECG signals. At first, the fetal heart is different from the adult heart and therefore clinical guidelines for interpretation need to be reconsidered. Secondly, the orientation of the fetus within the uterus varies not only between patients but also for the same patient. As a result of fetal movement, the fetus will change its orientation. These changes in orientation have immediate and substantial effects on the ECG signals recorded and derived from the abdominal recordings. As a result, clinical interpretation of the ECG signals is complicated; it can no longer be conclusively stated whether variations in the ECG signal originate from movement or from physiological events in the fetal health.

The outline of this part of the thesis is as follows. In Chapter 8 the physiological and electrical differences between the fetal heart and adult heart are discussed, demonstrating the effect of these differences on the fetal electrocardiogram (ECG). In Chapter 9 variations in the orientation of the fetus within the uterus are monitored to enable correction for fetal movement and hence avoid erroneous clinical interpretation of the fetal ECG and VCG. Finally, in Chapters 10 and 11 two examples of clinically interpretable ECG signals that are derived from the VCG are presented. In Chapter 10 the 12-lead ECG of fetal supraventricular extrasystoles is compared to the 12-lead ECG representation of normal fetal heartbeats and it is hypothesized that this ECG representation can be used to predict fetal congenital heart disease. In Chapter 11 the ECG representation is derived that resembles the invasively recorded fetal ECG and this ECG representation is subsequently used to perform fetal ST analysis. It is shown that the signal to noise ratio (SNR) of the non-invasive fetal ECG approaches that of the invasive fetal ECG. In addition, it is shown that the position of the currently employed invasive electrode (for fetuses that represent themselves in vertex position) is, in terms of the accuracy of the ST analysis, not that far from optimal.

Chapter 8

Electrical axis of the human fetal heart during pregnancy - insights into fetal electrocardiography

In this chapter the physiological and electrical differences between the fetal heart and the adult heart are discussed. The electrical properties of both hearts are assessed by determining the maternal VCG and the fetal VCG within the same frame of reference, hence enabling direct comparison. The consequence of the electrical differences between both hearts for ECG interpretation are illustrated by considering the Einthoven leads of the ECG.[1]

8.1 Introduction

Analysis of the electrocardiogram (ECG) of preterm born infants can have significant relevance for establishing a strategy for treatment of the newborn. However, clinical interpretation of the newborn's ECG is complicated due to the absence of adequate knowledge of what constitutes a normal ECG for these ages. The reason for this lack of standards is the fact that, due to the different cardiovascular circulation in fetal life as opposed to the adult circulation, the fetal heart is adapted to its intrauterine environment. This adaptation yields an abundance of cardiac muscle in the right ventricle. Accordingly, the electrical axis of the fetal ventricles is assumed to point to the right-anterior-inferior octant [59, 189]. Upon birth the circulation of the newborn drastically changes and the newborn's heart will start to adapt to this new situation. More particularly, the newborn's heart will grow towards an abundance of cardiac muscle in the left ventricle and accordingly, an electrical axis pointing towards the left-anterior-inferior octant. However, as this adaptation occurs gradually, ECG interpretation in the intermediate period is complicated.

[1]This chapter has been submitted as *R. Vullings, M.J.M. Hermans, C.H.L. Peters, J.W.M. Bergmans, S.G. Oei, P.F.F. Wijn, "Electrical axis of the human fetal heart during pregnancy – insights into fetal electrocardiography"* to be considered for publication.

With recent progresses made in the treatment of fetal congenital heart diseases [190, 191], the extrapolation of (lacking) neonatal ECG standards to the fetus is becoming more important. This extrapolation, among other factors, calls for a verification of the above-mentioned assumption that the mean electrical axis of the fetal ventricles indeed points towards the right-anterior-inferior octant. To the best of our knowledge, such a verification has hitherto not been attempted due to inadequate and insufficient technological means. With recent progresses made in the extraction of the fetal ECG and VCG from non-invasive electrophysiological recordings on the maternal abdomen [46, 140], we conceived a method to determine the electrical axis of the fetal heart. In this chapter we show that for 10 healthy fetuses with gestational ages ranging from 21 weeks to term, the electrical axis indeed points towards the right-anterior-inferior-octant.

On its own, this verification has little value in fetal monitoring. However, the combined information of the fetal VCG and the electrical axis provides a basis for interpretation of the fetal ECG. That is, by rotating the fetal VCG towards the adult frame of reference, i.e. the frame of reference in which for instance the 12-lead ECG is recorded, the VCG can be used to produce ECG leads of the fetal ECG that are familiar to cardiologists. The production of ECG leads from the VCG is detailed on in Section 8.2.1. However, to correctly interpret the fetal ECG, the orientation of the electrical axis should be taken into account. As an example, the correct identification of axis deviation and left or right bundle branch blocks benefits from *a priori* knowledge on the electrical axis; Not considering the different electrical axis of the fetal heart could lead to incorrect or inconclusive diagnosis.

To illustrate the differences between a heart with electrical axis pointing towards the left-anterior-inferior octant and a heart with electrical axis pointing towards the right-anterior-inferior octant, in this chapter, besides the electrical axis, also the fetal ECG in the adult frame of reference and the simultaneously recorded maternal ECG are presented alongside one another.

8.2 Materials and Methods

8.2.1 Relation between ECG and VCG

The heart contracts as a result of an action potential propagating through the cardiac tissues and depolarizing the cardiac cells. At any point in time, the combined effect of all the depolarized cells produces an electrical field that can be measured on the cutaneous surface: the ECG. During the cardiac cycle, this electrical field varies both in amplitude and orientation. The orientation for which the amplitude of the electrical field is largest is referred to as the electrical axis. When assuming the electrical field to originate from a single point, the time-path of the electrical field vector during the cardiac cycle is referred as the VCG [64].

In essence, this VCG contains all the electrical information about the heart. Consequently, any ECG signal can be derived from the VCG. This is done by projecting the VCG onto the vector that indicates the electrode positions that record the ECG of interest. For the application at hand, this means that calculation of the fetal VCG makes it possible to derive any ECG signal of interest. In other words, the fetal VCG can be rotated to the adult frame of reference and then projected onto e.g. the 12-lead ECG to yield a ”normal” 12-lead ECG of the fetal heart.

8.2.2 Fetal VCG assessment

The results presented in this chapter are obtained from 10 *in-vivo* measurements that form part of a study conducted at the Máxima Medical Center (Veldhoven, the Netherlands). In this study, for pregnant women, longitudinally across their pregnancy, the fetal ECG is recorded from the maternal abdomen. The measurements discussed here were performed on ten healthy mothers, with ages ranging between 28 and 37 years, all with a singleton pregnancy and gestational ages ranging from 21+4 to 40+1 weeks, and who have given informed consent. The use of 10 recordings ensures that statistical significance of the results can be achieved. All 10 pregnancies resulted in healthy babies with 1 minute Apgar scores ranging from 9 to 10, and 5 minute Apgar scores all 10, and no congenital heart diseases.

To enable rotation of the VCG towards the adult frame of reference, simultaneously with the fetal ECG recording, also an ultrasonic recording was performed, as depicted in Fig. 8.1. The abdominal fetal ECG signals are obtained with 8 self-adhesive electrodes on the maternal abdomen and are processed to suppress the interferences and artifacts from, among other factors, respiration and the maternal ECG (also indicated in Fig. 8.1). Subsequently, the fetal ECG signals are further enhanced by averaging 30 consecutive ECG complexes. Since the fetal heart rate is generally around 150 beats per minute, these 30 ECG complexes are recorded within a time frame smaller than 15 seconds. Within this time frame, no transient physiological events are anticipated and thus no significantly relevant clinical information is lost. To underpin this, the STAN® monitor (Neoventa Medical, Sweden) also analyzes fetal ECG complexes that constitute the average of 30 preceding ECG complexes. Finally, the fetal VCG is estimated from the enhanced fetal ECG complexes by a method referred to as patient-tailored vectorcardiography [140] (see Chapter 7). This method is an extension of the commonly known method proposed by Dower [47] and involves an automated, patient specific estimation of the ECG signal conduction, yielding an improved accuracy in VCG estimation.

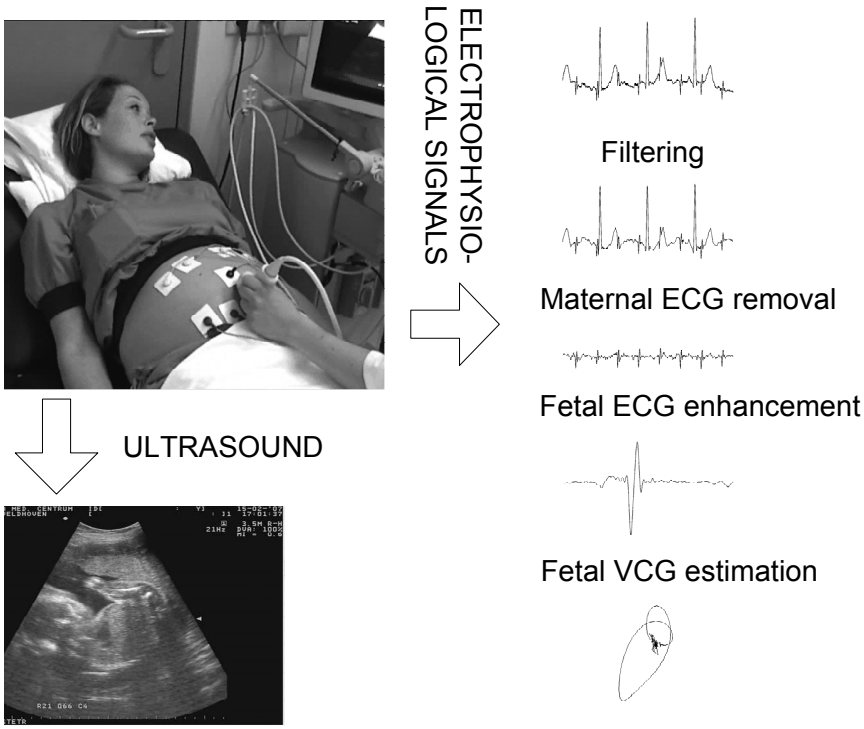

Figure 8.1: *The electrical axis is obtained in two steps. In the first step, the fetal ECG is recorded from the maternal abdomen (upper left photo) and processed by successive filtering, suppression of the maternal ECG, enhancement of the fetal ECG, and estimation of the fetal VCG (right panel). In the second step, the fetal VCG is rotated towards the fetal frame of reference, obtained from the ultrasound image (bottom left) to enable assessment of the electrical axis of the fetal heart.*

8.3 Results

In Fig. 8.2(a) the result of the determination of the electrical axis of the fetal heart is shown for a patient at 21+4 weeks of gestation. To exemplify that this axis is pointing in the opposite direction as it would for an adult, in Fig. 8.2(b) the electrical axis of the maternal heart is depicted. In these figures, both the VCG and the electrical axis are plotted together, with the electrical axis, as mentioned previously, defined as the direction in which the VCG exhibits the maximum amplitude. The VCG amplitude along the x-axis of the plot, referred to as V_x, constitutes the potential along the vector pointing normal to the frontal plane, from the posterior side to the anterior. The axis indicated with V_y points from the right to the left and the V_z axis points from the inferior side of the fetus to the superior side. The direction in which the QRS loop evolves over time is indicated as well.

The fetal VCG, more clearly than the maternal VCG, also shows that the direction of the electrical axis of the atria (i.e. the direction of the maximum P-wave amplitude) conforms to the electrical axis of the ventricles. The reason that the P-wave is not that clear in the maternal VCG is the non-standard electrode configuration that is used to assess the maternal VCG. That is, the maternal VCG is assessed from the same electrode configuration as is the fetal VCG (see Fig. 8.1).

In Figs. 8.2(c) and 8.2(d) the frontal view of the fetal and adult VCG's are shown again, together with their projections on the Einthoven triangle [62]. From these Einthoven leads of the ECG it is immediate clear that the ECG of a healthy fetus substantially differs from the ECG of a healthy adult, apart from the obviously lower signal amplitude (from Figs. 8.2(a) and 8.2(b) it can be deduced that the fetal ECG has an amplitude that is about 20 times as small as the amplitude of the maternal ECG). Where for the adult ECG, Einthoven III typically has a relatively small amplitude whereas Einthoven II has a large amplitude, for the fetal ECG this is the other way around. Consistently, the polarity of Einthoven I is inverted between the adult and fetal ECG.

To demonstrate that the findings of Fig. 8.2 are representative for the other 9 recordings, in Fig. 8.3 the directions of the electrical axes from all 10 fetuses and their mothers are depicted. From this figure it can be concluded that, on average, for all patients the direction of the fetal and maternal electrical axis is directed towards the same direction.

8.4 Discussion

The results in Fig. 8.2 and Fig. 8.3 indicate that the direction of the mean electrical axis of the fetal ventricles is, indeed, as assumed for many years, towards the right-anterior-inferior octant. In addition, the results indicate that full adaptation of the fetal

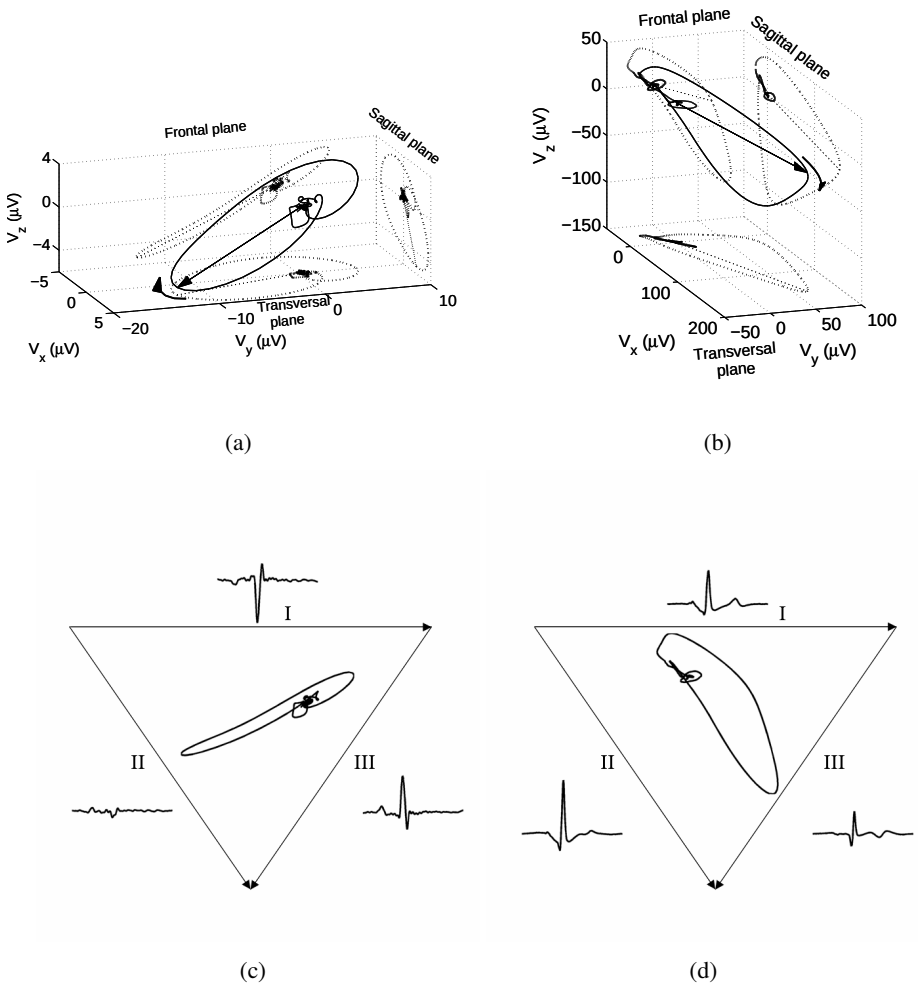

Figure 8.2: *(a) Fetal VCG and (b) Maternal VCG. Both VCG's are shown in the frontal plane, with projections onto this plane and onto the inferior transversal and left sagittal plane shown as well. The arrows in both plots indicate the direction of the electrical axis of the ventricles and the direction in which the VCG evolves over time. To facilitate visual comparison between the fetal VCG and the adult maternal VCG, both the VCG's in (a) and (b) are depicted under the same angle and with the same ratio between the lengths of the axes. Due to the smaller amplitude of the fetal VCG, the axes in (a) have smaller scales than the axes in (b). In (c) and (d) the frontal views of both VCG's are shown again, together with their projections on the I, II, and III ECG leads of the Einthoven triangle.*

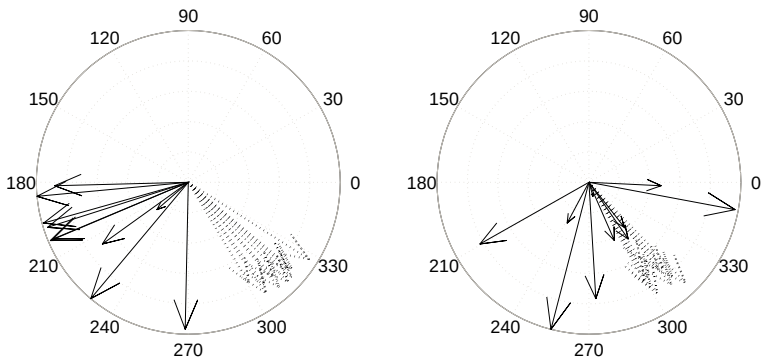

(a) (b)

Figure 8.3: *(a) Frontal view and (b) right-sagittal view of the direction of the electrical axis of both fetus and mother. All axes amplitudes have been normalized to enable simultaneous depiction for both the fetus and mother. The electrical axes of the fetal heart are depicted with a solid arrow. The electrical axes of the maternal heart are depicted with dotted arrows.*

heart to the larger mechanical load in the right ventricle can be seen at least as early as 21+4 weeks of gestation. This larger mechanical load of the right ventricle originates from the larger ejection volume of this ventricle, as opposed to the left ventricle. As both ventricles, due to the ductus arteriosus, eject into the same vascular bed, systolic pressure in both ventricles has to be the same [60]. Bearing this in mind, the direction of the electrical axis of the fetal atria, which at first sight is counter-intuitive due to the location of the sinoatrial node in the right atrium, can also be explained. Namely, because only one-third of the venous return flows through the foramen ovale from the right to the left atrium [60], the right atrium has to eject about twice as much blood to the right ventricle as the left atrium has to eject to the left ventricle.

The results in Figs. 8.2(c) and 8.2(d) show that the alternative direction of the fetal electrical axis has direct consequences in fetal electrocardiography. The projections of the fetal and adult VCG onto the Einthoven triangle [62] indicate that clinical interpretation of the fetal ECG should be made differently from clinical interpretation of the adult ECG. It can be concluded that our results verify existing assumptions on the electrical axis of the fetal heart, opening new research opportunities in the as yet uncharted field of fetal electrocardiography. When normal values for the fetal ECG can be established, diseases like bundle branch block, typically originating in the fetus around 18-20 weeks of gestation, can possibly be diagnosed and treated early. In addition, interpretation of the fetal ECG for assessment of fetal distress [2] could presumably improve with better knowledge on the electrical axis of the fetal heart. That is, when using the non-invasive fetal ECG for assessment of fetal hypoxia, full

comprehension of the fetal heart and ECG might lead to the derivation of ECG leads that exhibit advantageous properties for e.g. assessing ST changes.

8.5 Conclusion

In this report the authors have shown *in-vivo* that the healthy fetal heart, as assumed and proven in neonatal studies, is indeed adapted to its alternative circulation by increased mass of the right atrium and ventricle, already as early in pregnancy as 21 weeks. Moreover, the authors have shown that this adaptation of the fetal heart has substantial implications in the field of fetal electrocardiography. Notwithstanding these implications, the authors have shown that the presented methodology makes fetal ECG analysis possible and might, hence, in the future aid in the assessment of normal values for fetal electrocardiography. Finally, the presented methodology can similarly be applied to fetal magnetocardiographic signals, providing also a basis for signal interpretation in the field of fetal magnetocardiography.

Chapter 9

Vectorcardiographic loop alignment for non-invasive monitoring of fetal movement

In this chapter a method is presented that enables monitoring of variations in the fetal orientation. The method operates by estimating the rotation and scaling between consecutive VCG's. Because of its flexibility in the allowed scaling, the method can also be used to estimate the rotation between the fetal VCG and the maternal VCG. This rotation provides information on the orientation of the fetus within the uterus which in turn can be combined with the VCG to derive ECG signals that are familiar to clinicians. To ensure that this absolute fetal orientation is estimated accurately, the differences between the fetal and adult heart, discussed in the previous chapter, are taken into account.[1]

9.1 Introduction

High-risk pregnancies are generally monitored by cardiotocography (CTG), the combined assessment of fetal heart rate variability and maternal uterine activity. Unfortunately, the diagnostic value of CTG is relatively low and, therefore, in many cases additional information to assess the fetal condition is required [20].

A possible additional source of information is the fetal electrocardiogram (ECG). Analysis of the fetal ECG, recorded with an invasive electrode, in combination with CTG has been demonstrated to improve perinatal outcome [28]. Despite this improvement, the value of fetal ECG analysis in clinical practice is somewhat limited due to the fact that it requires an invasive electrode and can, therefore, only be applied during labor. Hence, non-invasive methods to support CTG in fetal monitoring and that can be applied in all stages of pregnancy – and not only during labor – are still

[1]This chapter has been submitted as *R. Vullings, C.H.L. Peters, S.G. Oei, and J.W.M. Bergmans, "Expectation-maximization for vectorcardiographic loop alignment and non-invasive assessment of fetal movement"* to be considered for publication.

urgently needed.

To extend the applicability of fetal ECG analysis to all stages of pregnancy, several attempts to record the fetal ECG from the maternal abdomen have been made over the years [46, 90, 92, 94, 95]. Notwithstanding the significant progress made, none of these methods is currently employed in clinical practice. This is due in part to difficulties in the clinical interpretation of the non-invasively obtained fetal ECG signals. A particular example of such difficulties arises in case of fetal movement. As a result of fetal movement the ECG signals will change. Without quantitative information on fetal movement, it is difficult to assess whether changes in the ECG originate from movement or from clinically relevant changes in the fetal physiological condition.

The monitoring of fetal movement can resolve this particular problem, facilitating clinical interpretation of the fetal ECG, and has an additional benefit. In most cases of fetal demise, fetal death is preceded by reduced fetal motility [53]. Moreover, as reduced fetal movement is also associated with fetal hypoxia and fetal growth restriction [72], using fetal movement assessment as a screening tool for fetal compromise could potentially become one of the mainstays in fetal surveillance. Presently, the most widely used method for fetal movement assessment is maternal perception. However, since maternal perception is liable to significant inter-patient variability, e.g. due to the variability in the position of the placenta, clinical actions based on fetal movement counting by the mother do not necessarily improve fetal outcome [192]. If it were possible, then, to assess fetal movement in a continuous, safe, objective, and automated way, this would resolve the issues on maternal partiality and could aid in the adoption of fetal movement monitoring in everyday clinical practice.

In a simplified model, the electrical activity of the heart can be fully described by the vectorcardiogram (VCG) [32, 64]. The VCG describes the evolution of the electrical field vector generated by the heart during each heartbeat. By tracking rotations between the fetal VCG of consecutive heartbeats and relating these rotations to fetal movement, it is possible to quantify fetal movement and hence facilitate both clinical interpretation of the fetal ECG and automated and objective monitoring of fetal movement. With respect to monitoring of fetal movement, it has to be noted that only a unidirectional relation between VCG rotations and fetal movement is anticipated. That is, in case VCG rotation is detected, this can be related to fetal movement. Conversely, no VCG rotation does not mean that the fetus is not moving. Limb movement, for instance, is not expected to lead to (significant) fetal rotational movement.

Rotations between the VCG's of consecutive heartbeats can be tracked by means of the maximum likelihood (ML) approach presented by Sörnmo [185]. In this approach, consecutive VCG's are modeled to be related to one another through a couple of transformations. Besides rotation, one of these transformations is scaling of the

complete VCG to account for contraction or dilatation. However, as discussed by Sörnmo, this scaling is not entirely realistic and improvements in the movement estimation are to be expected in case this scaling is extended to a lead-dependent scaling.

The method presented in this chapter (Section 9.2) builds on Sörnmo's approach but is extended with the above-mentioned lead-dependent scaling. The ML estimate for this scaling and the accompanying rotation estimate are successively inferred using the expectation-maximization (EM) algorithm. With respect to the intended goal of Sörnmo (i.e. vectorcardiographic loop alignment in adults) the extension with lead-dependent scaling is expected to yield only marginal improvements in accuracy. For the application mentioned above (i.e. tracking of fetal movement), the lead-dependent scaling is however particularly relevant. That is, translational movement of the fetus and maternal respiration are both anticipated to cause significant distortion of the fetal VCG. This distortion can be better accounted for by the lead-dependent scaling than by the single scaling proposed in Sörnmo. In turn, this improved scaling estimation results in an improved estimation of the VCG rotations.

The developed method is evaluated in two different ways. At first, the performance in VCG alignment for both adult and fetal ECG recordings is assessed quantitatively in terms of spatial variability and intralead variability of the aligned VCG's and compared to the performance of Sörnmo's approach (Section 9.3). Secondly, the developed method is applied on fetal ECG recordings and the determined fetal movement is evaluated qualitatively by comparing it to movement assessed from a simultaneously ultrasound recording (Section 9.4). To illustrate the potential of the lead-dependent scaling, the developed method is also applied on an extreme case of VCG mismatches (Section 9.4.3); determining the rotation between the maternal VCG and the fetal VCG both determined from the same abdominal recording. The estimated rotation yields a measure for the "absolute" fetal orientation within the uterus.

9.2 Vectorcardiographic loop alignment

9.2.1 Model for fetal rotation

As mentioned previously, the rotation between the VCG's of consecutive heartbeats can be used as a measure for fetal movement. Since they exhibit superior signal to noise ratio (SNR) with respect to other parts of the VCG and have an almost planar shape [134], the QRS loops of the VCG are particularly well-suited for this purpose. The superior SNR of the QRS loops stems from the fact that the QRS loops entail the parts of the VCG that are associated with electrical activation of the ventricles. As the ventricles comprise a relatively large fraction of the mass of the heart and the activation of the ventricles is well synchronized, the amplitude of the QRS loop is large with respect to other parts of the VCG, hence yielding a relatively large SNR.

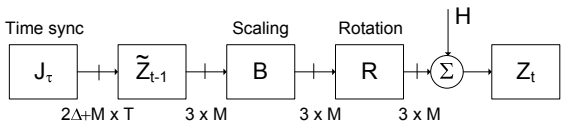

Figure 9.1: *Schematic overview of the model proposed by Sörnmo [185], with the extension that the scaling no longer entails a scalar but a matrix multiplication.*

A model that describes the relation between two consecutive VCG's has been proposed by Sörnmo [185] and evaluated extensively by Åstrom et al. [193]. In the model by Sörnmo, the QRS loop at time t is described by a $[3\times M]$ matrix $\mathbf{Z}_t$. In this matrix, each row vector contains the QRS loop of one of the three orthogonal leads of the VCG. In the model by Sörnmo, $\mathbf{Z}_t$ is assumed to be derived from the preceding QRS loop $\tilde{\mathbf{Z}}_{t-1}$, however altered by a series of transformations. The preceding reference loop $\mathbf{Z}_{t-1}$ is an $[3\times(M+2\Delta)]$ matrix and contains 2Δ additional samples to allow for QRS loops that constitute different subsets of M samples from $\tilde{\mathbf{Z}}_{t-1}$ (the tilde indicates that $\tilde{\mathbf{Z}}_{t-1}$ is augmented with additional samples).

The first of the above-mentioned transformations on $\tilde{\mathbf{Z}}_{t-1}$ is *time synchronization*, as indicated in Fig. 9.1. Time synchronization is considered to increase the resemblance between $\mathbf{Z}_t$ and $\tilde{\mathbf{Z}}_{t-1}$ [185]. Since the length of the QRS loop is determined by the time it takes an action potential to propagate through the ventricular tissues and since the ventricular propagation properties are rather constant over time, i.e. not regulated by the nervous system, the length of consecutive QRS loops can be assumed equal. This renders compression or expansion of the QRS loops superfluous. The time synchronization is described by the shift matrix $\mathbf{J}_\tau$, a $[(2\Delta+M)\times M]$ matrix defined by the time shift τ:

$$\mathbf{J}_\tau = \begin{pmatrix} \mathbf{0}_{\Delta+\tau} \\ \mathbf{I} \\ \mathbf{0}_{\Delta-\tau} \end{pmatrix} \tag{9.1}$$

with $\tau \in [-\Delta,\Delta]$. The zero-matrices in Eq. (9.1) are $[(\Delta+\tau)\times M]$ and $[(\Delta-\tau)\times M]$ matrices, respectively, and the identity matrix $\mathbf{I}$ has dimensions $[M\times M]$.

The second transformation applied on the preceding QRS loop is *scaling*. Scaling serves to compensate for loop distortion originating from variations in the location of the heart and in the conductivity of the surrounding tissues. Since these variations are expected to be different for the different electrode positions, a scalar multiplier, as suggested in Sörnmo [185], yields an inaccuracy in the model. This inaccuracy can be reduced, yet not fully overcome, by modeling the scaling as a $[3\times 3]$ diagonal matrix $\mathbf{B}$ with entries $\vec{\beta}$ ($B_{ij} = \beta_j\delta_{ij}$, with δ_{ij} the Kronecker delta). For the fetal VCG the variations in the location of the heart are expected to be even more prominent than

for adults as variations in the fetal position with respect to the recording electrodes on the maternal abdomen are more likely to occur.

The last transformation on $\tilde{\mathbf{Z}}_{t-1}$ is the *rotation*, which, as mentioned before, serves as a measure for fetal movement. In 3-dimensional space, the rotation between consecutive VCG's can be described by the rotation matrix $\mathbf{R}$.

Combining the three transformations, i.e. time synchronization, rotation, and scaling, gives the model (see Fig. 9.1):

$$\mathbf{Z}_t = \mathbf{R}\mathbf{B}\tilde{\mathbf{Z}}_{t-1}\mathbf{J}_\tau + \mathbf{H}. \tag{9.2}$$

Here, the QRS loop $\mathbf{Z}_t$ is assumed to be additively disturbed by the $[3\times M]$ Gaussian noise matrix $\mathbf{H}$.

9.2.2 Maximum likelihood estimation of alignment

With the model of Eq. (9.2), the loop alignment problem is reduced to a parameter estimation problem in which $\mathbf{R}$, $\mathbf{B}$, and τ constitute the parameters of interest. The uncertainty in the model and noise parameters suggests the use of a probabilistic approach for solving the parameter estimation problem. By assuming the noise to be white in all three VCG leads and have identical variances σ_v^2 [185] and by furthermore assuming no *a priori* information on the scaling and rotation matrices and the time synchronization parameter τ to be fixed, the likelihood of the model can be described as

$$p\left(\mathbf{Z}_t \left| \mathbf{R}, \mathbf{B}, \tilde{\mathbf{Z}}_{t-1}, \tau\right.\right) \propto \exp\left[-\frac{1}{2\sigma_v^2}\left\|\mathbf{Z}_t - \mathbf{R}\mathbf{B}\tilde{\mathbf{Z}}_{t-1}\mathbf{J}_\tau\right\|_F^2\right]. \tag{9.3}$$

Here, $\|\cdot\|_F^2$ denotes the Frobenius norm.

By maximizing this probability distribution with respect to both $\mathbf{B}$, $\mathbf{R}$, and τ, the ML estimation of these parameters can be assessed. This maximization is performed by finding expressions for the optimal estimates $\hat{\mathbf{B}}$ and $\hat{\mathbf{R}}$ under the assumption of fixed τ. By subsequently inferring for which value of τ the probability is maximal, the optimal estimate $\hat{\tau}$ can be determined.

To solve this maximization problem, let us for now assume that $\beta_i = \alpha$ for all i. As a result, after realizing that the matrix multiplication with $\mathbf{B}$ is equivalent to a scalar multiplication with α, the approach by Sörnmo can be followed. This approach stipulates that, since maximization of the probability of Eq. (9.3) is the same as minimization of $\|\mathbf{Z}_t - \mathbf{R}\mathbf{B}\tilde{\mathbf{Z}}_{t-1}\mathbf{J}_\tau\|_F^2$, the parameter estimation problem can be simplified to the minimization of

$$\mathrm{tr}\left(\mathbf{Z}_t^T\mathbf{Z}_t\right) + \alpha^2\mathrm{tr}\left(\mathbf{J}_\tau^T\tilde{\mathbf{Z}}_{t-1}^T\tilde{\mathbf{Z}}_{t-1}\mathbf{J}_\tau\right) - 2\alpha\mathrm{tr}\left(\mathbf{J}_\tau^T\tilde{\mathbf{Z}}_{t-1}^T\mathbf{R}^T\mathbf{Z}_t\right) \tag{9.4}$$

with respect to α and $\mathbf{R}$.

The ML estimate $\hat{\mathbf{R}}$ for $\mathbf{R}$ now follows from maximizing the last term in Eq. (9.4):

$$\hat{\mathbf{R}}_\tau = \Theta\Gamma^T \tag{9.5}$$

where Θ and Γ are the left and right eigenvectors of the matrix $\mathbf{Z}_t\mathbf{J}_\tau^T\tilde{\mathbf{Z}}_{t-1}^T$, respectively, and are obtained from the singular value decomposition (SVD) of this matrix. This ML estimate is indexed with τ to denote that it represents the ML estimate for a particular value of τ.

With $\hat{\mathbf{R}}$ determined, the ML estimate $\hat{\alpha}$ and, after that, the estimate $\hat{\tau}$ can be calculated from [185]

$$\hat{\alpha}_\tau = \frac{\operatorname{tr}\left(\mathbf{Z}_t^T\hat{\mathbf{R}}_\tau\tilde{\mathbf{Z}}_{t-1}\mathbf{J}_\tau\right)}{\operatorname{tr}\left(\mathbf{J}_\tau^T\tilde{\mathbf{Z}}_{t-1}^T\tilde{\mathbf{Z}}_{t-1}\mathbf{J}_\tau\right)} \tag{9.6}$$

$$\hat{\tau} = \arg\min_\tau \left\|\mathbf{Z}_t - \hat{\alpha}_\tau\hat{\mathbf{R}}_\tau\tilde{\mathbf{Z}}_{t-1}\mathbf{J}_\tau\right\|_F^2. \tag{9.7}$$

Let us now go back to the assumption of different scalings for each VCG lead ($\beta_i \neq \beta_j$ for $i \neq j$) and focus on the inference on the scaling matrix $\mathbf{B}$, irrespective of the rotation matrix $\mathbf{R}$. Furthermore, to clarify the notation somewhat, in the derivation presented below, the given variables/parameters $\tilde{\mathbf{Z}}_{t-1}$ and τ are omitted. In terms of probability distributions, the inference on $\mathbf{B}$ yields the maximization of the probability distribution $p(\mathbf{B}|\mathbf{Z}_t)$. Using Bayes'rule [150] and assuming no prior information on $\mathbf{B}$, it can be shown that

$$p(\mathbf{B}|\mathbf{Z}_t) \propto p(\mathbf{Z}_t|\mathbf{B}).$$

Consequently, maximizing of the log probability $\ln p(\mathbf{Z}_t|\mathbf{B})$ constitutes maximization of $\ln p(\mathbf{B}|\mathbf{Z}_t)$ as well. This log probability, in turn, can be re-expressed as:

$$\begin{aligned}\ln p(\mathbf{Z}_t|\mathbf{B}) &= \ln\int p(\mathbf{Z}_t|\mathbf{B},\mathbf{R})\,p(\mathbf{R}|\mathbf{B})\,\mathrm{d}\mathbf{R}\\ &= \ln\int p(\mathbf{Z}_t|\mathbf{B},\mathbf{R})\,\mathrm{d}\mathbf{R}.\end{aligned} \tag{9.8}$$

Here, for mathematical simplicity, the prior probability distribution $p(\mathbf{R}|\mathbf{B})$ is assumed to be uniformly distributed. When defining $p(\mathbf{R}|\mathbf{Z}_t,\hat{\mathbf{B}}^{\text{old}})$ to be the probability distribution for $\mathbf{R}$ given the VCG loops and an initial estimate of $\mathbf{B}^{\text{old}}$, then the probability distribution of Eq. (9.8) can be written as

$$\ln\int p(\mathbf{Z}_t|\mathbf{B},\mathbf{R})\,\mathrm{d}\mathbf{R} = \ln\int p\left(\mathbf{R}\middle|\mathbf{Z}_t,\mathbf{B}^{\text{old}}\right)\frac{p(\mathbf{Z}_t|\mathbf{B},\mathbf{R})}{p(\mathbf{R}|\mathbf{Z}_t,\mathbf{B}^{\text{old}})}\mathrm{d}\mathbf{R} \tag{9.9}$$

and using Jensen's inequality [132] it can be further bounded as

$$\begin{aligned}&\ln\int p\left(\mathbf{R}\middle|\mathbf{Z}_t,\hat{\mathbf{B}}^{\text{old}}\right)\frac{p(\mathbf{Z}_t|\mathbf{B},\mathbf{R})}{p\left(\mathbf{R}\middle|\mathbf{Z}_t,\hat{\mathbf{B}}^{\text{old}}\right)}\mathrm{d}\mathbf{R}\\ &\geq \int p\left(\mathbf{R}\middle|\mathbf{Z}_t,\hat{\mathbf{B}}^{\text{old}}\right)\ln p(\mathbf{Z}_t|\mathbf{B},\mathbf{R})\,\mathrm{d}\mathbf{R} - \int p\left(\mathbf{R}\middle|\mathbf{Z}_t,\hat{\mathbf{B}}^{\text{old}}\right)\ln p\left(\mathbf{R}\middle|\mathbf{Z}_t,\hat{\mathbf{B}}^{\text{old}}\right)\mathrm{d}\mathbf{R}\\ &= \mathbf{E}\left[p(\mathbf{Z}_t|\mathbf{B},\mathbf{R})\right] - \mathbf{E}\left[p\left(\mathbf{R}\middle|\mathbf{Z}_t,\hat{\mathbf{B}}^{\text{old}}\right)\right].\end{aligned} \tag{9.10}$$

Here, the expectations are expressed with respect to $p(\mathbf{R}|\mathbf{Z}_t, \hat{\mathbf{B}}^{\text{old}})$.

The derivation above essentially constitutes the EM algorithm [132, 194]. In the EM algorithm the lower bound on the righthand-side of Eq. (9.10) is defined by estimating $p(\mathbf{R}|\mathbf{Z}_t, \hat{\mathbf{B}}^{\text{old}})$. Subsequently, this lower bound is maximized, providing a new estimate for $\mathbf{B}$ that yields a larger likelihood than the old estimate $\hat{\mathbf{B}}^{\text{old}}$. In turn, for given $\mathbf{B}$, the ML estimate $\hat{\mathbf{R}}$ can be obtained using Eq. (9.5), where Θ and Γ are obtained from the SVD of the matrix $\mathbf{Z}_t \mathbf{J}_\tau^T \tilde{\mathbf{Z}}_{t-1}^T \hat{\mathbf{B}}^{\text{old}^T}$. This ML estimate $\hat{\mathbf{R}}$ can subsequently be used to define $p(\mathbf{R}|\mathbf{Z}_t, \hat{\mathbf{B}}^{\text{old}})$ as a Dirac delta function:

$$\text{(E-step):} \qquad p\left(\mathbf{R}\,\middle|\mathbf{Z}_t, \hat{\mathbf{B}}^{\text{old}}\right) = \delta\left(\mathbf{R} - \hat{\mathbf{R}}\right). \tag{9.11}$$

The use of the delta function in Eq. (9.11) implies that in the E-step the rotation matrix is assumed to equal the estimate $\hat{\mathbf{R}}$ that is determined in the previous iteration of the EM algorithm. Moreover, it has to be noted that the delta here constitutes the Dirac delta function, which is different from the Kronecker delta previously mentioned (Section 9.2.1).

Using Eq. (9.10) and (9.11), the maximization of the expectation of the log likelihood $\ln p(\mathbf{Z}_t|\mathbf{B})$ with respect to $\mathbf{B}$ reduces to finding the $\hat{\mathbf{B}}$ that satisfies

$$\text{(M-step):} \qquad \frac{\partial}{\partial \mathbf{B}} \left\| \mathbf{Z}_t - \hat{\mathbf{R}}\mathbf{B}\tilde{\mathbf{Z}}_{t-1}\mathbf{J}_\tau \right\|_F^2. \tag{9.12}$$

Here, the second term of Eq. (9.10) is omitted as this term does not depend on $\mathbf{B}$. By optimizing τ according to Eq. (9.7) after the M-step, the EM algorithm presented above operates as a three-step iterative process that maximizes the probability distribution of Eq. (9.3) with respect to $\mathbf{B}$, $\mathbf{R}$, and τ.

9.2.3 Quantification of fetal movement

Quantitative analysis of fetal movement in terms of monitoring the estimated rotation matrix $\hat{\mathbf{R}}$ is rather complicated. Specifically, visualization of evolutions in the $[3 \times 3]$ matrix over time is difficult. Hence, in this paper the movement is quantified by a single parameter: the l_2 norm of the rotation matrix $\mathbf{R}$. In fact, as no movement yields a rotation matrix that equals the $[3 \times 3]$ identity matrix $\mathbf{I}_3$, before taking the l_2 norm, $\mathbf{R}$ is adapted by subtracting $\mathbf{I}_3$:

$$\mathcal{M} = \sqrt{\sum (\mathbf{R} - \mathbf{I}_3)^2}. \tag{9.13}$$

The parameter $\mathcal{M}$ simplifies visualization of the movement, zero $\mathcal{M}$ being no movement at all and $\mathcal{M} = 2\sqrt{2}$ signifying maximal movement.

Table 9.1: *Medical conditions of the various patients and the number of patients for each of these diagnostic classes. For the patients in the class "unknown" no medical conditions were specified.*

Diagnostic class	Number of patients
Myocardial infarction	148
Cardiomyopathy/Heart failure	18
Bundle branch block	15
Dysrhythmia	14
Myocardial hypertrophy	7
Valvular heart disease	6
Myocarditis	4
Miscellaneous	4
Healthy controls	52
Unknown	22

9.3 Performance assessment of vectorcardiographic alignment

9.3.1 Signals for performance assessment

For the adult ECG, 549 recordings, most of them 60 seconds long, from 290 different patients are obtained from the MIT/BIH PTB diagnostic ECG database [184]. The medical conditions of the patients involved are detailed in Table 9.1. Besides the full 12-lead ECG, these recordings also comprise the Frank leads [64], i.e. three orthogonal leads that jointly compose the VCG.

As mentioned in Section 9.1, the developed method for estimating the rotation, scaling, and time-alignment between consecutive QRS loops (from here on, referred to as the EM method) is not expected to perform substantially better than Sörnmo's method in case of little variability in the QRS loop morphology. On the other hand, in cases of significant morphological variability, like for the fetal VCG, the difference between both methods is expected to be larger, favoring the developed method over Sörnmo's method. Therefore, both methods are also applied on fetal ECG recordings.

In total, eight fetal ECG recordings (gestational ages ranging from 23+6 to 40+5 weeks) of lengths ranging from 10 to 20 minutes are used to assess the performance of both VCG alignment methods. These ECG recordings are performed in the Máxima Medical Center (Veldhoven, the Netherlands) using contact electrodes that are placed upon the maternal abdomen. The ECG signals are acquired at a 1 kHz sampling rate using a NEMO system (Maastricht Instruments BV, the Netherlands) and are processed to eliminate the maternal ECG and some of the other interferences present [46]. The VCG can subsequently be determined from the processed signals by using

information on the electrode positions [47, 64]. In addition, to account for VCG distortion because of signal attenuation that originates from the different distances between the electrodes and the fetal heart, a statistical approach is employed that estimates the signal attenuation per electrode and exploits this information to infer a VCG that is less distorted [140].

9.3.2 Results of performance assessment

The performance of both methods is assessed in terms of spatial variability and intralead variability:

- *Spatial variability*: the spatial variability ε represents the difference between the aligned QRS loops, expressed as $\|\mathbf{Z}_t - \hat{\mathbf{R}}\hat{\mathbf{B}}\tilde{\mathbf{Z}}_{t-1}\mathbf{J}_{\hat{\tau}}\|_F^2$ for the developed method. For Sörnmo's method, the matrix $\hat{\mathbf{B}}$ is replaced by the scalar $\hat{\alpha}$.

- *Intralead variability*: the intralead variability is related to the standard deviation across the ensemble of heartbeats. That is, multiple aligned QRS loops are overlayed on one another and for each sample the standard deviation over this ensemble of QRS loops is determined. The intralead variability then constitutes the sum over (or area under) these standard deviations. To correct for variations due to noise, the standard deviations are corrected by subtracting the standard deviation obtained from intervals 50 ms before QRS onset and 50 ms after QRS end [185, 195]

For evaluation of both methods, the ECG signals are upsampled to 4 kHz to enable optimal performance of both methods [185]. Furthermore, to ensure fair comparison between both methods, Sörnmo's method is implemented in its multipass loop alignment scheme. In this scheme the reference loop $\mathbf{Z}_t$ is sequentially updated by averaging of the aligned QRS loops.

In Fig. 9.2 the effect of the loop alignment for both methods is illustrated on both an adult and a fetal ECG recording. In this figure, 50 consecutive beats are plotted on top of one another, both before and after alignment, demonstrating that the EM method performs better than Sörnmo's method in reducing the intralead variability (graphs on bottom row of Fig. 9.2) for both the adult and fetal recording.

In Fig. 9.3 the spatial variability and intralead variability for both the EM method and Sönrmo's method are depicted as a scatter plot. The standard deviation used for the assessment of the intralead variability is determined over an ensemble of 50 heartbeats and similarly, the spatial variability is averaged over the same heartbeats. Due to the fact that not all of the 549 recordings consisted of at least 50 heartbeats, in total 510 recordings are used in Fig. 9.3. Because only eight fetal ECG recordings are available, but because all these recordings contain, at least, over 1000 fetal heartbeats,

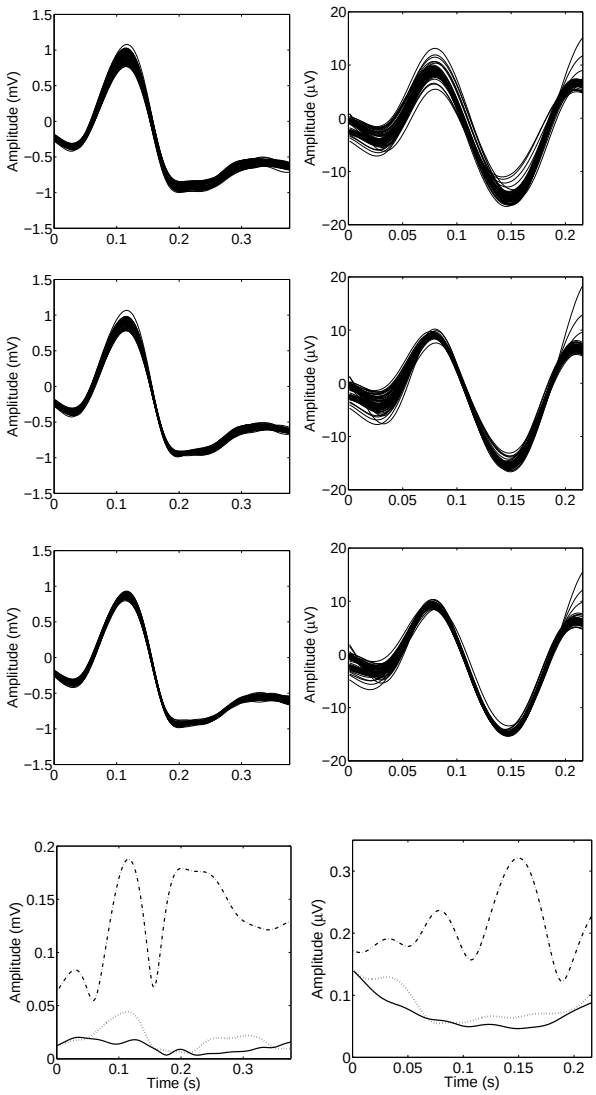

(a) (b)

Figure 9.2: *Example of 50 QRS complexes overlayed onto one another for both an adult (a) and a fetus (b) (for both lead X of the VCG). The top row shows the QRS complexes that are synchronized in time based on the maximum correlation (no rotation and scaling). The second row shows the QRS complexes that are aligned by Sörnmo's method. The third row shows the QRS complexes after alignment by the developed EM method. Finally, the bottom row shows the ensemble standard deviation. Here the '-.' line represents the standard deviation for the complexes that are only aligned in time, the dotted line represents Sörnmo's method, and the solid line represents the EM method.*

subsets of 50 heartbeats each are used to demonstrate the difference in the method's performances with respect to the performances on adult ECG recordings.

From Fig. 9.3(a), it can be seen that, in terms of minimizing the spatial variability, the EM method outperforms Sörnmo's method in all cases. This finding is conform expectation as the EM method entails an extension of Sörnmo's method, providing additional degrees of freedom in aligning the QRS loops. That is, the scaling is no longer represented by the scalar multiplier α but by the diagonal vector multiplier $\mathbf{B}$. In a worst case scenario, this diagonal obtains the form of a scalar times the identity matrix ($\mathbf{B} = \alpha\mathbf{I}$), yielding the same result as Sörnmo's method.

In terms of the intralead variability, the performance of the EM method is not by definition better than the performance of Sörnmo's method. However, Figs 9.3(b)-9.3(d) demonstrate that for most recordings the EM method performs better than Sörnmo's method. In addition, from Fig. 9.3 it can also (preliminarily) be concluded that for fetal ECG recordings the difference in performance between both methods is slightly larger. This finding can be explained by the fact that for the fetus more morphological variability between consecutive QRS loops is anticipated and this increased variability can be better accounted for by the EM method than by Sörnmo's method.

Despite the reductions in spatial and intralead variability that are achieved with the EM method, these reductions might also have a downside. Specifically, these reductions can go at the expensive of masking physiological changes. Clinically relevant changes in the morphology of the ECG might be obscured by the lead-dependent scaling, making it difficult or even impossible for clinicians to make an accurate diagnosis. In general, however, physiological changes in the ECG do not occur instantaneous but emerge rather gradual. Hence, by frequently updating the reference VCG loop $\mathbf{Z}_{t-1}$, the masking of physiological changes in the ECG can be kept relatively small. Irrespective of this comment, comparison between the performance of the EM method and Sörnmo's method, in terms of spatial and intralead variability, should nevertheless be made considering (or even correcting for) physiological changes in the ECG.

9.4 Monitoring fetal rotational movement

9.4.1 Signals and methodology for performance assessment

As mentioned previously, besides for vectorcardiographic loop alignment, the developed method can also be used to estimate movement of the fetal heart, either for facilitating clinical fetal ECG interpretation or for monitoring of fetal movement.

For evaluation of the latter application, simultaneously with the electrophysiological recordings, also ultrasound images are acquired using an Aloka SSD1100 ultrasound scanner (Aloka, Japan). Movement is determined from these ultrasound

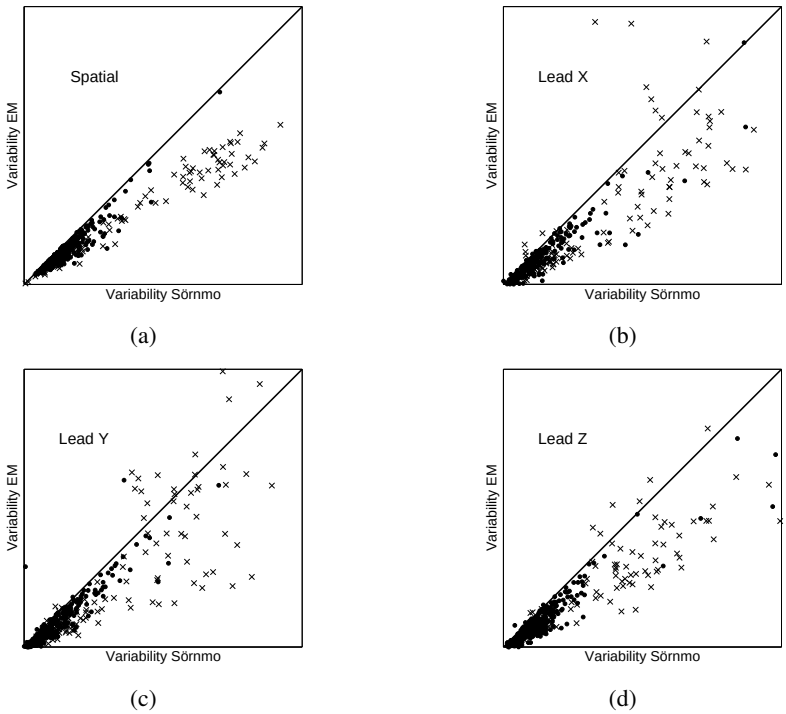

Figure 9.3: *Scatter plots of the spatial and intralead variability for both methods, for both the adult ('o') and fetal recordings ('x'). In (a) the spatial variabilities are plotted against one another. In (b)-(d) the intralead variabilities are plotted against each other. For scatter points below the line "y=x", the EM method outperforms the Sörnmo method. Vice versa, for points above the line, Sörnmo's method outperforms the EM method. For the fetal recordings, the variabilities (i.e. spatial and interlead) have been upscaled in order to visualize the fetal results next to the adult results.*

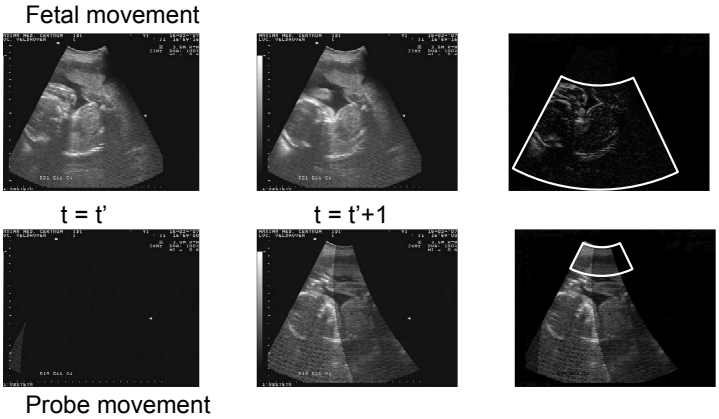

Figure 9.4: *Ultrasound images indicating either fetal movement (top row) or probe movement (bottom row). For each row, the panels on the left show the ultrasound image at time t, the center panels show the ultrasound images at the next point in time $t+1$, and the right panels show the difference between the first two panels. As fetal movement generally occurs rather gradually – for reasons of clarity – in the top row the time difference between the first two images is taken to be 0.8 s. For the probe movement, as this generally occurs more rapidly, the time difference between the first two images is taken 0.04 s. In the right panels, the ROI for fetal movement (top row) and the ROI for probe movement (bottom row) are indicated by the white frames.*

recordings in two different ways. In the first way, the movement is assessed based on visual inspection. In the second way, movement is assessed by determining the sum of absolute differences (SAD) [149] between consecutive images in the ultrasound recording. That is, the absolute difference between corresponding pixels in each ultrasound image is summed over an *a priori* assigned region of interest (ROI; see Fig. 9.4). To ensure that movement of the probe is not erroneously labeled as fetal movement, images for which the SAD is also relatively large outside the ROI (again see Fig. 9.4) are disregarded.

The automated analysis of fetal movement from ultrasound images presented above has the drawback that it cannot discriminate between movement of the limbs and movement of the heart. Hence, it can be anticipated that the ultrasound approach will show more movement than the VCG approach. For clinical practice, it can however be argued that this does not entail a major limitation to the VCG approach. Namely, one of the goals (and in this paper the principal goal) of VCG alignment is the correction for movement in the fetal ECG. In addition, because of the fact

that movement of the limbs will in some situations, due to the confined space of the uterus, result in movement of the fetal thorax (and its encompassing heart) as well, the movement assessed by the VCG approach could indeed be a reliable measure to support mothers or clinicians in fetal movement counting/monitoring.

9.4.2 Results of movement monitoring

In Fig. 9.5, for one of the fetal ECG recordings, the fetal movement $\mathcal{M}$ assessed from both the VCG recording and the ultrasound recording is simultaneously depicted. Here, the movement assessed from the VCG recordings is expressed in terms of $\mathcal{M}$.

To smoothen the movement traces depicted in Fig. 9.5 (i.e. both for the VCG recordings and the ultrasound images), they have been low-pass filtered at 0.6 Hz. The reason for this particular cut-off frequency is mainly to suppress respiration effects in the ultrasound images. That is, due to respiration, the maternal abdomen moves, causing variations between consecutive ultrasound images.

From Fig. 9.5 it can be seen that in essence all methods agree with one another. Only between 200 and 400 seconds, the ultrasound analysis shows significant elevation of the baseline, indicating movement in the ultrasound images, while this movement is not confirmed by the visual inspection. Fig. 9.5 also shows that the developed EM method is slightly more sensitive to movement than the Sörnmo method. This increased sensitivity can be explained by the fact that, due to the lead-dependent scaling in the EM method, the rotation matrix can be estimated more accurately. This improved estimation, in turn, leads to larger variations in the associated rotation angles [185].

The results for the other fetal ECG recording are consistent with the results of the recording visualized in Fig. 9.5. The correlation coefficients between the movement assessed from ultrasound and the movement assessed from either the EM method or the Sörnmo method range between 0.39 and 0.72 (average: 0.57) for EM and between 0.32 and 0.64 (average: 0.51) for Sörnmo. For the example depicted in Fig. 9.5 the correlation coefficients were 0.46 and 0.44, respectively.

9.4.3 Absolute fetal orientation estimation

As mentioned in Section 9.1, the EM method is also applied on a more extreme case of VCG mismatches: aligning the fetal QRS loop with the maternal QRS loop that is recorded simultaneously. The resulting estimate for the rotation matrix provides information on the absolute orientation of the fetus within the uterus. That is, by using *a priori* knowledge of the orientation of the maternal heart with respect to the abdominal electrodes and combining this knowledge with the estimated rotation between the fetal VCG and maternal VCG, the orientation of the fetal heart with respect to the abdominal electrodes can be assessed.

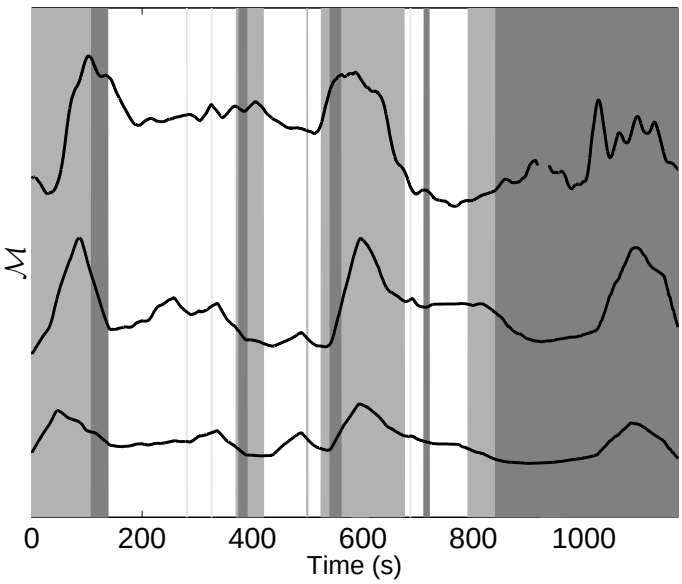

Figure 9.5: *Results of movement estimation from the ultrasound recordings (top line) and from the VCG recordings (center line for EM method and bottom line for Sörnmo's method) for the fetus at 24+4 weeks of gestation. To avoid unclarities due to overlapping of the lines, the results have been vertically shifted. The gaps in the movement trace from the ultrasound recordings are due to detected ultrasound probe movement. The shaded areas indicate the movement/events assessed from visual inspection of the ultrasound images. The lightest shade of grey indicates variations in the ultrasound images due to probe movements and external events such as changes in the intensity of the images. The darker shade of grey indicates movement of the limbs and the darkest grey indicates movement of the thorax and heart. It has to be noted here that in most cases movement of the heart is accompanied by movement of the limbs.*

Because each ECG signal basically constitutes the projection of the VCG onto the lead vector that describes the electrode position with respect to a reference position, the information on the orientation of the fetus within the uterus can be used to define lead vectors in such a way that ECG signals arise that are familiar to clinicians from adult electrocardiography. This makes clinical interpretation more easy. Moreover, when the fetal orientation can be accurately determined and the VCG can be accurately corrected for fetal movement, the developed EM method provides a platform for estimating any clinically relevant fetal ECG signal.

In order to align the fetal QRS loop with the maternal QRS loop, several signal processing and/or preparation steps have to be made that were not necessary for the VCG alignment applications discussed before. The first step is the determination of the maternal QRS loop from the abdominal recordings. This is performed the same way as discussed in Chapter 3, with the only difference that instead of subtracting the maternal ECG, this ECG is used to derive the maternal VCG. In the second step the maternal QRS loop is downsampled to match the length of the fetal QRS loop. Because the maternal heart is generally larger than the fetal heart also the maternal QRS lasts longer than the fetal QRS complex, making direct use of Eq. (9.2) impossible. The final step is compensation for the different orientation of the fetal VCG with respect to its heart. Specifically, for adults the electrical axis of the heart (i.e. the point of the VCG with maximum amplitude) on average points towards the left-anterior-inferior octant [9] (see Chapter 8). For the fetus, because it has an alternative cardiovascular circulation (e.g. septum defects and ductus arteriosus [9]), the electrical axis points towards the right-anterior-inferior octant. Alignment of the fetal VCG with the maternal VCG would therefore give an estimate for the fetal orientation that is still about 90° off [59].

In Fig. 9.6 an example of a maternal QRS loop and the aligned fetal QRS loops, determined by both the EM and the Sörnmo method, are depicted. This example is based on a fetal ECG recording performed at 24+4 weeks of gestation.

From Fig. 9.6 it can be seen that, due to the lead-dependent scaling, the alignment for EM method is much more accurate than for the Sörnmo method. For the EM method the aligned QRS loop is in the same plane as the maternal QRS loop, indicating accurate estimation of the rotation matrix $\mathbf{R}$. Conversely, the QRS loop aligned with Sörnmo's method is in a plane almost perpendicular to the plane of the maternal QRS loop.

As mentioned, the alignment between maternal and fetal QRS loops can be used to assess the absolute orientation of the fetus within the maternal uterus. The performance of this orientation estimation is evaluated by comparing the the fetal orientation determined from the VCG alignment to the orientation determined from the ultrasound recordings. The results of the evaluation are presented in Table 9.2.

The results in Table 9.2 demonstrate that the fetal orientations determined from

Table 9.2: *Estimates of fetal orientation for both fetal ECG recordings by means of ultrasound and VCG alignment. For the VCG alignment, the EM method is used. The gestational age is expressed in "weeks" + "days"*

Gestational age	23+6	24+1	24+4	36+0
Ultrasound				
VCG alignment				

	36+3	38+2	38+6	40+5
Ultrasound	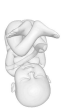			
VCG alignment				

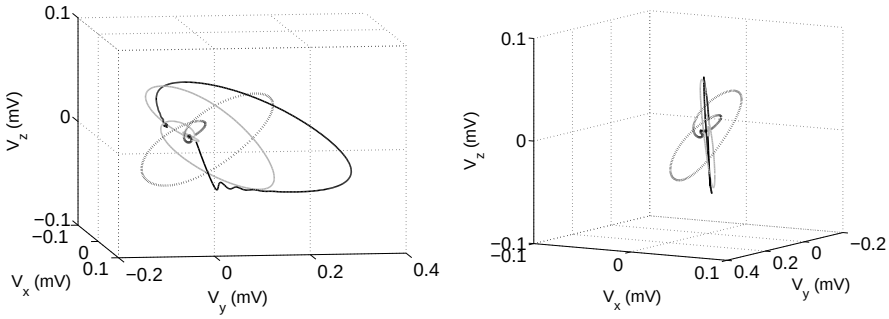

(a) (b)

Figure 9.6: *Maternal QRS loop (solid black line) jointly depicted with the aligned fetal QRS loops. The loop aligned by the EM method is depicted with the solid gray line. The loop aligned by Sörnmo's method is depicted with the dotted black line. To illustrate that the fetal QRS loop aligned by the EM method is indeed in the same plane as the maternal QRS loop, in (a) and (b) the same plot is shown from a different point of view.*

VCG alignment are consistent with the orientations determined from the ultrasound recordings. For practically all recordings, differences between the orientations assessed from ultrasound and from VCG alignment can nevertheless be seen. Whether these differences originate from insufficiencies in the model of Eq. (9.2) (e.g. because lead-dependent scaling is still not enough to accurately align both QRS loops) or from inaccuracies in the 90° correction discussed above remains to be studied in more detail. Nonetheless, based on the available recordings, the latter origin seems more likely as insufficiencies in the model of Eq. (9.2) are not confirmed to the same extent by all recordings. To conclusively state something about this, substantially more recordings are needed.

9.5 Discussion & Conclusions

In this paper a method for aligning vectorcardiographic loops has been developed. This method entails an extension of the method presented by Sörnmo [185] in that each lead of the VCG can be scaled separately, as opposed to a single scaling for Sörnmo's method. The developed method is based on the EM algorithm [132, 194] and, therefore, alignment by this method is referred to as EM alignment.

The EM alignment method is derived using a Bayesian probability framework, enforcing explicit statement of all assumptions made in the derivation. As such, the method provides a generalized framework for vectorcardiographic alignment meth-

ods, which can be tailored to each specific application by rephrasing any of the assumptions made. In contrast to this approach, in Stridh et al. [196] a specific solution to the alignment problem was presented that has a similar form as the presented EM method, but that is derived using a non-probabilistic approach. Although in this specific case the iterative method by Stridh is reported to converge for all ECG signals, this convergence cannot be straightforwardly established with mathematical proof [197] and might also depend on which of the parameters (i.e. $\mathbf{R}$ or $\mathbf{B}$) is estimated first [198]. Hence, in this paper, we have chosen to derive the alignment method using a probabilistic approach, ensuring both convergence of the maximum likelihood solution and simultaneous consideration of the parameters.

The EM method is evaluated by comparing its performance in aligning QRS loops from over 500 recordings to the performance of Sörnmo's method. From Figs. 9.2 and 9.3 it is clear that, in terms of the spatial variability, the developed method outperforms Sörnmo's method for all recordings. In terms of the intralead variability, on the other hand, the difference between both methods is less evident, albeit that the EM method still performs better than Sörnmo's method.

For the spatial variability the difference in performance can be explained by the fact that both methods strive to minimize this variability. With the EM method exploiting more degrees of freedom (i.e. separate scaling for each VCG lead instead of a common scaling for all leads), the EM method should always perform at least as well as Sörnmo's method.

Figs. 9.2 and 9.3 also indicate that the difference between the performance of both methods becomes larger in case of fetal ECG signals. This finding can be explained by the fact that for fetal ECG recordings, more variability between consecutive QRS loops is anticipated. This increased variability is likely to be more accurately modeled by the lead-dependent scaling than by the single scaling of Sörnmo's method. On this aspect, Sörnmo has raised the fair concern, which was already briefly addressed in Section 9.3.2, that the use of a lead-dependent scaling can mask physiological changes in the ECG signal. In Sörnmo [185] it is proposed to use an averaged QRS loop as the reference $\mathbf{Z}_t$ loop in the alignment procedure and to update this reference by including the newly aligned QRS loop in the averaged reference loop after each new heartbeat. Indeed, scaling and rotating all QRS loops towards this reference would mask physiological changes. However, since physiologically critical events in the fetal ECG are generally considered to occur at a time-scale of at least 15 seconds [1], by ensuring that the reference loop does not include contributions from heartbeats that are more than 15 seconds old, this masking can be prevented to a large extent. In fact, for the goal of correcting the fetal ECG signals for rotational movement of the fetus, it suffices to ignore the assessed scaling matrix $\hat{\mathbf{B}}$ and only correct for $\hat{\mathbf{R}}$. In this case, only the last QRS loop $\mathbf{Z}_{t-1}$ needs to act as reference loop for aligning $\mathbf{Z}_t$.

As mentioned previously, another use for the assessed fetal rotational movement

is to use it as a direct measure for fetal distress. The results for this movement detection are depicted in Fig. 9.5 alongside the results from automated and visual analysis of simultaneously performed ultrasound recordings and show relatively good consistency between the results.

Finally, in Fig. 9.6 and Table 9.2 the potential of the developed EM method is once more illustrated by demonstrating that the method can also be used to align fetal QRS loops with maternal QRS loops, providing information on the absolute orientation of the fetus within the uterus. However, this particular application of the EM method is at this moment accompanied by some inaccuracies or uncertainties. Namely, due to the alternative cardiovascular circulation of the fetus, the electrical axis of the fetal heart is shifted about 90° with respect to the electrical axis in the adult heart. In addition, the fact that the alignment now concerns QRS loops from different hearts can also lead to such large mismatches between the QRS loops that some elements in the estimated scaling matrix $\hat{\mathbf{B}}$ can become negative. Such negative scalings will significantly affect the estimated rotation matrix $\hat{\mathbf{R}}$ and with that, the assessed fetal orientation. To make conclusive statements on the influence of these inaccuracies on the performance of the EM method for assessing the fetal orientation, more data is required.

Additional data is also required to assess whether the EM method can provide information on fetal movement in all stages of pregnancy. Specifically, from the 28th week of gestation onwards the fetus gets covered by the vernix caseosa, a waxy electrically isolating layer that causes distortion of the VCG. Whether or not this distortion is so large that it prevents movement detection is as yet unclear. Similarly, this distortion can also complicate assessment of the absolute fetal orientation.

Besides distortion, the appearance of the vernix caseosa also causes a temporary reduction in the amplitude of the fetal ECG signals. Between about 28 and 32 weeks of gestation the vernix fully covers the fetus, significantly attenuating the ECG signals and, as a result, the SNR. After 32 weeks, gaps in the vernix appear and signal amplitudes return to their original range. For SNR values that have dropped below a certain level, Sörnmo's method is reported to break down [193]. Although it is expected that the EM method will show a similar breakdown in performance, this remains to be studied.

9.6 Comments

In Section 9.4.3 of this chapter, a method was presented to infer the fetal orientation within the uterus by aligning the fetal VCG with the maternal VCG. Although the results of this orientation inference are promising, the method is evaluated on too few measurements to conclusively state that the method performs well in all situations. Hence, for the assessment of the fetal orientation in the forthcoming two chapters ultrasound images will be used (similar as in Chapter 8).

Chapter 10

Can the 12-lead ECG representation of fetal supraventricular extrasystoles be used to assess congenital heart disease?

To illustrate the potential of the technologies developed throughout this thesis, they are all integrated for application on clinically interesting fetal ECG recordings. In this chapter, the 12-lead ECG representation of a fetus suffering from extrasystoles is presented.

10.1 Introduction

Congenital heart disease (CHD) is the most common origin of birth defects [199]. Assessment of CHD in fetuses with four chamber view echocardiography is reported to be only conclusive in about 65% of the cases [200]. This entails that, irrespective of the possibilities for treatment and management of CHD [78, 201–203], one of the main problems to be solved for reducing the incidence of infants born with CHD is to improve or extend the information on which clinicians can base their diagnosis.

Fetal arrhythmia are generally harmless and associated to the immaturity of the fetal heart [204]. However, a small number of arrhythmia originates from CHD [77, 205]. Because arrhythmia are rather easily detectable, the occurrence of arrhythmia could serve as screening tool for assessing fetuses at risk for CHD. What is still needed then is a way of inferring whether the arrhythmia originates from CHD or not.

In this chapter a possible approach towards this inference is discussed. This approach is based on the integration of all fetal electrocardiogram (ECG) and vectorcardiogram (VCG) processing techniques presented in this thesis to yield a means for estimating the 12-lead ECG of the fetus. This 12-lead ECG can be used to determine from where the arrhythmia originate and whether this origin can be related to CHD or innocent immaturity.

The hypothesis we pose is therefore that the 12-lead ECG presentation of fetal

arrhythmia can provide information on the origin of these arrhythmia and potentially relate them to fetal CHD. If so, in the near future for every fetus that shows prenatal arrhythmia a 12-lead ECG can be determined, providing additional support to clinicians in making an accurate diagnosis. In this chapter, we present the 12-lead ECG of two fetuses, one with no cardiac arrhythmia and one that has supraventricular extrasystoles . Note that neither of these fetuses suffers from CHD but that they do illustrate our hypothesis.

10.2 12-lead ECG of fetal supraventricular extrasystoles

The *in-vivo* measurements exemplified in this chapter form part of a larger study conducted at the Máxima Medical Center (Veldhoven, the Netherlands) in which for about 50 pregnant women, longitudinally across the pregnancy, the fetal electrocardiogram (ECG) is recorded from the maternal abdomen. The measurements were performed on two patients. The first was a healthy ”DES daughter” mother, 37 years of age with a singleton pregnancy of 39+0 weeks. The fetus showed supraventricular extrasystoles (SVES) with a repetition frequency of about 1 in 5, no pulmonary or cardiac oedema, no signs of CHD showed up during echocardiography, and the fetus was eventually born healthy without CHD and with 1 and 5-minute Apgar scores of 9 and 10, respectively. The second patient was a healthy mother, 35 years of age with a singleton pregnancy of 24+1 weeks, diagnosed as placenta previa totalis. This fetus showed no arrhythmia and was born after 36+5 weeks, with 1 and 5-minute Apgar scores of 9 and 10, respectively. Both mothers gave their informed consent.

The fetal ECG signals are obtained with 8 adhesive electrodes on the maternal abdomen and are processed to suppress the interferences and artifacts from, among other factors, respiration and the maternal ECG [46]. Subsequently, the information from all 8 electrodes is combined to yield the fetal vectorcardiogram (VCG) [47,140]. In essence this VCG constitutes a 3-dimensional representation of the ECG and enables the estimation of any ECG signal desired. More particularly, by combining the fetal VCG with information on the fetal orientation, obtained from a simultaneously performed ultrasound recording, it is not difficult to estimate the standardized 12-lead ECG. A schematic overview of the recording setup and ECG processing is depicted in figure 10.1.

In figures 10.2 and 10.3 the 12-lead ECG for both the fetus with SVES and the fetus without arrhythmia are respectively depicted. From figure 10.2 it can be clearly seen that the second and seventh heartbeat constitute a SVES, consistently with the above stated repetition frequency of 1 in 5. The correct clinical interpretation of the origin and nature of the SVES calls for a thorough consideration of the electrophysiological nature of the fetal ECG. That is, due to the adaptation of the fetal heart to its alternative cardiovascular circulation [57, 59, 206], the electrical axis of the heart

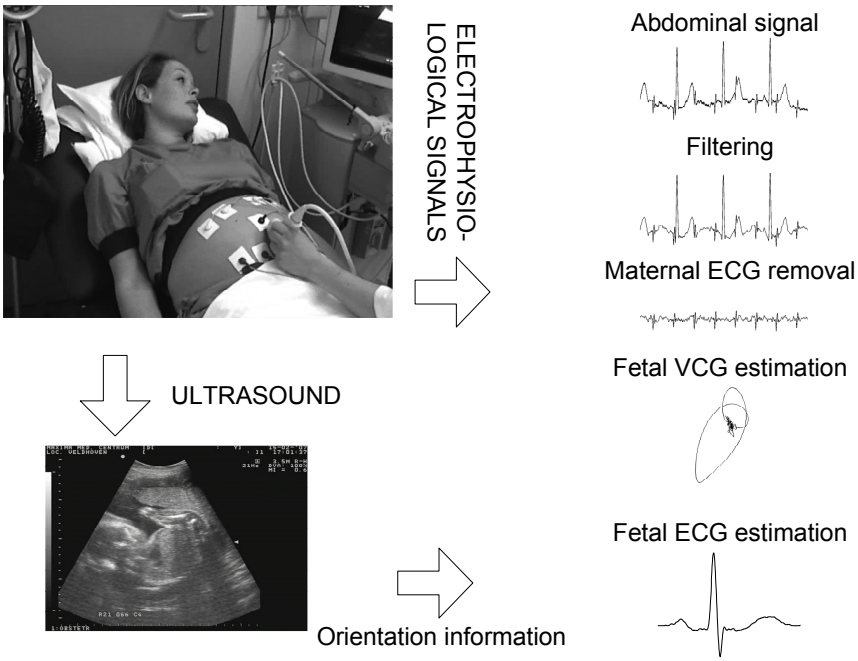

Figure 10.1: *Methodology for assessment of the 12-lead ECG of the fetal heart. This is achieved in two steps. In the first step, the fetal ECG is recorded from the maternal abdomen (upper left photo) and processed by successive filtering, suppression of the maternal ECG, enhancement of the fetal ECG, and estimation of the fetal VCG (right panel). In the second step, the fetal VCG is rotated towards the fetal frame of reference, obtained from the ultrasound image (bottom left) to enable estimation of the 12-lead ECG representation of the fetus.*

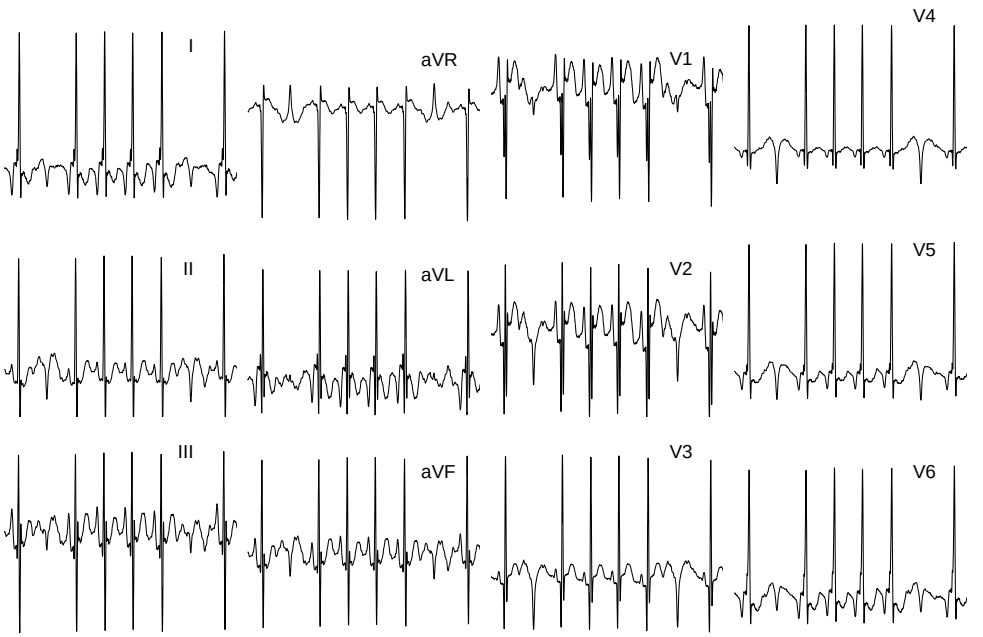

Figure 10.2: *12-lead ECG of the fetal heart. The 2nd and 7th heartbeat constitute SVES. It has to be noted that the ECG signals differ from the 12-lead ECG of an adult because the electrical axis of the fetal heart is typically oriented towards the right-anterior-inferior octant, rather than towards the left-anterior-inferior octant as in the adult heart.*

is shifted towards the right-inferior-anterior octant. This shift significantly affects the morphology of the presented ECG leads (see Chapter 8), rendering them largely different from the corresponding ECG leads in adult electrocardiography.

To provide a benchmark for assessing fetal cardiac pathophysiologies, the proposed 12-lead ECG method should also be applied to ECG recordings on healthy fetuses (as exemplified in figure 10.3). When analyzing the ECG in figure 10.2 relative to that in figure 10.3, it can be concluded that the arrhythmia indeed does not originate from any CHD, consistent with the result of the echocardiography.

Figures 10.2 and 10.3 also demonstrate that when analyzing the fetal ECG, some aspects need to be taken into account. Besides the aforementioned difference between the fetal and adult electrophysiology, also the small dimensions of the fetal heart and the fact that several (maternal) tissues shield the fetal heart from the abdominal electrodes have their effect on the visualized ECG signals. Specifically, both the small dimension and the intermediate tissues render the signal quality of the 12-lead fetal ECG signals relatively low when compared to the adult ECG signals, potentially

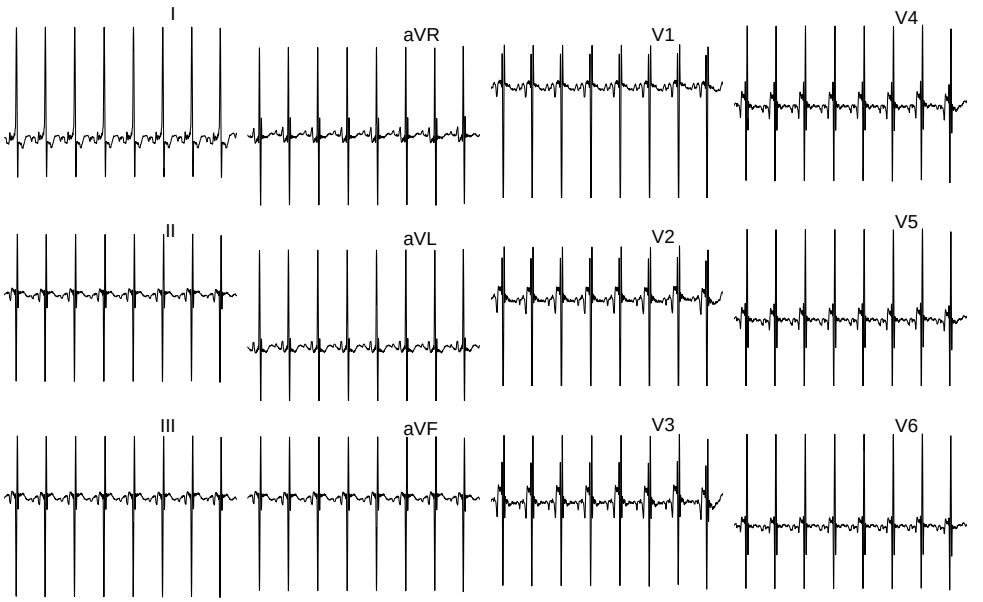

Figure 10.3: *12-lead ECG for the fetus with no fetal arrhythmia.*

complicating accurate diagnostics. In addition, it has to be noted that inaccuracies in the echocardiographic fetal orientation assessment lead to a relatively large inter-patient variability in the calculated ECG signals. That is, since the orientation cannot be accurately determined, the calculation of the 12-lead ECG also suffers from inaccuracies. Intuitively, these inaccuracies can be regarded as similar to inaccuracies in the adult 12-lead ECG that originate from inaccurate placement of the electrodes.

10.3 Discussion

In this chapter we hypothesized that visualization of fetal arrhythmia in the 12-lead ECG representation can aid in early diagnostics on whether the arrhythmia originate from fetal CHD or not. Early detection of CHD might facilitate treatment of the disease and improve expectancies on quality of life for the fetus. Although the presented data does not entail a fetus that suffers from CHD and therefore cannot be fully used to confirm (or refute) the hypothesis, it shows the potential of the 12-lead ECG representation of the fetal ECG.

The most diagnostic value for the 12-lead fetal ECG is expected in cases of fetal bradycardia. Nevertheless, also in cases of fetal tachycardia the 12-lead fetal ECG can have added value. Approximately half of all fetal bradycardia cases are caused by associated CHD [77]. With the relatively low sensitivity of four chamber view

echocardiography [200], only 65% of these bradycardia cases can be conclusively diagnosed as originating from CHD or not. Introducing the 12-lead fetal ECG in the standard work-up for fetal bradycardia might increase the sensitivity of the diagnosis for CHD and, furthermore, might reveal additional detail on the origin of the CHD, supporting decisions on treatment strategies.

Generally, fetal tachycardia is managed by transplacental administration of digoxin, sotalol, flecainide, or amiodarone to convert the heart rate back to sinus rhythm. In many situations these antiarrhythmic drugs cause a rise in heart rate variability [207], yielding Doppler cardiotocography inaccurate or even impossible. That is, most cardiotocography monitors detect the fetal heart rate by means of an autocorrelation algorithm [15, 143]. This algorithm operates by determining the average periodicity of the fetal cardiac activity within a fixed time window. The advantage of this approach is that it works relatively robustly. The drawback, on the other hand, is that in cases of high variability the average periodicity does not accurately reflect the true activity of the heart anymore. In addition, based on the autocorrelation algorithm alone, arrhythmia like SVES cannot be detected and classified, requiring the need for additional recording modalities such as M-mode echocardiography. From the fetal ECG not only these arrhythmia can be recognized, but also the fetal heart rate can be determined accurately and on a beat-to-beat basis.

Besides using the 12-lead ECG to assess fetal CHD only for patients that suffer from arrhythmia, the 12-lead ECG might also serve as standard screening tool for assessing CHD in early pregnancy. In (Dutch) gynaecology and obstetrics practice, around 20 weeks of gestation an echocardiographic examination is performed to, among other complications, search for CHD. Given the relatively low sensitivity of this echocardiographic examination, the 12-lead ECG, when available, might aid in the accurate detection of CHDs like tetralogy of Fallot and single-ventricle [208].

Nevertheless, before the 12-lead representation of the fetal ECG can have a truly added value in obstetrical diagnostics, the applications mentioned above need to be employable both robustly and cost efficiently. The robustness of the presented methodology concerns the fact that for all cases, the method should be able to provide a 12-lead ECG. In particular for the period in which the fetus is covered by the vernix caseosa, problems with the robustness are to be expected. Even when it is possible to non-invasively record the fetal ECG in this period, this ECG is likely to be distorted due to preferred propagation paths through the umbilical cord and over the oro-nasal cavity [105, 106]. This distortion of the ECG might render the correct interpretation of the fetal ECG impossible and could hence restrict the application of the 12-lead ECG to gestational ages for which the vernix caseosa has not yet been developed or has already been shed completely.

Finally, whether or not to introduce the proposed method in obstetrical diagnostics should strongly depend on the possibility of establishing a benchmark for healthy

fetuses and whether or not these benchmark ECG signals prove to be significantly different from ECG signals that are associated with CHD. So in conclusion, a large patient study will have to be performed to validate our hypothesis, map its robustness, and study its cost efficiency. When all positive, the proposed method could potentially lead to substantial improvement in the early diagnosis and treatment of CHD in the fetus.

Chapter 11

ST analysis of the non-invasive fetal electrocardiogram

Like for the previous chapter, also in this chapter the potential of the developed technologies is illustrated by applying them all on a clinically interesting case. Here, however, this interesting case does not concern a fetus suffering from some kind of physiological event or pathology, but it is intended to show the signal quality that can be achieved with the non-invasive recordings. In addition, in this chapter the optimal ECG signal for performing ST analysis is briefly addressed and compared to that of the invasive ECG signal used by the STAN® monitor.

11.1 Introduction

The assessment of intrapartum fetal hypoxia is complicated. Currently, cardiotocography (CTG; the simultaneous registration of the fetal heart rate and maternal uterine activity) is the most widespread method used for fetal surveillance. However, poor specificity of the CTG has led to an increase in the number of operative deliveries without a decrease in perinatal mortality or cerebral palsy [20]. Combined use of the CTG with automatic ST-waveform analysis of the fetal electrocardiogram (ECG) (STAN®, Neoventa Medical, Sweden) has been demonstrated to reduce the rates of severe metabolic acidosis at birth and unnecessary instrumental vaginal delivery for fetal distress [21, 28]. However, it also has been reported that patients showed no pathological changes in the ST-waveform, but were nevertheless born with evident metabolic acidosis [51]. In one of these cases, the reason for the absence of pathological changes was a temporary disconnection of the STAN® monitor [51]. During this disconnection the T/QRS ratio had risen significantly, but this rise was not correctly detected as after reconnection the STAN® monitor determined a new T/QRS baseline.

It is rather straightforward to argue that the occurrence of antepartum fetal metabolic acidosis cannot always be assessed using STAN®. Before sufficient cervical dilatation and membrane rupture the STAN® cannot be connected and once it

can, relevant changes in the T/QRS ratio might be obscured by a falsely established T/QRS baseline. Monitoring of the fetal ECG from the maternal abdomen might help in these cases, as shown for the ovine fetus [209]. Because these transabdominal recordings are performed non-invasively, they can provide the fetal ECG in stages of pregnancy earlier than labor. This avoids issues with late availability and potentially unreliable baseline assessment that are, in some situations, the case with the invasive recordings. Another potential disadvantage of the invasive ECG recordings, besides the risks of e.g. infections [210], is that they are expected to have suboptimal properties for their intended use. Specifically, out of all possible ECG leads available, the invasive ECG is not selected for its optimal properties for performing ST analysis, but for its accessibility; i.e. the invasive electrode is for vertex positions connected to the fetal scalp. For the transabdominal fetal ECG, any desired ECG lead can be made available and hence, the one with optimal properties for ST analysis can be selected. In addition, since the transabdominal recordings also provide information on fetal heart rates [92] and uterine activity [100], they have the potential to serve as a complete replacement of the invasively recorded fetal ECG.

Up till now, however, these non-invasive recordings are not widely used in clinical practice due to presumed technical difficulties, such as the lower quality of the non-invasive signals as opposed to the invasive fetal ECG signal. By exploiting the multi-lead information that can be obtained from the maternal abdomen [46, 140], nonetheless, most of these technical difficulties can be overcome, yielding fetal ECG signals that are no longer that inferior to the invasive ones. Notwithstanding the solution to the technical difficulties, ST analysis from non-invasive ECG recordings is complicated for physiological reasons as well. As reported in Cleal et al. [209], the amplitude of the fetal T-wave is significantly smaller in abdominal ECG signals than in the invasive ECG signal. The reason for this is the fact that the abdominal ECG signals need to propagate through the maternal volume conductor, consisting of vernix caseosa, amniotic fluids, muscle layers, fat and skin. This conductor is reported to act as a high-pass filter [37, 38] and hence does mainly affect low frequency events, such as the T-wave.

In this chapter, the authors quantify the filtering effect of the volume conductor *in-vivo* and use this quantitative information, together with *in-vitro* [37] and theoretical [38] characterizations of the volume conductor, to correct the transabdominal fetal ECG recordings for this filter. To enable the *in-vivo* quantitative characterization of the volume conductor, we have performed simultaneous fetal ECG recordings on both the maternal abdomen and on the fetal scalp. We also show the potential of the corrected non-invasive fetal ECG recordings for performing ST analysis. In addition, we show that the invasive scalp ECG lead is not that far from optimal for facilitating ST analysis.

11.2 Materials and Methods

11.2.1 Participants

The study was performed at the Máxima Medical Center (Veldhoven, the Netherlands) in 2006 and comprised the longitudinal monitoring of the fetal ECG and fetal heart rate from 14 weeks of gestation until term. Fifty healthy women were included in the study, all at least 18 years of age and with singleton pregnancies. The study was approved by the ethics committee of the hospital and all women gave their informed consent before entering the study. In this chapter, the results of only two different women are presented.

11.2.2 Fetal ECG recording

For the non-invasive recordings, the obstetric wards were equipped with a prototype of the NEMO system (NEMO Healthcare BV, Eindhoven, the Netherlands and Maastricht Instruments BV, Maastricht, the Netherlands). This system employs 500 times signal amplification, analog-to-digital data conversion at a rate of 1 kHz and signal processing to suppress interferences such as from the powerline grid [102] and the maternal ECG [46].

The recordings were performed by positioning 8 self-adhesive electrodes on the maternal abdomen with a common reference positioned near the umbilicus (Fig. 11.1) and a ground electrode in the side. The invasively recorded fetal ECG signal was simultaneously stored on the NEMO system.

As mentioned, the recordings from the maternal abdomen consist of eight fetal ECG signals, each recorded on a different position with respect to the fetus. These eight signals can be combined into the fetal vectorcardiogram (VCG) and this VCG, in turn, can be used to calculate any desired ECG lead. Naturally, for the comparison of the non-invasive fetal ECG with the invasively recorded ECG, the ECG lead that resembles the invasive ECG most will be used. By using ultrasound images to determine the fetal orientation within the uterus, this ”non-invasive scalp” ECG lead can be associated to a specific direction with respect to the fetal heart. Moreover, as mentioned before, the VCG can also be used to generate an ECG lead that has optimal properties for ST analysis. By evaluating the direction, corresponding to this ECG lead, with respect to the fetal heart (again using ultrasound images), it can be assessed to what extent the invasively recorded ECG is suitable for ST analysis. That is, when the ”optimal” direction is far from the direction used for the invasive ECG, the invasive ECG is suboptimal. On the other hand, directions close to one another render the invasive ECG not far from optimal.

Despite the fact that any desired ECG lead can be calculated from the VCG, the non-invasive ECG will nonetheless differ significantly from the invasive ECG. The

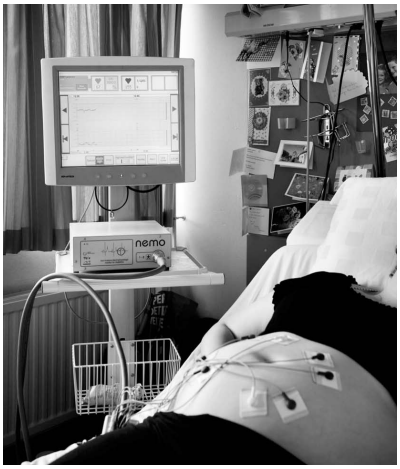

Figure 11.1: *Setup for the non-invasive fetal ECG recordings with the eight recording electrodes on the maternal abdomen. Neither the reference electrode, nor the ground electrode has yet been positioned. On the left the NEMO system can be seen. (Photo by Bart van Overbeeke.)*

reason for this is that the transabdominally recorded ECG signal need to propagate through the vernix caseosa, amniotic fluid, fetal membranes and maternal tissues [37]. The combined effect of all these tissues is a high-pass filter that mainly affects the amplitude of the fetal T-wave [37, 38] and hence complicates the non-invasive ST analysis [209]. With the simultaneous recording of the invasive and non-invasive ECG, this high-pass filter can be quantified *in-vivo*. Moreover, in this chapter we compare this so-called transfer function (i.e. quantification of the filter) between both patients and model it by a few filter coefficients. By subsequently inverting these coefficients, the non-invasive ECG recordings can be corrected for propagation effects to resemble the invasively recorded ECG and possibly improve non-invasive ST analysis.

The consistency between ST analyses performed on the invasively recorded fetal ECG and the non-invasively recorded fetal ECG is assessed by determining the T/QRS ratios. Naturally, the STAN® monitor also includes monitoring of biphasic ST segments, but as the transabdominal ECG cannot (yet) be analyzed by STAN®, comparing also these biphasic ST segment would require full copy of the STAN® and is beyond the scope of this chapter.

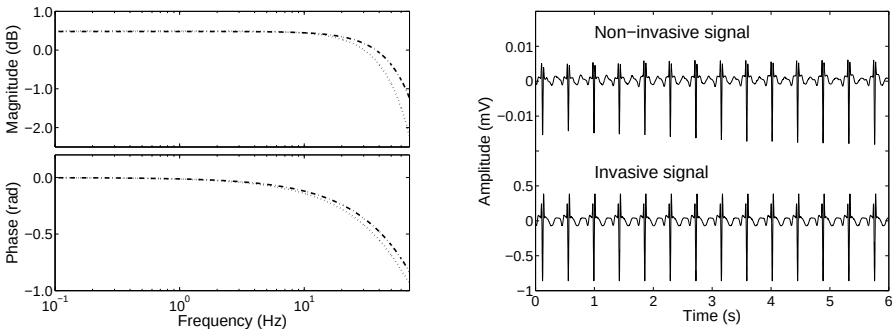

(a) (b)

Figure 11.2: *In (a) the magnitude and phase response of the inverted transfer function are depicted. Each line represents the result of one of the two patients. In (b) part of the non-invasively (after correcting for the volume conductor) and the invasively recorded fetal ECG signals are jointly depicted. Note that although the morphology of both ECG signals is similar, their scale is still different; the amplitude of the non-invasive ECG is significantly smaller.*

11.3 Results

In Fig. 11.2 the characteristics for the inverted transfer function are shown. Also in Fig. 11.2, the invasively recorded ECG and the resembling non-invasively recorded ECG (i.e. the ECG lead that resembles the invasive ECG most and that is enhanced by inverse filtering) are jointly depicted.

From the inverted transfer function in Fig. 11.2(a) it can be seen that correction for the volume conductor requires enhancement of low frequency events, such as the T-wave. This finding is consistent between both patients and with earlier findings in literature [37, 38, 209]. After correcting for the filtering effects of the volume conductor, the resemblance between the non-invasively and invasively recorded ECG signals shown in Fig. 11.2(b) is rather good (i.e. the correlation is 95%, $p<0.001$). For the patient not depicted in Fig 11.2(b), this resemblance was somewhat smaller (81%, $p<0.001$).

The resemblance between the invasively and non-invasively recorded fetal ECG is once more illustrated in Fig. 11.3 which shows the CTG and ST analysis (T/QRS ratios) obtained from both ECG signals. The activity of the uterus in Fig. 11.3(a) is determined from the transabdominal recordings using the electrohysterographic signal analysis technique presented in [100]. Since the output of a simultaneously applied tocodynamometer was not digitized, the uterine activity in Fig. 11.3(b) is also obtained from the transabdominal recordings and hence the same as in Fig. 11.3(a).

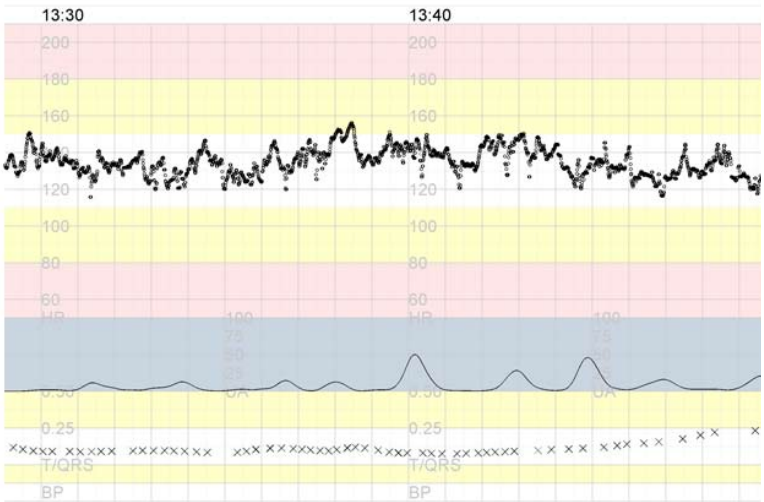

(a)

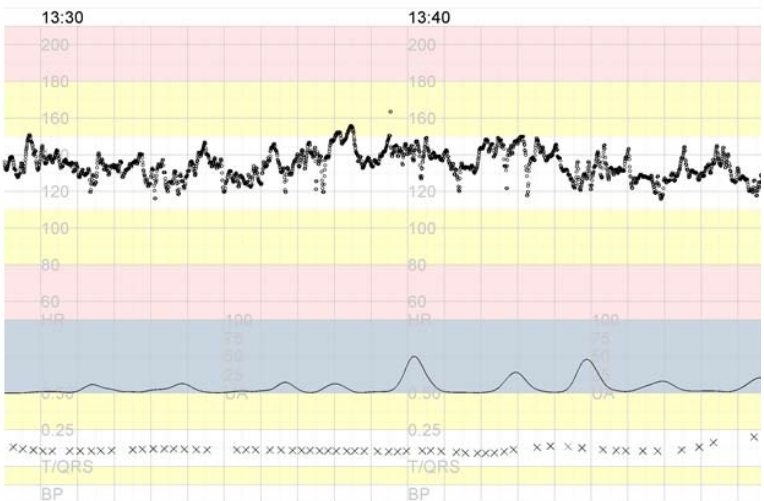

(b)

Figure 11.3: *In (a) the fetal cardiotocogram (CTG) and T/QRS ratios determined from the transabdominal recordings are depicted. In (b) the CTG and T/QRS ratios determined from the simultaneously performed invasive fetal ECG recording are depicted.*

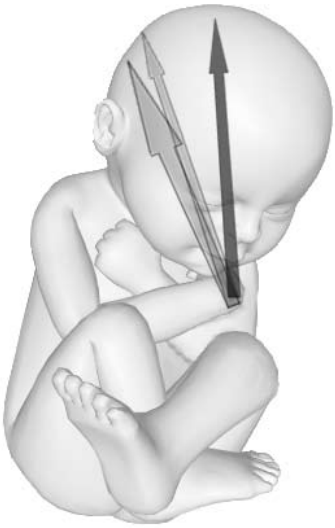

Figure 11.4: *Direction of the ECG lead that maximizes the accuracy of the ST analysis for the two patients involved in this study (light colored arrows) and the approximate direction of the invasively recorded ECG (dark colored arrow).*

The results depicted in Fig. 11.3 are for the same patient as the ECG signals in Fig. 11.2(b); The results for the other patient are consistent.

As mentioned previously, the VCG can also be used to calculate any desired ECG lead, including the one that is optimal for ST analysis. Since the ST analysis mainly involves the determination of the T/QRS ratio and the assessment whether the ST segment is biphasic, this analysis can be performed most accurately when the amplitude of the T-wave is maximal. That is, because in general the noise amplitude remains the same, a larger T-wave amplitude signifies a larger signal to noise ratio. In Fig. 11.4 for both patients the ECG lead direction that maximizes the T-wave is depicted. At the same time, also the approximate direction of the invasively recorded ECG is depicted, indicating that the direction of the invasively recorded ECG is rather close to optimal. The direction of the invasive fetal ECG is here approximated as the direction from the fetal heart to the scalp. In fact, the invasive fetal ECG is recorded as a bipolar recording with one electrode fixed in the fetal scalp and the other attached to the maternal leg: in literature often referred to as a unipolar recording [1, 28]. When assuming the maternal leg to be free of any fetal ECG components, the assumption of unipolarity is somewhat justified and the origin of the invasive ECG lead vector can be assumed to lie near the fetal heart [49].

11.4 Discussion

In this chapter, it was demonstrated that, using novel technologies, the human fetal ECG can be recorded non-invasively from the maternal abdomen with such quality that it enables ST analysis in stages of pregnancy earlier than labor. Naturally, the two recordings discussed in this chapter yield insufficient statistical significance to make any statements on the reliability of these recordings, but they clearly demonstrate the potential of present-day technologies. In fact, with regard to the reliability of these recordings, it is expected that the reliability is largest between 20 and 28 weeks of gestation and near term. In the former period, the fetal heart is large enough to generate ECG signals of sufficiently large amplitude. The same holds for the latter period. The intermediate period (i.e. from about 28 weeks till about 37 weeks), the fetus is fully (28-32 weeks) or partly (32 weeks and later) covered by the vernix caseosa [36]. This vernix electrically isolates the fetus from its surroundings, drastically affecting the amplitude of the ECG signals that can be recorded from the maternal abdomen.

In Fig. 11.2(b) one of the at-term fetal ECG signals, recorded from the maternal abdomen, was depicted alongside the simultaneously recorded invasive fetal ECG. The most striking difference between both ECG signals is the amplitude. Where the invasive signal is recorded close to the fetal heart, the non-invasive ECG signals have to propagate through amniotic fluids, uterine tissues, abdominal muscles, fat, skin, etc. These tissues cause significant signal attenuation – the amplitude of the non-invasive fetal ECG is about 100 times smaller than the amplitude of the invasive fetal ECG – and because of the even higher noise levels in the transabdominal recordings, this signal attenuation yields a significant reduction in signal-to-noise-ratio (SNR). However, as can be seen in Fig. 11.2(b), by processing the ECG signals this SNR can become similar to the SNR of the invasive recordings. In Fig. 11.2(b) it also strikes that the non-invasive transabdominal ECG signals have a smaller S-wave than the invasively recorded ECG. This difference can be explained by the fact that, although the non-invasive ECG lead is selected as such that it provides an ECG signal that resembles the invasive ECG, both ECG signals can never fully be the same. In this particular case, this difference expresses itself mainly in the S-wave. For ST analysis, this difference is not critical. ST elevations or biphasic ST segments will not be obscured by differences in the QRS amplitude; These amplitude differences merely affect the accuracy of the assessed T/QRS ratios.

In Fig. 11.3 the CTG and ST analysis on both ECG signals were presented; for the transabdominal ECG in Fig. 11.3(a) and for the invasive ECG in Fig. 11.3(b). The CTG's of both signals are consistent with one another and show a correlation of over 97% ($p<0.001$). The correlation between the T/QRS ratios is smaller: 65% ($p<0.001$). Because of the different ECG signals a lower correlation than for comparison between the ECG signals was expected here. Whether or not this correlation renders the non-invasive recordings reliable and accurate for assessment of signifi-

cant ST changes, e.g. because of fetal hypoxia, remains to be studied. Results from a study on the ovine fetus [209] are promising, but many more recordings are required to conclusively state something about this.

As discussed, the main advantage of the transabdominal ECG recordings lies in their non-invasiveness and the associated benefits that they do not expose either mother or fetus to any risks and they can be performed in earlier stages of pregnancy than the invasive recordings can. An additional advantage is that the non-invasive recordings can be performed using more electrodes providing more information than the single invasive electrode. Moreover, by combining the spatial information on the fetal ECG with information on the orientation of the fetus within the uterus (e.g. assessed by means of echography) any desired ECG signal can be estimated. Conversely, ECG signals calculated from the VCG can be linked to ultrasound images to approximate the direction of the corresponding ECG lead with respect to the heart. As an example, the ECG signals that optimize ST analysis were determined for both patients, indicating that the invasive ECG lead used by the STAN® monitor is in fact not far from optimal. Here again, it needs to be stressed that the two patients included in this study are not enough to ensure statistical significance of these conclusions. For future research, therefore, one of the goals should be to perform the determination of the transfer function, the non-invasive ST analysis, and the search for optimal ECG leads on more patients to assess whether the results presented in this chapter can be made statistically significant. In addition, a large patient study would ensure the inclusion of patients that suffer from metabolic acidosis, the principal target group for the non-invasive ST analysis.

11.5 Conclusions

In this chapter, it was shown that a similar ECG signal quality can be obtained with the non-invasive recordings as with the invasive recordings. In addition, a preliminary comparison between (partial) ST analyses performed on both an invasive and a non-invasive recording was presented. These partial ST analyses comprised the calculation of the T/QRS ratios and showed promising, but as yet not satisfactory, agreement between the invasive and non-invasive recordings. A larger patient study is required to further investigate the agreement between non-invasive and invasive ST analysis and assess whether the non-invasive recordings can be used to predict fetal hypoxia. Finally, it was studied whether the accuracy of the determined T/QRS ratios might be improved by calculating a different ECG lead from the fetal VCG; One that yields maximum amplitudes of the T-waves. It turned out that only small improvement in accuracy can be expected as the currently employed fetal scalp lead vector was demonstrated to be already close to the vector that maximizes the T-waves.

Chapter 12

Conclusions and future directions

12.1 Conclusions

The timely recognition of fetal distress is important to ensure that treatment or intervention of pregnancy can be done effectively. At present, the most widely used method to assess the fetal condition in the uterus is cardiotocography (CTG; the simultaneous monitoring of the fetal heart rate and maternal uterine activity). Unfortunately, the poor specificity of CTG has, since its introduction in clinical practice, resulted in increased rates of intervention without a significant reduction in perinatal mortality or cerebral palsy. The combined assessment of CTG and the fetal electrocardiogram (ECG) has been demonstrated to reduce the incidence of severe metabolic acidosis and the rate of instrumental deliveries. However, this fetal ECG must be measured invasively and consequently, this combined assessment is only possible during labor, after sufficient cervical dilatation and membrane rupture.

Monitoring of the non-invasively recorded fetal ECG, on the other hand, can, in principle, be performed in all stages of pregnancy and could hence become one of the mainstays in fetal surveillance. However, before the non-invasive fetal ECG can be applied in clinical practice several important aspects of this ECG need to be improved or studied. For instance, the reliability and signal quality of the non-invasive recordings need to be improved to ensure that clinical diagnosis based on the signals can be performed reliably at all times. In addition, the appropriate physiological context and background of the acquired signals need to be studied to make correct overall diagnosis possible. This thesis aims to contribute on the technological aspects (i.e. reliability and signal quality) and to advance the interpretation of the non-invasively recorded fetal ECG signals.

The main problems with reliability and signal quality stem from interferences that need to be suppressed. The maternal ECG is the dominant interference, but also interferences from the uterus, the abdominal muscles and powerline grid obscure the fetal ECG. The first part of this thesis (i.e. Chapters 3 to 7) deals with the suppression of some of these interferences and the estimation of the fetal vectorcardiogram (VCG). The VCG is used as starting point for studying the physiological aspects of

fetal ECG monitoring.

In Chapter 3, a technique was presented to suppress the maternal ECG from recordings performed on the maternal abdomen. The technique is referred to as weighted averaging of maternal ECG segments (WAMES) and can be viewed as an extension of existing template subtraction techniques. The main difference with existing techniques is that WAMES builds a template for each separate wave (segment) in the ECG, rather than generating a template for the ECG as a whole. The advantage of the latter approach is that it does not depend on the recognition of the separate segments and hence can be more robust. The disadvantage is that morphological variabilities in the ECG cannot be completely captured in the template. Although the inaccuracies in the template that originate from such variability are relatively small, they often lead to maternal ECG residues that are in the same order of magnitude as the fetal ECG. By *a priori* segmenting the ECG and generating templates for each separate segment, these variabilities can be more accurately modeled in the template. As a result of this accurate template, WAMES does not only outperform other template subtraction techniques in suppression of the maternal ECG, but also outperforms other maternal ECG suppression techniques such as adaptive filtering and blind source separation. Naturally, the need for ECG segmentation causes WAMES to be more susceptible to artifacts and noise. By including physiological information about the origin of the ECG in the segmentation, this susceptibility was minimized.

To further enhance the fetal ECG signals and suppress other interferences and noise, the quasi-periodicity of the fetal ECG can be exploited. Consecutive ECG complexes resemble one another to a large extent and hence averaging of several ECG complexes suppresses the noise without significantly distorting the ECG. However, to enable exploitation of the periodicity, the instantaneous fetal heart rate needs to be known. Conversely, for detecting the heart rate, the signal to noise ratio (SNR) of the signals needs to be sufficiently high. This yields a circular reasoning: to enhance the SNR the heart rate needs to be known, but to determine this heart rate the SNR needs to be sufficiently high. In Chapter 4 a method was presented that breaks this circular reasoning. It exploits *a priori* knowledge on the spatial correlation between fetal ECG signals recorded at different positions on the maternal abdomen. Based on this spatial correlation, a linear combination of the fetal ECG signals can be determined that has superior SNR with respect to the individual ECG signals. Moreover, because the method is based on physiological knowledge, it is relatively insensitive to noise levels and as such is more robust than blind source separation techniques like independent component analysis or principal component analysis.

To stress that the heart rate detected from the linear combination of ECG signals is still the correct heart rate, it needs to be mentioned that any linear combination of ECG signals still constitutes an ECG signal with the same periodicity. More specifically, each ECG signal is a one-dimensional projection of the three-dimensional elec-

trical activity of the heart. In a simplified model this three-dimensional activity can be represented by the VCG. As such, each ECG signal is the projection of the VCG onto the vector that indicates the recording position with respect to the reference position. Any linear combination of ECG signals therefore only entails the use of a different projection of the same three-dimensional electrical activity. In Chapter 5 a method was presented to detect the heart rate from the ECG signal. This method operates by transforming the signal, based on the physiology of the fetal QRS complexes, and subsequently detecting the QRS complexes in the transformed signal as local extrema exceeding a variable threshold. This method is not optimal in the sense of robustness and accuracy, but due to its computational simplicity and adequate performance, suffices for the purposes intended in this thesis.

The averaging of several ECG complexes, synchronized on their QRS complexes, entails a trade-off between signal enhancement and suppression of clinically relevant morphological variability. By averaging only few ECG complexes, the SNR will not be significantly enhanced, while averaging too many ECG complexes means that variations in the ECG are lost and their clinical relevance can no longer be assessed. In Chapter 6 a method was presented that, in essence, adaptively estimates the number of ECG complexes to be used in the averaging. In case of small morphological signal variations, this number is increased. Conversely, in case of significant signal variations this number is reduced. The presented method uses a Kalman filter with sequential adaptive noise covariance estimation. For the estimation of the measurement noise, the spatial correlation between ECG complexes recorded at several locations on the maternal abdomen was exploited. For the estimation of the process noise covariance (i.e. a measure for morphological signal variations), the evidence function of the Bayesian ECG estimation was maximized.

The performance of the developed filter was compared to the performance of a similar Kalman filter with fixed noise covariance. For this fixed Kalman filter the process noise covariance needs to be *a priori* estimated and hence, to ensure adequate performance of the filter, proper application of the filter requires rather detailed information on the ECG signal dynamics. The comparison between the fixed and adaptive Kalman filters demonstrated that the adaptive filter performs almost as well as the fixed Kalman filter in cases where the process noise covariance was chosen optimally. In other cases, the adaptive Kalman filter outperformed the fixed Kalman filter. In addition, for long term monitoring tasks in which the ECG signal characteristics change, the adaptive Kalman filter proved to be capable of quickly adapting its noise estimation to match the filter's output to the new input. The fixed Kalman filter, due to its less flexible estimation of the Kalman gain, was demonstrated to require about 10 seconds before it had adjusted its output to the new input.

As stipulated before, the VCG entails a simplified representation of the three-dimensional electrical activity of the heart. For adults, the VCG is generally recorded

using fixed electrode positions with respect to the heart, or by using a fixed transformation that converts a multitude of ECG signals into the VCG. For the fetus, neither of these approaches works. For each recording the position of the fetal heart with respect to the abdominal electrodes will be different and for each position of the heart, its distance to the electrodes on the maternal abdomen differs. As a result, the properties of the volume conductor through which the ECG signals have to propagate are different for each recording and are even expected to change during the recordings as a result of fetal movement. Hence, the use of either specific electrode positions or a fixed transformation does not work for the fetal VCG and an alternative method that can adapt to each specific recording is required. In Chapter 7 of this thesis, a method was presented that does exactly this. The method is based on a statistical model in which the volume conductor is approximated by a diagonal scaling matrix that represents an individual attenuation for each ECG signal. More specifically, each ECG signal is modeled to be a scaled projection of the VCG and additive noise. The VCG and the scaling matrix are inferred by maximizing the joint probability distribution over both variables, given the observed ECG signals. Since an analytic solution to the maximization of this probability distribution was not available, an approximation technique referred to as variational inference was used. Evaluation of the developed method showed that, as expected, the fetal VCG was determined more accurately than by using a fixed method. In addition, also for adults the developed method was demonstrated to provide a more accurate estimate of the VCG.

With the fetal VCG available, the relation between the VCG and the ECG described above was used in the second part of this thesis to calculate any desired ECG lead. In theory, the ECG signals that are frequently used in adult electrocardiography could be calculated, enabling clinicians to employ standardized guidelines for interpretation. Unfortunately, this approach is complicated by two distinct problems. Firstly, the fetal heart is not the same as the adult heart and thus similar ECG leads will provide different ECG morphologies. Secondly, due to variations in the fetal orientation the vectors onto which the VCG should be projected to obtain the desired ECG signals need to be assessed again for each individual case. In fact, upon every movement of the fetus, these vectors need to be reassessed. In Chapters 8 and 9 these two problems were discussed in more detail and, where possible, dealt with.

In Chapter 8 one of the main differences between the fetal and adult heart was discussed, namely the fact that the electrical axis of the fetal heart points in a different direction than the electrical axis of the adult heart. The reason for this difference lies in the alternative cardiovascular circulation of the fetus. In the adult circulation the blood is oxygenated in the lungs and then returns to the left side of the heart to be propelled throughout the body. Hence, the left side of the adult heart has more muscular tissue than the right side, causing the electrical axis to point towards the left ventricle. In the fetal circulation, on the other hand, the blood is oxygenated

in the placenta rather than in the lungs. The associated higher load that needs to be exerted by the right ventricle – as opposed to the left ventricle – yields a shift of the fetal electrical axis towards the right ventricle. In Chapter 8 this shift was visualized for the first time ever *in-vivo* and the consequences of this shift for the interpretation of the ECG were illustrated by projecting both the adult and fetal VCG onto standardized ECG leads.

In Chapter 9, the morphological variations in the ECG that arise as a result of variations in the fetal orientation were briefly discussed and a method to correct for these fetal movements was presented. This method operates by tracking the rotations between the VCG's of consecutive heartbeats. To this end, a statistical model was formulated that relates the VCG's of consecutive heartbeats to one another through a couple of transformations: rotation, lead-dependent scaling, and time-synchronization. The parameters associated with these transformations were assessed by maximizing the likelihood function of the statistical model, using the expectation-maximization (EM) algorithm. The presented method was evaluated by comparing its performance in aligning VCG's to that of the state-of-the-art method (i.e. a method in which the scaling is lead-independent); it was demonstrated that the presented method outperforms the state of the art under almost all circumstances, and especially at poor SNRs.

By correcting the VCG for the assessed rotations, the fetal VCG can be kept within the same frame of reference with respect to the abdominal electrodes during a recording. In addition, it was demonstrated that the presented method can also be used to determine the rotation between the fetal VCG and the maternal VCG. Combining this rotation with the orientation of the fetal heart axis (from Chapter 8), it is possible to estimate the absolute fetal orientation within the uterus. With this orientation determined, all information required to project the VCG onto standardized ECG leads has become available. Finally, besides facilitating correct interpretation of the fetal VCG, the tracking of fetal movement can have a direct value in clinical practice. Reduced fetal motility is associated with deterioration in the fetal condition. Although the VCG does not provide information on the movement of e.g. fetal limbs, the automated and objective means of monitoring fetal movement that has been made possible by the developed method could strongly aid clinicians in their diagnosis of the fetal condition.

To recapitulate, in this thesis technology has been developed that can be used to determine a fetal VCG of relatively high SNR from the maternal abdomen, correct this VCG for fetal movement, and interpret it within a clinically familiar frame of reference. To illustrate the potential value of this technology in clinical practice, in Chapters 10 and 11 two applications of the technology were presented; the standardized 12-lead ECG representation of both normal fetal heartbeats and fetal supraventricular extrasystoles (Chapter 10) and the derivation of a virtual invasively recorded

ECG signal for performing fetal ST analysis (Chapter 11). In the latter application, it was also shown that the currently employed invasive scalp electrode is, in terms of the electrode position, not that far from optimal for fetuses that present themselves in vertex position (i.e. the most common position during labor).

12.2 Future directions

Today, in general clinical practice, the fetal ECG is only monitored using an invasive electrode. Moreover, the only purpose of the recorded fetal ECG is to extract the fetal heart rate and to perform ST analysis. For long, clinicians and researchers have attempted to monitor the fetal ECG and its associated parameters in a non-invasive way, but in spite of the success achieved by some, none of these attempts has as yet led to an application that is used in clinical practice. Although it is unlikely that the methods presented in this thesis will quickly converge to such an application, they do (hopefully) provide a step in this direction and illustrate the potential of non-invasive ECG recordings. Not only is it possible to monitor the fetal ECG in earlier stages of pregnancy than just labor, but also do the non-invasive fetal ECG recordings facilitate the determination and clinical diagnosis of other parameters and signals than the heart rate and ST segment alone. Examples of these parameters and signals are fetal movement and the 12-lead ECG.

To increase the chances of the developed methods to lead to an actual non-invasive fetal ECG monitoring application, several improvements need to made. For each method the most critical points for improvement are listed and briefly discussed.

The maternal ECG suppression method that was presented in Chapter 3 suffers from the main drawback that it is computationally too complex. Although the method is capable of suppressing the maternal ECG online in about 4 channels using a standard PC, for employment in clinical practice the method should not only be able to suppress the maternal ECG from more than 4 channels, but also should the computational complexity be reduced so much that sufficient processor time is left for performing other required analyses.

Two of these required analyses were exemplified in Chapters 4 and 5. From the results presented in Chapter 4 it can, however, be concluded that – although the presented methods for finding fetal ECG source signals and detect the fetal heart rate perform more robustly than existing source separation techniques – their performance is not so good that a fetal heart rate can be determined for all patients and in all situations. The most critical improvement that is expected to be achievable here is in the detection of the fetal QRS complexes. The presented QRS detection method suffices for ECG signals in which the SNR is already relatively high. For low-SNR signals, on the other hand, the sensitivity and specificity of the method are expected to decrease significantly. By employing a method that is e.g. based on the com-

bination of wavelet analysis and a hidden Markov model more robustness to noise is anticipated. More specifically, by approximating the signals by wavelets and restricting the (quasi-)periodicity of these wavelets by means of a statistical model that describes the allowed and expected variations in the RR intervals, the effect of noise in the resulting fetal heart rate should be significantly reduced.

One of the critical improvements to be made in both the fetal ECG enhancement method presented in Chapter 6 and the fetal VCG estimation method presented in Chapter 7 is to loosen the rather restrictive assumptions of white Gaussian noise and Gaussian distributed model parameters. For one, due to preprocessing of the ECG signals by frequency-selective filtering and maternal ECG suppression (both presented in Chapter 3), the noise is (no longer) white. Similarly, in Chapter 7 it was discussed that the variational inference, in which the model parameters were assumed to be independent and Gaussian distributed, yields a relatively large inaccuracy in the estimated fetal VCG. Improvement of the methods by assuming colored noise or different distributions will however go at the expensive of the computational complexity and should, therefore, be a trade-off between this computational complexity and the increase in accuracy of the methods. Another key improvement that can be made to the VCG estimation in Chapter 7 is to omit the assumption of a fixed origin for the electrical field vector that describes the VCG. However, by admitting additional parameters in the model that describes the relation between the VCG and the recorded ECG signals (Eq. (7.3)), more ECG signals are required to infer these parameters [171–173], not only reducing patient comfort but also increasing the computational complexity.

The method for monitoring the fetal orientation that was presented in Chapter 9, is relatively robust to noise and has a limited computational complexity. However, the estimation of the fetal orientation with respect to the maternal abdomen can suffer from quite some inaccuracies. One of the main inaccuracies is the *a priori* assumed shift of 90° between the electrical axis of the fetal VCG and that of the maternal VCG. In practice, this shift is not expected to be exactly 90° and, moreover, is expected to differ between patients. Unfortunately, due also to the relatively large inaccuracy in the fetal orientation that is assessed from ultrasound images, the accuracy in the estimation of this shift in Chapter 8 is not expected to be easily improvable. Nevertheless, a large patient study (at least another 50 patients, but preferably more) should be performed to obtain some insights on both the amplitude of the shift and in the accuracy of the determined fetal orientation.

Such a large patient study could also aid in the assessment of the clinical relevance of the applications presented in Chapters 10 and 11. Not only is a large patient population more likely to yield fetuses with congenital heart diseases (CHD) like tetralogy of Fallot, single-ventricle, or bundle branch blocks, but also is this population more likely to yield fetuses that suffer from hypoxia during delivery. The former

group of fetuses can be used to assess whether the 12-lead ECG facilitates detection of these CHD. The latter group can be used to assess whether the non-invasive fetal ECG can be used for ST analysis that is as accurate as the ST analysis performed on the invasively recorded fetal ECG.

More in general, one of the ultimate goals of further technology development or improvement should be to boost the reliability of signal measurement and analysis, as well as communication availability, to such a standard that at-home monitoring of patients at risk can become routine procedure. This could not only spare the huge costs involved with hospitalizations and monitoring of pregnant women, but also could improve quality of life for these women and reduce the morbidity. To ensure broad application of this technology, the technology should be capable of providing the required information on the fetal condition at all times and for all patients. A factor that will play a large role in this technology development is the influence of the vernix caseosa on the signal quality. To obtain a thorough understanding of this factor and, in addition, to evaluate which aspects of the signal acquisition and analysis play a critical role in the further improvement of signal quality and interpretation, a large patient study would again be advisable. Another factor that will be of relevance in at-home monitoring is the comfort and positioning of the electrodes. Not only should the electrodes not restrict the mother in daily activities (too much) but also should the positions of the electrodes be monitored somehow to ensure that the spatial information in the ECG can be fully exploited (Chapters 4 and 7).

Finally, as mentioned throughout this thesis, some of the developed technologies also have the potential to contribute to other fields of healthcare as well. Examples are the enhancement of dynamic ECG signals (Chapter 6), the patient-tailored technique for estimating the (adult) VCG (Chapter 7), and the improved accuracy in vectorcardiographic loop alignment (Chapter 9). More study within the appropriate specialization fields of healthcare is, however, required to conclusively state something about this.

Bibliography

[1] A.K. Sundström, D. Rosén, and K.G. Rosén, "Fetal surveillance," Tech. Rep., Neoventa Medical AB, 2002.

[2] K.R. Greene, G.S. Dawes, H. Lilja, and K.G. Rosén, "Changes in the ST waveform of the fetal lamb electrocardiogram with hypoxemia," *Am J Obstet Gynecol.*, vol. 144, pp. 950–958, Dec. 1982.

[3] H.E. Cohn, E.J. Sacks, M.A. Heymann, and A.M. Rudolph, "Cardiovascular responses to hypoxemia and acidemia in fetal lambs," *Am J Obstet Gynecol*, vol. 120, pp. 817–24, 1974.

[4] L.L.H. Peeters, R.E. Sheldon, M.D. Jones Jr, E.L. Makowski, and G. Meschia, "Blood flow to fetal organs as a function of arterial oxygen content," *Am J Obstet Gynecol*, vol. 135, pp. 637–46, 1979.

[5] H. Asano, J. Homan, L. Carmichael, S. Korkola, and B. Richardson, "Cerebral metabolism during sustained hypoxemia in preterm fetal sheep," *Am J Obstet Gynecol*, vol. 170, no. 3, pp. 939–44, Mar 1994.

[6] B.S. Richardson, L. Carmichael, J. Homan, L. Johnston, and R. Gagnon, "Fetal cerebral, circulatory, and metabolic responses during heart rate decelerations with umbilical cord compression," *Am J Obstet Gynecol*, vol. 175, no. 4 Pt 1, pp. 929–36, Oct 1996.

[7] J. Itskovitz, E.F. LaGamma, and A.M. Rudolph, "Heart rate and blood pressure responses to umbilical cord compression in fetal lambs with special reference to the mechanism of variable deceleration," *Am J Obstet Gynecol*, vol. 147, no. 4, pp. 451–7, 1983.

[8] H. Lilja, K. Karlsson, I. Kjellmer, K. Lindecrantz, T. Olsson, and K.G. Rosén, "Heart rate variability and electrocardiogram changes in the fetal lamb during hypoxia and beta-adrenoceptor stimulation," *J Perinat Med*, vol. 12, no. 3, pp. 115–25, 1984.

[9] A.C. Guyton and J.E. Hall, *Textbook of Medical Physiology*, W.B. Saunders company, Philadelphia, USA, tenth edition, 2000.

[10] R. Eckert and D.J. Randall, *Animal physiology*, WH Freeman and Company, New York, 1983.

[11] W. de Jong, *Blood pressure variability in neonates*, Phd thesis, Technische Universiteit Eindhoven, Eindhoven, the Netherlands, 2000.

[12] I. Amer-Wåhlin, *Fetal ECG waveform analysis for intrapartum monitoring*, Phd thesis, Lund University, Lund, Sweden, 2003.

[13] E.H. Hon, "Instrumentation of fetal heart rate and fetal electrocardiography. II. a vaginal electrode," *Am J Obstet Gynecol*, vol. 86, pp. 772–84, 1963.

[14] W.L. Johnson, H.F. Stegall, J.N. Lein, and R.F. Rushmer, "Detection of fetal life in early pregnancy with an ultrasonic doppler flowmeter," *Obstet Gynecol*, vol. 26, pp. 305–7, Sep 1965.

[15] G.W. Lawson, R. Belcher, G.S Dawes, and C.W. Redman, "A comparison of ultrasound (with autocorrelation) and direct electrocardiogram fetal heart rate detector systems," *Am J Obstet Gynecol*, vol. 147, no. 6, pp. 721–722, Nov 1983.

[16] C. Kittel, W.D. Knight, and M.A. Ruderman, *Mechanics (Berkeley Physics Course)*, McGraw-Hill, USA, 1965.

[17] M. Peters, J. Crowe, J.F. Piéri, H. Quartero, B. H. Gill, D. James, J. Stinstra, and S. Shakespeare, "Monitoring the fetal heart non-invasively: a review of methods," *J. Perinat. Med.*, vol. 29, pp. 408–416, 2001.

[18] R.K. Freeman, T.J. Garite, and M.P. Nageotte, *Fetal heart rate monitoring*, Lippincott Williams & Wilkins, Philadelphia, PA, USA, 2003.

[19] FIGO subcommittee on Standards in Perinatal Medicine, "Guidelines for the use of fetal monitoring," *Int J Gynecol Obstet*, vol. 25, no. 3, pp. 159–67, 1987.

[20] Z. Alfirevic, D. Devane, and G.M.L. Gyte, "Continuous cardiotocography (CTG) as a form of electronic fetal monitoring (EFM) for fetal assessment during labor," *Cochrane Database of Systematic Reviews*, vol. Issue 3, pp. CD006066, Jul 2006.

[21] K.D. Nelson, J.M. Dambrosia, T.Y. Ting, and J.K. Grether, "Uncertain value of electronix fetal monitoring in predicting cerebral palsy," *New Eng J Med*, vol. 334, no. 10, pp. 613–8, Mar 1996.

[22] P. van den Berg, S. Schmidt, J. Gesche, and E. Saling, "Fetal distress and the condition of the newborn using cardiotocography and fetal blood analysis during labour," *Br J Obstet Gynaecol*, vol. 94, no. 1, pp. 72–5, Jan 1987.

[23] CH Peters, ED ten Broeke, P Andriessen, B Vermeulen, RC Berendsen, PF Wijn, and SG Oei, "Beat-to-beat detection of fetal heart rate: Doppler ultrasound cardiotocography compared to direct ECG cardiotocography in time and frequency domain," *Physiol Meas*, vol. 25, no. 2, pp. 585–593, Apr 2004.

[24] R.E. Myers, "Two patterns of perinatal brain damage and their conditions of occurrence," *Am J Obstet Gynecol*, vol. 116, no. 2, pp. 246–76, Jan 1972.

[25] K.G. Rosén and I. Kjellmer, "Changes in fetal heart rate and ECG during hypoxia," *Acta Physiol Scand*, vol. 93, pp. 59–66, 1975.

[26] K.G. Rosén, K.H. Hökegård, and I. Kjellmer, "A study of the relationship between the electrocardiogram and hemodynamics in the fetal lamb during asphyxia," *Acta Physiol Scand*, vol. 98, no. 3, pp. 275–84, Nov 1976.

[27] K.H. Hökegård, B.O. Eriksson, I. Kjellmer, R. Magno, and K.G. Rosén, "Myocardial metabolism in relation to electrocardiographic changes and cardiac function during graded hypoxia in the fetal lamb," *Acta Physiol Scand*, vol. 113, no. 1, pp. 1–7, Sep 1981.

[28] I. Amer-Wåhlin, C. Hellsten, H. Norén, H. Hagberg, A. Herbst, I. Kjellmer, H. Lilja, C. Lindoff, M. Månsson, L. Mårtensson, P. Olofsson, A. Sundström, and K. Marsál, "Cardiotocography only versus cardiotocography plus ST analysis of fetal electrocardiogram for intrapartum fetal monitoring: a swedish randomised controlled trial," *Lancet*, vol. 18, pp. 534–538, Aug 2001.

[29] The University of Nottingham, J.A. Crowe, D. James, B.R. Hayes-Gill, C.W. Barratt, and J.-F. Pieri, "Fetal surveillance," International patent WO/2005/039410, 2004-10-13.

[30] D. Gabor and C.V. Nelsen, "Determination of the resultant dipole of the heart from measurements on the body surface," *J Appl Phys*, vol. 25, no. 4, pp. 413–416, Apr 1954.

[31] J. Malmivuo and R. Plonsey, *Bioelectromagnetism - Principles and Applications of Bioelectric and Biomagnetic Fields*, Oxford University Press, New York, 1995.

[32] H.C. Burger and J.B. Van Milaan, "Heart-vector and leads," *Br Heart J.*, vol. 8, no. 3, pp. 157–161, July 1946.

[33] D.B. Geselowitz, "Dipole theory in electrocardiography," *Am. J. Cardiol.*, vol. 14, no. 9, pp. 301–306, 1964.

[34] D.B. Geselowitz, "On the theory of the electrocardiogram," *Proc of IEEE*, vol. 77, no. 6, pp. 857–876, 1989.

[35] E. Frank, "General theory of heart-vector projection," *Circ Res*, vol. 2, pp. 258–70, 1954.

[36] T.F. Oostendorp, A. van Oosterom, and H.W. Jongsma, "The effect of changes in the conductive medium on the fetal ECG throughout gestation," *Clin Phys Physiol Meas*, vol. 10, no. Suppl B, pp. 11–20, 1989.

[37] T.F. Oostendorp and A. van Oosterom, "Electrical properties of tissues involved in the conduction of foetal ECG," *Med Biol Eng Comput*, vol. 27, pp. 322–4, 1989.

[38] J.G. Stinstra and M.J. Peters, "The volume conductor may act as a temporal filter on the ECG and EEG," *Med Biol Eng Comput*, vol. 36, pp. 711–6, 1998.

[39] J.T. Oldenburg and M. Macklin, "Changes in the conduction of the fetal electrocardiogram to the maternal abdominal surface during gestation," *Am J Obstet Gynecol*, vol. 129, no. 4, pp. 425–433, Oct 1977.

[40] G. Tulzer, W. Arzt, R.C. Franklin, P.V. Loughna, R. Mair, and H.M. Gardiner, "Pulmonary valvuloplasty for critical pulmonary stenosis or atresia with intact septum," *Lancet*, vol. 360, pp. 1567–8, 2002.

[41] H.M. Gardiner, "In-utero intervention for severe congenital heart disease," *Best Pract Res Clin Obstet Gynaecol*, vol. 22, no. 1, pp. 49–, Feb 2008.

[42] B. Luke and M.B. Brown, "The changing risk of infant mortality by gestation, plurality, and race: 1989–1991 versus 1999–2001," *Pediatrics*, vol. 118, no. 6, pp. 2488–97, 2006.

[43] J.E. Tyson, N.A. Parikh, J. Langer, C. Green, and R.D. Higgins, "Intensive care for extreme prematurity - moving beyond gestational age," *New Engl J Med*, vol. 358, no. 16, pp. 1672–81, Apr 2008.

[44] R.L. Goldenberg, J.F. Culhane, J.D. Jams, and R. Romero, "Epidemiology and causes of preterm birth," *Lancet*, vol. 371, pp. 75–84, 2008.

[45] Y.W. Wu, G.J. Escobar, J.K. Grether, L.A. Croen, J.D. Greene, and T.B. Newman, "Chorioamnionitis and cerebral palsy in term and near-term infants," *JAMA*, vol. 290, no. 20, pp. 2677–84, Nov 2003.

[46] R. Vullings, C.H.L. Peters, R.J. Sluijter, M. Mischi, S.G. Oei, and J.W.M. Bergmans, "Dynamic segmentation and linear prediction for maternal ECG removal in antenatal abdominal recordings," *Physiol Meas*, vol. 30, pp. 291–307, 2009.

[47] G.E. Dower, H.B. Machada, and J.A. Osborne, "On deriving the electrocardiogram from vectorcardiographic leads," *Clin Cardiol*, vol. 3, pp. 87–95, 1980.

[48] L. Edenbrandt and O. Pahlm, "Vectorcardiogram synthesized from a 12-lead ECG: superiority of the inverse Dower matrix," *J Electrocardiol*, vol. 21, no. 4, pp. 361–367, 1988.

[49] F.N. Wilson, F.D. Johnston, F.F. Rosenbaum, H. Erlanger, C.E. Kossmann, H. Hecht, N. Cotrim, R. Menezes de Olivieira, R. Scarsi, and P.S. Barker, "The precordial electrocardiogram," *Am Heart J*, vol. 27, pp. 19–85, 1944.

[50] K.G. Rosén, A. Dagbjartsson, B.A. Henriksson, H. Lagercrantz, and I. Kjellmer, "The relationship between circulating catecholamines and ST waveform in the fetal lamb electrocardiogram during hypoxia," *Am J Obstet Gynecol*, vol. 149, no. 2, pp. 190–5, May 1984.

[51] M.E.M.H. Westerhuis, A. Kwee, A.A. van Ginkel, A.P. Drogtrop, W.J.A. Gyselaers, and G.H.A. Visser, "Limitations of ST analysis in clinical practice: three cases of intrapartum metabolic acidosis," *BJOG*, vol. 114, pp. 1194–201, 2007.

[52] M.E. Westerhuis, Visser G.H., K.G. Moons, E. van Beek, M.J. Benders, S.M. Bijvoet, H.J. van Dessel, A.P. Drogtrop, H.P. van Geijn, G.C. Graziosi, F. Groenendaal, J.M. van Lith, J.G. Nijhuis, S.G. Oei, H.P. Oosterbaan, M.M. Porath, R.J. Rijnders, N.W. Schuitemaker, L.M. Sopacua, I. van der Tweel, L.D. Wijnberger, C. Willekes, N.P. Zuithoff, B.W. Mol, and A. Kwee, "Cardiotocography plus ST analysis of fetal electrocardiogram compared with cardiotocography only for intrapartum monitoring: a randomized controlled trial," *Obstet Gynecol*, vol. 115, no. 6, pp. 1173–80, Jun 2010.

[53] P.A. Payne, A.N. Gordon, and T.R. Johnson Jr., "Fetal death without preceding fetal movement," *New Engl J Med*, vol. 303, pp. 1419–1420, Dec 1980.

[54] J.V. Tveit, E. Saastad, B. Stray-Pedersen, P.E. Børdahl, V. Flenady, R. Fretts, and J.F. Frøen, "Reduction of late stillbirth with the introduction of fetal movement information and guidelines - a clinical quality improvement," *BMC Pregnancy Childbirth*, vol. 9, no. 32, Jul 2009.

[55] J. Stinstra, E. Golbach, P. van Leeuwen, S. Lange, T. Menendez, W. Moshage, E. Schleussner, C. Kaehler, H. Horigome, S. Shigemitsu, and M.J. Peters, "Multicentre study of fetal cardiac time intervals using magnetocardiography," *BJOG*, vol. 109, pp. 1235–1243, Nov. 2002.

[56] J.G. Nijhuis, *Behavioural states in the human fetus*, Phd thesis, K.U. Nijmegen, Nijmegen, the Netherlands, 1984.

[57] G. Mielke and N. Benda, "Cardiac output and central distribution of blood flow in the human fetus," *Circulation*, vol. 103, no. 12, pp. 1662–8, 2001.

[58] J.A. Bernhards and L.N. Bouman, *Fysiologie van de mens*, Bohn Stafleu Van Loghum, 6th edition, 1994.

[59] N.P. DePasquale and G.E. Burch, "The electrocardiogram, ventricular gradient and spatial vectorcardiogram during the first week of life," *Am J Cardiol*, vol. 12, pp. 482–93, Oct 1963.

[60] M. Artman, L. Mahony, and D.F. Teitel, *Neonatal cardiology*, McGraw-Hill companies, USA, 2002.

[61] S. Yagel, N.H. Silverman, and U. Gembruch, *Fetal cardiology : embryology, genetics, physiology, echocardiographic evaluation, diagnosis and perinatal management of cardiac diseases*, Informa Healthcare Inc, New York, USA, 2nd edition, 2009.

[62] W. Einthoven, "Weiteres über das elektrokardiogram," *Pflüger Arch ges Physiol*, vol. 122, pp. 517–48, 1908.

[63] T. Oostendorp, *Modelling the foetal ECG*, Phd thesis, K.U.Nijmegen, The Netherlands, 1989.

[64] E. Frank, "An accurate, clinically practical system for spatial vectorcardiography," *Circulation*, vol. 13, pp. 737–749, 1956.

[65] G.S. Dawes, J.C. Mott, and H.J. Shelley, "The importance of cardiac glycogen for the maintainance of life in foetal lambds and newborn animals during anoxia," *J Physiol*, vol. 146, no. 3, pp. 516–38, Jun 1959.

[66] K.G. Rosén, I. Amer-Wåhlin, R. Luzietti, and H. Norén, "Fetal ECG waveform analysis," *Best Pract Res Clin Obstet Gynaecol*, vol. 18, no. 3, pp. 485–514, 2004.

[67] K.H. Hökegård, K. Karlsson, I. Kjellmer, and K.G. Rosén, "ECG changes in the fetal lamb during asphyxia in relation to β-adrenoreceptor stimulation and blockade," *Acta Physiol Scand*, vol. 105, no. 2, pp. 195–203, 1979.

[68] J.A. Westgate, L. Bennet, C. Brabyn, C.E. Williams, and A.J. Gunn, "ST waveform changes during repeated umbilical cord occlusions in near-term fetal sheep," *Am J Obstet Gynecol*, vol. 184, no. 4, pp. 743–51, Mar 2001.

[69] N.J. Outram, *Intelligent Pattern Analysis of the Foetal Electrocardiogram*, Phd thesis, University of Plymouth, 1997.

[70] J.I.P. de Vries, G.H.A. Visser, and H.F.R. Prechtl, "The emergence of fetal behaviour. i. qualitative aspects," *Early Hum Dev*, vol. 7, no. 4, pp. 301–22, Dec 1982.

[71] J.I.P. de Vries, G.H.A. Visser, and H.F.R. Prechtl, "The emergence of fetal behaviour. ii. quantitative aspects," *Early Hum Dev*, vol. 12, no. 2, pp. 99–120, Nov 1985.

[72] A.E. Heazell and J.F. Frøen, "Methods of fetal movement counting and the detection of fetal compromise," *J Obstet Gynaecol*, vol. 28, no. 2, pp. 147–54, Feb 2008.

[73] D.C. Stevens, R.L. Schreiner, R.A. Hurwitz, and E.L. Gresham, "Fetal and neonatal ventricular arrhythmia," *Pediatrics*, vol. 63, no. 5, pp. 771–7, 1979.

[74] M. Respondek, A. Wloch, P. Kaczmarek, D. Borowski, J. Wilczynski, and E. Helwich, "Diagnostic and perinatal management of fetal extrasystole," *Pediatr Cardiol*, vol. 18, no. 5, pp. 361–6, 1997.

[75] P. van Leeuwen, B. Hailer, W. Bader, J. Geissler, E. Trowitzsch, and D.H. Grönemeyer, "Magnetocardiography in the diagnosis of fetal arrhythmia," *BJOG*, vol. 106, no. 11, pp. 1200–8, Nov 1997.

[76] S. Comani, M. Liberati, D. Mantini, E. Gabriele, D. Brisinda, S. Di Luzio, R. Fenici, and G.L. Romani, "Characterization of fetal arrhythmias by means of fetal magnetocardiography in three cases of difficult ultrasonographic imaging," *Pacing Clin Electrophysiol*, vol. 27, no. 12, pp. 1647–55, Dec 2004.

[77] Y. Maeno, A. Hirose, T. Kanbe, and D. Hori, "Fetal arrhythmia: prenatal diagnosis and perinatal management," *J Obstet Gynaecol Res*, vol. 35, no. 4, pp. 623–9, 2009.

[78] D.C. Crawford, S.K. Chita, and L.D. Allan, "Prenatal detection of congenital heart disease: factors affecting obstetric management and survival," *Am J Obstet Gynecol*, vol. 159, no. 2, pp. 352–6, 1988.

[79] H. P. van Geijn and F. J. A. Copray, *A critical appraisal of fetal surveillance*, Excerpta Medica, Amsterdam, New York, 1994.

[80] E.M. Symonds, D. Sahota, and A. Chang, *Fetal electrocardiography*, Imperial College Press, Londen, UK, 2001.

[81] C.N. Smyth, "Experimental electrocardiography of the foetus," *Lancet*, vol. 1, no. 6771, pp. 1124–6, Jun 1953.

[82] C. Sureau, "Fetal electrocardiographic research during pregnancy and labor; first results of a new technic of registration by intrauterine electrodes," *Gynecol Obstet (Paris)*, vol. 55, no. 1, pp. 21–33, Jan–Mar 1956.

[83] S. Kaplan and S. Toyama, "Fetal electrocardiography; utilizing abdominal and intrauterine leads," *Obstet Gynecol*, vol. 11, no. 4, pp. 391–7, Apr 1958.

[84] S.D. Larks and G.G. Larks, "Components of the fetal electrocardiogram and intrauterine electrical axis: quantitative data," *Biol Neonat*, vol. 10, no. 3, pp. 140–52, 1966.

[85] S.D. Larks and G.G. Larks, "Comparative aspects of the fetal and newborn electrocardiograms. evidence for the validity of the method for calculation of the electrical axis of the fetal heart," *Am J Obstet Gynecol*, vol. 96, no. 4, pp. 553–5, Oct 1966.

[86] S.D. Larks and G.G. Larks, "The electrical axis of the fetal heart: a new criterion for fetal well-being or distress," *Am J Obstet Gynecol*, vol. 93, no. 7, pp. 975–83, Dec 1966.

[87] A. Kwee, C.W. van der Hoorn-van den Beld, J. Veerman, Dekkers A.H., and G.H. Visser, "STAN S21 fetal heart monitor for fetal surveillance during labor: an observational study in 637 patients," *J Matern Fetal Neonatal Med*, vol. 15, no. 6, pp. 400–7, Jun 2004.

[88] K. Ojala, M. Vääräsmäki, K. Mäkikallio, M. Valkama, and A. Tekay, "A comparison of intrapartum automated fetal electrocardiography and conventional cardiotocography–a randomised controlled study," *BJOG*, vol. 113, no. 4, pp. 419–23, Apr 2006.

[89] J.H. Van Bemmel, "Detection of weak foetal electrocardiograms by autocorrelation and crosscorrelation of envelopes," in *IEEE Transactions on Biomedical Engineering*, Jan. 1968, vol. 15, pp. 17–23.

[90] B. Widrow, J. R. Glover, J.M. McCool, J. Kaunitz, C. S. Williams, R. H. Hearn, J. R. Zeidler, E. Dong, and R. Goodlin, "Adaptive noise cancelling: principles and applications," *Proc. IEEE*, vol. 62, pp. 1692–1716, Dec. 1975.

[91] P. Bergveld and W. J. H. Meijer, "New technique for the suppression of the MECG," *IEEE Trans. Biomed. Eng.*, vol. 28, no. 4, pp. 248–353, 1981.

[92] S. Cerutti, G. Baselli, S. Civardi, E. Ferrazzi, A. M. Marconi, M. Pagani, and G. Pardi, "Variability analysis of fetal heart rate signals as obtained from abdominal electrocardiographic recordings," *J. Perinat. Med.*, vol. 14, no. 6, pp. 445–452, 1986.

[93] P.P. Kanjilal, S. Palit, and G. Saha, "Fetal ECG extraction from single-channel maternal ECG using singular value decomposition," *IEEE Trans Biomed Eng*, vol. 44, no. 1, pp. 51–9, Jan 1997.

[94] L. De Lathauwer, B. De Moor, and J. Vanderwalle, "Fetal electrocardiogram extraction by blind source subspace separation," *IEEE Trans Biomed Eng.*, vol. 47, no. 5, pp. 567–572, May. 2000.

[95] V. Zarzoso and A.K. Nandi, "Noninvasive fetal electrocardiogram extraction: blind separation versus adaptive noise cancellation," *IEEE Trans Biomed Eng.*, vol. 48, no. 1, pp. 12–18, Jan. 2001.

[96] M. Ungureanu and W.M. Wolf, "Basic aspects concerning the event-synchronous interference canceller," *IEEE Trans Biomed Eng.*, vol. 53, no. 11, pp. 2240–2247, Nov. 2006.

[97] C. Marque, J. Duchêne, S. Leclercq, G. Panczer, and J. Chaumont, "Uterine ehg processing for obstetrical monitoring," *IEEE Trans. Biomed. Eng.*, vol. BME-33, no. 12, pp. 1182–1187, Dec. 1986.

[98] C. Rabotti, *Characterization of uterine activity by electrohysterography*, Phd thesis, Technische Universiteit Eindhoven, Eindhoven, the Netherlands, 2010.

[99] S. Abboud and D. Sadeh, "Spectral analysis of the fetal electrocardiogram.," *Comput Biol Med.*, vol. 19, no. 6, pp. 409–415, 1989.

[100] C. Rabotti, M. Mischi, J.O.E.H. Van Laar, S.G. Oei, and J.W.M. Bergmans, "Estimation of internal uterine pressure by joint amplitude and frequency analysis of electrohysterographic signals," *Physiol. Meas.*, vol. 29, pp. 829–841, 2008.

[101] C. Buhimschi, M.B. Boyle, and R.E. Garfield, "Electrical activity of the human uterus during pregnancy as recorded from the abdominal surface.," *Obstet. & Gynecol.*, vol. 90, no. 1, pp. 102–111, Jul 1997.

[102] S.M. Martens, M. Mischi, S.G. Oei, and J.W.M. Bergmans, "An improved adaptive powerline interference canceller for electrocardiography," *IEEE Trans Biomed Eng.*, vol. 53, pp. 2220–2231, Nov. 2006.

[103] T.F. Oostendorp, A. van Oosterom, and H.W. Jongsma, "The fetal ECG throughout the second half of gestation," *Clin Phys Physiol Meas*, vol. 10, no. 2, pp. 147–60, 1989.

[104] J.G. Stinstra, *Reliability of the fetal magnetocardiogram*, Phd thesis, Universiteit Twente, Enschede, the Netherlands, 2001.

[105] A.R. Kahn, "Transmission characteristics in fetal electrocardiography," in *Proc. Sixteenth Ann. Conf on Engineering, Medicine and Biology*, Baltimore, USA, 1963, p. 134.

[106] J.B. Roche and E.H. Hon, "The fetal electrocardiogram v. comparison of lead systems," *Am J Obstet Gynecol*, vol. 92, pp. 1149–59, 1965.

[107] R.A. Brace, "Physiology of amniotic fluid regulation," *Clin Obstet Gynecol*, vol. 40, no. 2, pp. 180–9, Jun 1997.

[108] O.Z. Stern, "Sur Theorie der Elektrolytischen Doppelschit," *Electrochem*, vol. 30, pp. 508, 1924.

[109] K.H. Nicolaides, G. Azar, D. Byrne, C. Mansur, and K. Marks, "Fetal nuchal translucency: ultrasound screening for chromosomal defects in first trimester of pregnancy," *BMJ*, vol. 304, no. 6831, pp. 867–9, Apr 1992.

[110] R.E. Garfield, H. Maul, L. Shi, W. Maner, C. Fittkow, G. Olsen, and G.R. Saade, "Methods and devices for the management of term and preterm labor," *Ann N Y Acad Sci*, vol. 943, pp. 203–24, Sep 2001.

[111] M.J. Taylor, M.J. Smith, M. Thomas, A. R. Green, F. Cheng, S. Oseku-Afful, L. Y. Wee, N. M. Fisk, and H. M. Gardiner, "Non-invasive fetal electrocardiography in singleton and multiple pregnancies.," *BJOG*, vol. 110, no. 7, pp. 668–678, 2003.

[112] G.S. Dawes, G.H. Visser, J.D. Goodman, and C.W. Redman, "Numerical analysis of the human fetal heart rate: the quality of ultrasound records," *Am J Obstet Gynecol*, vol. 141, no. 1, pp. 43–52, Sep 1981.

[113] S.B. Thacker, D. Stroup, and M. Chang, "Continuous electronic heart rate monitoring for fetal assessment during labor," *Cochrane Database Syst Rev*, vol. 3, pp. CD000063, 2001.

[114] J.O.E.H. Van Laar, M.M. Porath, C.H.L. Peters, and S.G. Oei, "Spectral analysis of fetal heart rate variability for fetal surveillance: a review of the literature," *Acta Obstet Gynecol Scand*, vol. 87, no. 3, pp. 300–306, 2008.

[115] S.M. Siira, T.H. Ojala, T.J. Vahlberg, J.O. Jalonen, I.A. Välimäki, K.G. Rosén, and E.M. Ekholm, "Marked fetal acidosis and specific changes in power spectrum analysis of fetal heart rate variability recorded during the last hour of labour," *BJOG*, vol. 112, no. 4, pp. 418–423, Apr 2005.

[116] J. H. Van Bemmel and H. van der Weide, "Detection procedure to represent the foetal heart rate and electrocardiogram," *IEEE Trans Biomed Eng*, vol. 13, no. 4, pp. 175–82, 1966.

[117] P. Strobach, K. Abraham-Fuchs, and W. Härer, "Event-synchronous cancellation of the heart interference in biomedical signals," *IEEE Trans Biomed Eng.*, vol. 41, no. 4, pp. 343–350, Apr. 1994.

[118] M. Ungureanu, J.W.M. Bergmans, S.G. Oei, and R. Strungaru, "Fetal ECG extraction using an adaptive maternal beat subtraction technique," *Biomed Tech*, vol. 52, pp. 56–60, 2007.

[119] S.M.M. Martens, C. Rabotti, M. Mischi, and R.J. Sluijter, "A robust fetal ECG detection method for abdominal recordings," *Physiol. Meas.*, vol. 28, pp. 373–388, 2007.

[120] S. Comani, D. Mantini, A. Lagatta, F. Esposito, S. Di Luzio, and G. L. Romani, "Time course reconstruction of fetal cardiac signals from fmcg: independent component analysis versus adaptive maternal beat subtraction," *Physiological Measurement*, vol. 25, pp. 1305–1321, 2004.

[121] Plonsey, *Bioelectric Phenomena*, McGraw-Hill, New York, 1969.

[122] S.M.M. Martens, R.J. Sluijter, S.G. Oei, and J.W.M. Bergmans, "Improving QRS detection in multi-channel electrocardiography by principal component analysis," in *IFMBE Proc.*, Prague, Czech Republic, Nov. 2005.

[123] R. Vullings, C. Peters, M. Mischi, R. Sluijer, G. Oei, and J. Bergmans, "Artifact reduction in maternal abdominal ECG recordings for fetal ECG estimation," in *Proc. of IEEE EMBC*, Lyon, France, Aug. 2007, pp. 43–46.

[124] H. Künzi and W. Krelle, *Nichtlineare Programmierung*, Springer, Berlin, 1962.

[125] P. Comon, "Independent component analysis, a new concept?," *Signal Processing*, vol. 36, pp. 287–314, 1994.

[126] S. Abboud and D. Sadeh, "Power spectrum analysis of fetal heart rate variability using the abdominal maternal electrocardiogram.," *J. Biomed. Eng.*, vol. 12, no. 2, pp. 161–164, Mar. 1990.

[127] J.-F. Cardoso and A. Souloumiac, "Blind beamforming for nongaussian signals," *IEE Proc.-F*, vol. 140, no. 6, pp. 362–370, Dec. 1993.

[128] C. Peters, R. Vullings, J. Bergmans, G. Oei, and P. Wijn, "Heart rate detection in low amplitude non-invasive fetal ECG recordings," in *Proc. of IEEE EMBS*, New York, USA, 2006, pp. 6092–4.

[129] M. Kotas, J. Jezewski, T. Kupka, and K. Horoba, "Detection of low amplitude fetal QRS complexes," in *Proc. of IEEE EMBS*, Vancouver, Canada, 2008, pp. 4764–7.

[130] E.C. Karvounis, M.G. Tsipouras, and D.I. Fotiadis, "Detection of fetal heart rate through 3-D phase space analysis from multivariate abdominal recordings," *IEEE Trans Biomed Eng*, vol. 56, no. 5, pp. 1394–406, May 2009.

[131] S. Waldert, M. Bensch, M. Bogdan, W. Rosenstiel, B. Schölkopf, C.L. Lowery, H. Eswaran, and H. Preissl, "Real-time fetal heart monitoring in biomagnetic measurements using adaptive real-time ICA," *IEEE Trans Biomed Eng*, vol. 54, no. 10, pp. 1867–1874, Oct 2007.

[132] C.M. Bishop, *Pattern recognition and machine learning*, Springer Science+Business Media LLC, New York, 2006.

[133] S. Harmeling, F. Meinecke, and K.-R. Müller, "Analysing ICA components by injecting noise.," in *4th International Symposium on Independent Component Analysis and Blind Signal Separation*, Nara, Japan, Apr. 2003, pp. 149–154.

[134] F. Shellong, *Grundzüge einer klinischen Vektocardiographie des Herzens*, Springer-Verlag, Berlin, 1939.

[135] I.T. Jolliffe, *Principal Component Analysis*, Springer-Verlag, New York, 2nd edition, 2002.

[136] A. Hyvärinen and E. Oja, "Independent component analysis: algorithms and applications," *Neural Netw.*, vol. 13, pp. 411–430, 2000.

[137] A. Hyvärinen, "Fast and robust fixed point algorithms for independent component analysis," *IEEE Trans. On Neural Networks*, vol. 10, no. 3, pp. 626–634, 1999.

[138] F. Gritzali, G. Frangakis, and G. Papakonstantinou, "Detection of the P and T waves in an ECG," *Comput Biomed Res*, vol. 22, no. 1, pp. 83–91, Feb 1989.

[139] S.J. Ahn, W. Rauh, and H.-J. Warnecke, "Least-squares orthogonal distances fitting of circle, sphere, ellipse, hyperbola, and parabola," *Pattern Recognition*, vol. 34, pp. 2283–2303, 2001.

[140] R. Vullings, C.H.L. Peters, S.I. Mossavat, S.G. Oei, and J.W.M. Bergmans, "Bayesian approach to patient-tailored vectorcardiography," *IEEE Trans Biomed Eng*, vol. 57, no. 3, pp. 586–595, Mar 2010.

[141] G.D. Clifford and L. Tarassenko, "Quantifying errors in spectral estimates of HRV due to beat replacement and resampling," *IEEE Trans Biomed Eng*, vol. 52, no. 4, pp. 630–638, Apr 2005.

[142] C. Peters, R. Vullings, J. Bergmans, G. Oei, and P. Wijn, "The effect of artifact correction on spectral estimates of heart rate variability," in *Proc. of IEEE EMBC*, Vancouver, Canada, 2008, pp. 2669–72.

[143] T. Fukushima, C.A. Flores, E.H. Hon, and E.C. Davidson Jr, "Limitations of autocorrelation in fetal heart rate monitoring," *Am J Obstet Gynecol*, vol. 153, no. 6, pp. 685–92, Nov 1985.

[144] N.M. Gibson, W. Peasgood, J.M. Herbert, M.S. Woolfson, and J.A. Crowe, "Iterative method to derive an approximate matched filter template for fetal electrocardiogram signals," *Med Eng Phys*, vol. 17, no. 3, pp. 188–96, Apr 1995.

[145] A. Ruha, S. Sallinen, and S. Nissilä, "A real-time microprocessor QRS detector system with a 1-ms timing accuracy for the measurement of ambulatory HRV," *IEEE Trans Biomed Eng*, vol. 44, no. 3, pp. 159–67, Mar 1997.

[146] H.J. Ritsema van Eck, "Fiducial segment averaging to improve cardiac time interval estimates," *J Electrocardiol*, vol. 35, no. Suppl, pp. 89–93, 2002.

[147] C. Li, C. Zheng, and C. Tai, "Detection of ECG characteristic points using wavelet transforms," *IEEE Trans Biomed Eng*, vol. 42, no. 1, pp. 21–8, Jan 1995.

[148] S.Kadambe, R. Murray, and G. Faye Boundreaux-Bartels, "Wavelet transform-based QRS complex detector," *IEEE Trans Biomed Eng.*, vol. 46, no. 7, pp. 838–848, July. 1999.

[149] I.E.G. Richardson, *H.264 and MPEG-4 Video Compression: Video Coding for Next-generation Multimedia*, John Wiley & Sons Ltd, Chichester, 2003.

[150] E.T. Jaynes, *Probability theory: the logic of science*, Cambridge University Press, Cambridge, UK, 2003.

[151] J.M. Bland and D.G. Altman, "Statistical methods for assessing agreement between two methods of clinical measurement," *Lancet*, vol. 1, no. 8476, pp. 307–10, Feb 1986.

[152] M.S. Crouse, R.D. Nowak, and R.G. Baraniuk, "Wavelet-statistical signal processing using hidden markov models," *IEEE Trans Signal Processing*, vol. 46, no. 4, pp. 886–902, Apr 1998.

[153] K.M. Chang, "Portable obstructive sleep apnea screening system using overnight ECG and a PDA-based wireless transmission system," *Telemed J E Health*, vol. 15, no. 4, pp. 353–61, May 2009.

[154] W. Chen, C.L.W. Sonntag, F. Boesten, S. Bambang Oetomo, and L.M.G. Feijs, "A design of power supply for neonatal monitoring with wearable sensors," *Journal of Ambient Intelligence and Smart Environments-Special Issue on Wearable Sensors*, vol. 1, no. 2, pp. 185–196, 2009.

[155] A. Gruetzmann, S. Hansen, and J. Müller, "Novel dry electrodes for ECG monitoring," *Physiol Meas*, vol. 28, pp. 1375–1390, 2007.

[156] M. Oehler, V. Ling, K. Melhorn, and M. Schilling, "A multichannel portable ECG system with capacitive sensors," *Physiol Meas*, vol. 29, pp. 783–793, 2008.

[157] A.V. Oppenheim and R.W. Schafer, *Discrete-time signal processing*, Prentice Hall, 3rd edition, 2009.

[158] J.J. Bailey, A.S. Berson, A. Garson Jr, L.G. Horan, P.W. Macfarlane, D.W. Mortara, and C. Zywietz, "Recommendations for standardization and specifications in automated electrocardiography: bandwidth and digital signal processing. A report for health professionals by an ad hoc writing group of the Committee on Electrocardiography and Cardiac Electrophysiology of the Council on Clinical Cardiology, American Heart Association," *Circulation*, vol. 81, pp. 730–739, 1990.

[159] W.H. Press, B.P. Flannery, S.A. Teukolsky, and W.T. Vetterling, *Numerical recipes: the art of scientific computing*, Cambridge University Press, Cambridge, England, 1986.

[160] R Sameni, M.B. Shamsollahi, C. Jutten, and G.D. Clifford, "A nonlinear bayesian filtering framework for ecg denoising," *IEEE Trans Biomed Eng*, vol. 54, no. 12, pp. 2172–85, Dec 2007.

[161] A. Ben-Israel and T.N.E. Greville, *Generalized inverses*, Spinger, 2nd edition, 2003.

[162] J.F.G. De Freitas, M. Niranjan, and A.H. Gee, "Hierarchical Bayesian-Kalman models for regularisation and ARD in sequential learning," Tech. Rep., Department of Engineering, Cambridge University, 1998.

[163] Y. Bar-Shalom and X.R. Li, *Estimation and tracking: principles, techniques and software*, Artech House Inc, Norwood, MA, USA, 1993.

[164] R.E. Kalman, "A new approach to linear filtering and prediction problems," *Transactions of the ASME–Journal of Basic Engineering*, vol. 82, no. Series D, pp. 35–45, 1960.

[165] A.H. Jazwinski, "Adaptive filtering," *Automatica*, vol. 5, pp. 475–485, 1969.

[166] A. L. Goldberger, L. A. N. Amaral, L. Glass, J. M. Hausdorff, P. Ch. Ivanov, R. G. Mark, J. E. Mietus, G. B. Moody, C.-K. Peng, and H. E. Stanley, "PhysioBank, PhysioToolkit, and PhysioNet: Components of a new research resource for complex physiologic signals," *Circulation*, vol. 101, no. 23, pp. e215–e220, 2000 (June 13), Circulation Electronic Pages: http://circ.ahajournals.org/cgi/content/full/101/23/e215.

[167] S. Butterworth, "On the theory of filter amplifiers," *Experimental Wireless and the Wireless Engineer*, vol. 7, pp. 536–541, Oct 1930.

[168] M.R. Ford, S. Sands, and L Lew H, "Overview of artifact reduction and removal in evoked potential and event-related potential recordings," *Phys Med Rehabil Clin N Am*, vol. 15, no. 1, pp. 1–17, Feb 2004.

[169] L.G. Horan, N.C. Flowers, and D.A. Brody, "Principal factor waveforms of the thoracic QRS complex," *Circ Res*, vol. 15, pp. 131–145, 1964.

[170] L.G. Horan, N.C. Flowers, and C.B. Miller, "A rapid assay of dipolar and extradipolar content in the human electrocardiogram," *J Electrocardiol*, vol. 5, no. 3, pp. 211–224, 1972.

[171] R.M. Gulrajani, F.A. Roberge, and P. Savard, "Moving dipole inverse ecg and eeg solutions," *IEEE Trans Biomed Eng*, vol. BME-31, no. 12, pp. 903–910, Dec 1984.

[172] F. Greensite and G. Huiskamp, "An improved method for estimating epicardial potentials from the body surface," *IEEE Trans Biomed Eng*, vol. 45, no. 1, pp. 98–104, Jan 1998.

[173] B. He and D. Wu, "Imaging and visualization of 3-D cardiac electric activity," *IEEE Trans Inf Tech Biomed*, vol. 5, no. 3, pp. 181–186, Sep 2001.

[174] R. Hoekema, G.J.H. Uijen, and A. van Oosterom, "On selecting a body surface mapping procedure," *J Electrocardiol*, vol. 32, no. 2, pp. 93–101, 1999.

[175] S. Kenchaiah, J.C. Evans, D. Levy, P.W. Wilson, E.J. Benjamin, M.G. Larson, W.B. Kannel, and R.S. Vasan, "Obesity and the risk of heart failure," *N Engl J Med*, vol. 347, no. 5, pp. 305–313, Aug 2002.

[176] R Vullings, C.H.L. Peters, M. Mischi, S.G. Oei, and Bergmans J.W.M., "Fetal movement quantification by fetal vectorcardiography: a preliminary study," in *Proc. of IEEE EMBC*, Vancouver, Canada, 2008, pp. 1056–1059.

[177] A.J. Camm, T.F. Lüscher, and P.W. Serruys, *The ESC textbook of cardiovascular medicine*, Blackwell Publishing Ltd, Oxford, UK, 2006.

[178] E.H. Moore, "On the reciprocal of the general algebraic matrix," *Bulletin Am Math Soc*, vol. 26, pp. 394–395, 1920.

[179] R. Penrose, "A generalized inverse for matrices," *Proc Cambridge Phil Soc*, vol. 51, pp. 406–413, 1955.

[180] K.H. Knuth, "Bayesian source separation and localization," in *SPIE'98 Proceedings: Bayesian inference for inverse problems*, San Diego, July 1998, vol. 3459, pp. 147–158.

[181] R.C. Barr, M. Ramsey, and M.S. Spach, "Relating epicardial to body surface potential distributions by means of transfer coefficients based on geometry measurements," *IEEE Trans Biomed Eng*, vol. BME-24, no. 1, pp. 1–11, Jan 1977.

[182] Y. Yamashita and T. Takahashi, "Use of the finite element method to determine epicardial from body surface potentials under a realistic torso model," *IEEE Trans Biomed Eng*, vol. BME-31, no. 9, pp. 611–621, Sep 1984.

[183] G. Parisi, *Statistical field theory*, Perseus Books Publishing LLC, 1988.

[184] "http://www.physionet.org/physiobank/database/ptbdb/," accessed March 29 2010.

[185] L. Sörnmo, "Vectorcardiographic loop alignment and morphologic beat-to-beat variability," *IEEE Trans Biomed Eng*, vol. 45, no. 12, pp. 1401–1413, Dec 1998.

[186] Z. Liu, C. Liu, and B. He, "Noninvasive reconstruction of three-dimensional ventricular activation sequence from the inverse solution of distributed equivalent current density," *IEEE Trans Med Imaging*, vol. 25, no. 10, pp. 1307–1318, Oct 2006.

[187] W.D. Penny, N.J. Trujillo-Barreto, and K.J. Friston, "Bayesian fMRI time series analysis with spatial priors," *NeuroImage*, vol. 24, no. 2, pp. 350–362, 2005.

[188] M. Popescu, E.-A. Popescu, K. Fitzgerald-Gustafson, W.B. Drake, and J.D. Levine, "Reconstruction of fetal cardiac vectors from multichannel fMCG data using recursively applied and projected multiple signal classification," *IEEE Trans Biomed Eng*, vol. 53, no. 12, pp. 2564–2576, Dec 2006.

[189] P.E. Namin and R.A. Miller, "The normal electrocardiogram and vectorcardiogram in children," in *Electrocardiography in infants and children*, D.E. Cassel and R.F. Zugler, Eds., 1966, pp. 99–115.

[190] K. Mäkikallio, D.B. McElhinney, J.C. Levine, Marx G.R., Colan S.D., A.C. Marshall, J.E. Lock, E.N. Marcus, and W. Tworetzky, "Fetal aortic valve stenosis and the evolution of hypoplastic left heart syndrome: patient selection for fetal intervention," *Circulation*, vol. 113, no. 11, pp. 1401–5, Mar 2006.

[191] D.B. McElhinney, A.C. Marshall, L.E. Wilkins-Haug, D.W. Brown, C.B. Benson, V. Silva, G.R. Marx, A. Mizrahi-Arnaud, J.E. Lock, and W. Tworetzky, "Predictors of technical success and postnatal biventricular outcome after in utero aortic valvuloplasty for aortic stenosis with evolving hypoplastic left heart syndrome," *Circulation*, vol. 120, no. 15, pp. 1482–90, Oct 2009.

[192] L. Mangesi and G.J. Hofmeyr, "Fetal movement counting for assessment of fetal wellbeing," *Cochrane Database of Systematic Reviews*, vol. Issue 1, 2007.

[193] M. Åström, E. Carro Santos, L. Sörnmo, P. Laguna, and B. Wohlfart, "Vectorcardiographic loop alignment and the measurement of morphologic beat-to-beat variability in noisy signals," *IEEE Trans Biomed Eng*, vol. 47, no. 4, pp. 497–506, Apr 2000.

[194] F. Dellaert, "The expectation maximization algorithm," Tech. Rep., College of Computing, Georgia Institute of Technology, 2002.

[195] G.R. Shaw and P. Savard, "On the detection of QRS variations in the ECG," *IEEE Trans Biomed Eng*, vol. 42, no. 7, pp. 736–741, Jul 1995.

[196] M. Stridh and L. Sörnmo, "Spatiotemporal QRST cancellation techniques for analysis of atrial fibrillation," *IEEE Trans Biomed Eng*, vol. 48, no. 1, pp. 105–111, Jan 2001.

[197] A.P. Dempster, N.M. Laird, and D.B. Rubin, "Maximum likelihood from incomplete data via the EM algorithm," *J R Statist Soc, B*, vol. 39, no. 1, pp. 1–38, 1977.

[198] Y. Xing, T. Yu, Y.N. Wu, M. Roy, J. Kim, and C. Lee, "An expectation-maximization algorithm for probabilistic reconstructions of full-length isoforms from splice graphs," *Nucleic Acids Res*, vol. 34, no. 10, pp. 3150–60, 2006.

[199] U. Gemburch, "Prenatal diagnosis of congenital heart disease," *Prenat Diagn*, vol. 17, no. 13, pp. 1283–98, 1997.

[200] P. Randall, S. Brealey, S. Hahn, K.S. Khan, and J.M. Parsons, "Accuracy of fetal echocardiography in the routine detection of congenital heart disease among unselected and low risk populations: a systematic review," *BJOG*, vol. 112, no. 1, pp. 24–30, 2005.

[201] D. Bonnet, A. Coltri, G. Butera, L. Fermont, J. Le Bidois, J. Kachaner, and D. Sidi, "Detection of transposition of the great arteries in fetuses reduces neonatal morbidity and mortality," *Circulation*, vol. 99, no. 7, pp. 916–8, 1999.

[202] R.K. Kumar, J.W. Newburger, K. Gauvreau, S.A. Kamenir, and L.K. Hornberger, "Comparison of outcome when hypoplastic left heart syndrome and transposition of the great arteries are diagnosed prenatally versus when diagnosis of these two conditions is made only postnatally," *Am J Cardiol*, vol. 83, no. 12, pp. 1649–53, 1999.

[203] E.T. Jaeggi, G.F. Sholler, O.D. Jones, and S.G. Cooper, "Comparative analysis of pattern, management and outcome of pre- versus postnatally diagnosed major congenital heart disease: a population-based study," *Ultrasound Obstet Gynecol*, vol. 17, no. 5, pp. 380–5, 2001.

[204] D. Scagliotti and B.J. Deal, "Arrhythmia in the tiny, premature infant," *Clin Perinatol*, vol. 13, no. 2, pp. 339–50, 1986.

[205] C Kähler, V. Grimm, E. Schleussner, A. Schneider, U. Schneider, H. Nowak, L. Vogt, and H-J Seewald, "The application of fetal magnetocardiography (FMCG) to investigate fetal arrhythmia and congenital heart defects (CHD)," *Prenat Diagn*, vol. 21, no. 3, pp. 176–82, 2001.

[206] F.L. Hanley, "Fetal cardiac surgery," *Adv Cardiac Surg*, vol. 5, pp. 47–74, 1994.

[207] P.E. Vardas, E.M. Kanoupakis, G.E. Kochiadakis, E.N. Simantirakis, M.E. Marketou, and G.I. Chlouverakis, "Effects of long-term digoxin therapy on heart rate variability, baroreceptor sensitivity, and exercise capacity in patients with heart failure," *Cardiovasc Drugs Ther*, vol. 12, no. 1, pp. 47–55, Mar 1998.

[208] S.C. Mitchell, S.B. Korones, and H.W. Berendes, "Congenital heart disease in 56,109 births. incidence and natural history," *Circulation*, vol. 43, no. 3, pp. 323–32, Mar 1971.

[209] J.K. Cleal, M. Thomas, M.A. Hanson, S. Paterson-Brown, H.M. Gardiner, and L.R. Green, "Noninvasive fetal electrocardiography following intermittent umbilical cord occlusion in the preterm ovine fetus," *BJOG*, vol. 117, pp. 438–44, 2010.

[210] C.O. Onyeama, H. Srinivasan, M. Lotke, and D.L. Vickers, "Subgaleal abscess and E. coli septicemia following scalp electrode in a preterm newborn: a case report," *J Matern Fetal Neonatal Med*, vol. 22, no. 12, pp. 1201–3, Dec 2009.

Dankwoord

Het afronden van dit proefschrift betekent voor mij dat er een einde is gekomen aan een periode van enkele jaren waarin ik onderzoek heb gedaan naar nieuwe en verbeterde technologien voor de bewaking van de foetus in de buik van de moeder. De methodes en technieken die tijdens dit onderzoek ontwikkeld zijn hebben gaandeweg geleid tot een prototype bewakingssysteem, dat al snel NEMO (Non-invasive Electrophysiological Monitor for Obstetrics) werd gedoopt. Mijn promotieonderzoek, het ontwikkelen (en verbeteren) van dit NEMO systeem, kan logischerwijs als *Finding Nemo* betiteld worden. Al met al zijn de afgelopen jaren voorbij gevlogen en is het schrijven van het proefschrift redelijk voorspoedig gegaan. Met andere woorden, en om in de zwangerschapssfeer te blijven, het was geen heel zware bevalling. Niet in de laatste plaats valt dit toe te schrijven aan de onmisbare bijdrage en ondersteuning die ik van een groot aantal mensen heb mogen ontvangen en die ik hier graag wil benoemen.

In de eerste plaats wil ik mijn beide promotoren, Prof. Jan Bergmans en Prof. Guid Oei, bedanken voor de mogelijkheid die ze mij geboden hebben in dit onderzoeksproject deel te nemen. In het bijzonder wil ik Jan bedanken voor zijn bereidheid om mij te allen tijde te helpen en voor zijn (opbouwende) kritische houding ten opzichte van mijn werk. Volgens mij was de eerste versie van het manuscript dat tot hoofdstuk 3 van dit proefschrift heeft geleid na jouw eerste correcties meer rood dan zwart. Echter, deze kritische houding heeft er naar mijn mening wel toe geleid dat dit proefschrift zijn huidige niveau heeft bereikt en dat een aantal van de hoofdstukken inmiddels gepubliceerd is. Tevens wil ik je bedanken voor de tijd die je me hebt gegund om in alle rust te revalideren na mijn verkeersongeluk. Doordat ik geen enkele druk opgelegd kreeg om weer aan het werk te gaan (en zelfs afgeremd werd wanneer ik mijzelf wel enige druk oplegde) is het mogelijk geweest om vrijwel geheel te herstellen, al heeft dit uiteindelijk wel een heel jaar moeten duren. Guid, jou wil ik bedanken voor je enthousiasme en je klinische inbreng. De ontelbare voorbeelden die je aandroeg vanuit de klinische praktijk hadden een motiverend effect om toch weer door te gaan na elke tegenslag en hielpen ook om de klinische (ir)relevantie van de technologische uitdagingen te doorgronden.

De totstandkoming van dit proefschrift was nooit gelukt zonder de bijdrage van mijn co-promotor dr. Massimo Mischi en co-promovendus, voormalig afstudeerbegeleider en ”zaken partner” ir. Chris Peters. Massimo, thank you for your enor-

mous patience in reviewing papers, posters, presentations and, above all, my thesis. No matter how many times I carefully checked my work, every time you managed to find some errors or mistakes that I (and often also others) didn't see. I can only hope that I've picked up some of your meticulousness. Also thank you for all the nice times at conferences. Chris, jou wil ik in de eerste plaats bedanken voor de mogelijkheid die je me ooit geboden hebt om op dit onderwerp af te komen studeren. Zonder dat afstudeerproject zou ik nooit zijn gaan promoveren en zouden we nooit de plannen hebben gemaakt – en inmiddels met NEMO Healthcare zelfs gerealiseerd – om een eigen bedrijf op te zetten dat zich op bewakingstechnologie voor de verloskundige praktijk richt. Jouw vertrek uit Veldhoven om in Breda, en later Den Bosch, klinisch fysicus te worden maakte het minder gezellig in het MMC. Eerlijkheidshalve moet ik wel zeggen dat die gezelligheid af en toe een negatief effect had op mijn productiviteit (vooral wanneer er Subs gehaald moest worden of er "belangrijke dingen" verteld werden), maar dit werd over het algemeen ruimschoots gecompenseerd door de vruchtbare discussies die we hadden over alle inhoudelijke onderwerpen.

Prof. Karl Rosén, prof. Maria Signorini, and prof. Pieter Wijn are thanked for the efforts they made in reading and improving the thesis and for sitting on the core committee at the PhD defense. Prof. Frank Vandenbussche wordt bedankt voor het zitting nemen in de uitgebreide promotiecommissie. Pieter Wijn, behalve voor het zitting nemen in mijn promotiecommissie, wil ik je ook bedanken voor de mogelijkheid die je me hebt geboden om op jouw afdeling in het MMC te (blijven) werken en voor jouw inbreng in het totale onderzoek.

Dit promotie onderzoek was onderdeel van het 'electrophysiological monitoring of the fetal condition' project en werd financieel ondersteund door STW. Ik wil alle leden van de gebruikerscommissie bedanken voor hun opmerkingen, kritieken en suggesties tijdens de halfjaarlijkse voortgangsbesprekingen.

Natuurlijk kan ik in mijn dankwoord alle moeders (en baby's) die aan het onderzoek hebben meegedaan niet vergeten. Zonder de toewijding die zij hadden om elke keer weer naar het MMC te komen – wat voor sommigen een hele reis was – en bijna een uur stil te liggen, had ik nooit over de data kunnen beschikken die ik nu had en nooit deze resultaten kunnen verkrijgen. Gek genoeg waren de moeders die de beste metingen hebben opgeleverd juist die moeders die het beste op de hoogte waren van mijn onderzoek: betrokkenheid lijkt dus van invloed op de kwaliteit van de metingen. Ook bedankt aan Anne, Maartje, Judith, Marc, Lean en Rianne voor het uitvoeren en opzoeken van alle metingen en aan Barbara voor het onderhoud aan de meetopstelling.

Het feit dat de periode van mijn promotie onderzoek zo snel en prettig verlopen is heb ik ook te danken aan de vele collega's met wie ik samen heb kunnen werken en aan het werk van de studenten die ik heb mogen begeleiden bij hun stages (Fiere) of afstudeeronderzoeken (Satish en Maarten). Het werk van Maarten heeft (met een

kleine uitbreiding van 2D naar 3D) rechtstreeks geleid tot hoofdstuk 4 van dit proefschrift. Bedankt voor het werk dat je hiervoor hebt verricht en natuurlijk voor het Belgische bier, je verrijkingen aan de Nederlandse taal en alle verhalen over de illustere Bicky-burger. Ik heb er nog naar gezocht toen ik in de Ardennen was, maar het schijnt dat ze hem alleen in Vlaanderen kennen?!? De collega's en andere studenten (zowel op de TU/e als in het MMC) waarmee ik samen met mogen werken kan ik niet allemaal bij naam noemen, maar een aantal van hen wil ik toch specifiek vermelden. Iman, Bert, Rob, Yvonne, Anja, Diana, Tanya, Ward, Job, Carola bedankt voor jullie uiteenlopende bijdragen aan dit proefschrift, variërend van ondersteuning in administratieve zaken, tips over het gebruik van bepaalde computerprogramma's en feedback op stukjes van het onderzoek tot substantiële bijdragen in methodiek en berekeningen en de introductie in het voor mij nieuwe gebied van 'Bayesian machine learning' technieken. Chiara, thanks to you for all our discussions on pregnancy monitoring, the coffees, and the fun times during the various conferences. I have particular nice memories on the champagne in Lyon, the lunch on the hill in Florence, and the pubs in New York. Rian, bedankt voor alle gezellige ochtenden koffie drinken en alle koekjes en snoepjes die je meebracht.

Zonder af en toe te kunnen ontspannen en de moeders, foetussen en ECG's even te vergeten was mijn onderzoek nooit zo voorspoedig verlopen. Hiervoor wil ik dan ook een aantal mensen bedanken. Mijn vrienden voor de avondjes stappen, feesten, Wiien, Rikken (ik zal de nette naam maar gebruiken), weekendje(s), barbecues en weet ik veel wat nog meer, KDDB voor de altijd gezellige repetities en optredens en het voetbalteam Leunen 5+2-1 (elke jaargang weer met een langere naam). Ooit zal de dag komen dat jullie kampioen worden, ondanks (of juist vanwege) dat ik er niet meer bij ben.

Mijn familie wil ik bedanken voor alle steun en interesse tijdens mijn studie en mijn promotie, maar ook voor alle andere dingen (teveel om op te noemen). Jullie geduld met mij, als ik weer eens gefrustreerd was omdat een probleem niet meteen opgelost kon worden, was (en is) bewonderenswaardig. Fam. Schwachöfer wil ik bedanken voor de vakanties, weekendjes, etentjes en jullie enorme gastvrijheid: het is niet moeilijk om je bij jullie thuis te voelen. Janneke en Pleun worden bedankt voor hun foto's die ik in het proefschrift en/of op de kaft heb mogen gebruiken.

Tenslotte, maar zeker niet op de laatste plaats, wil ik Patricia bedanken voor alle leuke dingen die we samen gedaan hebben, voor je steun en geduld, niet alleen tijdens mijn promotie onderzoek, maar ook in de periode dat ik zolang thuis zat en niet bepaald een zonnetje zal zijn geweest, voor je liefde en voor nog zoveel andere dingen die ik hier niet allemaal kan vermelden. Helaas hebben we onlangs te horen gekregen dat je ziek bent, maar ik heb goede hoop en vertrouwen dat je snel weer helemaal beter zult zijn, vooral gezien jouw immer positieve instelling en vechtlust. Ik hoop dat we samen nog heel veel mooie en kankervrije tijden gaan beleven en ik

ben ervan overtuigd dat je volgend jaar je examens, die je nu helaas uit hebt moeten stellen, gaat halen. Op het moment van dit schrijven is het nog niet bekend of onze geplande reis naar Patagonië en Antarctica door zal gaan, maar ik hoop dat we samen heel veel van deze reis kunnen gaan genieten, bovenal omdat dit zou betekenen dat je weer beter bent.

Curriculum Vitae

Photograph of the author with the NEMO system.

Rik Vullings was born in Venray, the Netherlands, in 1980. In 1998 he graduated from the gymnasium at the Raayland College, Venray and started a study in Applied Physics at the Eindhoven University of Technology (TU/e), the Netherlands. During this study he completed two traineeships. The first one at the Gasdynamics group of the Applied Physics faculty at the TU/e, concerning the measurement and visualization of sound produced by air flowing through a Helmholtz resonator. The second one at the Radiation Oncology department of the Newcastle Mater Misericodiae Hospital in Newcastle, Australia. This traineeship involved the simulation of a linear accelerator in electron mode using the BEAM Monte Carlo code. In 2005 he received the M.Sc. degree *cum laude*. His graduation projected was conducted at the Clinical Physics department of the Máxima Medical Center (MMC) in Veldhoven, the Netherlands, and his master thesis was entitled ”The fetal electrocardiogram: determination of the fetal heart rate and electrocardiogram from abdominal recordings”.

Since 2005 he has been a PhD student within a joint project on fetal monitoring between the Signal Processing Systems group of the Electrical Engineering faculty of TU/e and the departments of Obstetrics & Gynecology and Clinical Physics at the MMC. The results of this PhD project are described in this dissertation. In May 2010, Rik Vullings co-founded a spin-off company, Nemo Healthcare BV, which aims to valorize knowledge and intellectual property of which a part is accumulated during his graduation project and his PhD project.

Index